APPENDIX C

ISSUES IMPORTANT TO QUANTIFICATION OF RISK

CONTENTS

FIGURES

TABLES

C.1 Introduction

It is well known that the methods of probabilistic risk assessment (PRA) have many kinds of uncertainties associated with them. To a varying extent, these uncertainties contribute to the imprecision in the estimates of risk to public health and safety from nuclear reactor accidents. The NRC contractor work underlying this report (Refs. C.1.1 through C.1.14) addresses many of these uncertainties and quantifies their impact on selected measures of risk. The method to incorporate uncertainties in the quantification of reactor risk involves identifying uncertainty "issues." In this context, an issue is a physical parameter, process, or event that cannot be characterized precisely but is potentially important to the frequency of core damage or to severe accident progression. Examples are operator error rates, hydrogen generation during core meltdown, and direct containment heating.

The total number of issues that was considered in the present analyses is quite large. A complete description of all issues is available in the contractor reports. To give the reader a feel for what information is available, three tables and the description of those tables from the Surry analysis (Ref. C.1.10) have been included in this section.

This appendix summarizes the way in which a few important issues were treated in the five PRAs addressed in this report. In this context, "important" refers to subjective judgments made by the NRC staff and its contractors (based on results of the detailed analyses) that a particular issue has substantial influence on the quantification of risk. The objective of these descriptions is twofold:

1. To provide an answer to the following question: What aspects of the knowledge base supporting probabilistic risk assessment for nuclear power reactors are the principal contributors to our inability to precisely calculate risk?

2. To describe how areas known from previous work to have substantial uncertainty were addressed in the analyses described in NUREG–1150.

It should be noted that issues contributing to the uncertainty in risk are not necessarily significant contributors to a particular estimate of reactor risk. For example, issues that are threshold in nature (e.g., those governing the outcome of an event that either occurs or does not occur) can be important contributors at one end of the spectrum of risk estimates, yet be an insignificant contributor to risk estimates at the opposite end of the spectrum. Such issues may not even be major contributors to the mean value of risk. It is important to identify these issues—particularly those that contribute to estimates of risk near the high end of the spectrum. Improvements in the precision with which reactor risk analysis can be performed may be achieved by focusing future research on topics that are major contributors to the uncertainty in risk. Confidence that a selected measure of reactor risk is below some value can be improved by focusing research on topics that contribute to estimates of risk near the upper end of the spectrum.

Issues important to risk uncertainty are described in the following sections, which are organized in a similar fashion. First, an issue is defined in the context of its application within the risk analyses in this study. Since most issues are relatively high-level representations of uncertainty (i.e., they represent a composite of several interrelated sources of uncertainty), the specific source(s) of uncertainty included within each issue are delineated as part of the definition. The process of characterizing the contributing factors to the uncertainty associated with an issue is termed "issue decomposition." An example of issue decomposition is provided in Figure C.1.1, which considers the hypothetical issue of containment bypass. Underlying this hypothetical issue are a variety of more basic events and processes. Each of these may have an associated uncertainty. Quantification of the uncertainty associated with the main issue, therefore, involves the aggregation of uncertainties of several interrelated items. This process can become quite complicated and is not addressed in detail in this appendix. A summary of each issue's quantification and the technical basis that supports this quantification is provided. For greater detail regarding issue decomposition and quantification of individual contributors to uncertainty, the reader is referred to References C.1.1 through C.1.7 for issues related to estimating core damage frequency and References C.1.8 through C.1.14 for issues related to accident progression and consequences. Finally, the manner in which an issue was incorporated in the PRA(s) is described. Results of statistical analyses and other indicators of an issue's importance to risk uncertainty are presented.

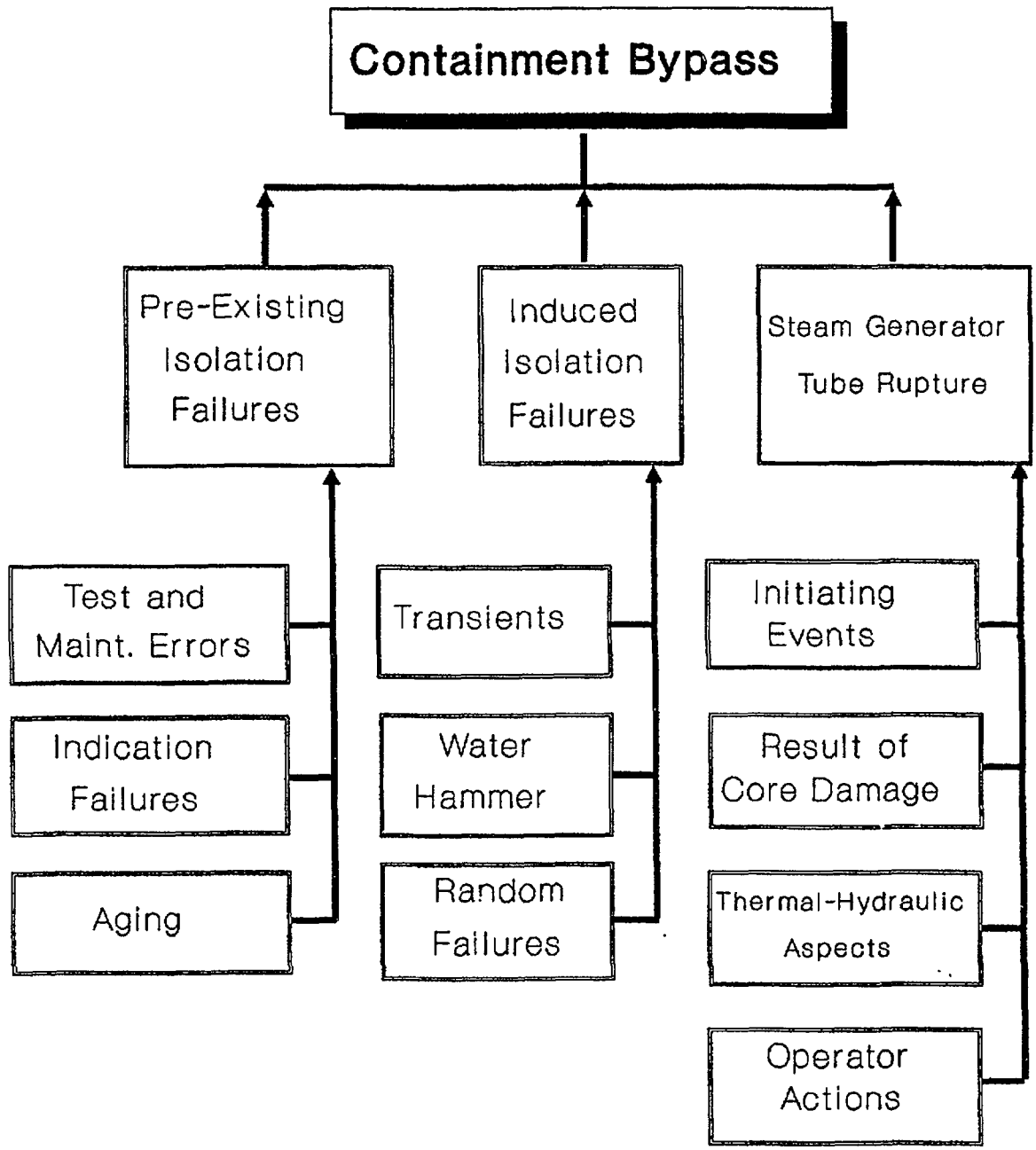

Figure C.1.1 Example of NUREG–1150 "issue decomposition."

C.1.1 Description of Table C.1.1; Variables Sampled in Accident Frequency Analysis

In the accident frequency analysis for internal events, a large number of variables were sampled. (A list of these variables may be found in Ref. C.1.3.) Only those variables found to be important to the uncertainty in the accident frequencies were selected for sampling in the integrated risk analysis. These variables are listed and defined in Table C.1.1. For the regression analysis, identifiers of eight characters or less were required, and these are listed in the first column. Where these differ from the identifiers used in the fault trees, these identifiers are listed in the description in brackets. Generally, the eight-character identifiers have been selected to be as informative as possible to those not familiar with the conventions used in systems analysis. For example, while Event K is commonly used to indicate the failure of the reactor protection system (RPS) to insert enough control rods to make the reactor subcritical, the identifier AU-SCRAM was chosen since it was felt that "auto scram" conveys more meaning to most readers than "K."

The second column in Table C.1.1 gives the range of the distribution for the variable, and the third column indicates the type of distribution used and its mean value. The entry "Experts" for the distribution indicates that the distribution came from the accident frequency analysis expert panel. The fourth and fifth columns in Table C.1.1 show whether the variable is correlated with any other variable, and the last column describes the variable. More complete descriptions and discussion of these variables may be found in the Surry accident frequency analysis report (Ref. C.1.3). This report also gives the source or the derivation of the distributions for all these variables.

Only two accident frequency variables were correlated in the integrated analysis. As indicated in Table C.1.1, DG-FRUN1 and DG-FRUN6 were correlated with each other since they represent failures to run for different times for the same equipment. The failures to run for the steam-turbine-driven auxiliary feedwater (AFW) pump (ATP-FR6 and ATP-FR24) should have been correlated for the same reason, but this correlation was omitted because of an oversight. Neither of the AFW pump failure-to-run variables was important in determining the uncertainty in risk, so the effect of omitting the correlation between them is not significant.

Table C.1.1 Variables sampled in accident frequency analysis for internal initiators.

Variable	Range	Distribution	Correlation	Correlation With	Description
V-TRAIN	1.8E-13 1.5E-5	Experts Mean=5.5E-7	None		Initiating event: frequency (1/yr) of check valve failure in one of the LPIS trains.
IE-LOSP	2.6E-5 0.28	LOSP Data Mean=0.077	None		Initiating event: frequency (1/yr) of LOSP. [IE-T1]
IE-A	5.0E-5 0.0032	Lognormal Mean=5E-4	None		Initiating event: frequency (1/yr) of a large (dia. > 6 in.) break in the RCS (LOCA).
IE-S1	1.0E-4 0.0063	Lognormal Mean=0.001	None		Initiating event: frequency (1/yr) of an intermediate size (6 in. > dia. > 2 in.) LOCA.
IE-S2	1.0E-4 0.0063	Lognormal Mean=0.001	None		Initiating event: frequency (1/yr) of a small break (2 in. > dia. > 0.5 in.) in the RCS.
IE-S3	0.0013 0.082	Lognormal Mean=0.013	None		Initiating event: frequency (1/yr) of a very small (0.5 in. > dia.) break in the RCS (LOCA).

Table C.1.1 (continued)

Variable	Range	Distribution	Correlation	Correlation With	Description
IE-T-ALL	0.67 41.6	Lognormal Mean=6.6	None		Initiating event: frequency (1/yr) of all transients that require scram (Surry data). [IE-T]
IE-T-HIP	0.60 37.2	Lognormal Mean=5.9	None		Initiating event: frequency (1/yr) of all transients from high (>25%) power that require scram (Surry data). [IE-TN]
IE-LMFWS	0.096 5.9	Lognormal Mean=0.94	None		Initiating event: frequency (1/yr) of transients due to loss of the main feedwater system (Surry data). [IE-T2]
IE-SGTR	0.001 0.063	Lognormal Mean=0.01	None		Initiating event: frequency (1/yr) of SGTRs (PWR data). [IE-T7]
IE-DCBUS	2.5E-5 0.14	Lognormal Mean=0.005	None		Initiating event: frequency (1/yr) for loss of a dc power bus. [IE-T5]
DG-FRUN1	9.9E-6 0.057	Lognormal Mean=0.002	Rank 1	DG-FRUN6	Probability that the diesel generator fails to run for 1 h, given that it starts. [DGN-FR-1HR]
DG-FRUN6	6.0E-5 0.34	Lognormal Mean=0.012	Rank 1	DG-FRUN1	Probability that the diesel generator fails to run for 6 h, given that it starts. [DGN-FR-6HR]
DG-FSTRT	0.0022 0.14	Lognormal Mean=0.022	None		Probability that the diesel generator fails to start, given a demand to start. [DGN-FS]
UNFV-MOD	1.8E-4 0.27	Lognormal Mean=0.014	None		Fraction of the time that the reactor operates with an unfavorable moderator temperature coefficient. [Z]
AU-SCRAM	1.8E-6 7.6E-4	Lognormal Mean=6E-5	None		Probability of failure of the RPS to automatically insert sufficient control rods to terminate the reaction. [K]
MN-SCRAM	0.017 1.0	Max. Entropy Mean=0.17	None		Probability of failure to effect manual scram due to operator error and hardware faults. [R]
AUTO-ACT	4.8E-5 0.020	Lognormal Mean=0.0016	None		Probability of failure of one train of an automatic actuation system (generic). [ACT-FA]

Table C.1.1 (continued)

Variable	Range	Distribution	Correlation	Correlation With	Description
CCF-RWST	1.5E-6 0.0085	Lognormal Mean=3E-4	None		Probability of common-cause failure of the recirculation mode *transfer system due to miscali*-bration of the water level sensors in the RWST (human error). [RMT-CCF-FA-MSCAL]
BETA2MOV	0.0089 0.55	Lognormal Mean=0.088	None		Beta factor for common-cause failure of two motor-operated valves (generic). [BETA-2MOV]
BETA-AFW	0.0057 0.35	Lognormal Mean=0.056	None		Beta factor for common-cause failure of the AFWS motor-driven pumps (generic).
BETA-LPI	0.015 0.94	Lognormal Mean=0.15	None		Beta factor for common-cause failure of the LPIS pumps (generic).
AFW-STMB	2.0E-8 0.0070	Lognormal Mean=1.0E-4	None		Probability of common-cause failure of all AFWS due to steam binding (backleakage through check valves from MFWS). [CCF-LK-STMBD]
MDP-FSTR	1.5E-5 0.085	Lognormal Mean=0.003	None		Probability of failure to start (per demand) for motor-driven pumps for which specific plant data were not available (generic). [MDP-FS]
AFWMP-FS	6.4E-4 0.040	Lognormal Mean=0.0063	None		Probability of failure to start (per demand) for AFW motor-driven pumps (from Surry data). [AFW-MDP-FS-FW3B]
AFWTP-FS	5.5E-5 0.31	Lognormal Mean=0.011	None		Probability of failure to start (per demand) for AFW steam-turbine-driven pump (from Surry data). [TDP-FS]
ATP-FR6	1.5E-4 0.85	Lognormal Mean=0.030	None		Probability of failure to run for 6 h for the AFW steam-turbine-driven pump (generic). [TDP-FR-6HR]
ATP-FR24	0.01 1.0	Max. Entropy Mean=0.12	None		Probability of failure to run for 24 h for the AFW steam-turbine-driven pump (generic). [TDP-FR-24HR]
PORV-BLK	0.0041 0.25	Lognormal Mean=0.040	None		Probability of failure to open (per demand) for the PORV block valves (MOVs). [PPS-MOV-FT]

Table C.1.1 (continued)

Variable	Range	Distribution	Correlation	Correlation With	Description
LPRS-MOV	2.6E-5 0.15	Lognormal Mean=0.0052	None		Probability of failure (per demand) for the suction MOVs in the LPRS due to hardware failures or plugging. [LPR-MOV-FT]
MOV-FT	1.5E-5 0.085	Lognormal Mean=0.003	None		Probability of failure to transfer (per demand) for motor-operated valves (generic).
MNV-PG1	4.1E-6 2.5E-4	Lognormal Mean=3.6E-5	None		Probability of failure due to plugging for manual valves that are flow-tested every month (generic). [XVM-PG-1MO]
MOV-PG3	1.0E-5 6.3E-4	Lognormal Mean=1.0E-4	None		Probability of failure due to MOVs that are flow-tested every 3 months (generic). [MOV-PG-3MO]
MOV-PG12	4.5E-5 0.0028	Lognormal Mean=4.4E-4	None		Probability of failure due to plugging for MOVs that are flow-tested every 12 months (generic). [MOV-PG-12MO]
AFW-OCC	1.5E-5 9.5E-4	Lognormal Mean=1.5E-4	None		Probability of common-cause failure of AFWS due to an inadvertently open crossconnect to Unit 2 (flow diversion). [AFW-PSF-FC]
PORV-REC	1.5E-4 0.85	Lognormal Mean=0.030	None		Probability of failure of the pressurizer PORVs to reclose after opening (generic). [SOV-OO]
SSRVO-SB	0.030 1.0	Max. Entropy Mean=0.27	None		Probability of failure of an SG SRV to reclose within 1 h during SBO (faulted steam generator). [QS-SBO]
SSRVO-U2	0.016 1.0	Max. Entropy Mean=0.16	None		Probability of failure of a secondary system SRV at Unit 2 to reclose within 1 h during SBO at both units. [QS-UNIT2]
SOV-FT	1.0E-4 0.0063	Lognormal Mean=0.001	None		Probability of failure to transfer (per demand) for solenoid-operated valves (generic).
CKV-FT	1.0E-5 6.3E-4	Lognormal Mean=1E-4	None		Probability of failure to open (per demand) for check valves (generic).

Table C.1.1 (continued)

Variable	Range	Distribution	Correlation	Correlation With	Description
HE-FDBLD	0.0071 0.71	Max. Entropy Mean=0.071	None		Probability of failure of the operator to initiate feed and bleed (human error—open PORVs, and start charging pump and align suction and discharge valves). [HPI-XHE-FO-FDBLD]
HE-PORVS	0.0044 0.44	Max. Entropy Mean=0.044	None		Probability of failure of the operator to initiate feed and bleed (human error; diagnose situation and open PORVs). [PPS-XHE-FO-PORVS]
HE-CST2	0.0065 0.65	Max. Entropy Mean=0.065	None		Probability of failure of the operator to align the AFWS suction to the backup CST during an SBO with a faulted SG. [AFW-XHE-FO-CST2]
HE-UNIT2	0.0036 0.36	Max. Entropy Mean=0.036	None		Probability of failure of the operator to provide AFW from Unit 2 via the crossconnect. [XHE-FO-UNIT2]
HE-SKILL	1.3E-5 0.077	Lognormal Mean=0.0026	None		Probability of human error for skill-based human errors (rudimentary actions performed from memory). [XHE-FO-SKILLBASE]
RCP-SL-F		Experts	None		Probability of RCP seal failure before the onset of core damage.

C.1.2 Description of Table C.1.2; Questions in Surry APET

In addition to the number and name of the question, Table C.1.2 indicates if the question is sampled, and how the question is evaluated or quantified. In the sampling column, an entry of DS indicates that the sampling is from a distribution provided by one of the expert panels, or from the electric power recovery distribution. The item sampled may be either the branching ratios or the parameter defined at that question. For questions that are sampled and that were quantified internally, the entry ZO in the sampling column indicates that the question was sampled zero-one, and the entry SF means the questions were sampled with split fractions. The difference may be illustrated by a simple example. Consider a question that has two branches and a uniform distribution from zero to 1.0 for the probability for the first branch. If the sampling is zero-one, in half of the observations the probability for the first branch will be 1.0, and in the other half of the observations it will be zero. If the sampling is split fraction, the probability for the first branch for each observation is a random fractional value between zero and 1.0. The average over all the fractions in the sample is 0.50. The implications of ZO or SF sampling are discussed in Reference C.1.8.

If the sampling column is blank, the branching ratios for that question, and the parameter values defined in that question, if any, are fixed. The branching ratios of the plant damage state (PDS) questions change

to indicate which PDS is being considered. Some of the branching ratios depend on the relative frequency of the PDSs that make up the PDS group being considered. These branching ratios change for every sample observation but may do so for some PDS groups and not for others. If the branching ratios change from observation to observation for any one of the seven PDS groups, SF is placed in the sampling column for the PDS questions.

The abbreviations in the quantification column of Table C.1.2 are given below, with the number of questions that have that type of quantification.

Type of Quantification	Number of Questions	Comments
PDS	11	Determined by the PDS
AcFrqAn	1	Determined in the accident frequency analysis
Other	4	See Notes 1 through 4
Internal	17	Quantified internally in this analysis
Summary	17	The branch taken at this question follows directly from the branches taken at previous questions
ROSP	3	The probability of the recovery of offsite power is determined by distributions derived from the electric power recovery data for this plant
UFUN–Str.	3	Calculated in the User Function, using distributions from the structural response expert panel
UFUN–Int.	2	Calculated in the User Function, using an adiabatic pressure rise calculation determined internally
In-Vessel	5	Distributions from the in-vessel accident progression expert panel
Loads	2	Distributions from the containment loadings expert panel
Struct.	1	Distribution from the containment structural performance expert panel
N.A.	5	Fan cooler questions not applicable to Surry

In some cases, a question may have more than one function so the entry under Quantification in Table C.1.2 can be only indicative. For example, Questions 43, 52, and 64 are listed as being quantified by the user function, based on distributions generated by the containment structural performance expert panel. The actual situation is that a portion of the user function is evaluated which determines whether the containment fails using the load pressure and the failure pressure. The load pressure is determined in Questions 39 and 40 based on aggregate distributions from the containment loadings expert panel. The containment failure pressure is determined in Question 42 from the aggregate distributions from the containment loadings expert panel. If the failure pressure is lower than the load pressure, then the containment fails and the mode of failure is determined using the random number defined in Question 42 and a table of conditional failure mode probabilities contained in the user function. This table was also generated by the containment structural performance expert panel. The sampling is indicated to be zero-one because one of the four branches of these questions always has a probability of 1.0, and the other three always have a probability of zero.

Table C.1.2 Questions in Surry APET.

Question Number	Question	Sampling	Quantification
1.	Size & location of RCS break when the core uncovers?	SF	PDS
2.	Has the reaction been brought under control?	SF	PDS
3.	For SGTR, are the secondary system SRVs stuck open?	SF	PDS
4.	Status of ECCS?	SF	PDS
5.	RCS depressurization by the operators?	SF	PDS
6.	Status of sprays?	SF	PDS
7.	Status of fan coolers?		N.A.
8.	Status of ac power?		PDS
9.	RWST injected into containment?	SF	PDS
10.	Heat removal from the steam generators?	SF	PDS
11.	Did the operators depressurize the secondary before the core uncovers?	SF	PDS
12.	Cooling for RCP seals?	SF	PDS
13.	Initial containment condition?		AcFrqAn
14.	Event V—break location under water?	SF	Note 1
15.	RCS pressure at the start of core degradation?		Summary
16.	Do the PORVs stick open?	SF	Note 2
17.	Temperature-induced RCP seal failure?	ZO	Note 3
18.	Is the RCS depressurized before breach by opening the pressurizer PORVs?		Internal
19.	Temperature-induced SGTR?	DS	In-Vessel
20.	Temperature-induced hot leg or surge line break?	DS	In-Vessel
21.	Is ac power available early?	SF	ROSP
22.	Rate of blowdown to containment?		Summary
23.	Vessel pressure just before vessel breach?	ZO	Internal
24.	Is core damage arrested? No vessel breach?	SF	Internal
25.	Early sprays?		Summary
26.	Early fan coolers?	N.A.	
27.	Early containment heat removal?		Summary
28.	Baseline containment pressure before VB?		Internal
29.	Time of accumulator discharge?		Summary
30.	Fraction of zirconium oxidized in-vessel during core degradation?	P	In-Vessel
31.	Amount of zirconium oxidized in-vessel during core degradation?		Summary
32.	Amount of water in the reactor cavity at vessel breach?		Summary

Table C.1.2 (continued)

Question Number	Question	Sampling	Quantification
33.	Fraction of core released from the vessel at breach?	P	In-Vessel
34.	Amount of core released from the vessel at breach?		Summary
35.	Does an alpha event fail both vessel & containment?	SF	Note 4
36.	Type of vessel breach?	ZO	In-Vessel
37.	Does the vessel become a "Rocket" and fail the cont.?		Internal
38.	Size of hole in vessel (after ablation)?	ZO	Internal
39.	Total pressure rise at vessel breach? Large hole cases	P	Loads
40.	Total pressure rise at vessel breach? Small hole cases	P	Loads
41.	Does a significant ex-vessel steam explosion occur?		Internal
42.	Containment failure pressure?	P	Struct.
43.	Containment failure and type of failure?	ZO	UFUN-Str.
44.	Sprays after vessel breach?		Internal
45.	Is ac power available late?	SF	ROSP
46.	Late sprays?		Summary
47.	Late fan coolers?		N.A.
48.	Late containment heat removal?		Summary
49.	How much hydrogen burns at vessel breach?	SF	Internal
50.	Does late ignition occur?		Internal
51.	Resulting pressure in containment?		UFUN-Int.
52.	Containment failure and type of failure?	ZO	UFUN-Str.
53.	Amount of core available for CCI?		Summary
54.	Is the debris bed in a coolable configuration?		Internal
55.	Does prompt CCI occur?		Summary
56.	Is ac power available very late?	SF	ROSP
57.	Very late sprays?		Summary
58.	Very late fan coolers?		N.A.
59.	Very late containment heat removal?		Summary
60.	Does delayed CCI occur?		Summary
61.	How much hydrogen is produced during CCI?		Internal
62.	Does very late ignition occur?	P	Internal
63.	Resulting pressure in containment?		UFUN-Int.
64.	Containment failure and type of failure?	ZO	UFUN-Str.
65.	Sprays after very late CF?		Internal
66.	Fan coolers after very late CF?		N.A.
67.	Containment heat removal after very late CF?		Summary
68.	Eventual basemat meltthrough (BMT)?		Internal

Table C.1.2 (continued)

Question Number	Question	Sampling	Quantification
69.	*Eventual overpressure failure of containment?*		*Internal*
70.	BMT before overpressure failure?		Internal
71.	Final containment condition?		Summary

Note 1. Whether the location of the break in the low-pressure piping would be under water in Event V at the time the core was uncovered was determined by a special panel that considered only this problem for the draft version of this analysis. As there was no new information available, there was no reason to change the conclusions reached by this group.

Note 2. There is little or no data on the failure rate of PORVs when passing gases at temperatures considerably in excess of their design temperature. The quantification was arrived at by discussions between the accident frequency analyst and the plant analyst.

Note 3. In the accident frequency analysis, a special panel was convened to consider the issue of the failure of RCP seals. The quantification of this question is not as detailed as that done in the accident frequency analysis but relies on the information produced by this panel.

Note 4. The alpha mode of vessel and containment failure was considered by the Steam Explosion Review Group a few years ago. The distribution used in this analysis is based on information contained in the report of this group.

Key to Abbreviations in Table C.1.2

AcFrqAn The quantification was performed as part of the accident frequency analysis.

DS The branch probabilities are taken from a distribution; depending on the distribution, the sampling may be SF or ZO.

Internal The quantification was performed at Sandia National Laboratories by the plant analyst with the assistance of other members of the laboratory staff.

In-Vessel This question was quantified by sampling from an aggregate distribution provided by the expert panel on in-vessel accident progression.

Loads This question was quantified by sampling from an aggregate distribution provided by the expert panel on containment loadings.

N.A. Not Applicable.

P A parameter is determined by sampling from a distribution, in most cases an aggregate distribution from an expert panel.

PDS The quantification follows directly from the definition of the plant damage state.

ROSP This question was quantified by sampling from a distribution derived from the offsite power recovery data for the plant.

SF Split fraction sampling – the branch probabilities are real numbers between zero and one.

Struct. This question was quantified by sampling from an aggregate distribution provided by the containment structural performance expert panel.

Summary The quantification for this question follows directly from the branches taken at preceding questions or the values of parameters defined in preceding questions.

UFUN-Str. This question is quantified by the execution of a part of the User Function, using distributions from the containment structural performance expert panel.

UFUN-Int. This question is quantified by the execution of a part of the User Function, using an adiabatic calculation for the pressure rise due to hydrogen combustion.

ZO Zero-One sampling—the branch probabilities are either 0.0 or 1.0.

C.1.3 Description of Table C.1.3; Variables Sampled in Source Term Analysis

The variables that were sampled in the source term analysis are listed and summarized in Table C.1.3. Those variables quantified by the source term expert panel are marked with an asterisk in Table C.1.3.

Table C.1.3 Variables sampled in source term analysis.

Variable	Description
FCOR*	Fraction of each fission product group released from the core to the vessel before or at vessel breach. There are two cases: high and low zirconium oxidation.
FVES*	Fraction of each fission product group released from the vessel to the containment before or at vessel breach. There are four cases: RCS at system setpoint pressure, RCS at high or intermediate pressure, RCS at low pressure, and Event V.
VDF	Decontamination factor for pool scrubbing for Event V when the break location is underwater at the time of the release. There is one distribution, which applies to all radionuclide classes except inert gases.
FCONV*	Fraction of each fission product group in the containment from the RCS release that is released from the containment in the absence of mitigating factors such as sprays. There is one distribution for each case, which applies to all radionuclide classes except inert gases. There are five cases: containment leak at or before vessel breach with sprays operating, containment leak at or before vessel breach with sprays not operating, containment rupture at or before vessel breach, very late containment rupture, and Event V. Note that FCONV does not account for fission product removal by the sprays. The case differentiation on spray operation is to account for differences in containment atmosphere temperature and humidity between the two cases.
FCCI*	Fraction of each fission product group in the core material at the start of CCIs that is released to the containment. There are four cases: low zirconium oxidation in the core and no overlaying water, high zirconium oxidation in the core and no overlaying water, low zirconium oxidation in the core with overlaying water, and high zirconium oxidation in the core with overlaying water.
FCONC*	Fraction of each fission product group in the containment from the CCI release that is released from the containment in the absence of mitigating factors such as sprays. The five cases are the same as those for FCONV, but there are separate distributions for each radionuclide class.
SPRDF	Decontamination factor for sprays. Internal elicitation was used to develop a distribution for this variable, which was used for all fission product groups except the noble gases. There is one distribution for each case, which applies to all radionuclide classes except inert gases. There are three cases: RCS release at high pressure and CF at VB, RCS releases not covered by the first case, and CCI releases.

Table C.1.3 (continued)

Variable	Description
LATEI*	Fraction of the iodine deposited in the containment that is revolatilized and released to the environment late in the accident. This variable applies only to iodine.
FLATE*	Fraction of the deposited amount of each fission product group in the RCS that revolatilized after VB and released to the containment. There are two cases: one large hole in the RCS and two large holes in the RCS.
DST*	Fraction of each fission product group in the core material that becomes aerosol particles in a direct containment heating event at VB that is released to the containment. There are two cases: VB at high pressure (1000 to 2500 psia) and VB at intermediate pressure (200 to 1000 psia).
FISGFOSG	Fraction of each fission product group released from the reactor vessel to the steam generator, and from the steam generator to the environment, in an SGTR accident. There are two separate distributions, FISG and FOSG, each of which has two cases: SGTRs in which the secondary SRVs reclose and SGTRs in which the secondary SRVs stick open.
POOL-DF	Decontamination factor for a pool of water overlaying the core debris during CCI. There are two cases: a completely full (depth about 14 ft) cavity and a partially full cavity (accumulator water only, depth about 4 ft).

*Quantified by source term expert panel.

REFERENCES FOR SECTION C.1

C.1.1 D.M. Ericson, Jr., (Ed.) et al., "Analysis of Core Damage Frequency: Internal Events Methodology," Sandia National Laboratories, NUREG/CR-4550, Vol. 1, Revision 1, SAND86-2084, January 1990.

C.1.2 T.A. Wheeler et al., "Analysis of Core Damage Frequency from Internal Events: Expert Judgment Elicitation," Sandia National Laboratories, NUREG/CR-4550, Vol. 2, SAND86-2084, April 1989.

C.1.3 R.C. Bertucio and J.A. Julius, "Analysis of Core Damage Frequency: Surry Unit 1," Sandia National Laboratories, NUREG/CR-4550, Vol. 3, Revision 1, SAND86-2084, April 1990.

C.1.4 A.M. Kolaczkowski et al., "Analysis of Core Damage Frequency: Peach Bottom Unit 2," Sandia National Laboratories, NUREG/CR-4550, Vol. 4, Revision 1, SAND86-2084, August 1989.

C.1.5 R.C. Bertucio and S.R. Brown, "Analysis of Core Damage Frequency: Sequoyah Unit 1," Sandia National Laboratories, NUREG/CR-4550, Vol. 5, Revision 1, SAND86-2084, April 1990.

C.1.6 M.T. Drouin et al., "Analysis of Core Damage Frequency: Grand Gulf Unit 1," Sandia National Laboratories, NUREG/CR-4550, Vol. 6, Revision 1, SAND86-2084, September 1989.

C.1.7 M.B. Sattison and K.W. Hall, "Analysis of Core Damage Frequency: Zion Unit 1," Idaho National Engineering Laboratory, NUREG/CR-4550, Vol. 7, Revision 1, EGG-2554, May 1990.

C.1.8 E.D. Gorham-Bergeron et al., "Evaluation of Severe Accident Risks: Methodology for the Accident Progression, Source Term, Consequence, Risk Integration, and Uncertainty Analyses," Sandia National Laboratories, NUREG/CR-4551, Vol. 1, Draft Revision 1, SAND86-1309, to be published.*

C.1.9 F.T. Harper et al., "Evaluation of Severe Accident Risks: Quantification of Major Input Parameters," Sandia National Laboratories, NUREG/CR-4551, Vol. 2, Revision 1, SAND86-1309, December 1990.

C.1.10 R.J. Breeding et al., "Evaluation of Severe Accident Risks: Surry Unit 1," Sandia National Laboratories, NUREG/CR-4551, Vol. 3, Revision 1, SAND86-1309, October 1990.

C.1.11 A.C. Payne, Jr., et al., "Evaluation of Severe Accident Risks: Peach Bottom Unit 2," Sandia National Laboratories, NUREG/CR-4551, Vol. 4, Draft Revision 1, SAND86-1309, to be published.*

C.1.12 J.J. Gregory et al., "Evaluation of Severe Accident Risks: Sequoyah Unit 1," Sandia National Laboratories, NUREG/CR-4551, Vol. 5, Revision 1, SAND86-1309, December 1990.

C.1.13 T.D. Brown et al., "Evaluation of Severe Accident Risks: Grand Gulf Unit 1," Sandia National Laboratories, NUREG/CR-4551, Vol. 6, Draft Revision 1, SAND86-1309, to be published.*

C.1.14 C.K. Park et al., "Evaluation of Severe Accident Risks: Zion Unit 1," Brookhaven National Laboratory, NUREG/CR-4551, Vol. 7, Draft Revision 1, BNL-NUREG-52029, to be published.*

*Available in the NRC Public Document Room, 2120 L Street NW., Washington, DC.

C.2 Common-Cause and Dependent Failures

Since the completion of the Reactor Safety Study over 10 years ago, more than 25 PRAs have been completed. These PRAs and other reliability analyses performed on nuclear power plant systems indicate that among the major contributors to the estimated total frequency of core damage are events that involve dependent failures.

Dependent failures are failures that defeat the redundancy or diversity in engineered plant safety systems. In the absence of dependent failures, separate trains of a redundant system, or diverse methods of providing the same safety function, may be regarded as independent. However, actual operating experience indicates that not all components of redundant systems are free from dependent failures; simultaneous failure of similar independent components occur as a result of a common cause. Such failures occur infrequently, and their interdependence can be very subtle. As a result, dependent failure data are too sparse to accurately estimate common-cause failure rates for many types of components. Also, dependent failure mechanisms are often plant specific in nature, further limiting the availability of directly usable data.

System analysts generally try to include explicit dependencies in the basic plant logic model (i.e., in the structure of the fault and event trees). Functional dependencies arising from the reliance of frontline systems on support systems, such as emergency coolant injection on service water or on electrical power, are examples of types of dependent failures that are usually modeled as an integral part of the fault and event tree structure. Interaction among various components within systems, such as common maintenance or test schedules, common control or instrumentation circuitry, and co-location within plant buildings (common operating environments), are often included as basic events on system fault trees. Even though the fault and event tree models include the major dependencies that have been identified, in some cases it is not possible to identify the specific mechanisms of common-cause failure from the available data bases (e.g., Licensee Event Reports—LERs). In other cases, where there can be many different types of common-cause failure, each with low probability, it is not practical to model each type separately. A relatively simple method is often used to account for the collective contribution of these residual common-cause failures to system or component failure rates. The method correlates the common-cause failure rate of multiple similar components to the failure rate of a single component of the same type. This method, known as the modified beta factor method (Ref. C.2.1), was applied in the system analyses for this study. Quantification of the beta factors (the common-cause failure rate correlation parameters) for important components is based on limited data and was treated as an uncertainty issue.

C.2.1 Issue Definition

The Fleming report is used as a basis for beta factors for common-cause faults involving the failure of two out of two components (Ref. C.2.2). Quantification of higher order common-cause events, such as three of three or four of four, is based on an additional set of multipliers (e.g., those developed by Atwood (Ref. C.2.3)). These multipliers are applied to the beta factors to calculate failure rates for higher order common-cause faults. For the elicitation, the higher order multipliers are not treated specifically in this issue; but because the quantifiable estimates of higher order common-cause failures are functions of Fleming-based data factors, the treatment of the beta factors in this issue will also affect the higher order factors. The uncertainties associated with this issue center on the appropriateness, robustness, and interpretation of the Fleming data. A beta factor represents that fraction of component faults that could also result in faults for similar components in the same service. It is also the conditional probability of a component failure, given that a similar component has failed. Such failures are concurrent, or approximately so, and are not due to any other component fault. Mathematically, Fleming's data are manipulated to derive beta factors defined by

$$\beta = A / (A+B),$$

where

$$A = N_{ac} + W_c N_{pc} + 1$$

$$B = N_{ai} + W_i N_{pi} + 1$$

N_{ac} = number of actual component failures due to common cause,

N_{pc} = number of potential* component failures due to common cause,

N_{ai} = number of actual independent failures,

N_{pi} = number of potential independent failures, and

W_i, W_c = weighting factors for considering potential failures as actual failures.

Not all common-cause beta factors used in the present analyses are based on the Fleming report because either a more component-specific analysis existed elsewhere or the Fleming report did not analyze data for certain components. The beta factors *not* based on Fleming's work, are:

- BWR safety relief valves (fail to reclose)
- Batteries
- Air-operated valves

The BWR SRV failure to reclose common-cause event was modeled with data from Reference C.2.2, using a nonparametric model instead of the beta factor model. BWRs have from eight to ten SRVs, so it was necessary to model the failure of various combinations of these valves. This is an exception to the assumption that was used for most other components, where the common-cause failure of k redundant components was modeled for only one failure combination, all k components. These SRV failures include all multiple SRV failures to reclose. The probabilities of these outcomes include the contribution of combinations of independent failures as well as common-cause failures. Reference C.2.4 discusses in detail the approach that was used to derive the common failure rate used in these situations for BWR SRVs failing to reclose.

The dc power study (Ref. C.2.5) was the source for the beta factor for a common-cause failure of two redundant batteries. That study suggests a worst case beta factor of 0.4 for a two-battery configuration in the minimum standard dc power system reported. Higher order beta factors were calculated with a formula based on the assumption that the conditional probability of the k_{th} (k>2) battery failing, given that "k–1" have failed, is the average of 1.0 and the beta for "k–1" of k batteries failing:

$$\beta_k = \prod_{i=2}^{k} [(2^{i-2} - 1.0 + B_2)/(2^{i-2})]$$

Air-operated valve (AOV) failures were not specifically addressed in the various references on common-cause failures. A screening value of 0.1 was chosen as a beta factor for two or even more AOVs failing from a common cause. This was the result of an expert judgment elicitation performed among the project staff (Ref. C.2.6).

C.2.2 Technical Bases for Issue Quantification

The results of the common-cause beta factor statistical analysis of the Fleming data are shown on Table C.2.1 for pumps and Table C.2.2 for valves. Using Fleming's model, 5^{th}, 50^{th}, and 95^{th} binomial confidence intervals were calculated to measure the uncertainty in the data. The Fleming model weights the potential failures by a factor of 0.1 (i.e., 10 percent of potential failures evolve into actual failures). The importance of considering potential failures in quantifying common-cause beta factors was examined in a sensitivity study that examined two extreme cases. The first (denoted β_a) case assumed all potential failures become actual component failures (W_c, W_i = 1.0); the second (denoted β_d) case assumed no contribution from potential failures (W_c, W_i = 0.0). The impact of these assumptions on the median value of the common-cause beta factor for each of several components is indicated in Tables C.2.1 and C.2.2.

*Potential failures involve components that are capable of performing their functions but exhibit a degraded performance or an incipient condition which, if not corrected, could lead to failure.

Table C.2.1 Beta factor analysis for pumps—based on Fleming data.

Pumps		Binomial Confidence Intervals 5	50	95	Data* N_{ac}	N_{pc}	N_{ai}	N_{pi}
LPCI/LPCS/RHR	β	0.10	0.15	0.25	7	4	40	27
	β_a		0.16					
	β_d		0.13					
PWR Safety Injection	β	0.15	0.21	0.26	15	4	59	18
	β_a		0.20					
	β_d		0.21					
PWR Aux. Feedwater	β	0.036	0.056	0.093	9	6	107	11
	β_a		0.079					
	β_d		0.053					
PWR Containment Spray	β	0.047	0.11	0.25	2	2	25	7
	β_a		0.14					
	β_d		0.11					
Service Water/	β	0.012	0.026	0.065	2	10	111	4
Component	β_a		0.075					
Cooling Water	β_d		0.026					

β = Beta factor

β_a = Beta factor calculated by weighting all potential failures (N_{pc}, N_{pi}) at 1.0.

β_d = Beta factor calculated by weighting all potential failures from the model.

* See text for definition of terms.

Table C.2.2 Beta factor analysis for valves—based on Fleming data.

Valves		Binomial Confidence Intervals 5	50	95	Data* N_{ac}	N_{pc}	N_{ai}	N_{pi}
Motor-Operated Valves	β	0.08	0.09	0.11	72	43	778	64
	β_a		0.12					
	β_d		0.08					
Safety Relief Valves	β	0.022	0.07	0.30	0	0	11	19
(PWR)	β_a		0.03					
	β_d		0.08					
Relief Valves	β	0.16	0.22	0.28	27	23	107	29
	β_a		0.27					
	β_d							

β = Beta factor

β_a = Beta factor calculated by weighting all potential failures (N_{pc}, N_{pi}) at 1.0.

β_d = Beta factor calculated by weighting all potential failures from the model.

* See text for definition of terms.

The β_a and β_d values are not always respectively higher and lower than the base case values. This is because the assumption to disregard or fully credit potential events also affects the denominator of the Fleming model, which includes terms for potential common-cause and independent failures.

Expert judgment was elicited from two experienced system analysts regarding the uncertainty in beta factor estimates due to potential misclassification of available data:

Alan Kolaczkowski—Science Applications International Corp., and
Arthur Payne, Jr.—Sandia National Laboratories.

Their consensus is that this uncertainty is adequately accounted for in current models. Their rationale is as follows:

1. **Inclusion of Potential Failures in Data Base**

   The β_a and β_d factors on Tables C.2.1 and C.2.2 indicate that the inclusion of potential common-cause and independent failures in the data base does not represent a significant source of model uncertainty. The most significant impact of assuming that all potential events in the data are actual failures is an increase by a factor of 2.9 (service water system pump). There is almost no impact of deleting all potential failures from the data base.

2. **Classification of Independent Failures**

   The beta factor model is highly sensitive to the number of independent failures. This number dominates the denominator of the beta factor equation. A factor of n increase in the number of independent failures would result roughly in a factor of n decrease in the beta factor. A factor of n decrease in independent failures would have the inverse effect. It seems highly unlikely that the data classification could be so erroneous that enough independent failures could have been miscategorized to create significant error in the parameter estimates.

3. **Classification of Common-Cause Failures**

   A sensitivity analysis was performed to examine the impact of reclassifying common-cause data. In this analysis, Fleming's common-cause data were assumed to have been miscategorized by a factor of two (i.e., the observed failures were assumed to be common cause in nature twice as often or, alternatively, half as often as categorized by Fleming). The resulting range of beta factor values for these cases fell well within the uncertainty ranges of the current models (Ref. C.2.6). As a result, the experts whose judgments were elicited on this issue believe it unreasonable that the data could have been misinterpreted to such an extent that current models inadequately represent this uncertainty.

Because it is unlikely that significant misclassifications of events have occurred, the experts believe that the distributions for common-cause beta factors are peaked near the median and fall off rapidly from the median. Given the lack of information and historical insensitivities of the accident sequence analysis results to the actual distribution selected, the experts believe that the lognormal distributions indicated on Table C.2.3 adequately characterize the data and modeling uncertainties for this issue.

C.2.3 Treatment in PRA and Results

The beta factors described above were used in the quantification of the system fault trees for each plant. An indication of the importance of individual common-cause and dependent failures in the fault tree analysis for these plants is the decrement by which the total core damage frequency would be reduced if these failures were not to occur. This decrement (known as the risk-reduction measure) is shown in Table C.2.4 for selected common-cause events in the Surry and Peach Bottom analyses. Note that several of the common-cause events shown in Table C.2.4 were not quantified using Fleming's data (e.g., diesel generator failures). For these events, plant-specific information was used when available. A complete listing of the risk-reduction measures is provided in References C.2.7 through C.2.11.

The collective contribution of common-cause failures to the mean total core damage frequency was investigated by performing a sensitivity study in which all beta factors were assigned a single (point

Table C.2.3 Beta factor models from EPRI NP-3967.

Pumps	Mean	Error Factor	Valves	Mean	Error Factor
Low-Pressure Coolant Injection	0.15	3	Motor Operated	0.088	3
Low-Pressure Core Spray	0.15	3	Safety Relief (PWR)	0.07	3
Residual Heat Removal	0.15	3	Relief (BWR)	0.22	3
High-Pressure Safety	0.21	3			
PWR Aux. Feedwater (Motor-driven)	0.056	3			
PWR Containment Spray	0.11	3			
Service Water/Component Cooling Water	0.026	3			

All distributions are assumed to be lognormal.

Table C.2.4 Risk-reduction measures for selected common-cause events in Surry and Peach Bottom analysis.

Common-Cause Event	Mean Event Probability	Risk-Reduction Measure*
Surry (mean total core damage frequency = 4.01E-5)		
BETA-2MOV (failure of 2 motor-operated valves)	8.80E-2	2.72E-6
BETA-3DG (failure of 3 diesel generators)	1.80E-2	2.66E-6
BETA-2DG (failure of 2 diesel generators)	3.80E-2	2.25E-6
BETA-LPI (failure of multiple motor-driven pumps, low-pressure injection)	1.50E-1	6.75E-7
Peach Bottom (mean total core damage frequency = 4.50E-6)		
BETA-5BAT (failure of 5 station batteries)	2.50E-3	1.97E-7
BETA-3AOVS (failure of 3 air-operated valves)	5.50E-2	9.75E-8
BETA-4DGNS (failure of 4 diesel generators)	1.30E-2	3.52E-8
BETA-2SIPUMPS (failure of 2 safety injection pumps)	2.10E-1	1.81E-8

*Decrement by which the total core damage frequency would be reduced if this event were not to occur.

estimate) value of zero, and the core damage frequency distribution was recalculated. The results of this analysis are summarized in Table C.2.5, which shows the extent to which the mean total core damage frequency for Surry, Sequoyah, Peach Bottom, and Grand Gulf is reduced when common-cause failures are eliminated.

Table C.2.5 Results of sensitivity study in which common-cause failures were eliminated from fault trees.

Plant	Base Case Analysis	Sensitivity Study No Common-Cause Failures	Percent Reduction
Surry	4.01E-5	3.08E-5	23
Sequoyah	5.72E-5	4.57E-5	20
Peach Bottom	4.50E-6	4.07E-6	10
Grand Gulf	4.05E-6	3.10E-6	26

REFERENCES FOR SECTION C.2

C.2.1 Pickard, Lowe and Garrick, Inc., "Procedures for Treating Common Cause Failures in Safety and Reliability Studies, Procedural Framework and Examples," NUREG/CR-4780, Vol. 1, EPRI NP-5613, January 1988.

C.2.2 K.N. Fleming et al., "Classification and Analysis of Reactor Operation Experience Involving Dependent Failures," Pickard, Lowe and Garrick, Inc., EPRI NP-3967, June 1985.

C.2.3 C.L. Atwood, "Common Cause Fault Rates for Pumps," EG&G Idaho, Inc., NUREG/CR-2098, EGG-EA-5289, February 1983.

C.2.4 D. M. Ericson, Jr., (Ed.) et al., "Analysis of Core Damage Frequency: Internal Events Methodology," Sandia National Laboratories, NUREG/CR-4550, Vol. 1, Revision 1, SAND86-2084, January 1990.

C.2.5 P. W. Baranowsky et al., "A Probabilistic Safety Analysis of DC Power Supply Requirements for Nuclear Power Plants," NUREG-0666, April 1981.

C.2.6 T.A. Wheeler et al., "Analysis of Core Damage Frequency from Internal Events: Expert Judgment Elicitation," Sandia National Laboratories, NUREG/CR-4550, Vol. 2, Part 2 of 2—"Project Staff," SAND86-2084, April 1989.

C.2.7 R.C. Bertucio and J.A. Julius, "Analysis of Core Damage Frequency: Surry Unit 1," Sandia National Laboratories, NUREG/CR-4550, Vol. 3, Revision 1, SAND86-2084, April 1990.

C.2.8 A.M. Kolaczkowski et al., "Analysis of Core Damage Frequency: Peach Bottom Unit 2," Sandia National Laboratories, NUREG/CR-4550, Vol. 4, Revision 1, SAND86-2084, August 1989.

C.2.9 R.C. Bertucio and S.R. Brown, "Analysis of Core Damage Frequency: Sequoyah Unit 1," Sandia National Laboratories, NUREG/CR-4550, Vol. 5, Revision 1, SAND86-2084, April 1990.

C.2.10 M.T. Drouin et al., "Analysis of Core Damage Frequency: Grand Gulf Unit 1," Sandia National Laboratories, NUREG/CR-4550, Vol. 6, Revision 1, SAND86-2084, September 1989.

C.2.11 M.B. Sattison and K.W. Hall, "Analysis of Core Damage Frequency: Zion Unit 1," Idaho National Engineering Laboratory, NUREG/CR-4550, Vol. 7, Revision 1, EGG-2554, May 1990.

C.3 Human Reliability Analysis

Human performance has been found to be a dominant factor in major safety-related incidents at nuclear power plants, both in the United States and elsewhere. Examples include events such as those at Three Mile Island Unit 2, Davis-Besse, and Oyster Creek in the United States and at Chernobyl in the U.S.S.R. In each of these, a complex interaction between humans and hardware led to a significant hazardous event and, in two cases, to offsite releases. Deficiencies in human performance occurred both before the initiation of the event, in areas such as maintenance, training, and planning, and in response to the event.

In the evaluation of human performance, different types of human errors have been identified. The first is generally an error where an intended action is not carried out, usually because of lapses in memory or lack of attention. Examples of these types of errors involve an operator missing a step in a procedure or accidentally selecting a wrong switch. The second type of human error is generally an action performed in accordance with a plan that is inadequate for the situation. The plan may be inadequate because there is an error in diagnosing the type of event or because the type of event has not been considered in preparing the plan and is not part of the operator's experience and training. The third type of human error is a deliberate deviation from practices thought necessary to maintain safety. These kinds of errors can be either routine (as in taking shortcuts) or exceptional (as in the case of Chernobyl).

Techniques have been developed for modeling some, but not all, of these types of human errors in PRAs. In particular, the first two kinds of error described above are analyzed in the present analysis. Other types of errors have not been addressed in this analysis, principally because no methods have been developed to provide quantitative estimates of error rates for them. Those errors considered in this study, and the methods for modeling them, are discussed below.

C.3.1 Issue Definition

Human reliability was not analyzed as a separate issue in these analyses; that is, the influence of alternative methods, models, or data were not evaluated. Rather, uncertainty distributions of the individual failure probabilities were estimated using standard human reliability methods. These failure probabilities were incorporated in the accident sequence quantifications.

In most cases, human errors were modeled as failures of people to take actions specified in procedures, including maintenance procedures, operating procedures, and emergency operating procedures. In a few cases, innovative actions were identified as ways to arrest sequences prior to the onset of core damage; failure probabilities for such actions were estimated. There were no evaluations of the consequences of mistakes, as in "if the operators mistook scenario A for scenario B, then they would ...."

The kinds of human actions represented in the analyses included human errors before the onset of an accident and errors and recovery actions following the start of an accident. The pre-accident errors are mostly failures by test and maintenance personnel to restore components to operation following maintenance (hence, rendering a system unavailable) or miscalibration of multiple sensors, such as containment pressure or reactor level sensors (hence, failing automatic initiation signals at the correct setpoint). Other pre-accident errors are failures of operators to perform tests correctly, such as failing to restore the standby liquid control system after testing, resulting in its being unavailable in the event of a demand.

Post-accident failures include failures to initiate or control emergency core cooling systems (ECCS), control rods, the standby liquid control system, etc., or their critical support systems, following their failure to start or run automatically during an accident. Examples include recovering the operability of failed diesel generators and arranging crossconnections of service water systems between units following single-unit failures. In addition, there are post-accident actions that must be performed manually during certain accidents to prevent core damage; these are not simply starting systems that failed to start automatically. Examples include the implementation of feed and bleed or the changeover from high-pressure injection to recirculation cooling following depletion of the refueling water storage tank (RWST) during loss-of-coolant accidents at some PWRs (e.g., Sequoyah).

C.3.2 Technical Bases for Issue Quantification

Quantitative estimates were made for the likelihoods of human errors using documented human reliability models. Failures in test and maintenance actions were quantified using a simplified version of the

technique for human error rate prediction (THERP) (Ref. C.3.1). The original THERP method (Ref. C.3.2) was developed and applied in the Reactor Safety Study to model human errors that can be analyzed using a task analysis (a step-by-step decomposition of an activity into simple items, such as "read meter," "turn switch," etc.). The THERP documentation provided a data base and rules of application for this approach to human reliability analysis. In the simplified approach developed for this study, bounding values were initially assigned for overall tasks, such as "restore pump," without performing a task analysis. A nominal failure probability of 3E-2 was assigned for all pre-accident failures, with adjustments made for factors such as people performing independent checks and the use of written verification sheets. Each of these factors reduced the nominal value by a factor of 10. Hence the existence of three factors would reduce the failure probability from 3E-2 to 3E-5.

The post-accident actions were categorized as to whether misdiagnosis of the plant state was considered credible. Misdiagnosis was not considered credible for manual scrams following failure of the automatic scram system, where operators are well trained and written procedures exist. Misdiagnosis was included for operators failing to recognize the condition of the plant and responding with an inappropriate strategy. These misdiagnosis errors were quantified, using a time-reliability correlation described in Reference C.3.1. A time-reliability correlation provides an estimate of failure probability based on a time available for operators to take action following the onset of an event; this is a commonly used type of technique for this type of error.

These human reliability techniques provide single best estimate values with associated ranges of uncertainties. Table C.3.1 shows representative errors and associated uncertainty ranges used in the Grand Gulf accident sequence analysis.

Table C.3.1 Representative ranges of human error uncertainties (taken from Grand Gulf analysis).

Human Error	Error Rate*	Uncertainty Range*
Common-mode miscalibration of instrument	2.5E-5	10
Failure during isolation and repair of pump	3.0E-5	16
Operator failure to initiate level control (ATWS)	1.0E-3	5

*Error rates and uncertainty ranges are expressed as the median and error factors of the distributions used in the sequence quantification.

C.3.3 Treatment in PRA and Results

In this analysis, as in most published PRAs, human errors are most commonly represented in the system fault trees (much like component failures within systems), in the event trees (representing procedural actions), and in the recovery analysis of accident sequence cut sets. Therefore, many human errors are scattered throughout the system analysis models.

A small number of operator actions are represented in event trees. These are where a single action has a direct effect on the progression of an accident, as in the case of manual depressurization of a PWR to achieve "feed and bleed." Similarly, manual reactor trips are represented in ATWS-related event trees.

It is not possible to state what range of uncertainty in the core damage frequencies and other risk measures results only from uncertainties in human reliability. However, analyses were performed to evaluate the sensitivity of core damage frequencies to human reliability values. These sensitivity studies were conducted by setting the human error probabilities for post-accident actions to zero and comparing the resulting core damage frequencies to those for the base case analyses. Requantifying the core damage frequency with these human error probabilities equal to zero led to reductions in the range of 3.5 to 6.6—a significant potential reduction. These are summarized in Table C.3.2. The highest factor, 6.6 for Grand

Gulf, resulted largely from eliminating all cut sets involving diesel failure, because zero human error implied perfect recovery of the failed diesel. The core damage frequency for Grand Gulf is dominated by station blackout, and, hence, eliminating diesel failure results in a significant reduction in core damage frequency. It must be remembered that the calculated reduction in core damage frequency includes unrealistic equipment behavior as well as unrealistic human performance as a result of simplifying assumptions in the analysis. Specifically, "perfect" human repairs would be effective for only a subset of possible equipment failure modes. Recovery of diesel operability following major equipment damage within a short time is meaningless, regardless of the quality of the human performance. (To be more realistic, the analysis would require separating recoverable failure modes from unrecoverable failure modes and associating perfect recovery only with recoverable failure modes.)

In a different sense, these calculated reductions in core damage frequency are an upper bound. During analyses such as this, recovery actions (human actions to terminate sequences prior to core damage) are identified only for sequences important to the total core damage frequency; this is done to simplify the analysis and focus the analysts' efforts on the important factors in the analysis. Setting the human error probability to zero eliminates the initially dominant sequences that already include recovery actions, but no reconsideration of recovery was evaluated for the remaining sequences that did not include recovery. It is likely that recovery actions could be postulated in some of these sequences. Adding recovery actions to these newly dominant sequences would yield further reductions in core damage frequencies.

Table C.3.2 Core damage frequencies with and without human errors.

Plant	Core Damage Frequency		Factor of Reduction
	Base Case	No Errors	
Grand Gulf	4.1E-6	6.2E-7	6.6
Peach Bottom	4.5E-6	9.5E-7	4.8
Sequoyah	5.7E-5	2.5E-5	3.5
Surry	4.0E-5	1.1E-5	3.8

REFERENCES FOR SECTION C.3

C.3.1 A.D. Swain III, "Accident Sequence Evaluation Program—Human Reliability Analysis Procedure," Sandia National Laboratories, NUREG/CR-4772, SAND86-1996, February 1987 (with errata).

C.3.2 A.D. Swain III and H.E. Guttmann, "Handbook of Human Reliability Analysis with Emphasis on Nuclear Power Plant Applications," Sandia National Laboratories, NUREG/CR-1278, Revision 1, SAND80-0200, October 1983.

C.4 Hydrogen Combustion Prior to Reactor Vessel Breach

LWR fuel assemblies and core structures contain substantial quantities of metallic materials that oxidize when heated to sufficiently high temperatures (i.e., those calculated to accompany core meltdown accidents). Oxidation of these metals, principally Zircaloy and stainless steel, can liberate sufficient quantities of hydrogen to generate substantial containment loads if released to the containment building and allowed to accumulate and subsequently burn. It is estimated (Ref. C.4.1) that approximately 270–370 kilograms of hydrogen were generated and released to the containment during the accident at Three Mile Island Unit 2 (TMI–2). Combustion of this hydrogen during the TMI–2 accident resulted in a containment pressure spike of approximately 28 psig (peak pressure). Since the design pressure of the TMI–2 containment is approximately 60 psig, this pressure rise did not pose a serious threat to containment integrity. However, the pressure spike observed during the accident at TMI–2 provided much of the motivation for subsequent changes in NRC regulations regarding containment hydrogen control (10 CFR 50.44). These changes involved hardware backfits for plants with pressure-suppression containments—BWR Mark I, II, and III and PWR ice condensers.

Hydrogen combustion is the dominant contributor to early containment failure for both Grand Gulf (BWR Mark III) and Sequoyah (PWR ice condenser). The importance of hydrogen combustion for these plants stems from the fact that both plants have relatively small free volumes, have low containment failure pressures, and incorporate pressure-suppression systems, which condense steam released from the vessel and thereby allow flammable mixtures of hydrogen and air to form. Accidents that result in early containment failure allow radionuclides that are released during the core damage process to escape to the environment. Because these accidents result in an early release, the time available for many of the emergency response actions to mitigate the accident is reduced. Because of its importance to risk, a large amount of effort was devoted to modeling and representing the uncertainty in these events.

Hydrogen can be generated during three phases of the accident: during the core damage process, at vessel breach, and late in the accident from the interaction of the core debris with concrete. The first two sources of hydrogen are generally more important to risk because they can lead to early containment failure.

During the core degradation process, the oxidation of metal with steam in the reactor produces hydrogen, which is subsequently released to the containment. During transient-type accidents in a BWR, hydrogen is released through the safety relief valve (SRV) tailpipes into the suppression pool. Similarly, during transients in a PWR, the hydrogen is released through the power-operated relief valves (PORVs) into the containment. Hydrogen can also be released directly to the containment during a loss-of-coolant accident (LOCA). If this hydrogen is allowed to accumulate, combustible mixtures can form. Although both Grand Gulf and Sequoyah have hydrogen ignition systems that are designed to burn the hydrogen at low concentrations, during station blackouts (i.e., accidents in which both onsite and offsite ac power are lost), these systems are not available. Subsequent ignition of this hydrogen by either random ignition sources or by the recovery of ac power can result in loads that can threaten the integrity of the containment. Depending on the concentration of the hydrogen at the time of ignition, both deflagrations and detonations are possible.

In the analyses performed for this study, hydrogen combustion phenomena were decomposed into smaller parts or issues. The various issues that were considered included in-vessel hydrogen production, ignition probability, detonation probability, peak pressure rise from a deflagration, dynamic load from a detonation, structural capacity of the containment to quasistatic pressurization events, and structural capacity of the containment to dynamic loads. Each of these issues in itself is very complicated and involves a substantial amount of uncertainty. Because of the large amount of uncertainty associated with these issues and because of their importance to early containment failure and risk, many of these issues were presented to panels of experts. The amount of hydrogen produced in the reactor during the core degradation process was addressed by the in-vessel accident progression expert panel. Hydrogen combustion phenomena before vessel breach and containment loads at vessel breach were addressed by the containment loadings expert panel. The structural response to these loads was provided by the containment structural performance expert panel.

The interfaces and the transfer of information between the various related issues are managed in the accident progression event tree (APET). A brief description of the relationship between these issues is

provided below. The amount of hydrogen that is produced in-vessel is obtained from distributions provided by the expert panel. This amount of hydrogen depends on the type of accident that is being analyzed and the conditions in the reactor vessel during the core damage process. A certain fraction of hydrogen produced during core damage is released to the containment. The distribution of the hydrogen in the various compartments of the containment depends on the accident. Based on the amounts of hydrogen, steam, and air that are present in the containment, the flammability of the mixture is determined. If the mixture is flammable, the likelihood that it is ignited by a random source is determined. The ignition probability in the absence of igniters was provided by the containment loadings expert panel and is a function of the concentration of steam and hydrogen in the containment. If the hydrogen concentration is high enough, it is possible for a deflagration-to-detonation transition to occur. If the hydrogen burns as a deflagration, a quasistatic pressure load results, whereas a detonation would impose a dynamic load on the containment.

The peak pressure that results from a deflagration depends on hydrogen concentration, burn completeness, effectiveness of the heat transfer to surrounding structures, and the degree to which gases are vented to other compartments within the containment. The magnitude of the dynamic load that results from a detonation is a function of hydrogen concentration, steam concentration, and the geometry of the containment compartment within which the burn occurs. Given that a hydrogen combustion event occurs, it must be determined if the load is sufficient to fail the containment. The load obtained from the combustion event is compared to structural capacity of the containment. If the load is greater than the containment failure pressure, the containment fails. Based on the pressure at which the containment fails and the magnitude of the load, the mode of failure is determined (i.e., leak or rupture). The APET accesses Fortran subroutines, which are used to track the amount of hydrogen and oxygen in the containment during the course of the accident, to determine the hydrogen concentration and the flammability of the atmosphere in the containment during various time periods, and to determine the pressure rise due to hydrogen burns.

Combustion events can also occur at the time of vessel breach or late in the accident. At the time of vessel breach, hydrogen is produced by the rapid oxidation of metal that accompanies energetic events such as ex-vessel steam explosions and direct containment heating. The ejection of hot core debris from the vessel also provides numerous ignition sources. Because of the availability of both hydrogen and ignition sources, the likelihood of hydrogen combustion is high at the time of vessel breach. However, because the pressure rise at vessel breach results from many phenomena (e.g., direct containment heating (DCH), ex-vessel steam explosions, and hydrogen combustion) and hydrogen combustion is only one component, a single distribution was used to characterize the uncertainty in the pressure rise from these events. Thus, the pressure rise at vessel breach is addressed as a separate issue. Late in the accident, the interaction of the core debris with concrete produces both hydrogen and carbon monoxide, both of which are combustible. The approach used to determine the likelihood of containment failure from late hydrogen and carbon monoxide combustion is similar to the approach used before vessel breach.

As an example, a detailed description of the hydrogen issue, hydrogen combustion prior to reactor vessel breach, is presented below.

C.4.1 Issue Definition

Because of significant differences in containment configuration and other design features, this issue was posed in a slightly different way for each plant. However, in each case, the issue was posed to answer the following two fundamental questions:

1. What distributions characterize the uncertainty in the probability that hydrogen combustion will occur in the containment building prior to vessel breach?

2. Given that combustion occurs, what distributions characterize the uncertainty in the attendant peak static pressure and the maximum impulse loading (to the drywell wall for Grand Gulf and to the ice condenser walls for Sequoyah)?

The answers to these questions may depend on the accident scenario postulated. Therefore, a case structure was established to distinguish the initial conditions associated with accident sequences found to be important contributors to a plant's estimated core damage frequency. The case structure also provides

a convenient tool for applying the generated probability distributions to the Grand Gulf and Sequoyah PRAs (as described in Section C.4.3).

Containment loads due to hydrogen combustion in Grand Gulf represent a significant challenge to containment integrity only during station blackout accident sequences, during which the igniters are inoperable. The case structure for Grand Gulf combustion loads, therefore, considers three variations of the station blackout accident sequence. These are summarized below:

Case	Steam Partial Pressure (psia)	Steam Partial Pressure (kPa)	Air Partial Pressure (psia)	Air Partial Pressure (kPa)	ac Power Recovered?	Containment Sprays Operate After Power Recovery?
1	7	5	17	115	No	No
2	7	50	17	115	Yes	Yes*
3	20	135	18	120	Yes	Yes*

Case 1 represents station blackout scenarios during which ac power is not recovered and a hydrogen burn is ignited spontaneously from a random ignition source. Cases 2 and 3 represent station blackout scenarios during which ac power is recovered prior to vessel breach; they differ from each other only in containment initial conditions.

Variations of station blackout are also the only accident scenarios in Sequoyah for which containment loads from hydrogen combustion represent a significant challenge to containment integrity. As in Grand Gulf, the ignition system is inoperable during these sequences; however, numerous "random" ignition sources are available in the Sequoyah containment. For example, sparks can be generated from movement of the intermediate deck doors in the ice condenser. The case structure for Sequoyah involves four variations of station blackout accident sequences, each of which yields different thermodynamic initial conditions. These may be summarized as follows:

Case 1: Station blackout; cycling power-operated relief valve (PORV) with the reactor pressure vessel at 2000–2500 psia.

Case 2: Station blackout; loss of pump seal cooling induces failure(s) of one or more reactor coolant pump (RCP) seals, resulting in a relatively low leak rate.

Case 3: Station blackout; loss of pump seal cooling induces failure(s) of one or more RCP seals, resulting in a relatively large leak rate.

Case 4: Station blackout; high temperatures in the reactor vessel upper plenum induce a creep rupture failure of hot leg piping of sufficient size to rapidly depressurize the reactor vessel.

For readers familiar with Reactor Safety Study (Ref. C.4.2) nomenclature for labeling accident sequences, Case 1 is the classic TMLB' accident scenario. Case 2 represents accident scenarios similar to S_3B, Case 3 represents scenarios similar to S_2B, and Case 4 represents scenarios similar to AB.

The following discussion of this issue only addresses the potential range of containment loads that may result from the combustion of hydrogen prior to reactor vessel breach for the Grand Gulf and Sequoyah plants. Containment response analyses for the other three plants addressed in the present work did consider hydrogen combustion in the evaluation of containment loads; however, the importance of early hydrogen combustion to the uncertainty in reactor risk for these plants is minor in comparison to that observed in the Grand Gulf and Sequoyah analyses. Additionally, questions regarding safety concerns that may result from hydrogen combustion in the containment, such as equipment survivability, initiation of building fires, etc., are not part of this issue.

*Sprays are assumed to initiate approximately 90 seconds after ignition.

C.4.2 Technical Bases for Issue Quantification

The principal bases for quantifying the probability of hydrogen combustion during station blackout accident scenarios and the accompanying containment loads are calculations performed with several computer codes. These include early calculations performed with the MARCH2 code (Ref. C.4.3), more recent MARCH3 analyses (Refs. C.4.4 and C.4.5), HECTR calculations of hydrogen burns in an ice condenser containment (Refs. C.4.6 and C.4.7), parametric analyses of Grand Gulf containment response to hydrogen burns using MELCOR (Ref. C.4.8), and calculations performed in support of the IDCOR program (Ref. C.4.9). These calculations are supplemented by a large body of information, available in the open literature, which discusses the strengths and weaknesses of the models employed by these codes, the experimental evidence on which many of the models are based, and the sensitivity of calculated containment loads to uncertain modeling parameters. The number of reports describing this information is too large to list here; however, a reasonably complete list is presented in References C.4.1 and C.4.10.

It is not uncommon for a relatively wide range of estimates of containment loads due to hydrogen combustion to be generated if several different analysts are asked to provide an estimate. Even for well-defined initial and boundary conditions (e.g., rate of release of a hydrogen/steam mixture to containment), the selection of different analytical tools and judgments regarding appropriate modeling parameters (e.g., flame speed, burn completeness) inevitably results in significant differences in containment loads. Although the sensitivity of estimated containment loads to many important modeling parameters has been quantified in a fairly comprehensive fashion, an analyst's judgment is still required to select the combination of parameters most appropriate to the particular problem being evaluated.

To characterize the distribution of containment loads that reflects the current state of knowledge and uncertainties in hydrogen combustion modeling, this issue was presented to a panel of experienced severe accident analysts. For each plant, three analysts were asked to provide a distribution representing the probability that various mixtures of combustible gas, air, and diluents would ignite (in the absence of an operating igniter system) and a distribution for the attendant peak static pressure and/or maximum impulse. Participating in the Grand Gulf evaluations were:

James Metcalf—Stone & Webster Engineering Corp.,
Louis Baker—Argonne National Laboratory, and
Martin Sherman—Sandia National Laboratories.

Participating in the Sequoyah evaluations were:

Patricia Worthington—U.S. Nuclear Regulatory Commission,
James Metcalf—Stone & Webster Engineering Corp., and
Martin Sherman—Sandia National Laboratories.

The following discussion summarizes the collective judgment of the panels and selected individual assessments where significant differences in judgment were observed.

Quantification of Ignition Frequency

As indicated in the issue definition, there is some uncertainty regarding how and with what frequency a combustible mixture would ignite in the Grand Gulf or Sequoyah containment if the igniter system is inoperative. There is some evidence that the propensity for combustible mixtures to spontaneously ignite (because, for example, of the discharge of accumulated static charges) increases with increasing molar concentrations of combustible gas. The likelihood of spontaneous ignition of a given combustible gas concentration also increases with time.

An additional source of ignition during loss-of-ac-power accident scenarios in Sequoyah is the generation of sparks from movement of the intermediate and deck doors of the ice condenser. These doors, illustrated in Figure C.4.1, are normally closed to isolate the ice compartment from warm regions of the containment. Under accident conditions, when steam or other reactor coolant system effluents enter the bottom of the ice condenser, the doors open upward against their own weight. During severe accidents, gas flow rates through the ice condenser are not likely to be sufficiently high to hold all the doors open, and several doors may cycle open and shut as flow fluctuates. A comparable ignition source was not identified in the Grand Gulf containment building.

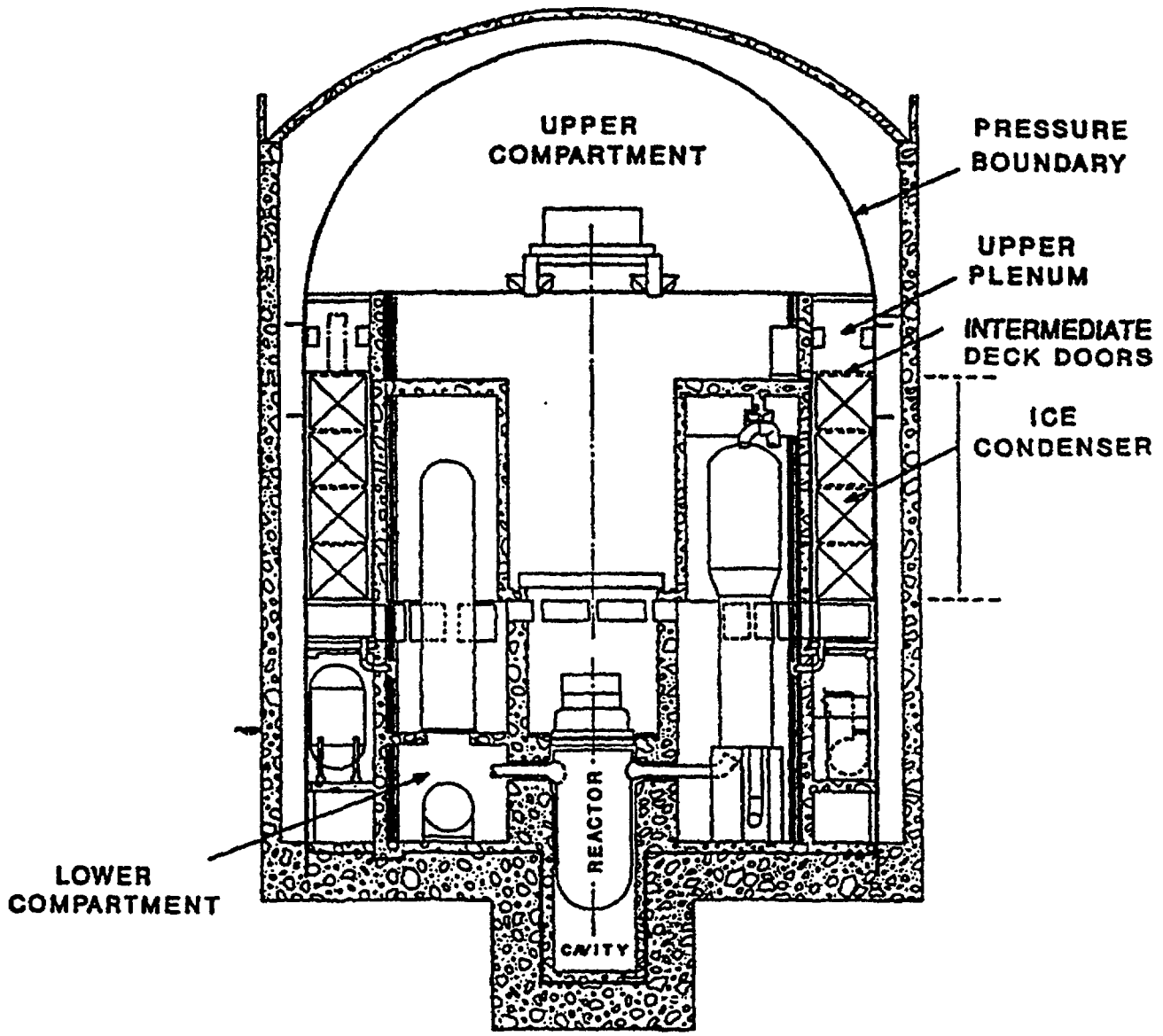

Figure C.4.1 Cross section of Sequoyah containment.

Each panelist was asked to provide a distribution that represented his or her estimate for the probability that a given concentration of combustible gas would ignite in the absence of an operating ignition system. For the Sequoyah containment, separate distributions were elicited for the ice condenser (i.e., region below the intermediate deck doors), the ice condenser upper plenum (i.e., region between the intermediate and top deck doors), and the containment upper compartment. Each of these regions is indicated in Figure C.4.1.

Distributions were elicited only for the outer containment in Grand Gulf (illustrated in Fig. C.4.2). The composition of the gas mixture in the drywell region of the Grand Gulf containment will be noncombustible (i.e., absent of sufficient oxygen or hydrogen to support combustion) prior to vessel breach, thus precluding ignition.

The panel's aggregate distribution (arithmetic average of the panelists' distributions) for Grand Gulf are shown in Figure C.4.3. The frequency of ignition in Grand Gulf is strongly dependent on the initial concentration of hydrogen. The absence of a readily identifiable ignition source in Grand Gulf results in relatively low probabilities of ignition for low hydrogen concentrations. Ignition frequency in the Sequoyah containment (shown in Fig. C.4.4) is less sensitive to initial hydrogen concentration than to the region of containment being considered. The potential for sparks from ice condenser door movement results in generally higher probabilities of ignition in the ice condenser upper plenum than in other areas.

Quantification of Containment Loads Due to Hydrogen Combustion

As indicated in the issue definition, combustion loads are characterized for each of two possible events: deflagration and detonation. Loads accompanying a deflagration are characterized by a distribution for the attendant peak static pressure. Detonation loads are characterized by the maximum impulse (to the drywell wall for Grand Gulf and to the ice condenser walls for Sequoyah). The likelihood that a particular combustion event would result in a deflagration or detonation is described by a conditional probability distribution (i.e., given the occurrence of a combustion event, what is the probability that it takes the form of a detonation?).

An aggregate distribution was generated for each permutation of cases (listed in Section C.4.1) and various ranges of plausible initial hydrogen and/or steam concentration. The ranges of initial conditions considered were:

Grand Gulf:

- Deflagration Loads: <4%(H), 4–8%(H&L), 8–12%(H&L), 12–16%(H&L), >16%(H&L)
- Conditional Probability of Detonation: 12–16%(H), 16–20%(H&L), >20%(L)
- Detonation Loads: >12%(H&L)

Sequoyah:

- Deflagration Loads: Loads calculated in containment event tree*
- Conditional Probability of Detonation: 14–16%, 16–21%, >21%
- Detonation Loads: >14%

Nomenclature: % refers to hydrogen mole fraction
H refers to a"high" steam mole fraction (40–60%)
L refers to a"low" steam mole fraction (20–30%)

Distributions for each of the case/initial-condition permutations are not presented in this report. Selected aggregate distributions are shown and discussed below to illustrate the range of values used in the PRA. The reader is encouraged to review Reference C.4.11 for complete documentation of individual panelists' judgments as well as the panel aggregate for each case.

*Formula used to estimate peak static pressure is based on information provided by expert panelists. This formula is described in Reference C.4.11.

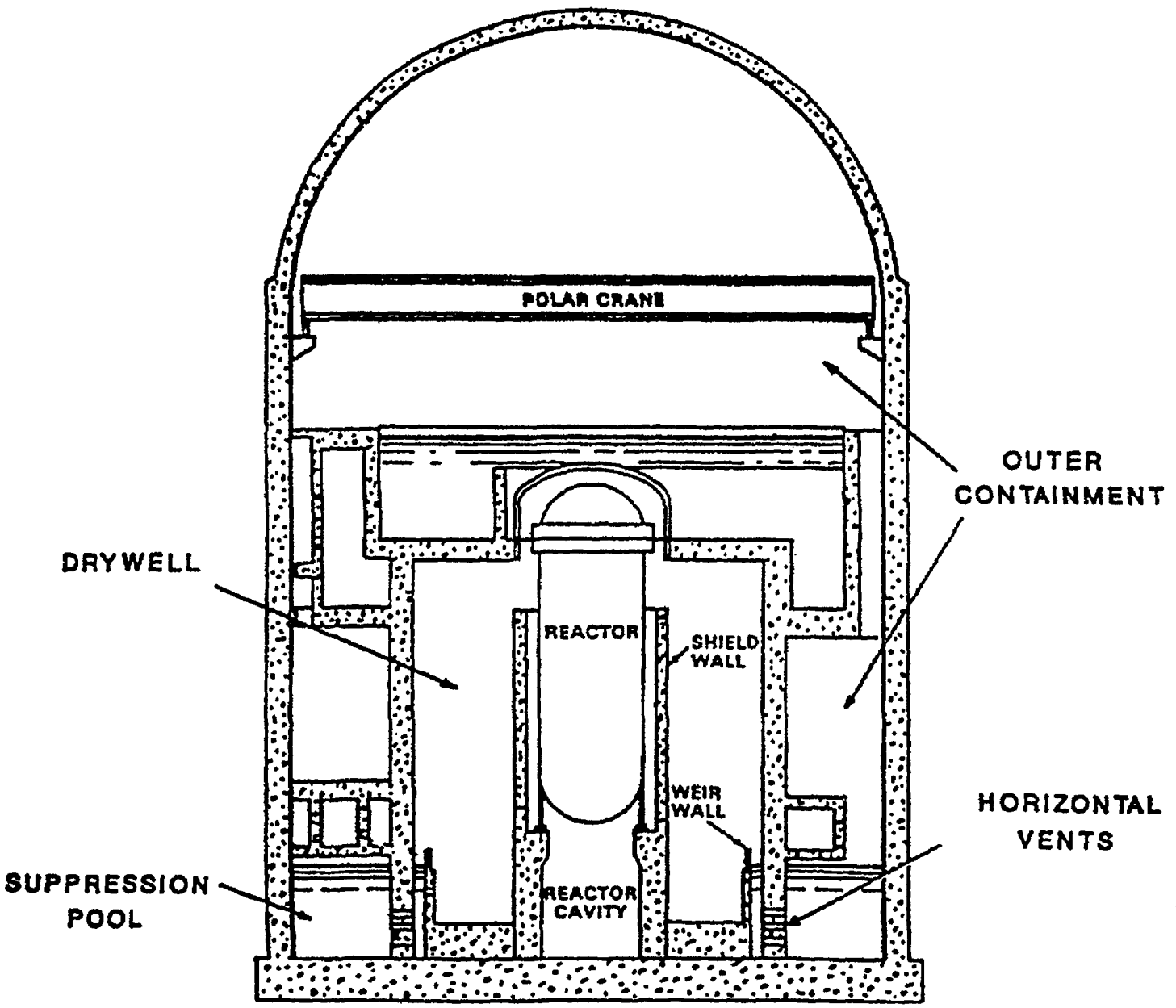

Figure C.4.2 Cross section of Grand Gulf containment.

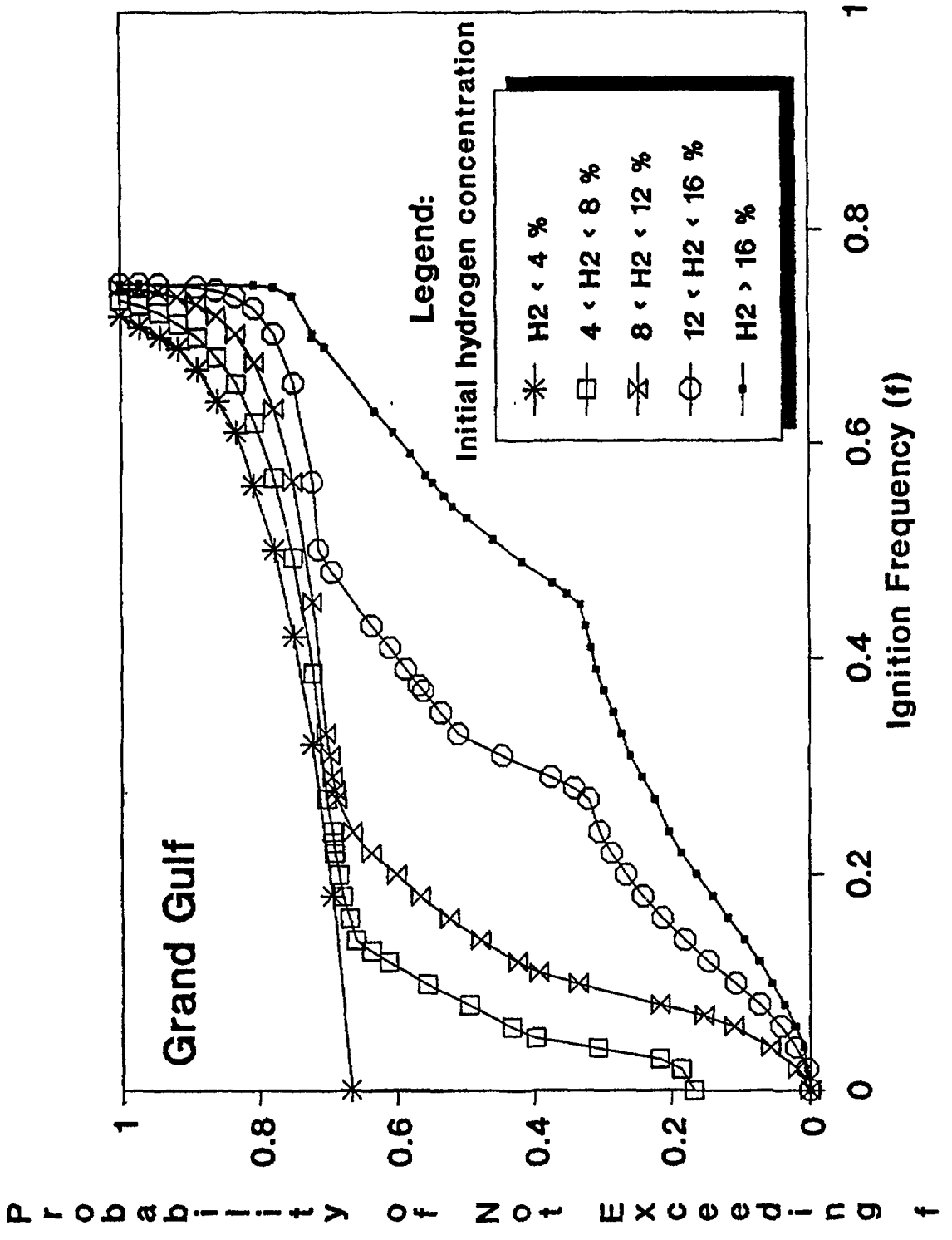

Figure C.4.3 Ignition frequency as a function of initial hydrogen concentration in the Grand Gulf containment building (outer containment-wetwell region for accident progressions in which the RPV is at high pressure).

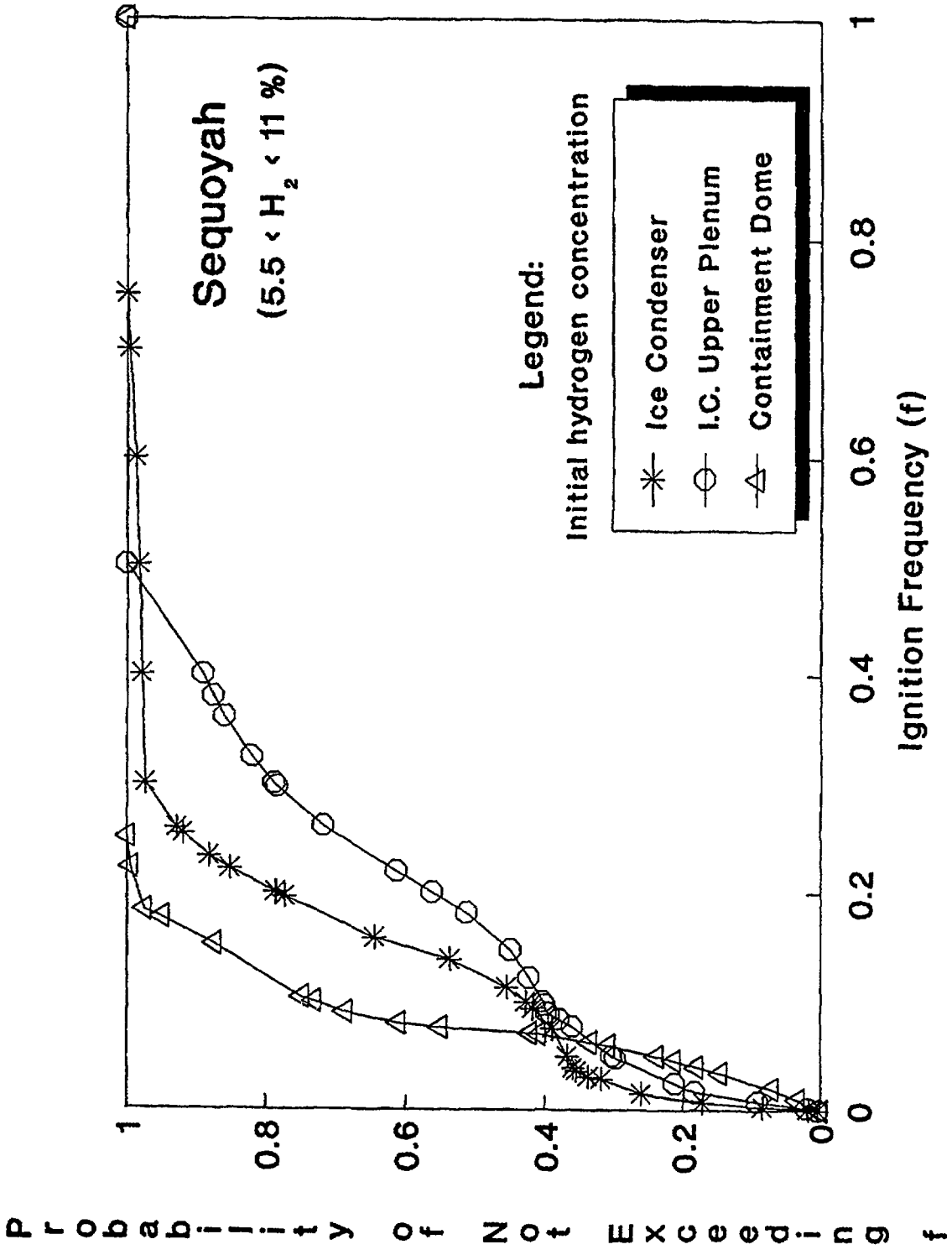

Figure C.4.4 Ignition frequency for various regions of the Sequoyah containment—illustrated for an assumed initial hydrogen concentration between 5.5 and 11 volume percent.

Selected Distributions for Grand Gulf

The range of estimated loads on the Grand Gulf containment generated by a hydrogen deflagration, initiating from various hydrogen concentrations, is shown in Figures C.4.5 and C.4.6. The former represents accident progressions in which the concentration of steam in containment at the time of ignition is relatively high, and the latter represents accident progressions with low initial steam concentrations. The distribution for the estimated strength of the containment pressure boundary and the wall separating the drywell from the outer containment is also indicated on these figures to illustrate the potential for structural failure. The likelihood of coincident failure of the containment shell and drywell wall is discussed in Section C.4.3.

Selected Distributions for Sequoyah

The range of estimated loads on the Sequoyah containment generated by a hydrogen deflagration is shown in Figures C.4.7 and C.4.8. The former illustrates the range of loads generated during fast station blackout sequences, the latter illustrates the range of loads generated during slow blackout sequences with an intermediate-size break in the reactor coolant pump seals. In both figures, distributions for containment loads are shown for cases in which the quantity of hydrogen released to the containment corresponds to that generated from the oxidation of 20, 60, and 100 percent of the core Zircaloy inventory. To illustrate the potential for these loads to cause containment failure, the distribution for the estimated strength of the containment pressure boundary is also indicated on these figures.

Quantification of Hydrogen Detonation Frequency

Detonations can occur if hydrogen is allowed to accumulate to concentrations greater than 12–14 volume percent in the presence of an ignition source and a sufficient concentration of oxygen. The current analysis indicates that the possibility of developing such conditions in either Grand Gulf or Sequoyah is low but cannot be dismissed. Figures C.4.9 and C.4.10 show aggregate distributions for the frequency of hydrogen detonations in Grand Gulf and Sequoyah, respectively (each showing the dependence on initial hydrogen concentration). The frequencies shown in these figures are conditional on hydrogen concentrations exceeding the values shown in the figure legends. The discontinuities in the distributions are a result of averaging the distributions of experts with substantially different judgments regarding detonation frequency, some of whom believe the frequency distribution to have thresholds (i.e., frequency cannot be lower than x or higher than y).

The conditions under which detonations were considered in the two plants are quite different, however. In Grand Gulf, large quantities of hydrogen may accumulate in the outer containment (as a result of substantial in-vessel metal-water reaction) and a global detonation may result. In the case of Sequoyah, a deflagration-to-detonation transition is a more likely means of creating a hydrogen detonation. The configuration of the ice condenser (a vertically oriented enclosed compartment with obstacles in the flow path) can promote flame acceleration and initiate a detonation in upper portions of the ice bed or the upper plenum.

C.4.3 Treatment in PRA and Results

The probability distributions for this issue were implemented in the Grand Gulf and Sequoyah accident progression event trees. These trees (one for each plant) provide a structured approach for evaluating the various ways in which a severe accident can progress, including important aspects of the reactor coolant system thermal-hydraulic response, core melt behavior, and containment loads and performance. The accident progression event tree for each plant is a key element in the assessment of uncertainties in risk by accommodating the possibility that a particular accident sequence may proceed along any one of several alternative pathways (i.e., alternative combinations of events in the severe accident progression). The probability distributions (or split fractions) for individual and combinations of events within the tree provide the "rules" that determine the relative likelihood of various modes of containment failure.

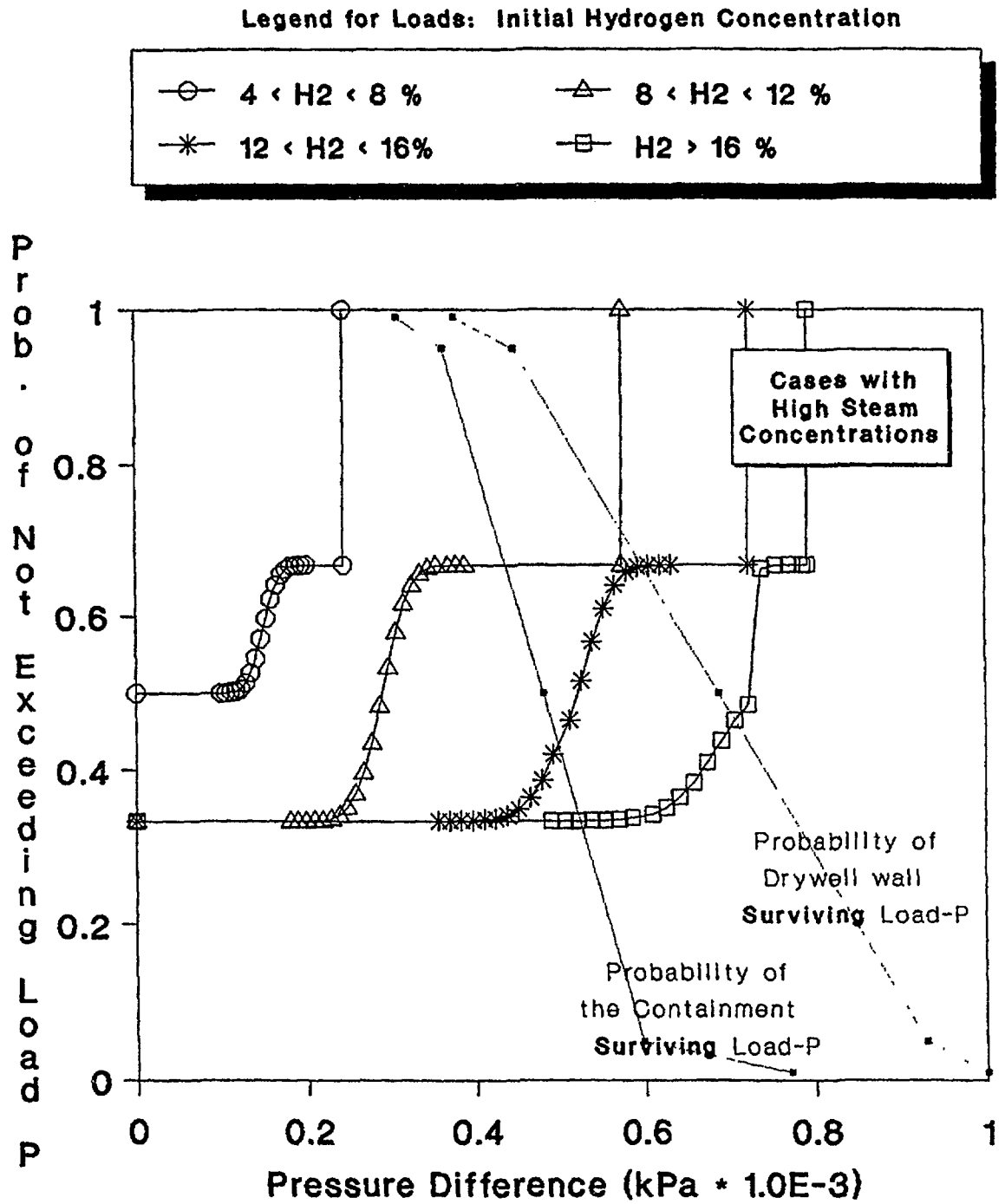

Figure C.4.5 Range of Grand Gulf containment loads in comparison with important structural pressure capacities (various initial hydrogen concentrations and *high* initial steam concentrations).

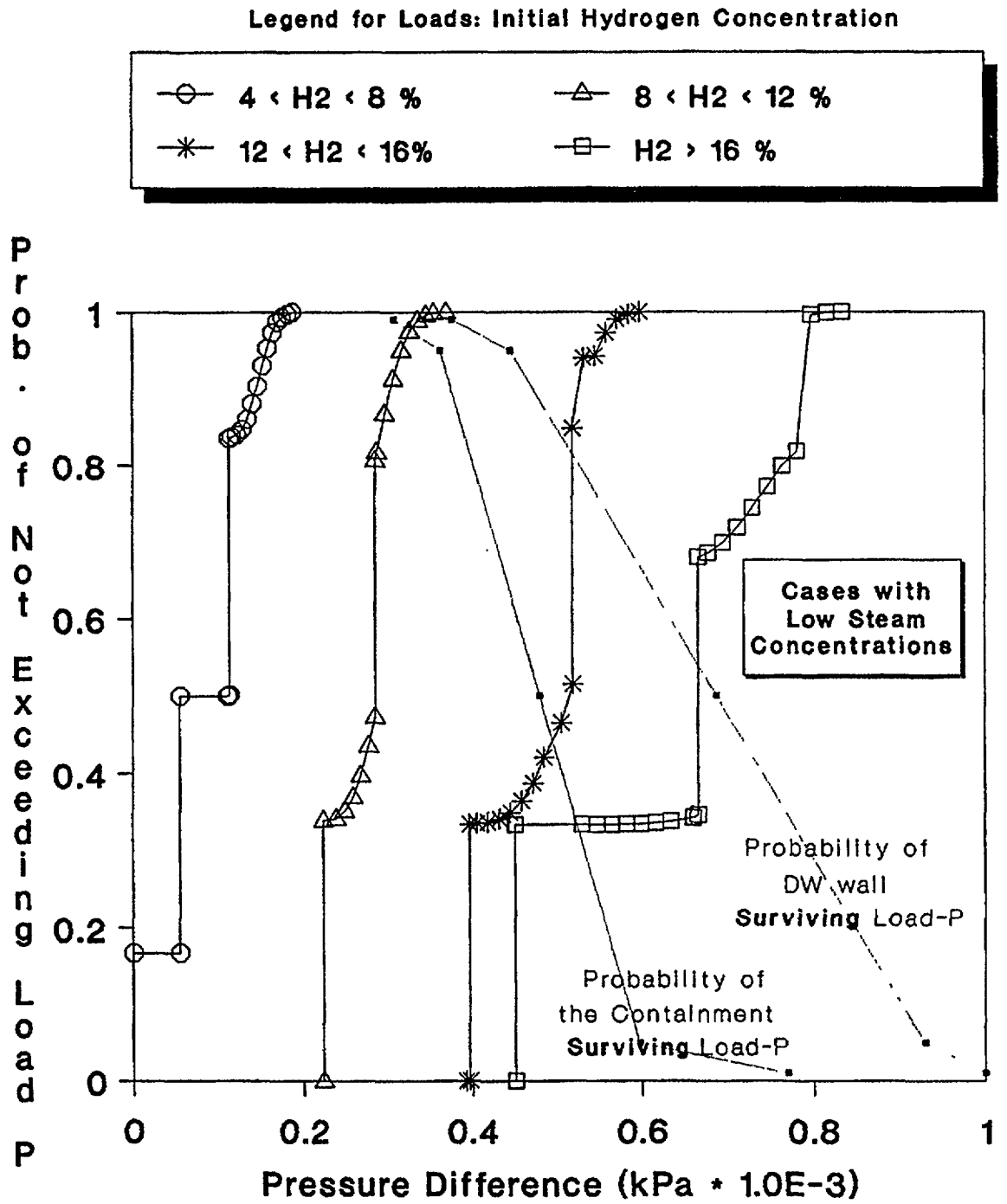

Figure C.4.6 Range of Grand Gulf containment loads in comparison with important structural pressure capacities (various initial hydrogen concentrations and *low* initial steam concentrations).

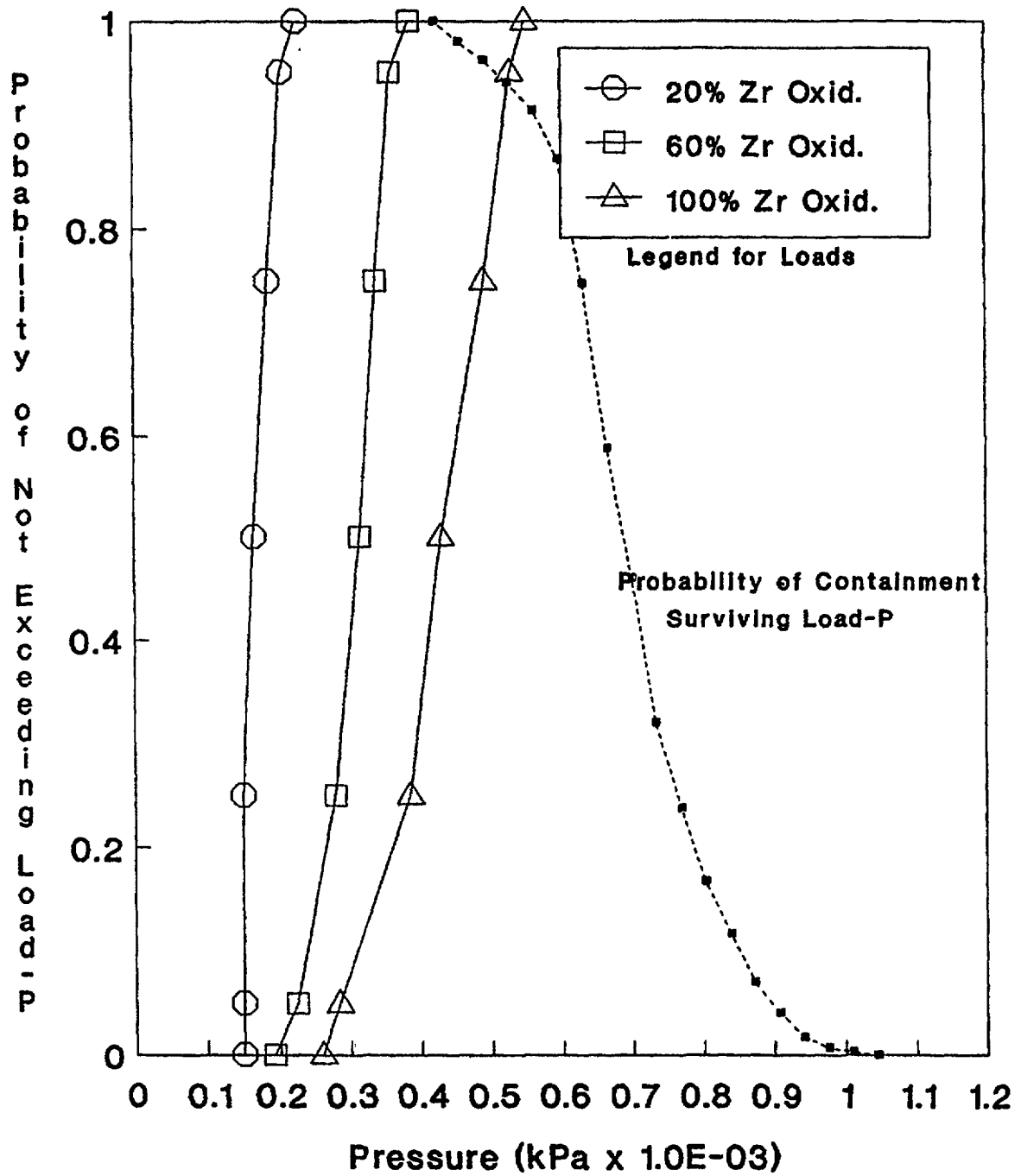

Figure C.4.7 Range of Sequoyah containment loads from hydrogen combustion in comparison with containment pressure capacity (fast station blackout scenarios with various levels of in-vessel cladding oxidation).

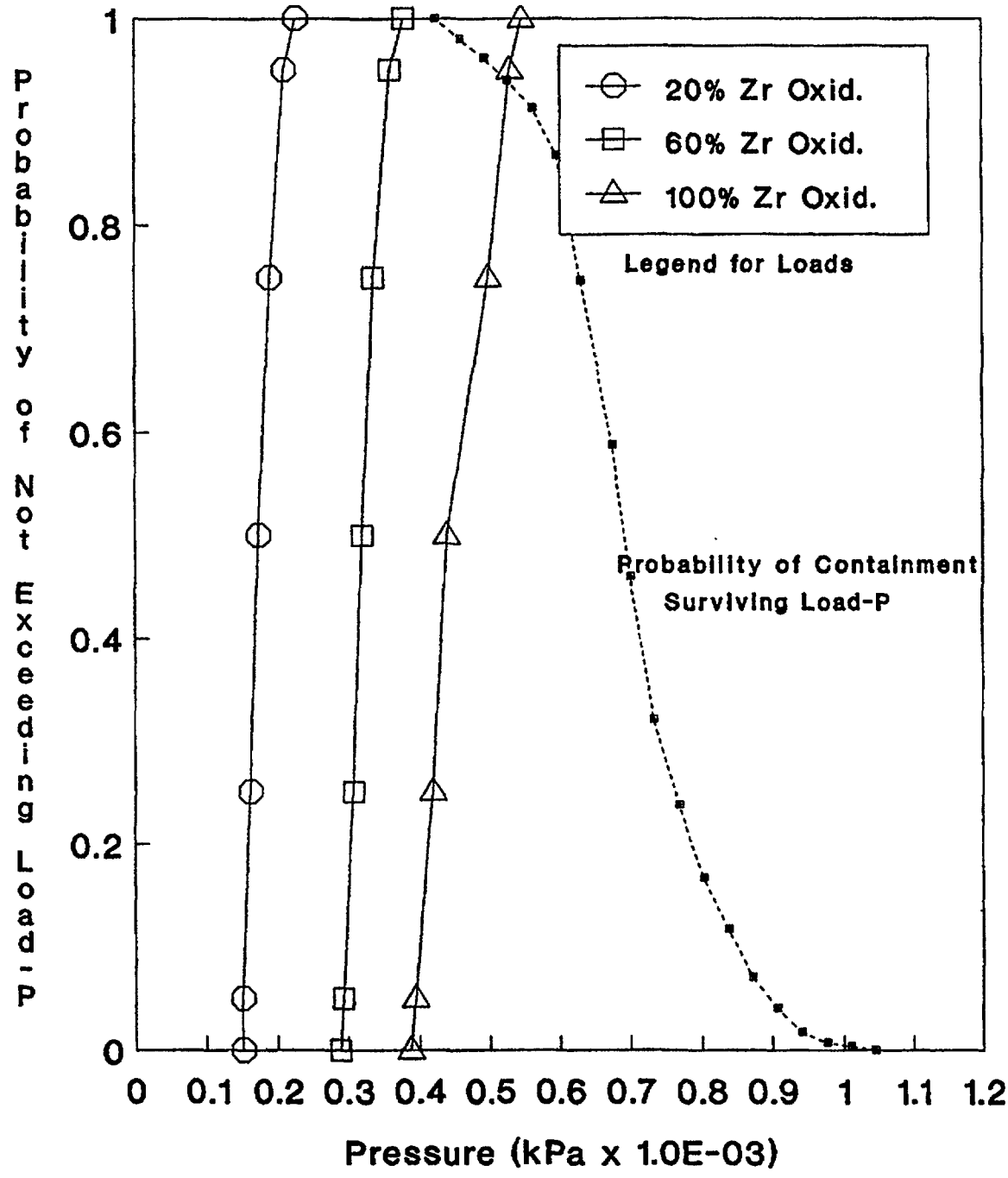

Figure C.4.8 Range of Sequoyah containment loads from hydrogen combustion in comparison with containment pressure capacity (slow station blackout accidents with induced reactor coolant pump seal LOCA and various levels of in-vessel cladding oxidation).

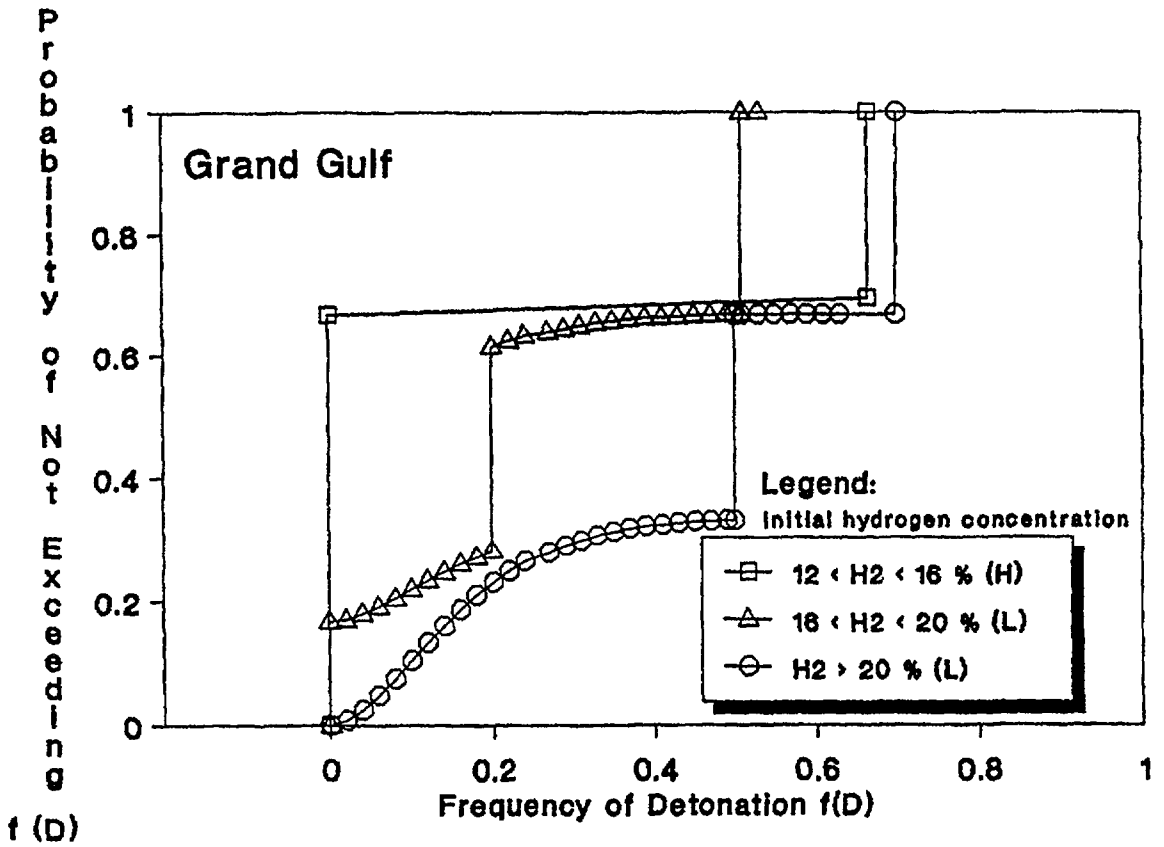

Figure C.4.9 Frequency of hydrogen detonations in Grand Gulf containment (probability of a detonation per combustion event—i.e., given ignition). H and L refer to high and low steam concentrations, respectively.

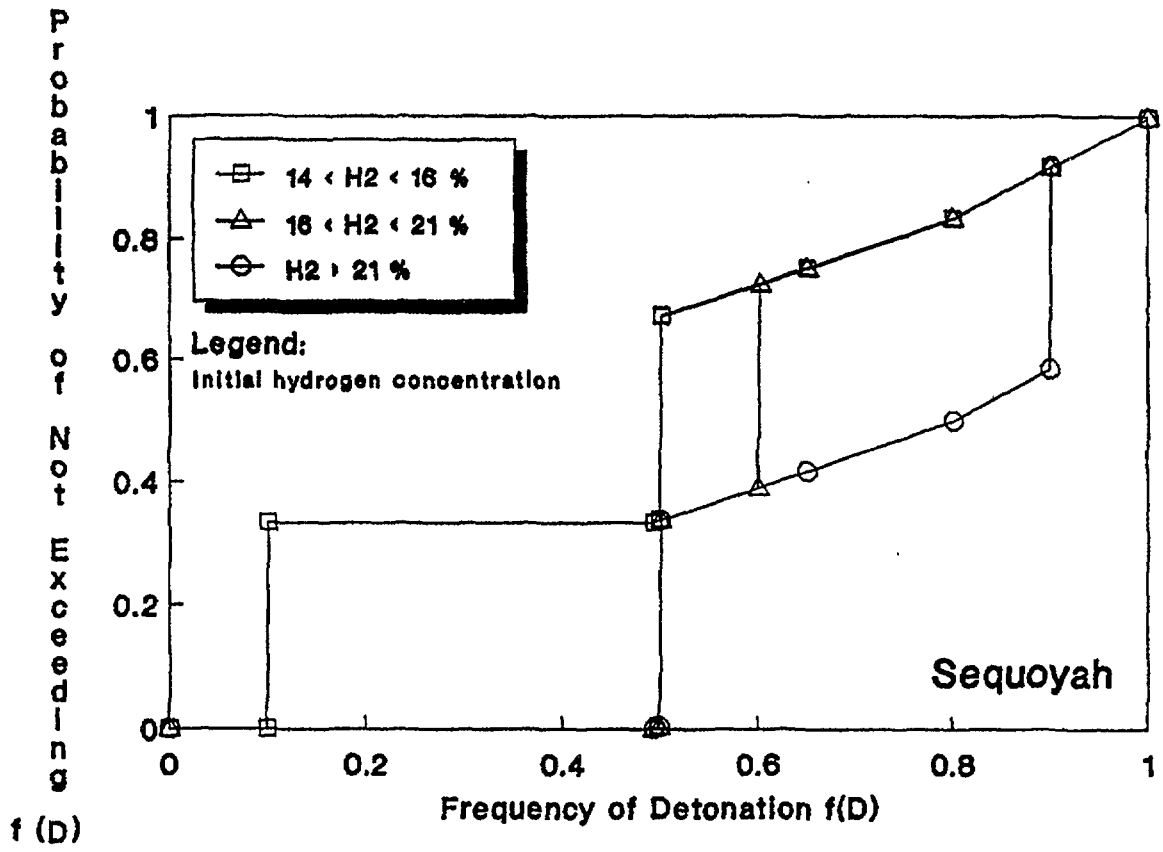

Figure C.4.10 Frequency of hydrogen detonations in Sequoyah ice condenser or upper plenum (probability of a detonation per combustion event).

As mentioned above, distributions for combustion loads were provided as input to the Grand Gulf accident progression event tree directly from the results of expert panel elicitations. An algorithm was created within the Sequoyah tree to calculate combustion loads as a function of "upstream" conditions such as the mass of hydrogen released from the reactor vessel, the distribution of the hydrogen through the containment, the compartment of the containment in which ignition took place, and other variables accounted for in the tree (e.g., burn completeness, potential for flame propagation). For each pass through the event tree in the risk uncertainty analysis, the likelihood of containment failure (and drywell failure for Grand Gulf) was determined by comparing the sampled value of the combustion loads against the sampled value of the containment pressure capacity.

Station blackout dominates the estimated core damage frequency for Grand Gulf, therefore rendering the igniters unavailable for most of the accident sequences important to risk. The attendant potential for hydrogen to accumulate and spontaneously ignite at relatively high concentrations received particular attention in this analysis. Of particular interest was the potential for hydrogen burns to induce a breach of the containment pressure boundary and result in suppression pool bypass. This combination of events could occur if a hydrogen burn were of sufficient magnitude to fail the containment shell and the drywell wall.

The outer containment (wetwell) pressure boundary is not an extremely strong structure in the BWR Mark III design (e.g., the Grand Gulf outer containment design pressure is 15 psig—103 kPa). As with all the pressure-suppression containment designs, heavy reliance is placed on the suppression pool to reduce thermodynamic loads on this structure. The structures forming the drywell, however, are much stronger (design pressure of 30 psid—207 kPa). The present analysis considers the possibility of combustion-generated loads failing either or both structures. If the containment pressure boundary is breached, but the drywell remains intact, the pressure-suppression pool is available throughout the accident to reduce the magnitude of the radioactive release to the environment. If, however, the loads accompanying a hydrogen burn (or some other event) are of sufficient magnitude to damage the drywell walls and allow for suppression pool bypass, the accompanying radioactive release can be substantial.

The contribution of hydrogen combustion to early containment loads in Grand Gulf is evident in the fraction of accident progressions with early containment failure caused by hydrogen burns. These are summarized below for each type of accident sequence that contributes greater than 1 percent of the mean total core damage frequency:

Type of Accident	Fractional Contribution to Mean Total Core Damage Frequency	Fraction Resulting in Early Containment Failure	Fraction of Early Containment Failures Caused by Hydrogen Burn or Detonation
Short-term station blackout	0.94	0.46	0.96
Long-term station blackout	0.02	0.86	0.44
ATWS	0.03	0.85	0.36
Transients	0.01	0.56	0.98

The vast majority of early containment failures for short-term station blackout (the dominant contributor to the Grand Gulf core damage frequency) is shown to be caused by loads generated by hydrogen combustion.

A substantially smaller fraction of the accident progressions in Sequoyah are estimated to result in early containment failure from hydrogen burns. The fraction results in early containment failure for the two most important types of core damage accidents in Sequoyah are summarized as follows:

Type of Accident	Fractional Contribution to Mean Total Core Damage Frequency	Fraction Resulting in Early Containment Failure from Hydrogen Burns
LOCA	0.63	0.001
Station blackout	0.25	0.05

The majority of cases in which hydrogen combustion produces a load sufficiently large to compromise containment integrity involves deflagration (quasistatic) loads, not detonations (dynamic loads).

REFERENCES FOR SECTION C.4

C.4.1 National Research Council, *Technical Aspects of Hydrogen Control and Combustion in Severe Light-Water Reactor Accidents*, National Academy Press, Washington, DC, 1987.

C.4.2 U.S. Nuclear Regulatory Commission, "Reactor Safety Study—An Assessment of Accident Risks in U.S. Commercial Nuclear Power Plants," WASH-1400 (NUREG-75/014), October 1975.

C.4.3 J.A. Gieseke et al., "Radionuclide Release Under Specific LWR Accident Conditions," Battelle Columbus Laboratories, BMI-2104, Vols. III and IV, July 1984.

C.4.4 R.S. Denning et al., "Radionuclide Release Calculations for Selected Severe Accident Scenarios," Battelle Columbus Division, NUREG/CR-4624, BMI-2139, Vols. 2 and 4, July 1986.

C.4.5 R.S. Denning et al., "Radionuclide Release Calculations for Selected Severe Accident Scenarios: Supplemental Calculations," Battelle Columbus Division, NUREG/CR-4624, Vol. 6, BMI-2139, August 1990.

C.4.6 A.L. Camp et al., "MARCH-HECTR Analysis of Selected Accidents in an Ice-Condenser Containment," Sandia National Laboratories, NUREG/CR-3912, SAND83-0501, January 1985.

C.4.7 S.E. Dingman et al., "Pressure-Temperature Response in an Ice Condenser Containment for Selected Accidents," *Proceedings of the 13th Water Reactor Safety Research Information Meeting* (Gaithersburg, MD), NUREG/CP-0072, February 1986.

C.4.8 S.E. Dingman et al., "MELCOR Analyses for Accident Progression Issues," Sandia National Laboratories, NUREG/CR-5331, SAND89-0072, to be published.*

C.4.9 Technology for Energy Corporation, "Integrated Containment Analysis," IDCOR Task 23.1, 1984.

C.4.10 A.L. Camp et al., "Light Water Reactor Hydrogen Manual," Sandia National Laboratories, NUREG/CR-2726, SAND82-1137, September 1983.

C.4.11 F.T. Harper et al., "Evaluation of Severe Accident Risks: Quantification of Major Input Parameters," Sandia National Laboratories, NUREG/CR-4551, Vol. 2, Revision 1, SAND86-1309, December 1990.

*Available in the NRC Public Document Room, 2120 L Street NW., Washington, DC.

C.5 PWR Containment Loads During High-Pressure Melt Ejection

During certain severe reactor accidents, such as those initiated by station blackout or a small-break loss-of-coolant accident (LOCA), degradation of the reactor core can take place while the reactor coolant system remains pressurized. Left unmitigated, core materials will melt and relocate to lower regions of the reactor pressure vessel. Molten material will eventually accumulate on the inner radius of the vessel bottom head and attack lower head structures. If the bottom head of the reactor vessel is breached, core debris may be ejected into the containment under pressure.* The blowdown of reactor coolant system gases atomizes ejected molten material and transports the resulting particles through the containment atmosphere. The attendant exothermic oxidation of metal constituents of the molten particles and rapid transfer of sensible heat to the containment atmosphere is referred to as "direct containment heating." The pressure rise in containment induced by high-pressure melt ejection (HPME) can be large enough to challenge containment integrity. Since containment failure immediately following reactor vessel breach can lead to a relatively large environmental release of radionuclides (and proportionally high consequences), uncertainties in the magnitude of containment loads at vessel breach are important contributors to the uncertainty in reactor risk.

A significant rise in containment pressure can be produced by HPME in PWR (large dry, subatmospheric, and ice condenser) containments and BWR (Mark I, II, and III) containments. These loads were, therefore, considered in the analyses for each of the plants examined in this study. The magnitude of the pressure rise depends strongly on details of reactor cavity (PWR)/pedestal (BWR) geometry and is, therefore, highly plant-specific. For the two BWRs examined in the present study, containment loads attributable to high-pressure melt ejection were not found to be the dominant contributor to the likelihood of early containment failure. This is a result of several factors, including the comparatively lower nominal reactor vessel pressure in BWRs, the capability of the suppression pool to attenuate, to some extent, the energy released from HPME, and (in Peach Bottom) the relatively high likelihood of other containment failure mechanisms (e.g., drywell shell meltthrough—refer to Section C.7). The discussion presented in the remainder of this section, therefore, focuses on PWR containment loads during HPME.

The containment loads associated with HPME are generated by the addition of mass and energy to the containment atmosphere from several sources:

1. Blowdown of reactor coolant system steam and hydrogen inventory into the containment.
2. Combustion of hydrogen released prior to and during HPME.
3. Interactions between molten core debris and water on the containment floor.
4. Direct containment heating.

Uncertainties in containment loads at vessel breach arise from the nonstochastic nature of some of these events (e.g., hydrogen burns), as well as a poor understanding of the phenomena governing others (e.g., direct containment heating).

In the preliminary containment response analyses (i.e., published in the February 1987 draft for comment release of this report), each of these contributors to containment loads was treated individually. An estimate of the total rise in containment pressure at vessel breach was generated by the superposition of pressure increments from each contributor. This approach was acknowledged to compromise the synergistic aspects of the phenomena involved but was analytically convenient. Among the motivations for taking this approach was the desire to isolate the uncertainties associated with direct containment heating, a controversial and highly uncertain phenomenon that can have a significant impact on the estimation of risk.

Although more experimental and analytical information regarding direct containment heating has been generated for and incorporated into the final analyses for this study, substantial uncertainties persist and

*In roughly 70+ percent of the PWR accident scenarios during which core degradation begins while the reactor pressure is at elevated pressures, an unisolatable breach in the primary system pressure boundary opens in hot leg piping, the pressurizer surge line, steam generator tubes, reactor coolant pump seals, or via a stuck-open power-operated relief valve. This break is sufficiently large to depressurize the reactor vessel prior to vessel breach. Containment loads during high-pressure melt ejection apply to the scenarios represented by the remaining 30 percent of the cases. The mechanisms for and likelihood of reactor vessel depressurization are treated as a separate uncertainty issue and are discussed in Section C.6.

the phenomenon continues to generate controversy. The motivation for isolating direct containment heating remains valid; however, the arguments in favor of treating containment response during this important stage of severe accident progression in a physically self-consistent manner prevailed. In the current analyses (presented in this document and NUREG/CR-4551 (Refs. C.5.1 through C.5.7)), containment pressure rise at vessel breach is treated as a single issue representing the combined uncertainties associated with the synergism of the four events listed above. As a result, the pressure increment attributable to an isolated phenomenon (e.g., direct containment heating) is not separable.

C.5.1 Issue Definition

This issue characterizes the uncertainties in containment loads that accompany reactor vessel breach. These uncertainties have been characterized over the entire range of possible initial reactor coolant system pressures. The largest loads (and, thus, the most significant challenges to containment integrity), however, are generated when the reactor vessel is breached while at elevated pressures. The following discussion will, therefore, focus on accident scenarios in which reactor vessel breach occurs at pressures between 500 psia (35 bar) and 2500 psia (170 bar). Further, pressure increments are characterized for three PWR containment designs—Surry Unit 1 (subatmospheric), Zion Unit 1 (large, dry), and Sequoyah Unit 1 (ice condenser). Diagrams of the Surry and Zion containments are shown in Figures C.5.1 and C.5.2, respectively. A similar diagram of the Sequoyah containment was discussed in Section C.4 (refer to Fig. C.4.1).

A rise in containment pressure may result from one or more of the four events listed earlier. The blowdown of steam and hot gases from the reactor coolant system into the containment can be calculated with reasonable precision. The pressure rise attributable to this event may be augmented by the steam production accompanying an interaction of core debris and water on the cavity floor, the generation of energy from hydrogen combustion, and energy addition from direct containment heating. Each of these potential contributors to containment loads at vessel breach is subject to physical limitations.

- Potential ex-vessel interactions between core debris and water are of concern only for accident scenarios during which water covers the reactor cavity floor prior to vessel breach. In general, this implies the successful operation of containment sprays or a LOCA or both.

- Combustion of sufficient hydrogen to generate a substantial pressure rise is subject to physical requirements regarding minimum hydrogen concentrations, oxygen availability, and maximum inerting gas concentrations. Hydrogen concentrations in containment prior to vessel breach depend upon in-vessel core melt progression (primarily the fraction of the core Zircaloy oxidized before vessel breach, which was addressed as a separate issue) and the type of accident scenario being considered.

- Direct containment heating is a term that refers to a series of physicochemical processes that have been postulated to accompany the ejection of molten core debris from a reactor vessel under high pressure. If a large fraction of the ejected molten core debris is dispersed into the containment as fine particles, a substantial portion of the debris' sensible heat can be transferred rapidly to the atmosphere. The containment pressure rise accompanying direct containment heating depends on reactor cavity geometry, the mass of material dispersed by reactor vessel blowdown, and several other parameters described later.

The resulting pressure rise can be further supplemented by the release of chemical energy associated with the oxidation of metals in the particulate melt as they are transported through the containment atmosphere. The total energy release, and thus the pressure rise, attributable to these phenomena depend on the fraction of the core (molten mass) participating in the process and the model used to represent the events that accompany reactor pressure vessel breach.

Distinct cases are established to consider separately each plausible combination of debris characteristics and containment initial conditions. The case structure accounts for uncertainties in selected severe accident events and phenomena that precede reactor vessel breach. Uncertainties associated with the containment loads generated by processes and events that occur after the core debris leaves the reactor vessel are represented by the distribution of plausible pressure increments assigned to each case. The specific parameters and range of values used to define the case structure are:

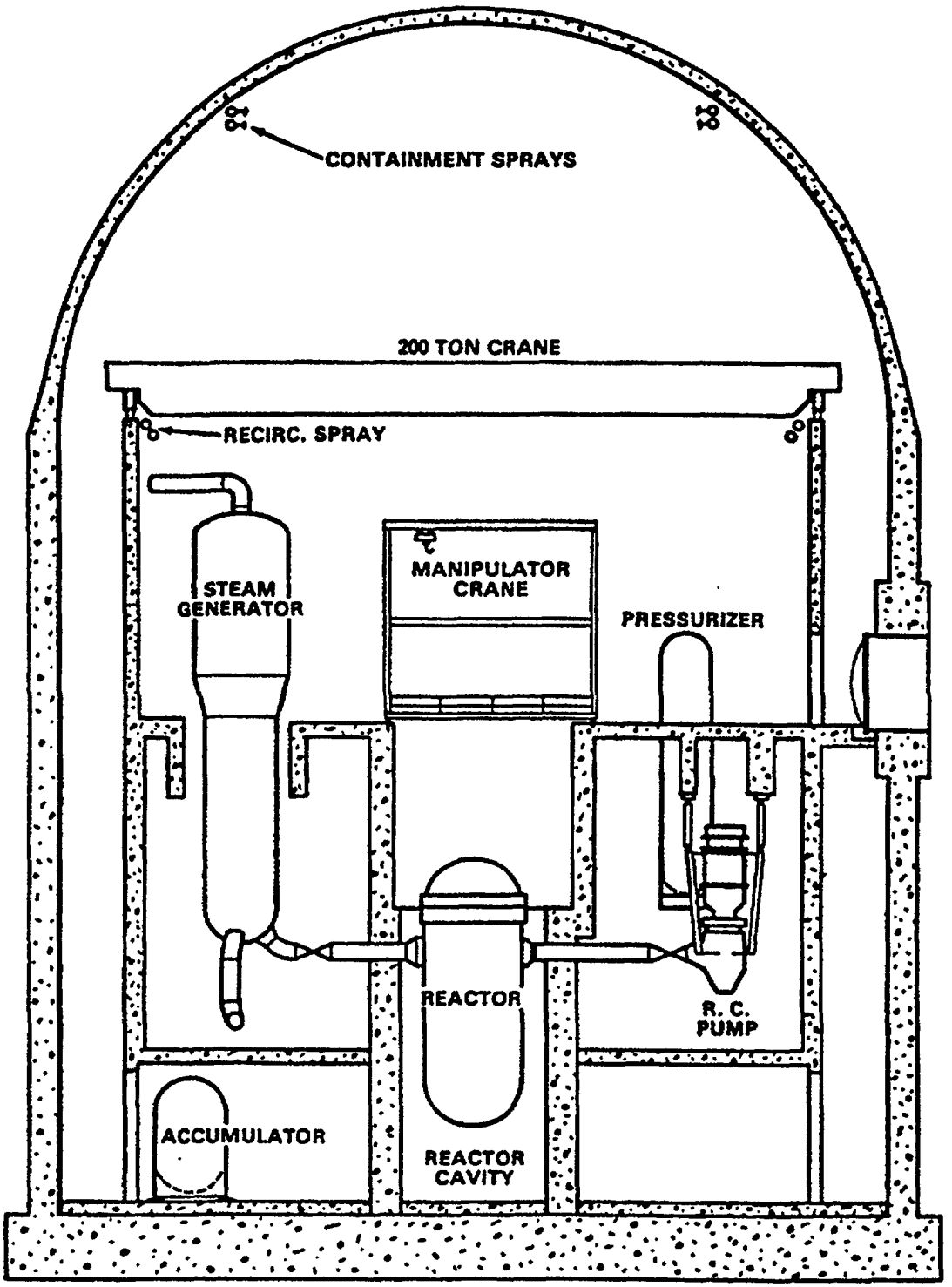

Figure C.5.1 Cross section of Surry Unit 1 containment.

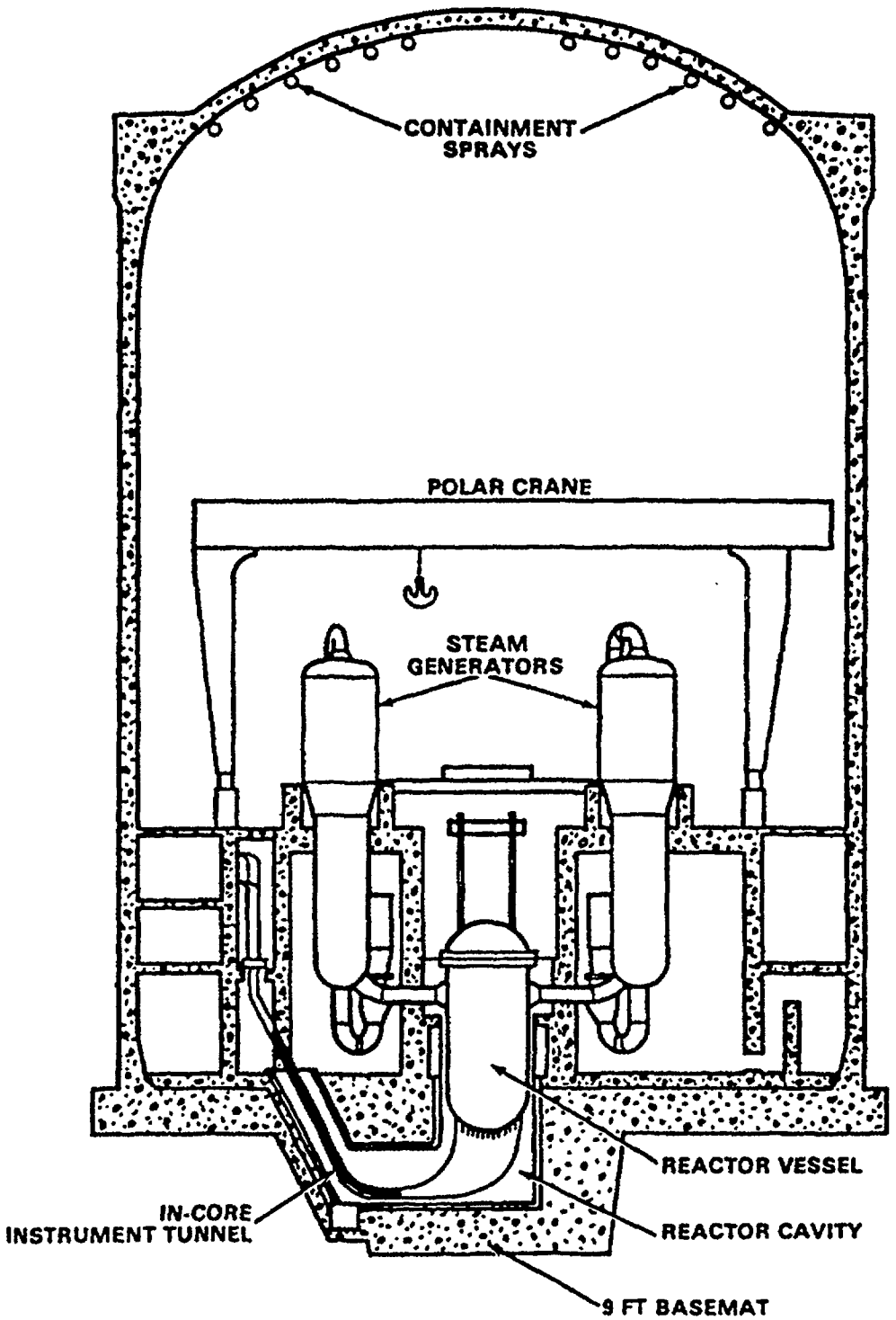

Figure C.5.2 Cross section of Zion Unit 1 containment.

Parameters Defining Case Structure	Values Considered
1. Reactor vessel pressure prior to vessel breach	**High, Medium, Low** p > 1000 psia 500 < p < 1000 psia p < 200 psia
2. Amount of unoxidized metal in melt	**High, Low** 60 percent of initial inventory 25 percent of initial inventory
3. Fraction of molten core debris ejected	**High, Medium, Low** Approx. 50 percent of total Approx. 33 percent of total Approx. 10 percent of total
4. Initial size of hole in reactor vessel lower head when breached	**Large, Small** Approx. 2.0 sq-meters Approx. 0.1 sq-meters
5. Presence (or lack) of water in reactor cavity	**Full, Half-full, Dry**
6. Containment spray operation during HPME	**Yes:** Operating **No:** Not operating

A distribution of values for the incremental rise in containment pressure was generated for each PWR containment type analyzed (large dry, subatmospheric, and ice condenser) and for each combination of parameter values in the case structure. The relative likelihood of the cases was not considered as part of this issue but is determined in the evaluation of the accident progression event tree. Section C.5.3 discusses application of the estimated pressure increments for each case in the risk uncertainty analysis.

A qualitative description of how the above parameters influence containment response follows. The technical bases (experimental evidence, calculational results, or engineering judgment) for quantifying these influences are also indicated.

Reactor Vessel Pressure

Reactor vessel pressure at the time of vessel breach characterizes the internal energy stored in reactor coolant system gases and provides the motive force for core debris dispersal. Higher initial pressures lead to larger pressure increments from reactor coolant system blowdown. Provided the initial reactor vessel pressure is sufficient to transport hot gases and reactive material (molten debris particles) to upper regions of the containment, the pressure rise attributable to direct containment heating is probably insensitive to the initial reactor vessel pressure. Attempts have been made to define a cutoff pressure (pressure below which substantial direct containment heating does not occur); however, the technical basis for a cutoff pressure is weak. In this assessment, direct containment heating is regarded as possible if the reactor vessel pressure at the time of vessel breach is greater than approximately 200 psia (14 bar). The likelihood of, and pressure rise associated with, hydrogen combustion and ex-vessel core-coolant interactions are largely insensitive to initial reactor vessel pressure.

Unoxidized Metal Content in Melt

Among the important contributors to containment loads during high-pressure melt ejection is the energy release associated with the oxidation of unreacted metals (particularly Zircaloy) in the melt. The fragmentation and dispersal of debris throughout the containment atmosphere can significantly enhance the rate of Zircaloy oxidation by exposing a large surface area of unreacted metal to the containment atmosphere. The conceptual picture of hot, unreacted metals being dispersed in air atmosphere might suggest a strong relationship between the total energy released and the mass of unoxidized metal being

dispersed. However, CONTAIN calculations (Ref. C.5.8) suggest that containment loads are relatively insensitive to the extent of in-vessel Zircaloy oxidation (mass of Zircaloy consumed in-vessel and, therefore, unavailable for oxidation during melt ejection). These calculations indicate only minor differences in containment pressurization when the unoxidized fraction of metal in the melt (dispersed at vessel breach) is increased from 50 to 70 percent of the initial inventory. It is not clear that a similar trend would be observed if the mass of dispersed metals were less than 50 percent of the initial inventory (i.e., if greater than 50 percent of the metal mass oxidized in-vessel or if a small fraction of the total mass of debris were to be ejected).

Fraction of Molten Debris Ejected

The amount of core material ejected from the vessel depends on the fraction of the core that has melted and collected at the bottom of the reactor vessel at the time of vessel breach. This is governed by the model used to represent in-vessel core melt progression (addressed in other uncertainty issues). Three nominal values were considered in this assessment (0.50, 0.33, and 0.10) to represent large (greater than 40 percent), medium (between 20 and 40 percent), and small (less than 20 percent) fractions of core melted and available for ejection, respectively. The results of parametric studies performed with the CONTAIN computer code (Ref. C.5.8) indicate that the containment pressure increment at vessel breach increases substantially with increasing fraction of melt ejected. Illustrative results of these calculations are shown in Figure C.5.3, which presents the predicted peak pressure for variations of a station blackout accident scenario in which progressively greater fractions of the initial core mass were assumed to be ejected. In these calculations, all the melt ejected is assumed to participate in direct containment heating. Results of scaled high-pressure melt ejection experiments in the Surtsey facility (Refs. C.5.9 through C.5.13) indicate that not all ejected debris may participate, however.

Initial Size of Hole in Vessel When Breached

Alternative conceptual models for in-vessel core melt progression suggest quite different modes of reactor vessel breach. One model assumes that a localized thermal attack of the vessel lower head results in the failure of one or more lower head penetrations. Such a model suggests an initial hole size in the neighborhood of 0.1 m^2. Much larger hole sizes are conceivable, however, particularly if the reactor vessel lower head fails by creep rupture or when the hole is ablated. The primary parameter affected by the initial hole size is the rate at which vessel blowdown occurs (larger initial hole size implying more rapid blowdown and melt ejection). The CONTAIN parametric studies referenced above also examined this sensitivity by varying the length of time required to blow down the reactor vessel. Substantially larger pressure rises were predicted when the blowdown period was shortened from 30 seconds to 10 seconds.

Presence of Water in Reactor Cavity

At least two scenarios are conceivable when water interrupts the pathway for debris dispersal following reactor vessel breach (as it would if the reactor cavity were filled with water). One scenario is that one or more steam explosions will occur after only a fraction of the debris has been injected into the cavity and that the cavity water will then be dispersed ahead of the bulk of the injected debris. Another possibility is that the relatively cold water will be co-dispersed with the debris, exiting the cavity region as small droplets intermixed with the transported debris, steam, and hydrogen. Experiments with water-filled cavities (Ref. C.5.13) have been inconclusive, in part because of the tendency of the experimental facilities to be destroyed by the debris-water interactions. Reality may involve some combination of these two scenarios.

The scenario resulting in co-dispersed water has received considerable attention. Of principal interest is the nature of the interaction between the debris particles and water droplets. The water may continue to quench the debris, mitigating the effects of direct containment heating. However, the fate of the steam generated by this quenching is uncertain. It could simply increase the partial pressure of steam in the containment, thereby producing a moderate addition to containment loads, or it might act as a source of oxygen for unquenched debris and substantially enhance the oxidation of metallic particles. This tradeoff was investigated in some detail in the CONTAIN sensitivity studies referenced above. The effects of co-dispersed water were shown to be quite sensitive to the timing and location of water addition, assumptions regarding droplet-debris reaction kinetics, and the amount of water involved.

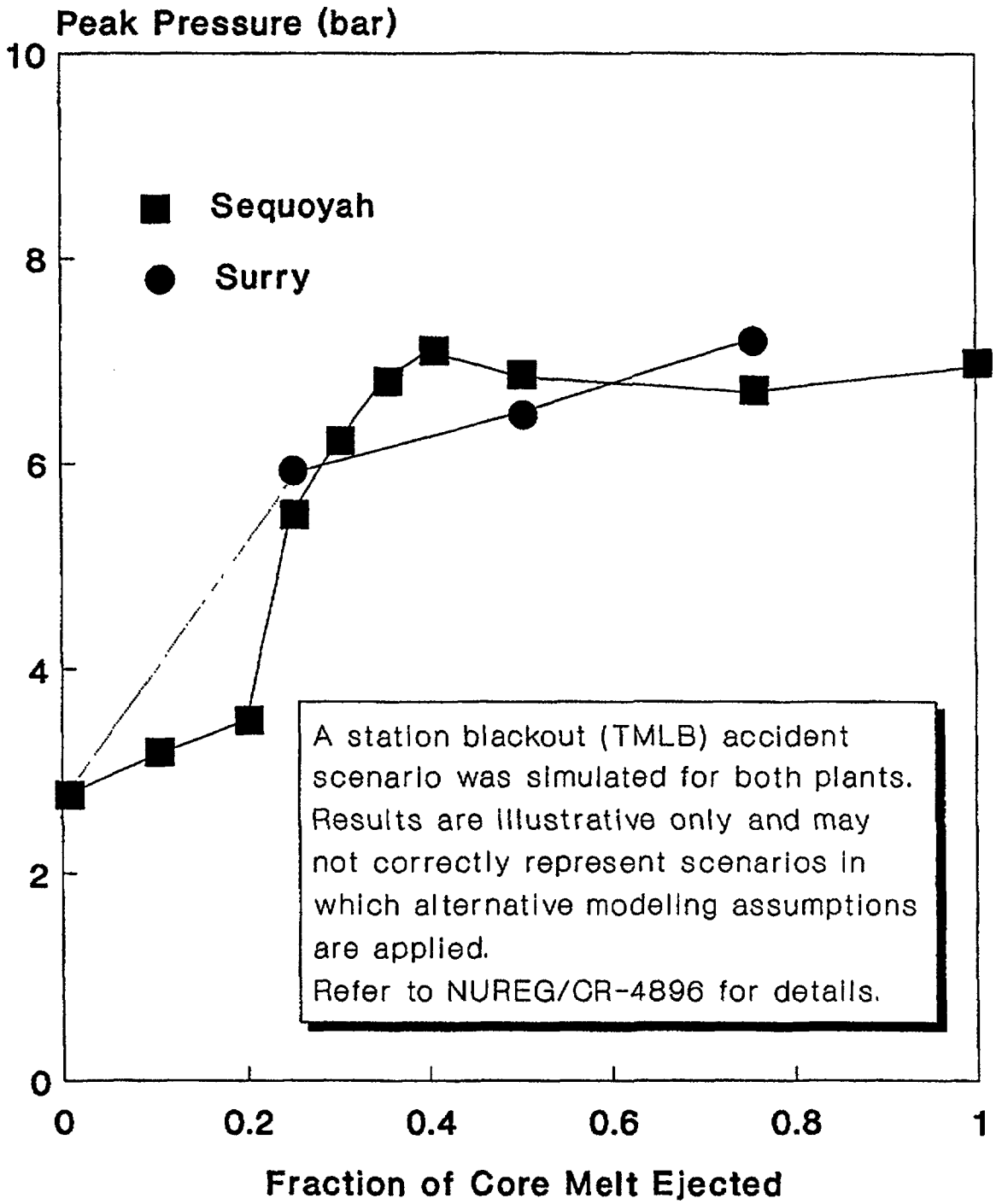

Figure C.5.3 Calculated containment peak pressure as a function of molten mass ejected (Ref. C.5.8).

Containment Sprays and Ice Condenser

The effect of containment sprays on containment loads from reactor vessel blowdown has been relatively well characterized by numerous containment response computer code calculations. In Surry, for example, it has been estimated (Ref. C.5.2) that the operation of containment sprays reduces the pressure rise at vessel breach by approximately 30 to 45 psi (2 to 3 bar). The impact of sprays on dispersed core debris is not well understood and was not explicitly examined in the CONTAIN sensitivity analyses (Ref. C.5.8). For some plants, however, early spray operation may ensure a substantial inventory of water in the reactor cavity. The uncertainties in estimating the effect of this water were described above.

The presence of the ice condenser in the Sequoyah containment introduces significant uncertainties in estimating HPME loads for this plant. There are no experimental data regarding ice condenser performance under conditions representative of those accompanying HPME. In the present study, quantitative assessments of core debris capture and pressure suppression during HPME is largely based on the subjective judgment of experienced containment response analysts. Topics of particular concern include the potential for "channeling" (the preferential melting of a vertical column of ice, creating an early ice bypass pathway) and hydrogen detonations. The possibility of a rapid release of large quantities of hydrogen following reactor vessel breach, accompanied by effective steam condensation as the steam/hydrogen mixture passes through the ice beds, can generate conditions that favor hydrogen detonations in the upper regions of the ice condenser. The dynamic loads generated from such events are not explicitly included in this issue. The reader is referred to Section C.4 for more details on the treatment of hydrogen combustion phenomena in this containment design.

C.5.2 Technical Bases for Issue Quantification

This issue was presented to a panel of experienced severe accident analysts. Six panelists addressed containment loads for the three PWR plants:*

Louis Baker—Argonne National Laboratory,
Kenneth Bergeron—Sandia National Laboratories,
Theodore Ginsberg—Brookhaven National Laboratory,
James Metcalf—Stone & Webster Engineering Corp.,
Martin Plys—Fauske & Associates, Inc., and
Alfred Torri—Pickard, Lowe & Garrick, Inc.

Each panelist provided a distribution of values for containment pressure rise following reactor vessel breach for each of the cases outlined in Section C.5.1. These distributions characterize the panelist's judgment for the range of plausible containment loads for each case and the relative confidence (i.e., degree of belief) that particular values within that range are the "correct" ones for the conditions specified by the issue case structure. Panelists based their judgments on the current body of experimental evidence and analytical information, a sample of which was summarized above.

A summary of the expert panel's judgments is provided below. In most instances, aggregate distributions (arithmetic average among the panelists for a particular case) are presented to illustrate observable trends between cases. Examples of individual panelists' distributions are also shown to illustrate the variance of opinion within the panel. Complete documentation of the elicitation of expert judgment from these analysts is provided in Reference C.5.2.

An estimate of containment loads has little meaning if isolated from a corresponding estimate of static pressure capacity. Therefore, for each plant, the appropriate distribution for its static failure pressure (discussed in detail in Section C.8) is shown on each plot of containment loads. An example display of containment loads versus a reference static failure pressure is shown in Figure C.5.4. The curve for containment loads (base pressure plus the pressure increment accompanying reactor vessel breach) is shown as a cumulative distribution function (CDF). The static failure pressure is shown as a complementary cumulative distribution function (CCDF). The reason for this display format is to allow the reader to perform the following visual exercise:

*A minimum of three panelists addressed each plant. In general, each panelist was responsible for addressing the uncertainties in containment loads for two of the three PWR plants (Surry, Zion, or Sequoyah). If any analyst wished to provide a judgment for more than two, he was free to do so.

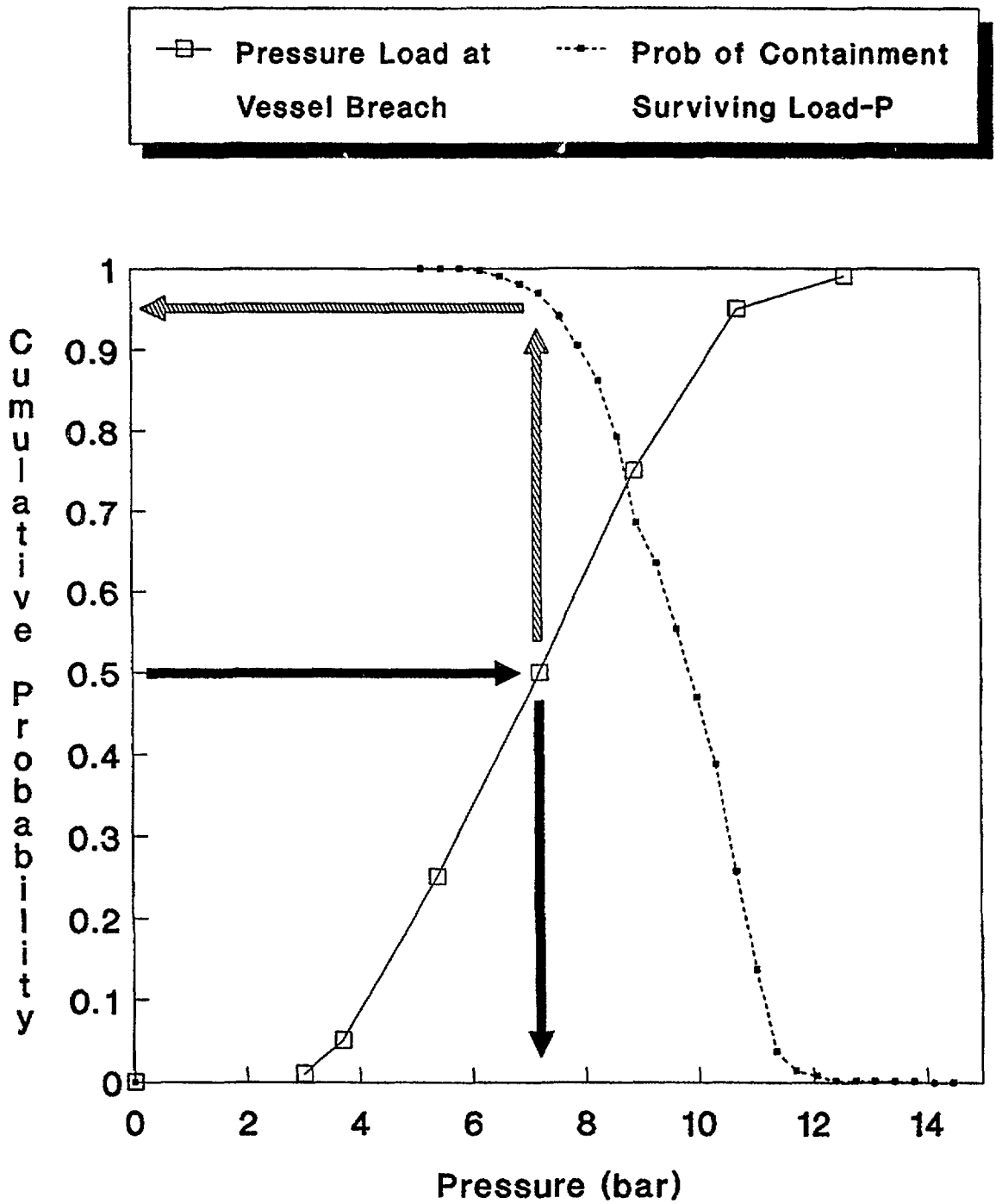

Figure C.5.4 Example display of distributions for containment loads at vessel breach versus static failure pressure.

Select a value (0.5 in the example—the median of the distribution) for the probability that the containment load at vessel breach is equal to or below some level. Read (horizontally) along the selected probability value, and determine the corresponding containment load (approximately 7 bar in the example). This means that the probability that the containment load at vessel breach is 7 bar or less is approximately 0.5. Next, read vertically upward to determine the point on the static failure pressure curve that intersects the same value of pressure, then left, back to the ordinate. This final value of probability (0.95 in the example) is the probability that the containment will survive the imposed load (7 bar in the example).

This format for displaying the containment performance information allows the reader to examine the relative likelihood of the containment surviving a particular load and the corresponding likelihood of that load being produced. In performing this exercise, it must be remembered that the distributions displayed in this manner apply only to the initial and boundary conditions specified by the case structure.

Containment Load Distributions for Surry

An important parameter in characterizing containment loads for high-pressure accident scenarios in Surry is the operation of containment sprays (or more specifically, the presence of water in the reactor cavity). Figures C.5.5 and C.5.6 show the estimated containment loads for HPME cases with sprays operating and not operating, respectively, for vessel failure with the reactor coolant system at high pressure. In each figure, the four curves for containment loads represent the aggregate (arithmetic average) distribution for the expert panel for each of four cases (identified in the legend). The variables that change among these cases are the initial size of the hole in the reactor vessel lower head at vessel breach and the fraction of molten debris ejected. (Each may take on high or low values as indicated in Section C.5.1. Curves are not given for cases with a "medium" fraction of the core ejected.) The largest loads are generated when both parameters take on high values (with or without sprays operating). Significantly lower loads are likely for cases in which containment sprays operate.

The likelihood that the Surry containment would survive the median (50th percentile) loads is greater than approximately 90 percent for all cases in which the sprays operate or provided a small fraction of the core debris is ejected (with or without sprays). It should be noted that accident sequences for which containment sprays are assumed to operate generally result in a cavity at least partially filled with water. The distributions shown in Figure C.5.5, therefore, assume a full cavity; those in Figure C.5.6, likewise, assume a dry cavity.

For Surry, the variance in the estimated containment loads among panelists is comparable to the variance among cases. Figure C.5.7 shows the distributions generated by each panelist for the four cases shown in Figure C.5.5. The range of median values for pressure rise among the panelists spans 30 to 60 psi (2 to 4 bar). This range increases to 120 psi (8 bar) at the distributions' upper bound. This trend is typical of virtually all the Surry cases.

Containment Load Distributions for Zion

Example distributions of containment loads at vessel breach in the Zion Unit 1 containment are shown in Figures C.5.8 and C.5.9 (with and without containment sprays operating, respectively). The boundary conditions represented by the cases illustrated in these figures are the same as those shown in Figures C.5.5 and C.5.6 for Surry. The Zion containment is shown to be able to withstand high-pressure melt ejection loads (even at the upper end of the uncertainty range) with very high confidence.

The variance in the estimated containment loads (among panelists) for Zion is also very similar to that for Surry. The variance indicated in the individual distributions displayed in Figure C.5.7 (for Surry) is representative of that observed for Zion. Individual panelists' distributions for Zion are, therefore, not displayed in this document; the reader is encouraged to review Reference C.5.2 for this information.

Containment Load Distributions for Sequoyah

The case structure for this plant includes an additional variable to account for uncertainties related to ice condenser performance (namely, the fraction of ice remaining at vessel breach). Distributions for Sequoyah containment loads for the cases similar to those displayed previously for Surry and Zion are

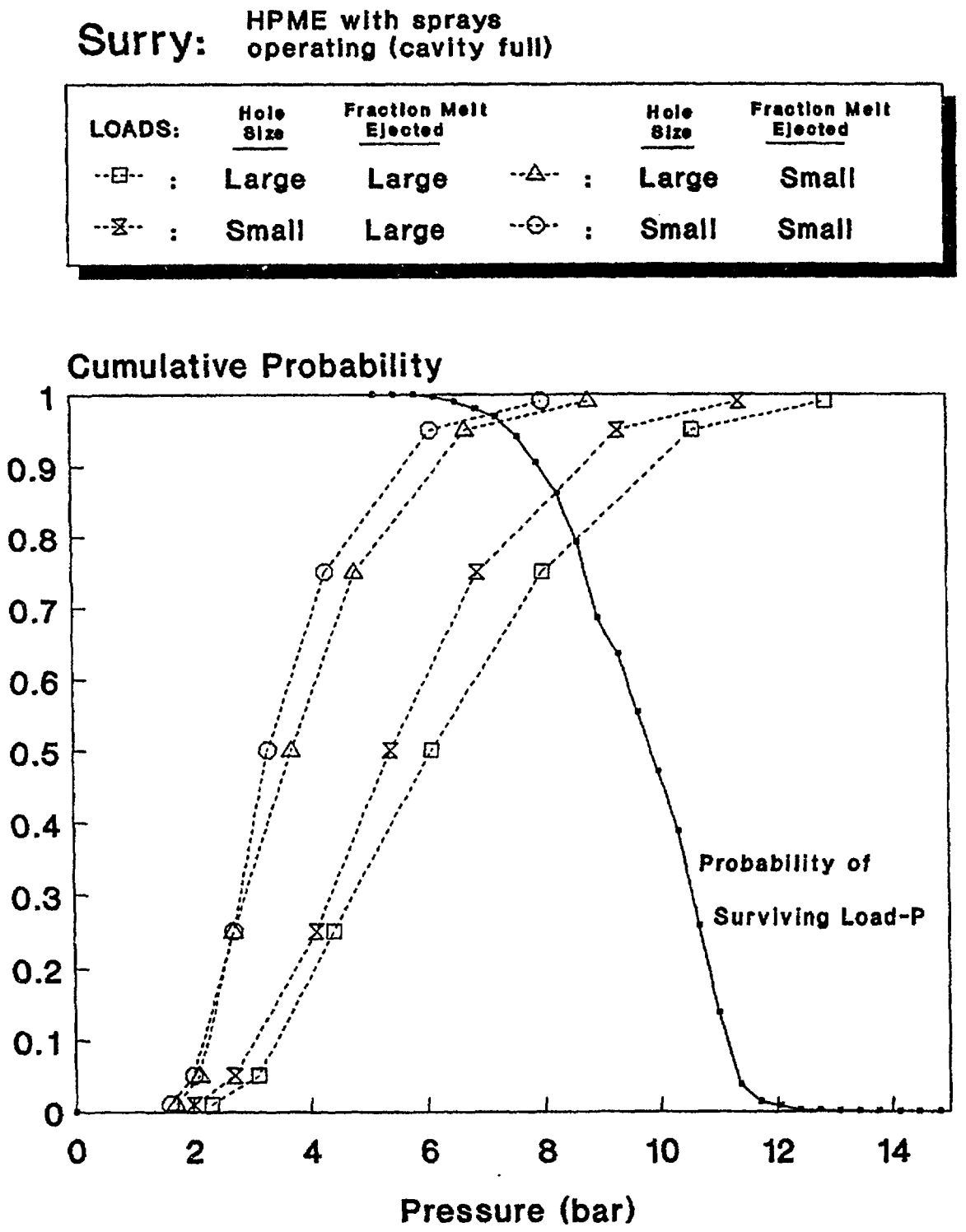

Figure C.5.5 Surry containment loads at vessel breach; cases involving vessel breach at high pressure with containment sprays operating (wet cavity).

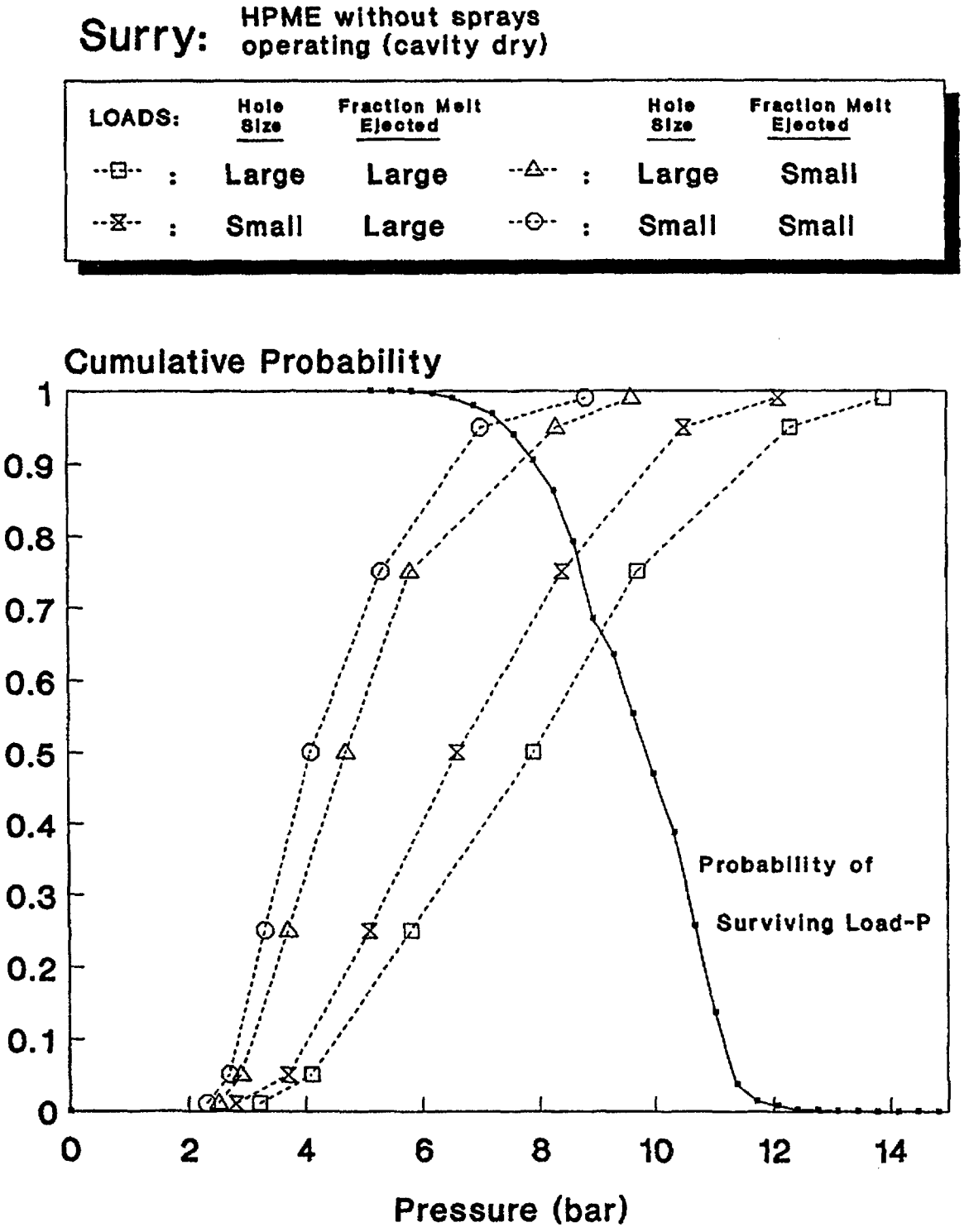

Figure C.5.6 Surry containment loads at vessel breach; cases involving vessel breach at high pressure without containment sprays operating (dry cavity).

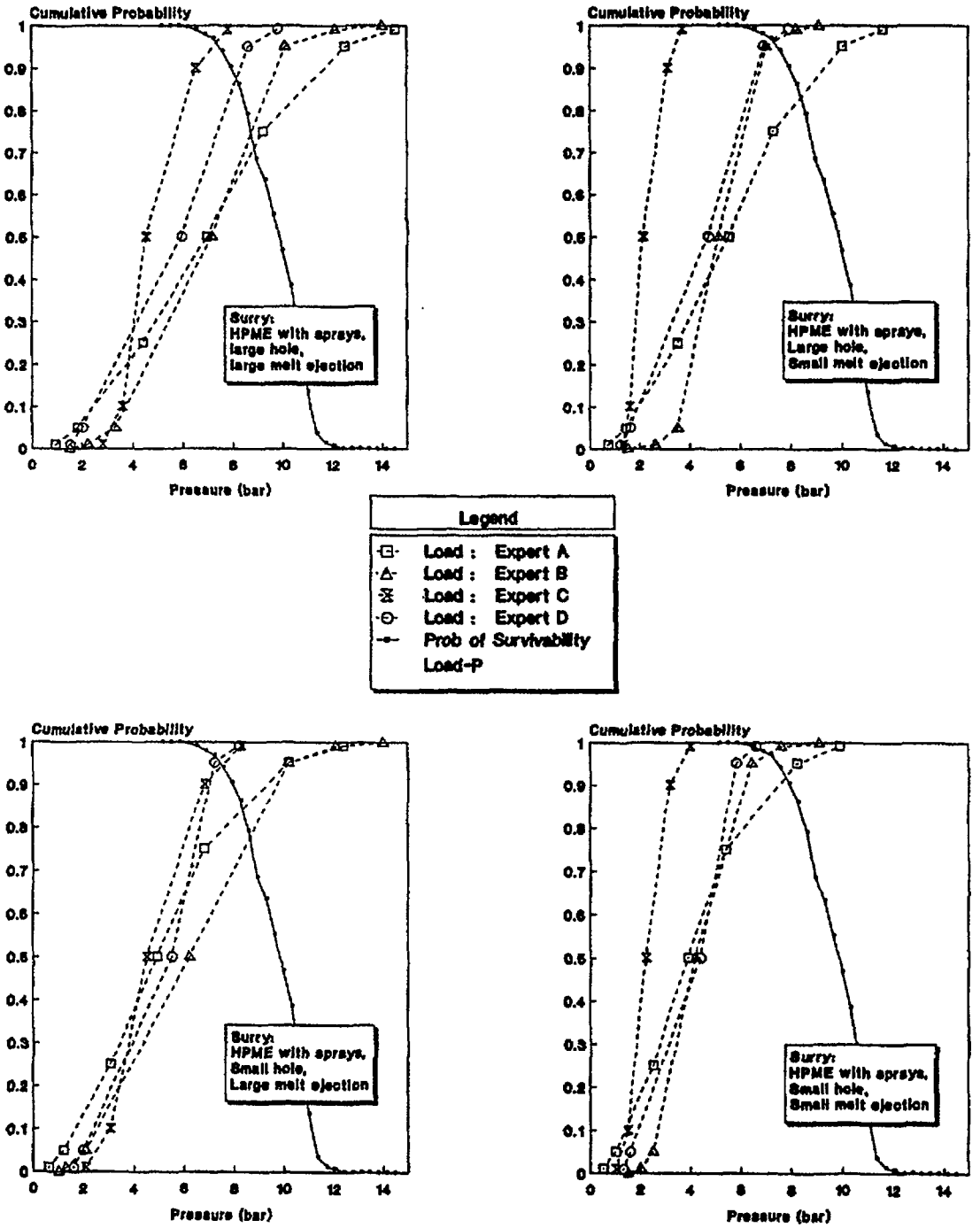

Figure C.5.7 Surry containment load distributions generated by composite of individual experts for each of the cases shown in Figure C.5.5.

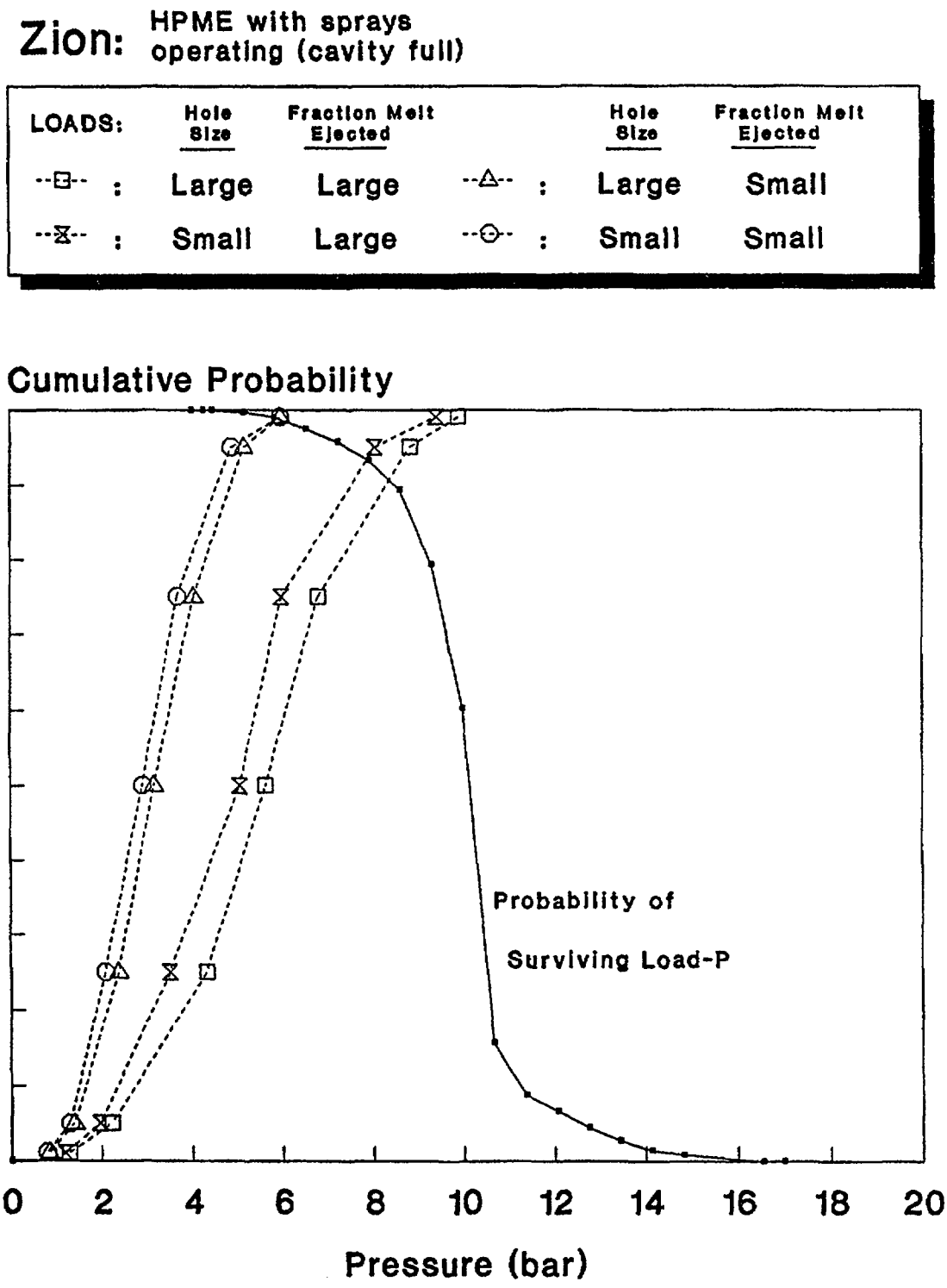

Figure C.5.8 Zion containment loads at vessel breach; cases involving vessel breach at high pressure with containment sprays operating (wet cavity).

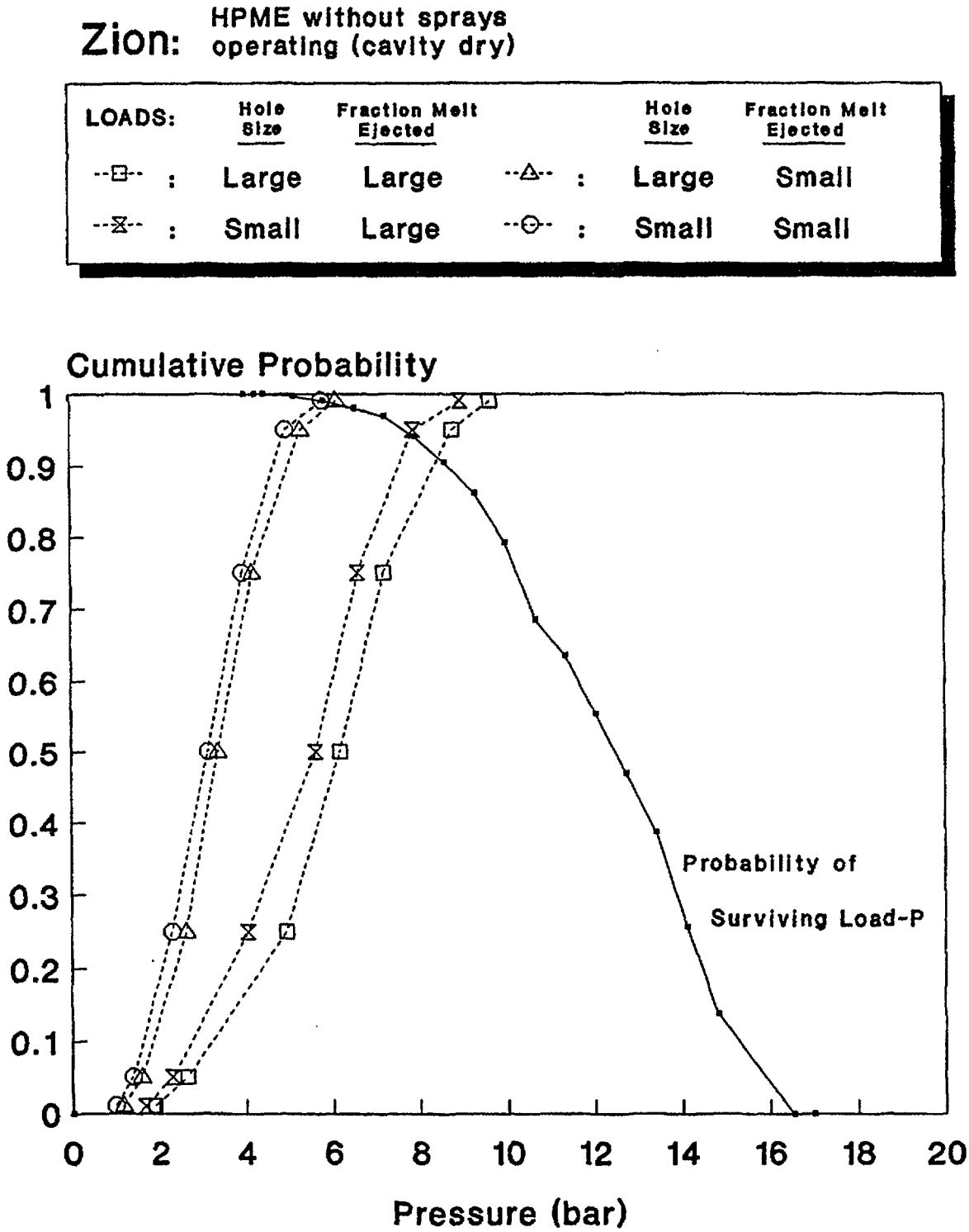

Figure C.5.9 Zion containment loads at vessel breach; cases involving vessel breach at high pressure without containment sprays operating (dry cavity).

shown in Figures C.5.10 and C.5.11 (i.e., they represent the loads for high-pressure accident scenarios with and without containment sprays operating, respectively). Note that, for cases with a wet reactor cavity,* the distributions for containment pressure rise were observed to be relatively insensitive to the assumed size of the hole generated in the reactor vessel bottom head at vessel breach. Separate distributions are, therefore, not displayed in Figure C.5.10 for cases with different assumed hole sizes. At Sequoyah, there are accident progressions when the reactor cavity is deeply flooded** (water level is well above the bottom of the reactor vessel, attaining a level as high as the hot legs). The expert judgment concerning this plausible situation is that pressure rise attendant to HPME is substantially mitigated. Containment loads for the deeply flooded cases were assessed separately from the dry and wet cavity cases and, because the threat to containment integrity is minimal, they are not presented here. The reader is encouraged to consult Reference C.5.2 for full details of the containment loads for the cases with a deeply flooded cavity.

In Figures C.5.10 and C.5.11, the load distributions represent accident situations in which a substantial fraction (greater than 50 percent) of the initial inventory of ice remains in the ice condenser at vessel breach. Such conditions may arise during small-break LOCAs or station blackout. Other accident scenarios, however, may result in substantial ice depletion prior to reactor vessel breach (such as small-break LOCAs with failure of ECCS in the recirculation mode). Representative distributions of containment loads at vessel breach for these cases are shown in Figure C.5.12.

The value of the ice condenser for containment pressure suppression is readily apparent when comparing the distributions in Figure C.5.12 with those in Figures C.5.10 and C.5.11. The Sequoyah containment is considerably more likely to survive the static pressure loads generated at vessel breach if a substantial quantity of ice (i.e., greater than 10 percent of the initial inventory) remains in the ice condenser than when the ice inventory is depleted. The influence of containment spray operation on containment performance is noticeable, but far less dramatic.

C.5.3 Treatment in PRA and Results

The probability distributions for this issue were implemented in the PWR accident progression event trees. These trees (one for each plant) provide a structured approach for evaluating the various ways in which a severe accident can progress, including important aspects of reactor coolant system thermal-hydraulic response, core melt behavior, and containment loads and performance. The accident progression event tree for each plant is a key element in the assessment of uncertainties in risk; it considers the possibility that a particular accident sequence may proceed along any one of several alternative pathways (i.e., alternative combinations of events in the severe accident progression). The probability distributions for individual and combinations of events within the tree provide the rules that determine the relative likelihood of various modes of containment failure.

As mentioned in the introduction to Section C.5, uncertainties in containment loads accompanying high-pressure melt ejection are not major contributors to the overall uncertainty in risk for any of the three PWRs examined in this study. There are two reasons for this. First, comparison of the range of potential loads against the estimated strength of the large, dry containments (Surry and Zion) indicates high confidence that these containments can accommodate the pressure increment accompanying high-pressure melt ejection. A similar conclusion cannot be supported for the Sequoyah containment without additional assurance that some of the containment safety features operate (e.g., a substantial inventory of ice remains at the time of vessel breach). Secondly, accident sequences that have traditionally been considered as "high-pressure" core meltdown accidents (e.g., a fast station blackout***) are estimated to result in a depressurized reactor vessel by the time of reactor vessel breach with a relatively high frequency. Depressurization mechanisms considered in the present analysis include temperature-induced hot leg failure and steam generator tube ruptures, reactor coolant pump seal

*For substantial quantities of water to accumulate on the containment floor and overflow into the Sequoyah cavity, the refueling water storge tank (RWST) inventory must dump onto the containment floor (e.g., via containment sprays) and approximately 25 percent of the ice inventory must melt.

**Deep flooding of the cavity occurs with approximately 50 percent of the ice inventory and transfer of the RWST inventory onto the containment floor.

***A fast station blackout involves the loss of electrical power and failure of steam-driven auxiliary feedwater, thus rendering all decay heat removal systems unavailable.

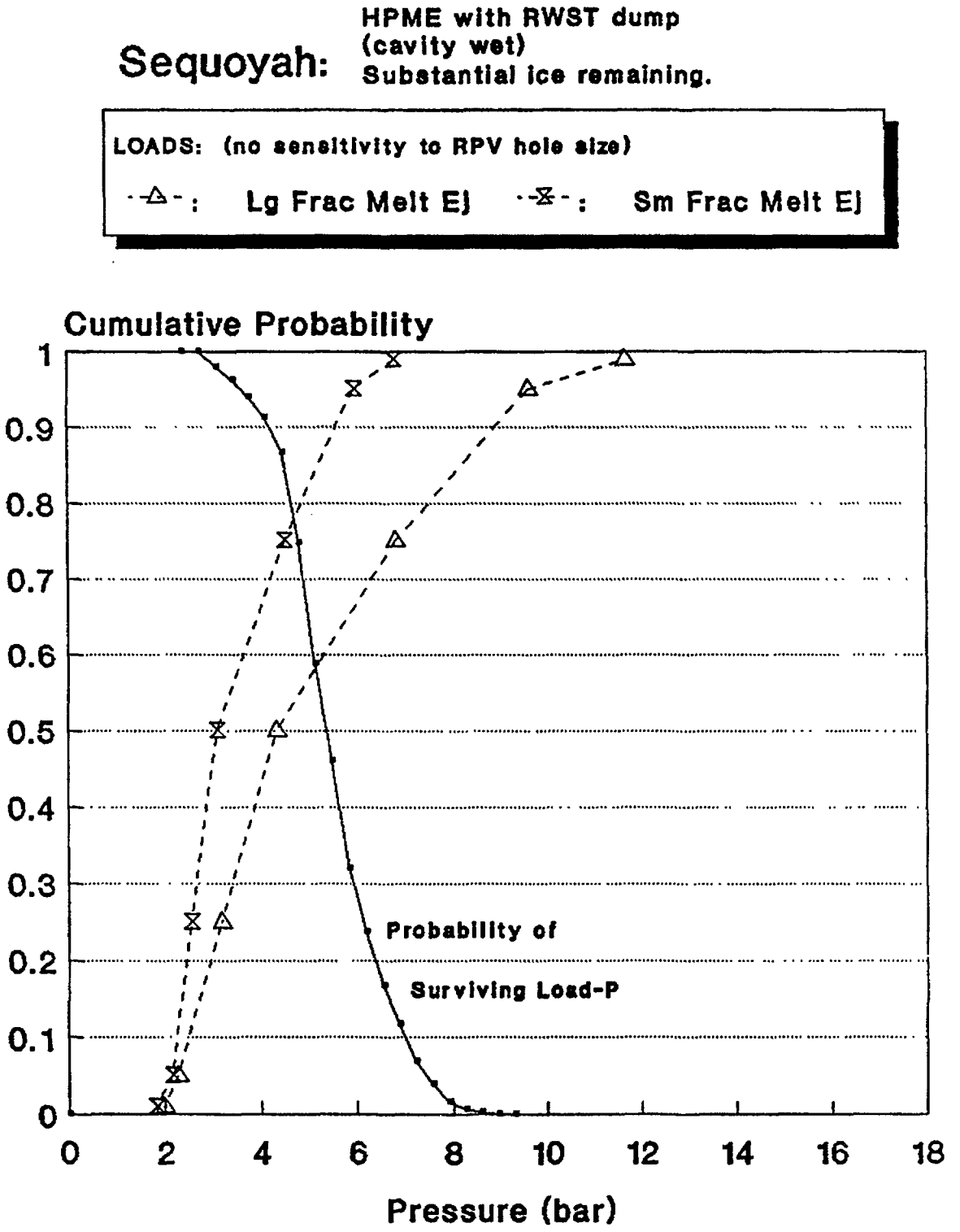

Figure C.5.10 Sequoyah containment loads at vessel breach; cases involving vessel breach at high pressure with containment sprays operating (wet cavity) and a substantial inventory of ice remaining.

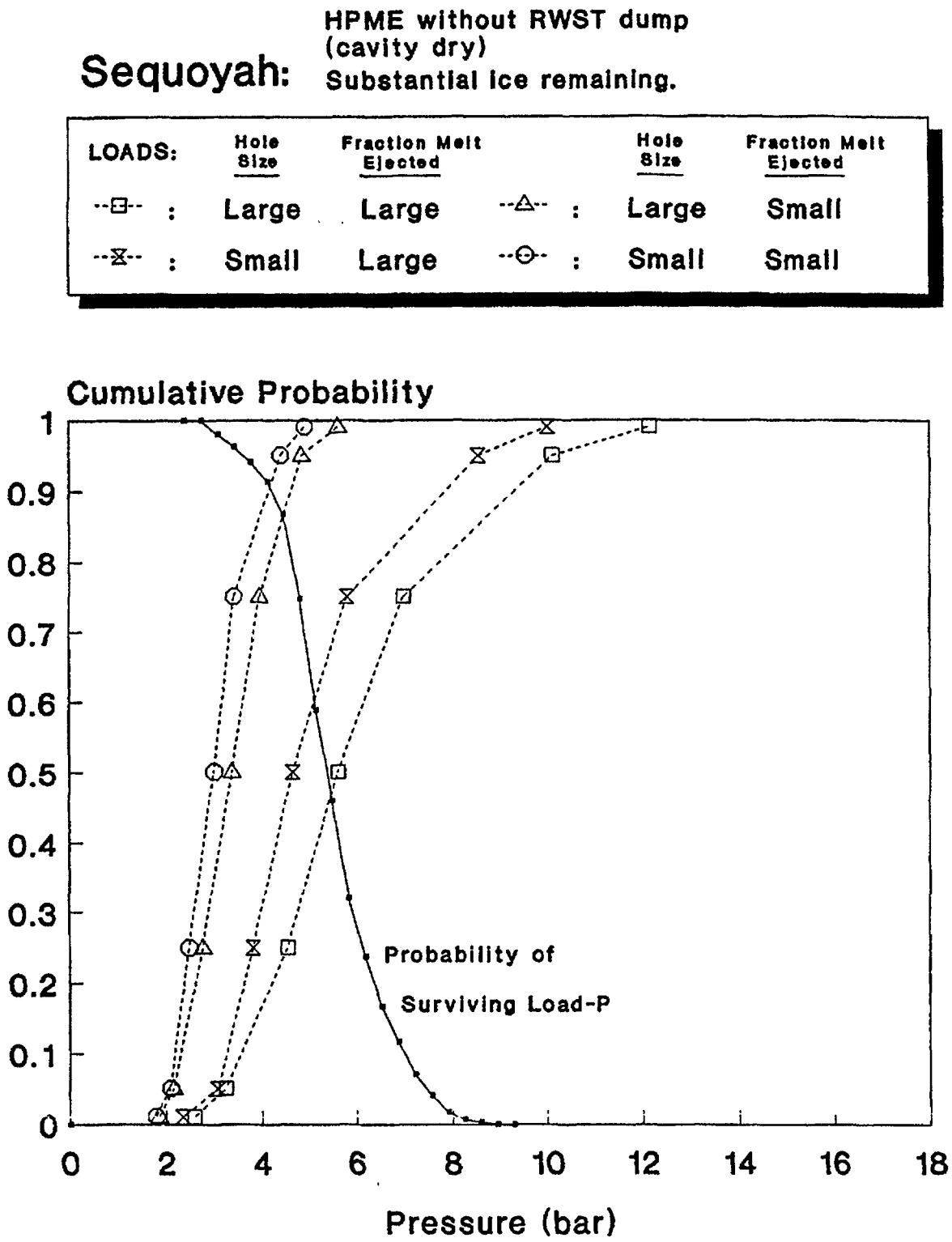

Figure C.5.11 Sequoyah containment loads at vessel breach; cases involving vessel breach at high pressure without containment sprays operating (dry cavity) and a substantial inventory of ice remaining.

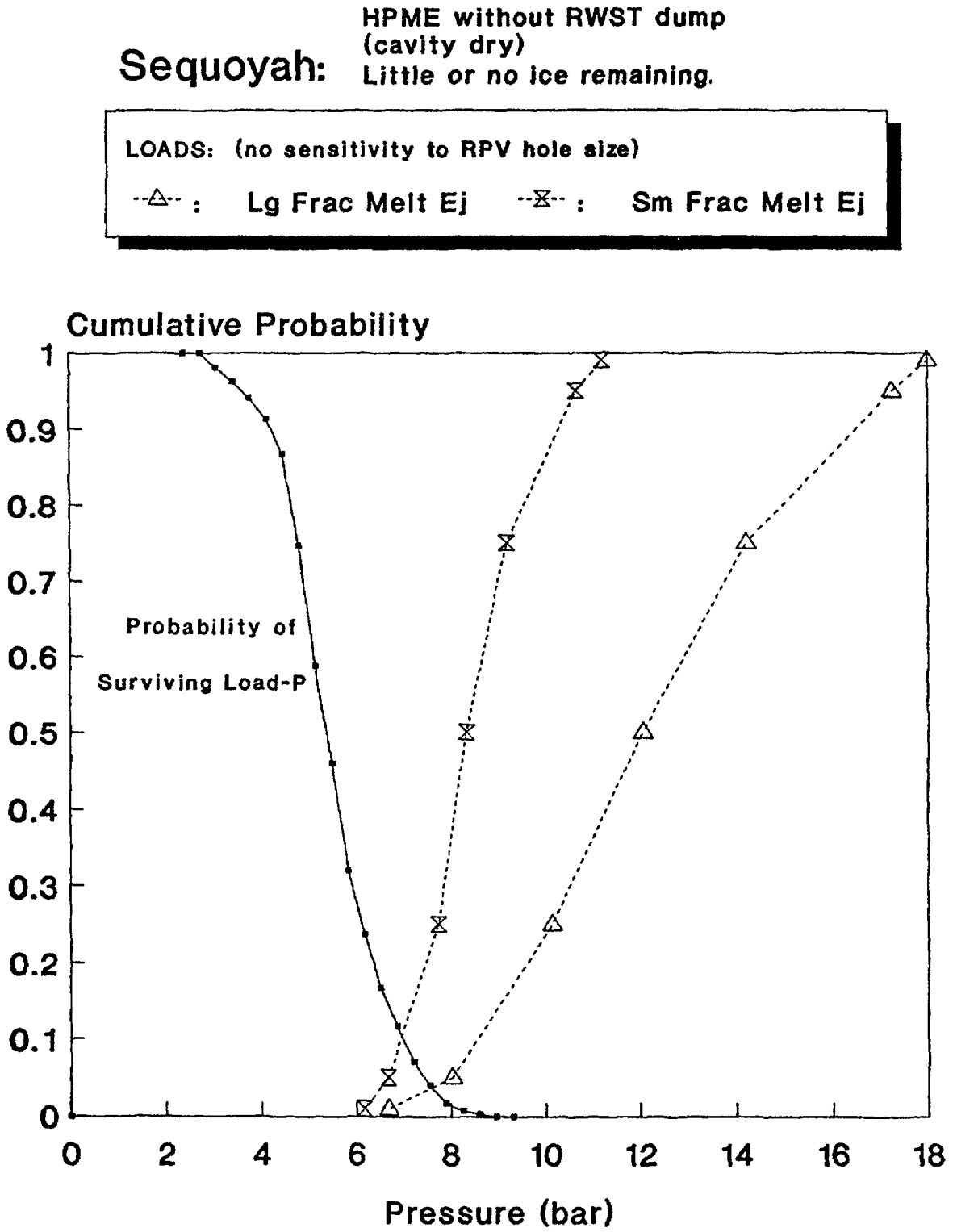

Figure C.5.12 Sequoyah containment loads at vessel breach; cases involving vessel breach at high pressure without containment sprays operating (dry cavity) and a negligibly small inventory of ice remaining.

failures, and stuck-open power-operated relief valves (PORVs). These mechanisms are described in detail in Section C.6. The result of incorporating the potential for reactor vessel depressurization prior to vessel breach is a reduced frequency of high-pressure melt ejection and reduced containment loads at vessel breach. Another potential means of mitigating HPME loads at Sequoyah is deep flooding of the reactor cavity. However, deep flooding introduces a potential for an ex-vessel steam explosion. Challenges to containment integrity from ex-vessel steam explosions are discussed in Section C.9.

As an illustration of the reduced frequency of high-pressure melt ejection and a resulting reduced frequency of early containment failure in the present analysis (from that estimated in the preliminary analyses—published in the February 1987 draft for comment release of this report (Ref. C.5.14)), Table C.5.1 summarizes the relative likelihood of various modes of containment failure for each of the PWRs examined. The numbers shown in this table are frequency-weighted averages (i.e., they are the mean probability of containment failure given core damage). It is important to note that the probability of no containment failure is significant, and the average probability of early containment failure is shown to be low for all three plants.

Table C.5.1 Mean conditional probability of containment failure for three PWRs.

Containment Failure Mode	Surry	Zion	Sequoyah
Early failure with reactor vessel at pressure > 200 psi	0.004	0.02	0.04
Early failure with reactor vessel at pressure < 200 psi	0.0	—	0.02
Late containment failure	<0.01	—	0.04
Containment bypass	0.12	0.006	0.06
Others (alpha,* basemat meltthrough)	0.06	0.22	0.18
No containment failure or arrested core damage with no vessel breach	0.81	0.76	0.66

*Steam explosion-induced containment failure. The analyses supporting the quantification of this mode of containment failure are described in Section C.9.

C.5.4 Differences in Treatment of HPME and DCH Between First and Second Drafts of NUREG-1150

There are important differences in the role played by high-pressure melt ejection/direct containment heating (HPME/DCH) in the second and final versions of NUREG-1150 versus its role in the first draft. In the latter, DCH contributed about 80 percent to the mean early fatality risk at Surry, while the contribution is substantially less in the current version of NUREG-1150, about 17 percent. Similar trends resulted for Zion. For Sequoyah, however, the change was in the opposite direction: HPME/DCH was a very minor contributor in the first draft of NUREG-1150, while it is significant in the current version of NUREG-1150.

Some of the implications of NUREG-1150 may be understood by first examining the reasons for the changes between the final version of NUREG-1150 and the first draft of NUREG-1150 results. A large number of factors are involved, with the following being especially noteworthy:

1. In the final version of NUREG-1150, much higher probabilities were assigned for partial or total depressurization of the vessel prior to vessel breach (VB) because of the occurrence of induced failures of the RCS boundary: hot leg and surge line LOCAs, pump seal LOCAs, and failure of PORVs to reclose. In the Surry analysis for the first draft, for example, the vessel remains pressurized in about 66 percent of the TMLB' accidents, while partial or complete depressurization occurs in 97 percent of the Surry TMLB' accidents in the final version.

2. The final version of NUREG-1150 takes credit for offsite power recovery during the period between the onset of core degradation and the occurrence of VB in station blackout accidents, which are the

principal accident sequences leading to HPME/DCH. In Surry, for example, recovery occurs in 60 percent of the cases, and recovery arrests the accident (preventing HPME/DCH) in 90 percent of the recovered cases. The PWR analyses in the first draft of NUREG-1150 did not consider core damage arrest between onset of core degradation and VB.

3. The high end of the distribution for HPME/DCH loads in large, dry containments was reduced somewhat, relative to the first draft of NUREG-1150, but these changes were not large; containment-threatening loads were still considered quite credible. (In Surry, there was also an increased estimate of containment strength.) In ice condenser plants, however, the assessed threat was substantially increased, both because of increased appreciation of the potential role played by hydrogen in augmenting the DCH threat in these plants and also because of the recognition of the possibility of containment failure due to direct impingement of melt on the containment shell.

4. The ultimate strengths of the containment building under severe accident loads increased somewhat.

5. In the final version of NUREG-1150, steam generator tube ruptures (SGTRs) were included as accident initiators, and they contribute significantly to the role of bypass accidents for some consequence measures (their contribution is minor for early fatality risks, however). The first draft of NUREG-1150 did not consider SGTRs as initiators for severe accidents.

It should be noted that the changes summarized in points 1 and 3 above were heavily influenced by results from the Severe Accident Research Program during the interim period between the first and second drafts of NUREG-1150. Review of the NUREG-1150 expert elicitation documentation (Ref. C.5.2) shows that these research results played an important role in guiding the uncertainty distributions supplied for many important parameters, including both those governing DCH loads and those governing the probability of RCS depressurization.

The results noted above indicate that the most important single reason for the reduced contribution of HPME/DCH to mean risk in the large, dry containments is the perception that HPME/DCH scenarios are more likely to be prevented by the occurrence of unintentional RCS depressurization associated with induced failures of the RCS boundary and, to a lesser extent, by power recovery. In Sequoyah, this effect is more than compensated for by the increase in perceived threat from HPME/DCH phenomenology itself.

The degree to which the reduced importance of HPME/DCH in the Surry analysis depends upon RCS depressurization is especially noteworthy because this conclusion hinges upon such uncontrollable and unplanned factors as the temperature-induced failure of RCS components. This behavior is highly dependent on code predictions of core melt progression and the response of the RCS during degraded core accidents; the predictions have not been validated experimentally. The TMI-2 accident is also interesting in this regard because it provides evidence that degraded core accidents can progress quite far at elevated pressure without approaching temperature-induced failure of RCS components.

REFERENCES FOR SECTION C.5

C.5.1 E.D. Gorham-Bergeron et al., "Evaluation of Severe Accident Risks: Methodology for the Accident Progression, Source Term, Consequence, Risk Integration, and Uncertainty Analyses," Sandia National Laboratories, NUREG/CR-4551, Vol. 1, Draft Revision 1, SAND86-1309, to be published.*

C.5.2 F.T. Harper et al., "Evaluation of Severe Accident Risks: Quantification of Major Input Parameters," Sandia National Laboratories, NUREG/CR-4551, Vol. 2, Revision 1, SAND86-1309, December 1990.

C.5.3 R.J. Breeding et al., "Evaluation of Severe Accident Risks: Surry Unit 1," Sandia National Laboratories, NUREG/CR-4551, Vol. 3, Revision 1, SAND86-1309, October 1990.

C.5.4 A.C. Payne, Jr., et al., "Evaluation of Severe Accident Risks: Peach Bottom Unit 2," Sandia National Laboratories, NUREG/CR-4551, Vol. 4, Draft Revision 1, SAND86-1309, to be published.*

*Available in the NRC Public Document Room, 2120 L Street NW., Washington, DC.

C.5.5 J.J. Gregory et al., "Evaluation of Severe Accident Risks: Sequoyah Unit 1," Sandia National Laboratories, NUREG/CR-4551, Vol. 5, Revision 1, SAND86-1309, December 1990.

C.5.6 T.D. Brown et al., "Evaluation of Severe Accident Risks: Grand Gulf Unit 1," Sandia National Laboratories, NUREG/CR-4551, Vol. 6, Draft Revision 1, SAND86-1309, to be published.*

C.5.7 C.K. Park et al., "Evaluation of Severe Accident Risks: Zion Unit 1," Brookhaven National Laboratory, NUREG/CR-4551, Vol. 7, Draft Revision 1, BNL-NUREG-52029, to be published.*

C.5.8 D.C. Williams et al., "Containment Loads Due to Direct Containment Heating and Associated Hydrogen Behavior: Analysis and Calculations with the CONTAIN Code," Sandia National Laboratories, NUREG/CR-4896, SAND87-0633, May 1987.

C.5.9 M. Pilch and W.W. Tarbell, "Preliminary Calculations of Direct Heating of a Containment Atmosphere by Airborne Core Debris," Sandia National Laboratories, NUREG/CR-4455, SAND85-2439, July 1986.

C.5.10 W.W. Tarbell et al., "Results from the DCH-1 Experiment," Sandia National Laboratories, NUREG/CR-4871, SAND86-2483, June 1987.

C.5.11 M. Pilch et al., "High Pressure Melt Ejection and Direct Containment Heating in Ice Condenser Containments," *Proceedings of the International Topical Meeting on Operability of Nuclear Power Systems in Normal and Adverse Environments, ANS/ENS* (Albuquerque, NM), September 29-October 3, 1986, SAND87-2141C.

C.5.12 M. Pilch and W.W. Tarbell, "High Pressure Ejection of Melt from a Reactor Pressure Vessel—The Discharge Phase," Sandia National Laboratories, NUREG/CR-4383, SAND85-0012, September 1985.

C.5.13 W.W. Tarbell et al., "Pressurized Melt Ejection into Scaled Reactor Cavities," Sandia National Laboratories, NUREG/CR-4512, SAND86-0153, October 1986.

C.5.14 U.S. Nuclear Regulatory Commission, "Reactor Risk Reference Document," NUREG-1150, Vols. 1-3, Draft for Comment, February 1987.

*Available in the NRC Public Document Room, 2120 L Street NW., Washington, DC.

C.6 Mechanisms for PWR Reactor Vessel Depressurization Prior to Vessel Breach

The previous section addressed the range of thermodynamic loads to a PWR containment accompanying penetration of the reactor pressure vessel lower head by molten core debris and subsequent ejection of material into the containment atmosphere. These loads can present a significant challenge to containment integrity if penetration of the reactor vessel occurs at sufficiently high vessel pressure. For the three PWRs examined in this study, however, a substantial fraction of the severe accident progressions that started with the reactor vessel at high pressure depressurized before vessel breach. That is, many of the accident scenarios important to risk result in—by one means or another—a breach in the reactor coolant system (RCS) pressure boundary of sufficient size to reduce reactor vessel pressure below approximately 200 psi before reactor vessel lower head failure. An outcome of this result is that the uncertainties in high-pressure melt ejection loads are observed to have a relatively small impact on the overall uncertainties in reactor risk. This observation is a substantial change in results from those of preliminary analyses published in draft form in February 1987.

Unlike the BWRs examined in this study, the PWRs do not have a system specifically designed to manually depressurize the reactor vessel. Feed-and-bleed operations can effect limited depressurization if the necessary systems are operable. Many of the accident sequences leading to core damage in the three PWRs examined in this study, however, include combinations of failures that render feed-and-bleed operations unavailable. This section addresses the other means by which the reactor vessel pressure may be reduced to levels below which high-pressure melt ejection loads do not threaten containment integrity:

- Temperature-induced failure of steam generator tubes,
- Temperature-induced failure of primary coolant hot leg piping or the pressurizer surge line,
- Failure of reactor coolant pump seals,
- Stuck-open power-operated relief valves (PORVs), and
- Manual (operator) actions to depressurize the RCS.

The estimated frequency of each of these events and their influence on reactor vessel pressure was incorporated in the accident progression analysis for the Surry, Sequoyah, and Zion plants. Manual depressurization was found to be ineffective for most PWR accident sequences because of limitations in the appropriate emergency procedures and the need for ac power to operate relief valves. This mechanism is, therefore, not discussed further. The manner in which the other hypothetical events were considered, the means of quantifying their likelihood, and illustrations of the impact they have on the results are discussed in the following sections.

C.6.1 Issue Definition

The general issue is the frequency with which PWR severe accident progressions involve a breach in the RCS pressure boundary of sufficient size to reduce the reactor vessel pressure below approximately 200 psia. The mechanisms for depressurizing the reactor vessel that are considered in the present analysis are those listed in the introduction above. The first two mechanisms involve temperature-induced (i.e., creep rupture) failures of RCS piping. In both cases, the heat source for such failures is hot gases transported from the core via natural circulation or exiting the RCS through the PORV. The natural circulation pattern may involve an entire RCS coolant loop if water in the loop seals has cleared. If the loop seals have not cleared, a countercurrent natural circulation flow pattern may be established within the hot leg piping, transporting superheated gases and radionuclides from the core region of the reactor vessel to the steam generators. Effective cooling of the steam generator tubes is not available in many of the accident sequences considered in this analysis because of depletion of secondary coolant inventory earlier in the accident. Decay heat from radionuclides deposited in the steam generator inlet plenum and inside the tubes may also contribute to local tube heating. In either case, natural circulation flow (if established) may be interrupted by the frequent cycling of the pressurizer PORV or by the accumulation (and stratification) of hydrogen in the reactor vessel upper plenum and hot legs. The specific parameter to be quantified is the frequency with which creep rupture of hot leg piping or steam generator tubes results from the transfer of heat from the core (via gas circulation) to RCS structures. The temperature-induced failures of interest here are limited to those that occur before reactor vessel failure.

Degradation and failure of reactor coolant pump seals may also result from overheating. In this case, overheating results from the loss of seal cooling water flow or loss of heat removal from the seal cooling water system. A number of potential "seal states" have been identified in reactor coolant pump performance studies, which result in a range of plausible leak rates from the reactor coolant system. The parameters to be quantified are the frequency of pump seal LOCAs, the relative likelihood of various leak rates that result from these failures, and the resulting value of reactor vessel pressure at the time of vessel breach.

The fourth mechanism considered in this analysis, stuck-open PORV(s), may result following the repeated cycling (opening and reseating) of the PORVs during the course of an accident. Such events have been observed (with relatively low frequency) during transient events in which plant conditions never exceed design basis conditions. PORVs have also been tested for their reliability to close after repeated cycles at design basis conditions. This issue considers the effect of beyond design basis conditions on the frequency with which PORVs fail to close after several cycles.

C.6.2 Technical Bases for Issue Quantification

Two of the four mechanisms, temperature-induced hot leg failure and steam generator tube ruptures, were presented to a panel of experienced severe accident analysts. Each panelist was asked to provide a probability distribution representing his estimate of the frequency of each event. Their judgments were to be based on current information, made available to each of the panelists, and their own professional experience. The panelists participating were:

Vernon Denny—Science Applications International Corp.,
Robert Lutz—Westinghouse Electric Corp., and
Robert Wright—U.S. Nuclear Regulatory Commission.

The individual distributions prepared by these panelists were then combined (i.e., an aggregate distribution was generated by averaging those of the three panelists) to develop a single distribution for application in the PRA. The methods used to aggregate individual panelists' distributions are described in Reference C.6.1.

The frequency of reactor coolant pump seal failures was addressed by an expert panel in support of the systems analysis for the PWRs (Ref. C.6.2). This panel's judgments were adopted for use in the accident progression event tree. Very limited data are available to support an assessment of the frequency of PORVs sticking open when subjected to severe accident conditions. A broad distribution was, therefore, assigned to the frequency of stuck-open PORVs. A summary of the technical bases for quantifying the frequency of RCS depressurization for each of these four mechanisms is given below.

Frequency of Hot Leg Failure

A case structure was established to consider a spectrum of plausible severe accident conditions for which the frequency of hot leg failures needed to be quantified. The case structure was formulated around accident sequences that represent a significant contribution to the total core damage frequency. The cases considered were:

Case 1: A classic TMLB'* scenario (station blackout). RCS pressure is maintained near 2500 psia by the continuous cycling of the PORV. The secondary side of the steam generator is at the steam relief valve setpoint pressure (approx. 1000 psia) and is depleted of coolant inventory. Reactor coolant pump seal cooling is maintained at the nominal flow rate.

Case 2: Station blackout sequence during which reactor pump coolant seals fail, yielding a leak rate equivalent to a 0.5-inch-diameter break in each coolant loop. The steam generator secondary coolant inventory is depleted and the auxiliary feedwater system is unavailable.

Case 3: Same as Case 2 except the steam generators maintain an effective RCS heat sink with auxiliary feedwater operating.

*Reactor Safety Study [WASH-1400] nomenclature for accident sequence delineation. The alphabetical characters represent compound failures of plant equipment leading to the loss of plant safety functions. The characters TMLB' represent a transient initiating event, loss of decay heat removal, and loss of all electrical power.

The technical bases used by the panelists for characterizing the frequency of temperature-induced hot leg failures for each case were dominated by calculations performed with various severe accident analysis computer codes and by several different organizations. Those cited by the panelists in their elicitations (Ref. C.6.1) included TRAC/MELPROG calculations of TMLB' scenarios in Surry (Ref. C.6.3), RELAP5/SCDAP calculations of similar accident scenarios (Ref. C.6.4), CORMLT/PSAAC calculations for Surry and Zion (Refs. C.6.5 and C.6.6), and MAAP calculations performed in support of the Ringhals Unit 3 PRA (Ref. C.6.7) and the Seabrook PSA (Refs. C.6.8 and C.6.9). Ringhals Unit 3 is a three-loop plant with an NSSS similar to that of Surry; Seabrook is a four-loop plant with an NSSS similar to those of Sequoyah and Zion.

Only two specific references were cited by the panelists regarding experimental data or other physical evidence of natural circulation and its effect on heating RCS structures. These were the natural circulation experiments sponsored by EPRI (Ref. C.6.10) and the results of post-accident examinations of the Three Mile Island Unit 2 core debris and RCS structures (Ref. C.6.11). Information from neither of these sources is believed to have significantly influenced the panelists' judgments on this issue.

The aggregate distribution for the frequency of temperature-induced hot leg failures are shown in Figure C.6.1 for Cases 1 and 2 outlined above. The probability that Case 3 would result in an induced hot leg failure was judged to be essentially zero. The distributions shown in Figure C.6.1 are displayed in the form of a cumulative distribution function (CDF); that is, the curve displays the probability that the frequency of an induced hot leg failure is not greater than a particular value. The likelihood of an induced hot leg failure, given a station blackout accident during which the reactor vessel pressure remains high (i.e., no reactor coolant pump seal LOCAs, stuck-open PORVs, etc.), is shown to be relatively high; the median frequency is greater than 95 percent. In contrast, lower reactor vessel pressures in Case 2 (with an early pump seal LOCA) make an induced hot leg failure unlikely; there is an 83 percent chance that a hot leg failure will not occur.

Frequency of Induced Steam Generator Tube Ruptures

Essentially the same information (results of several computer code calculations) were used to characterize induced steam generator tube rupture (SGTR) frequency. All three panelists agreed that the likelihood of an induced SGTR is quite low. The three panelists noted that temperature-induced tube ruptures are driven by the same phenomena that drive temperature-induced hot leg failure (natural circulation flow of hot gases from the reactor vessel); therefore, the frequency distributions are correlated. Two of the panelists believed that the frequency of SGTR is very small because of the assumption that the hot leg would fail first, and neither of their distributions for frequency of induced SGTR exceeded a value of 0.0005. The aggregate distribution (shown in Fig. C.6.2) is dominated by a single panelist, whose distribution was strongly influenced by consideration of pre-existing flaws in steam generator tubes, resulting in the assumption that SGTR might occur before hot leg failure.

Frequency of Induced Reactor Coolant Pump Seal LOCAs

The frequency of pump seal LOCAs of various sizes (corresponding to various pump seal states) was considered by a panel of experts as a systems analysis issue. Degradation mechanisms for reactor coolant pumps are highly plant- (or pump-) specific and can be quite complicated. Details of the analyses leading to the characterization of the various pump seal states and the corresponding spectrum of possible leak rates are not provided here but are available in the documentation of the expert panel elicitations (Ref. C.6.2). An indication of the potential importance of modeling pump seal LOCAs, however, can be found by examining the accident progressions for which the reactor vessel pressure remains at or near the system setpoint (e.g., station blackouts with no other breach in the RCS pressure boundary). In the Surry analysis, approximately 71 percent of these accident progressions result in a failure of the seals in at least one reactor coolant pump. Of these, roughly one-third are estimated to result in a large enough leak rate to depressurize the reactor vessel to less than approximately 200 psia prior to reactor vessel breach; another third result in leak rates small enough to preclude any significant depressurization. In the remaining one-third of the cases, the reactor vessel is at intermediate pressure (200–600 psia) at the time of vessel breach (Ref. C.6.12).

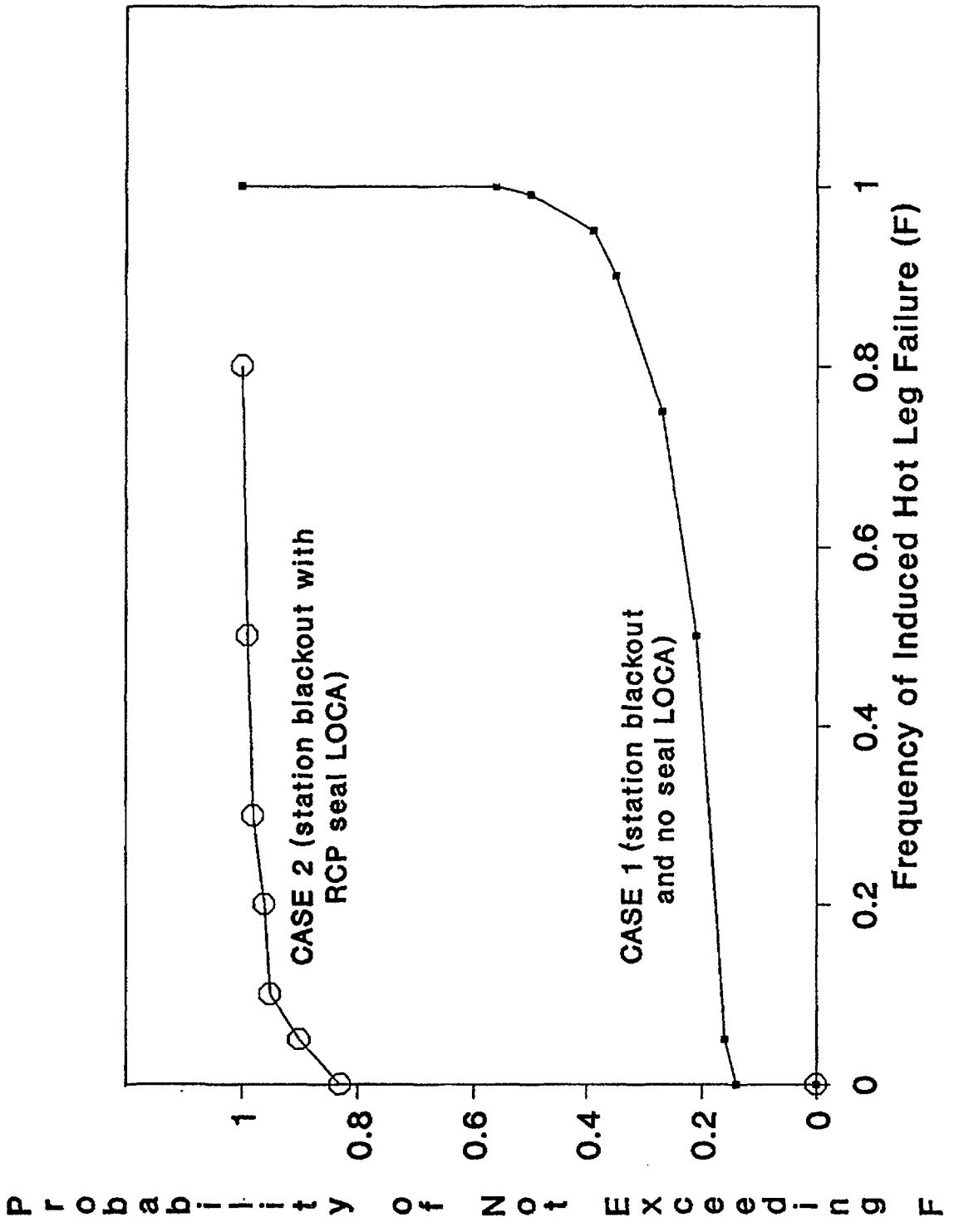

Figure C.6.1 Aggregate distribution for frequency of temperature-induced hot leg failure (Surry, Zion, and Sequoyah).

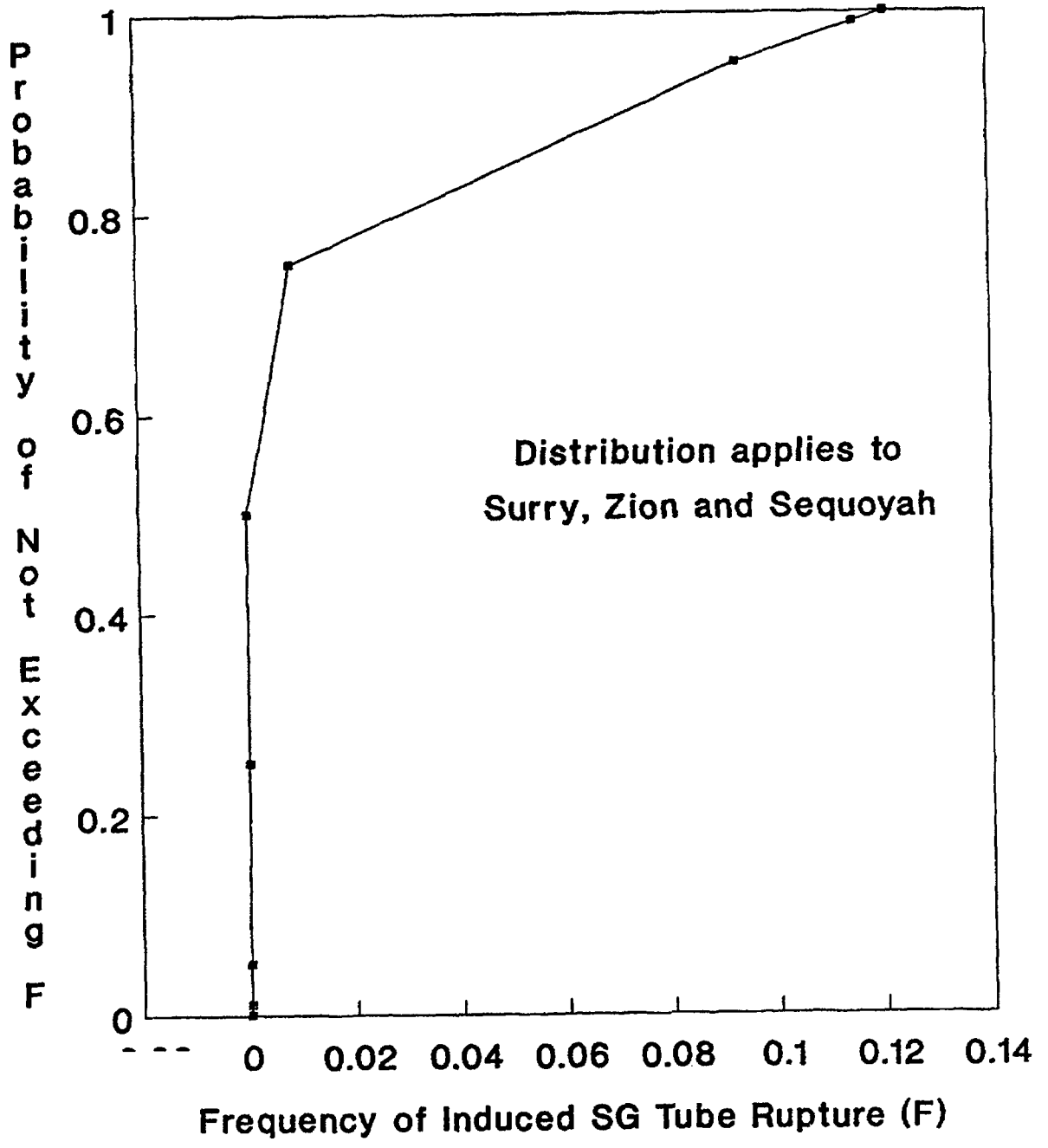

Figure C.6.2 Aggregate distributions for frequency of temperature-induced steam generator tube rupture.

Frequency of Stuck-Open PORVs

This issue was also addressed in the "front-end" analysis as an uncertainty issue (Ref. C.6.2). The RCS conditions under which PORVs will cycle after the onset of core damage, however, are expected to be significantly more severe than those for which the valves were designed and more severe than the conditions under which PORV performance has been tested. In lieu of specific analyses, test data, or operating experience, an estimate of frequency with which a PORV will stick open and an estimate for the resulting RCS pressure were generated as follows:

> The valve is expected to cycle between 10 to 50 times during core degradation and prior to vessel breach. Extrapolation of the distributions for the frequency of PORV failure-to-close from the front-end elicitations indicates an overall failure rate (for 10 to 50 demands) in the neighborhood of 0.1 to 1.0. A uniform distribution from zero to 1.0 was, therefore, used in the Surry and Sequoyah analyses.
>
> TRAC/MELPROG and Source Term Code Package (STCP) analyses were reviewed to characterize the rate at which a stuck-open PORV could depressurize the reactor vessel (Ref. C.6.12). The results of this review resulted in an estimate that there is an 80 percent probability that the reactor vessel pressure at the time of vessel breach will be less than 200 psia; in the remaining 20 percent of the cases, the vessel pressure will be at intermediate levels (200–600 psia).

C.6.3 Treatment in PRA and Results

The probability distributions for this issue were implemented in the PWR accident progression event trees. These trees (one for each plant) provide a structured approach for evaluating the various ways in which a severe accident can progress, including important aspects of RCS thermal-hydraulic response, core melt behavior, and containment loads and performance. The accident progression event tree for each plant is a key element in the assessment of uncertainties in risk; it considers the possibility that a particular accident sequence may proceed along any one of several alternative pathways (i.e., alternative combinations of events in the severe accident progression). The probability distributions for individual and combinations of events within the tree provide the rules that determine the relative likelihood of various modes of containment failure.

For the issue of reactor vessel depressurization, probability distributions for each of the mechanisms discussed above were incorporated in the accident progression event tree to determine reactor vessel pressure prior to vessel breach. As indicated in Section C.5, the containment loads accompanying vessel breach strongly depend on reactor vessel pressure. The load at vessel breach assigned to a particular accident progression, therefore, depends on the outcome of questions in the tree regarding reactor vessel depressurization. Selected results from the accident progression event tree analysis are summarized below.

The pressure history (as determined by the Surry accident progression event tree) for slow station blackout accident sequences* is summarized in Table C.6.1. This table shows the fraction of slow station blackout accident progressions for which the RCS pressure is at the PORV setpoint at high, intermediate, and low levels at the time the core uncovers and the time of reactor vessel breach.

A substantial fraction of the slow blackout accident progressions that start out with the RCS pressure at the PORV setpoint pressure are depressurized by one (or more) of the mechanisms described in Reference C.6.1 and result in a low pressure by the time of vessel breach.

A sensitivity study was performed to examine the effect of neglecting temperature-induced hot leg failure and steam generator tube ruptures on the observed results. Table C.6.2 summarizes the results of this study (presented in an identical format as Table C.6.1).

The results for pressure when the core uncovers are not affected by the change since temperature-induced hot leg failure and steam generator tube ruptures can only occur after the onset of core damage. The elimination of the possibility of these failures does affect the fraction of accident progressions involving reactor vessel breach at high pressure. The occurrence of high-pressure melt ejection is observed to roughly double in frequency.

*Slow station blackout accident sequences contribute more than one-half of the mean total core damage frequency for Surry. The results indicated for this group of accident sequences are not generally applicable to other Surry accident sequences or other plants.

Table C.6.1 Surry reactor vessel pressure at time of core uncovery and at vessel breach.

	Fraction of Slow Blackout Accident Progressions With Pressure-P at the Time of:	
RCS Pressure (psia)	Core Uncovery	Reactor Vessel Breach
2500	0.54	0.06
1000—1400	0.13	0.10
200—600	0.33	0.19
<200	0.0	0.65

Table C.6.2 Surry reactor vessel pressure at time of core uncovery and at vessel breach (sensitivity study without induced hot leg failure and steam generator tube ruptures).

	Fraction of Slow Blackout Accident Progressions With Pressure-P at the Time of:	
RCS Pressure (psia)	Core Uncovery	Reactor Vessel Breach
2500	0.54	0.25
1000—1400	0.13	0.10
200—600	0.33	0.19
<200	0.0	0.46

The increase in accident progressions resulting in vessel breach at high pressure is not observed to significantly affect the likelihood of early containment failure, however. Table C.6.3 shows the fraction of slow blackout accident progressions that results in various modes of containment failure (including no failure) for the Surry base case analysis and for the sensitivity analysis in which induced hot leg failures and steam generator tube ruptures were eliminated.

The insignificant change in results is largely attributable to the strength of the Surry containment and its ability to withstand loads as high as those estimated to accompany high-pressure melt ejection with a relatively high probability (refer to Section C.5).

Qualitatively similar results are observed for Sequoyah. Elimination of the potential for early reactor vessel depressurization by induced hot leg failure or steam generator tube rupture (via a sensitivity analysis) has a noticeable, but not dramatic, influence on the likelihood of high-pressure melt ejection. Table C.6.4 shows the fraction of Sequoyah accident progressions (for two important types of core melt accidents) that results in high-pressure melt ejection* for the base case analysis and the sensitivity analysis. In adjacent columns of this table are the fractions of the time that high-pressure melt ejection occurs and results in containment failure by overpressurization.

*The values shown only account for cases in which high-pressure melt ejection occurs in a cavity that is not deeply flooded. Cases in which the cavity is deeply flooded do not usually generate loads sufficiently large to threaten containment integrity.

Table C.6.3 Fraction of Surry slow blackout accident progressions that results in various modes of containment failure (mean values).

Containment Failure Mode	Fraction of Slow Blackout Accident Progressions Resulting in Containment Failure Mode X: Base Case Analysis	Sensitivity Analysis
Structural Rupture	0.01	0.01
Leak	0.01	0.01
Basemat Meltthrough	0.07	0.06
Containment Bypass	< 0.01	0.0
No Failure*	0.91	0.92

*Included in this category are accident progressions in which core damage is arrested in-vessel, thus preventing reactor vessel breach and containment failure. For Surry, these cases comprise approximately 60–65 percent of the "No Failure" scenarios.

Table C.6.4 Fraction of Sequoyah accident progressions that results in HPME and containment overpressure failure.

Type of Core Damage Accident	Fraction Resulting in HPME Without a Flooded Cavity: (A) Base Case Analysis	(A) Sensitivity Analysis	Fraction of Columns (A) Cases in Which Containment Overpressure Failure Occurs: Base Case Analysis	Sensitivity Analysis
LOCA	0.11	0.11	0.16	0.16
Station Blackout	0.16	0.21	0.20	0.21

As might be expected, no change is observed for the LOCA accident scenarios. Negligible changes are also observed for station blackout scenarios.

REFERENCES FOR SECTION C.6

C.6.1 F.T. Harper et al., "*Evaluation of Severe Accident Risks: Quantification of Major Input* Parameters," Sandia National Laboratories, NUREG/CR-4551, Vol. 2, Revision 1, SAND86-1309, December 1990.

C.6.2 T.A. Wheeler et al., "Analysis of Core Damage Frequency from Internal Events: Expert Judgment Elicitation," Sandia National Laboratories, NUREG/CR-4550, Vol. 2, SAND86-2084, April 1989.

C.6.3 J.E. Kelly et al., "MELPROG-PWR/MOD1 Analysis of a TMLB' Accident Sequence," Sandia National Laboratories, NUREG/CR-4742, SAND86-2175, January 1987.

C.6.4 P.D. Bayless, "Natural Circulation During a Severe Accident: Surry Station Blackout," EG&G Idaho, Inc., EGG-SSRE-7858, 1987.

C.6.5 V.E. Denny and B.R. Sehgal, "PWR Primary System Temperatures During Severe Accidents," *ANS Transactions,* 47, (317-319).

C.6.6 B.R. Sehgal et al., "Effects of Natural Circulation Flows on PWR System Temperatures During Severe Accidents," *1985 National Heat Transfer Conference*, (223–234), 1985.

C.6.7 R.J. Lutz, Jr., et al., "Ringhals Unit 3 Severe Accident Analyses to Support Development of Severe Accident Procedures," Westinghouse Nuclear Technology & Systems Division, WCAP–11607, 1987.

C.6.8 M.G. Plys et al., "Seabrook Steam Generator Integrity Analysis," Fauske & Assoc., FAI/86–39, 1986.

C.6.9 K.N. Fleming et al., "Risk Management Actions to Assure Containment Effectiveness at Seabrook Station," Pickard, Lowe and Garrick, PLG–0550, 1987.

C.6.10 W.A. Stewart et al., "Experiments on Natural Circulation Flow in a Scale Model PWR Reactor System During Postulated Degraded Core Accidents," *Proceedings of Third International Topical Meeting on Reactor Thermal Hydraulics* (Newport, RI), ANS, Vol. 1, October 1985.

C.6.11 American Nuclear Society, *Transactions of the ANS/ENS Topical Meeting on the TMI–2 Accident* (Washington, DC), October 30–November 4, 1988.

C.6.12 J.E. Kelly memorandum to R.J. Breeding, Sandia National Laboratories, "RCS Pressure at Vessel Breach," dated January 27, 1989 (with errata dated February 15, 1989).

C.7 Drywell Shell Meltthrough

The potential for early containment failure is an important contributor to the potential consequences of severe accidents and, thus, to risk. In this context, "early" means before or immediately following the time at which molten core debris penetrates the lower head of the reactor vessel. A number of plausible mechanisms for early containment failure were identified in the Reactor Safety Study, many of which have since been determined to be of extremely low probability and are currently considered to be negligible contributors to risk. More recent containment performance studies have identified a few mechanisms that were not considered in the Reactor Safety Study and have been found to be important contributors to the uncertainty in risk for some plants.

An early failure mechanism that has received a great deal of attention is penetration of a BWR Mark I containment resulting from thermal attack of the steel containment shell by molten core debris. The scenario for this mode of containment failure postulates that, as core debris exits the reactor pressure vessel and is deposited on the floor within the reactor pedestal, it flows out of the pedestal region through an open doorway in the pedestal wall and onto the annular drywell floor. For the debris to contact the drywell shell, it must flow across the drywell floor until it contacts the steel containment shell along the line where the shell is embedded in the drywell floor. Figures C.7.1 and C.7.2 show the relevant geometry of the Peach Bottom drywell in vertical and horizontal cross sections, respectively. If hot debris contacts the drywell shell, two failure modes may occur: the combined effects of elevated containment pressure and local heating of the steel shell may result in creep rupture, or, if hot enough, the debris may melt through the carbon steel shell. Both of these plausible modes are considered in this issue and are collectively referred to as "drywell shell meltthrough."

C.7.1 Issue Definition

This issue represents the ensemble of uncertainties associated with the conditional probability of drywell shell meltthrough. (Failure is conditional on core meltdown progressing to the point that core debris penetrates and is discharged from the lower head of the reactor pressure vessel.) This probability is known to depend on the condition of the core debris (physical state, composition, release rate from the reactor vessel, etc.) as it relocates to the reactor pedestal floor. Distinct cases are established to consider separately each plausible combination of debris conditions at vessel breach. The case structure accounts for uncertainties in severe accident events and phenomena that precede the potential challenge to drywell integrity by drywell shell meltthrough.

Uncertainties associated with the processes and events that occur after core debris leaves the reactor vessel are represented by the probability distribution assigned to each case. The parameters considered in the case structure are:

Parameters Defining Case Structure	Values Considered
1. Rate at which core debris flows out of the reactor vessel.	High: R > 100 kg/sec Med: 50 kg/sec > R > 100 kg/sec Low: 50 kg/sec > R
2. Reactor vessel pressure when core debris first begins to exit the vessel.	High: Near 1000 psia Low: < 200 psia
3. Amount of unoxidized metals in melt.	High: 65 percent of initial inventory (representing range: 50–80 percent) Low: 35 percent of initial inventory (representing range: 20–50 percent)
4. Amount of debris superheat (temperature above melting point of debris).	High: > 100K Low: < 100K

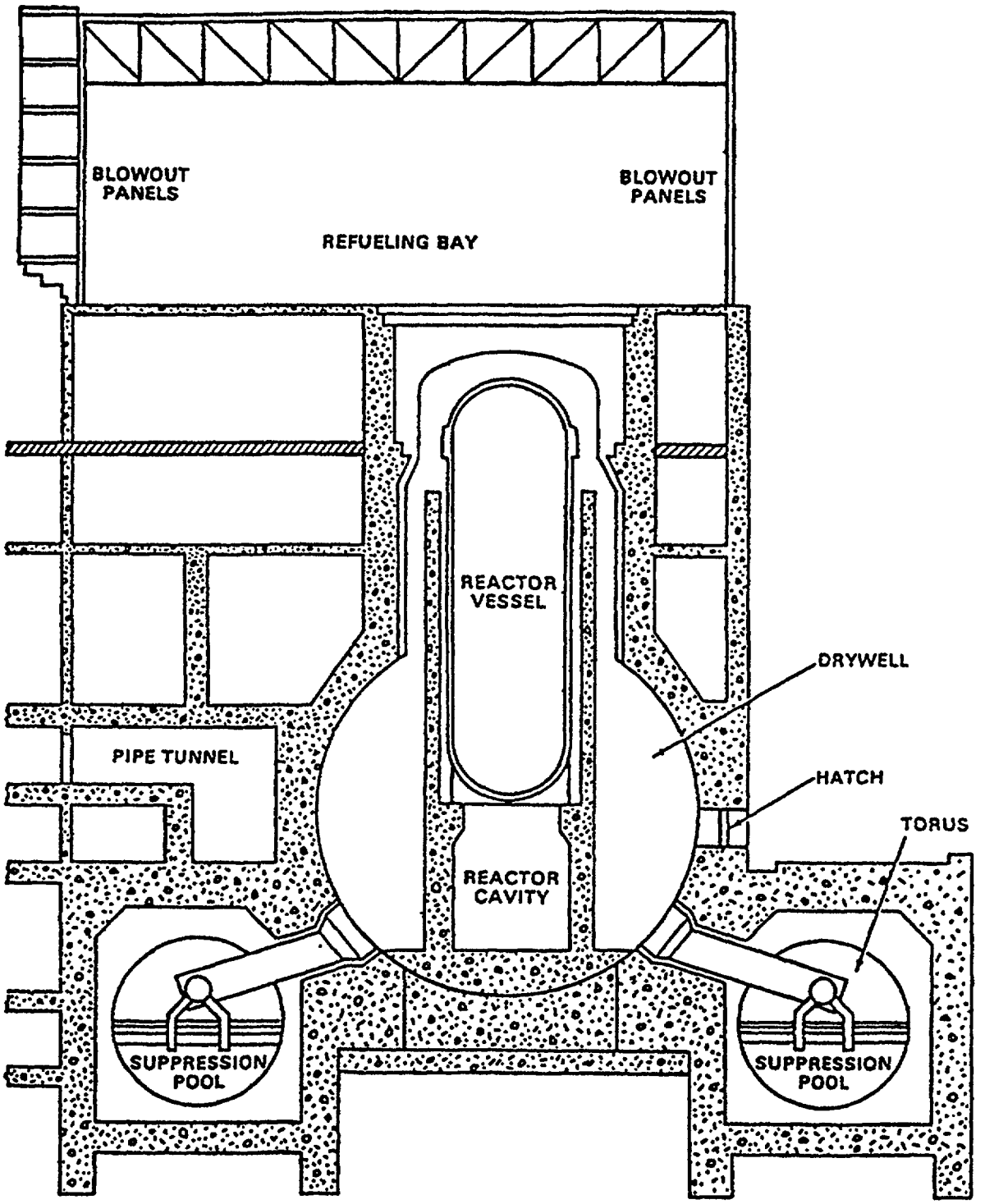

Figure C.7.1 Configuration of Peach Bottom drywell shell/floor—vertical cross section.

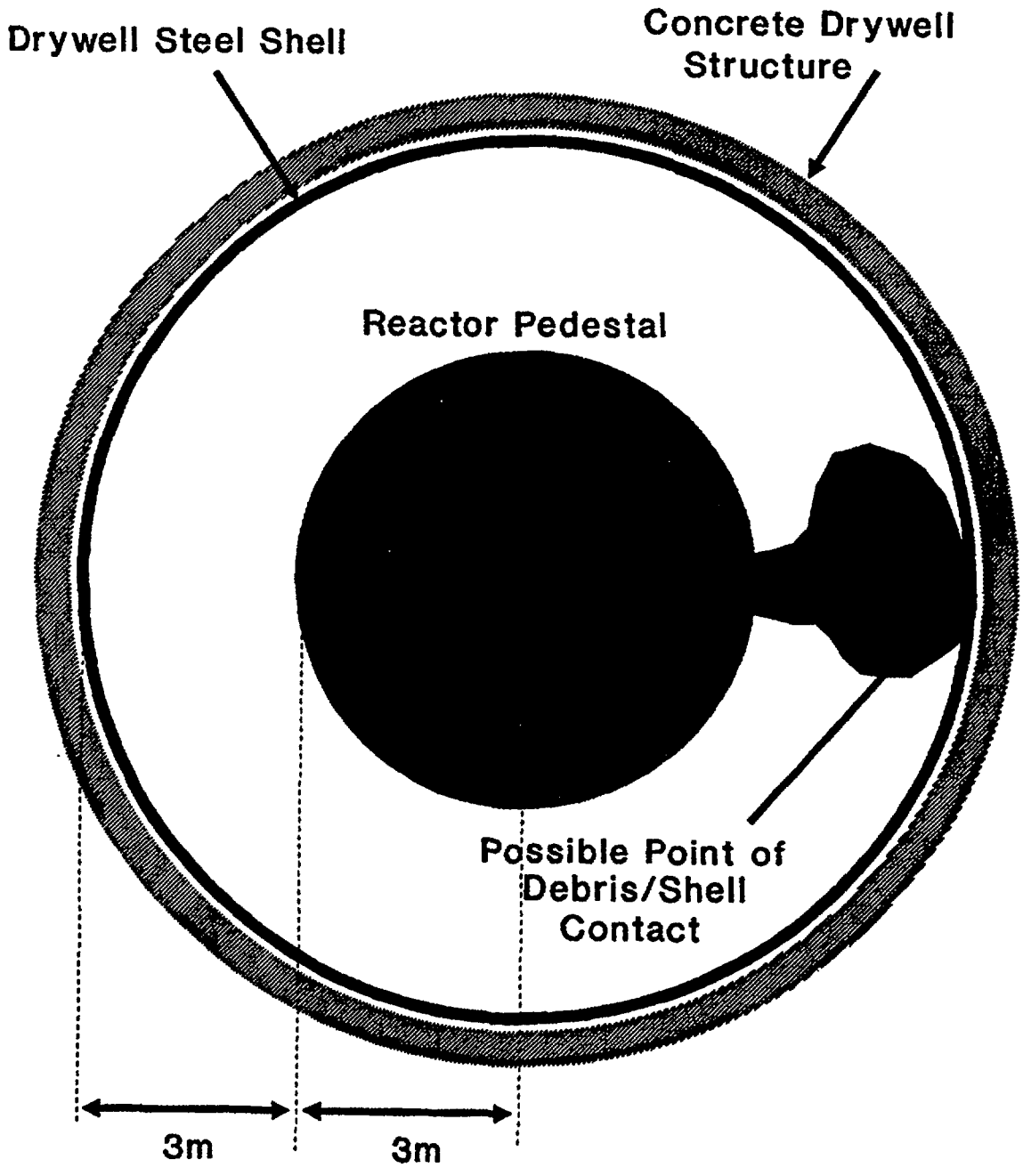

Figure C.7.2 Configuration of Peach Bottom drywell shell/floor—horizontal cross section.

5. Presence (or lack of) water on drywell floor before debris is expelled from reactor vessel.*	Yes: Sufficient to overfill sumps and replenishable No: No water on drywell floor

To account for the possibility that any permutation of these parameters may be important, the conditional probability of containment failure is quantified for each of the 48 cases. For each case, the containment failure probability is allowed to vary with time (after reactor vessel failure).

The uncertainties considered in characterizing the failure probabilities for each case include:

- Heat transfer characteristics of the debris on the concrete floor (e.g., thermal properties of melt and concrete, heat transfer coefficients for competing mechanisms, physical configuration of debris constituents, rate of internal heat generation).
- Heat transfer characteristics of the melt/steel shell interface (e.g., anticipated configuration and composition of debris in contact with steel, mechanism(s) for deterioration of shell thickness, properties of interfaces between debris and steel, and the steel shell and materials outside the shell).
- Debris transport characteristics when flowing across drywell floor (e.g., rheology of molten corium, drywell floor area covered by debris, barriers to flow—sump pits, pedestal wall).
- Structural behavior of the carbon steel drywell shell when in contact with molten material (e.g., formation of eutectics, alternative failure mechanisms).

C.7.2 Technical Bases for Issue Quantification

This issue was presented to a panel of six experienced severe accident analysts:

David Bradley—Sandia National Laboratories,
Michael Corradini—University of Wisconsin,
George Greene—Brookhaven National Laboratory,
Michael Hazzan—Stone & Webster Engineering Corp.,
Mujid Kazimi—Massachusetts Institute of Technology, and
Raj Sehgal—Electric Power Research Institute.

The panelists' individual judgments for the conditional probability of containment failure by drywell shell meltthrough formed the basis for quantifying this issue. Each of the panelists used the results of several published analyses in their deliberations. References C.7.1 through C.7.6 are among those identified by the panelists as having had an influence on their technical judgments. Complete documentation of the elicitation of expert judgment is provided in Reference C.7.7. A summary of the probability distributions that were generated by this process and a description of important areas of agreement and disagreement are presented below.

Each panelist generated a conditional probability distribution for each of the 48 cases outlined above. However, as will be shown, the uncertainties associated with this issue (i.e., the divergence in quantitative judgment among the panelists) are quite large. Although collectively divergent, the panelists' judgments are individually self-consistent. As a result, the collective judgment of the panel for all cases can be reasonably characterized by a handful of aggregate probability distributions. To preserve the true characteristics of the panel's case-by-case judgments, however, the distributions for individual cases are retained in the analysis for Peach Bottom documented in Reference C.7.8 (refer to Section C.7.3). The aggregate distributions are quite useful for illustrating important similarities and differences in the rationales of the panelists and are discussed later.

Before discussing specific topics dominating uncertainty, it should be noted that there are some aspects of this issue on which the technical community appears to agree. The appropriate failure criterion for the drywell steel shell is generally accepted as a shell temperature exceeding 1100–1300K. This range

*This parameter includes the effects of spray operation.

envelopes the uncertainties related to alternative mechanisms for failure of the drywell pressure boundary. At the lower end of this range, breach of the drywell pressure boundary could occur by creep rupture, particularly at elevated containment pressures. Alternatively, localized penetration of the steel shell by molten debris might occur if the debris in contact with the shell is sufficiently hot.

It is also generally agreed that the composition and temperature of the debris exiting the reactor pressure vessel are important properties to characterize when estimating the likelihood of hot debris reaching the drywell floor/wall interface. Specifying these properties, however, is limited by large uncertainties in core melt progression. These uncertainties have been treated parametrically (i.e., they are addressed through the case structure outlined above).*

Unfortunately, the harmony ends here. Most panelists expressed a strong allegiance to a specific technical rationale that, in many cases, was physically inconsistent with rationales expressed by other panelists. These dramatic differences in technical judgment reflect the polarized views on this issue that have developed in recent years. Over the full spectrum of plausible severe accident conditions, roughly half the technical community (as represented by the expert panel) appears to believe with near certainty that the drywell shell will fail following many core meltdown accidents; the other half is equally certain that it will not fail. If drywell shell meltthrough does occur, the containment pressure boundary is most likely to be breached within the first hour following reactor vessel penetration.

The variation of the conditional probability of drywell meltthrough among the 48 cases considered in this issue is not very wide. The net probability (i.e., arithmetic average of all panelists) of drywell shell meltthrough is no smaller than 0.33 and no larger than 0.87. The lowest failure probabilities correspond to cases in which water is assumed to cover the drywell floor; the highest correspond to cases in which the drywell floor is dry and debris flow rate, debris temperature (superheat), and debris unoxidized metal content are all at the high end of their range.

An illustration of the overall result for this issue is shown in Figure C.7.3. As mentioned above, the probability distributions for the 48 cases examined as part of this issue can be aggregated into five classes without introducing substantial error. These are displayed in the figure. Two classes characterize all the cases with low or medium flow rates of debris from the reactor vessel. The only single parameter significantly affecting the failure probability for these cases is the presence (or lack) of replenishable water on the drywell floor (all other parameters are observed to have a relatively minor influence on the probability of failure). Each of the remaining three classes represent "high flow" cases; one represents cases with water covering the drywell floor, and two represent cases without water on the drywell floor. Again, the presence (or lack) of water is the only single parameter significantly affecting the outcome. The values of other parameters (in certain combinations) influenced the panelists' judgments for these cases, however. The highest probability of drywell shell meltthrough is observed for cases in which two of the remaining three parameters take on values at the high end of their range (denoted 2/3H in the figure's legend). Lower values are observed when at least two of the three parameters take on low values (denoted 2/3L).

A conclusion that might be drawn from Figure C.7.3 is that the probability of drywell shell meltthrough is lowered by ensuring the presence of water on the drywell floor. This position is supported by some, but not all, of the panelists. It is important to keep in mind that the values displayed in Figure C.7.3 are averages of individual experts' judgments. As such, they tend to mask the divergence of technical views on many of the topics important to quantifying this issue. In this appendix, we do not intend to elaborate on the details of technical rationales expressed by individual panelists. The reader is encouraged to study Reference C.7.7 to gain a more thorough understanding of the phenomena and modeling assumptions disputed within the technical community. The following example is provided, however, to illustrate the divergence of technical views and explain why the average value of drywell shell meltthrough, displayed in Figure C.7.3, can be misleading.

Figure C.7.4 displays the probability distributions generated by each panelist for four specific cases. The case definition is noted in the legend on each plot. The upper two cases represent scenarios with low core debris flow rates. The case shown in the upper left represents a scenario in which the drywell floor is dry;

*The relative likelihood of one case over another is treated as a separate issue.

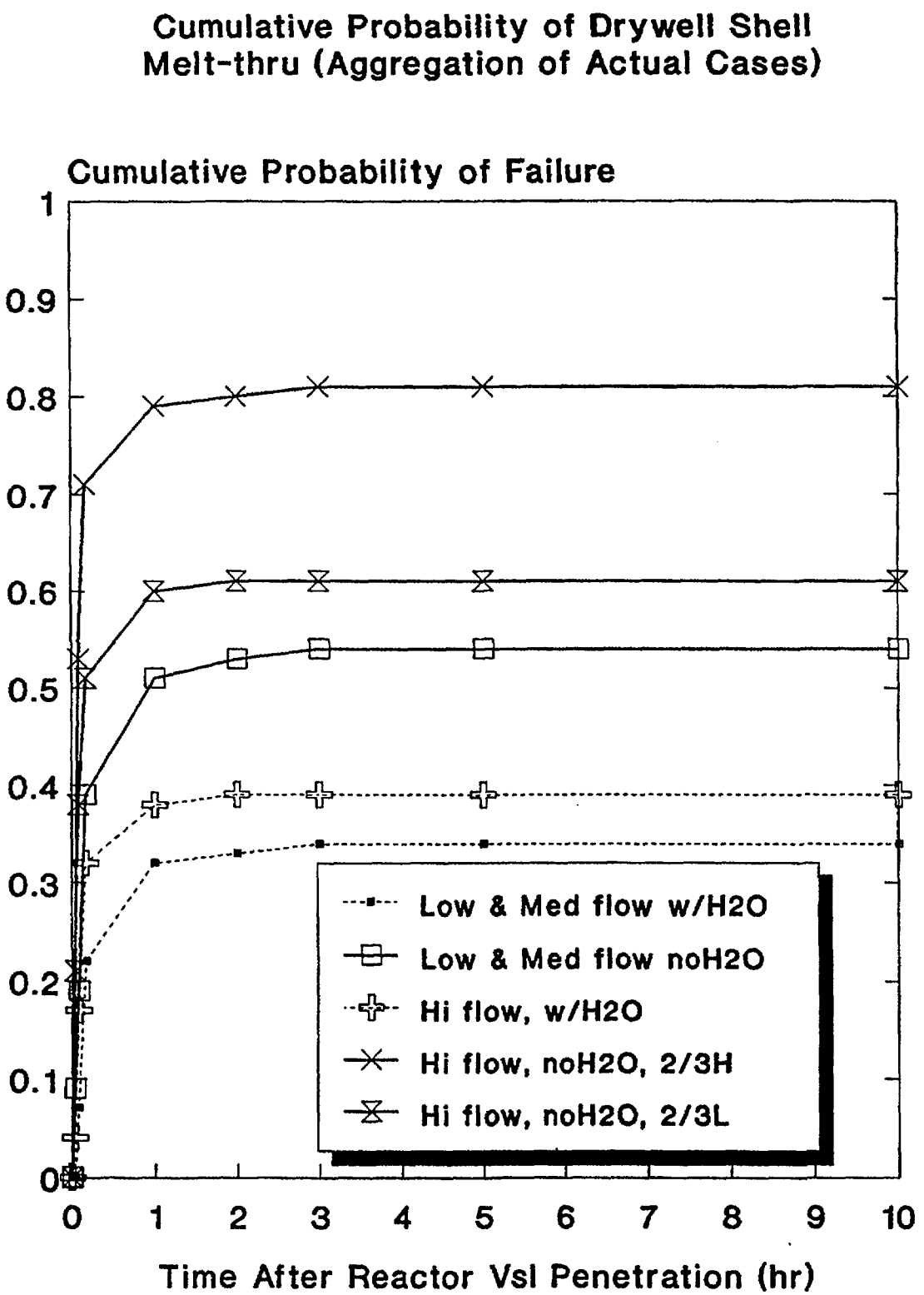

Figure C.7.3 Aggregate cumulative conditional probability distributions for Peach Bottom drywell shell meltthrough.

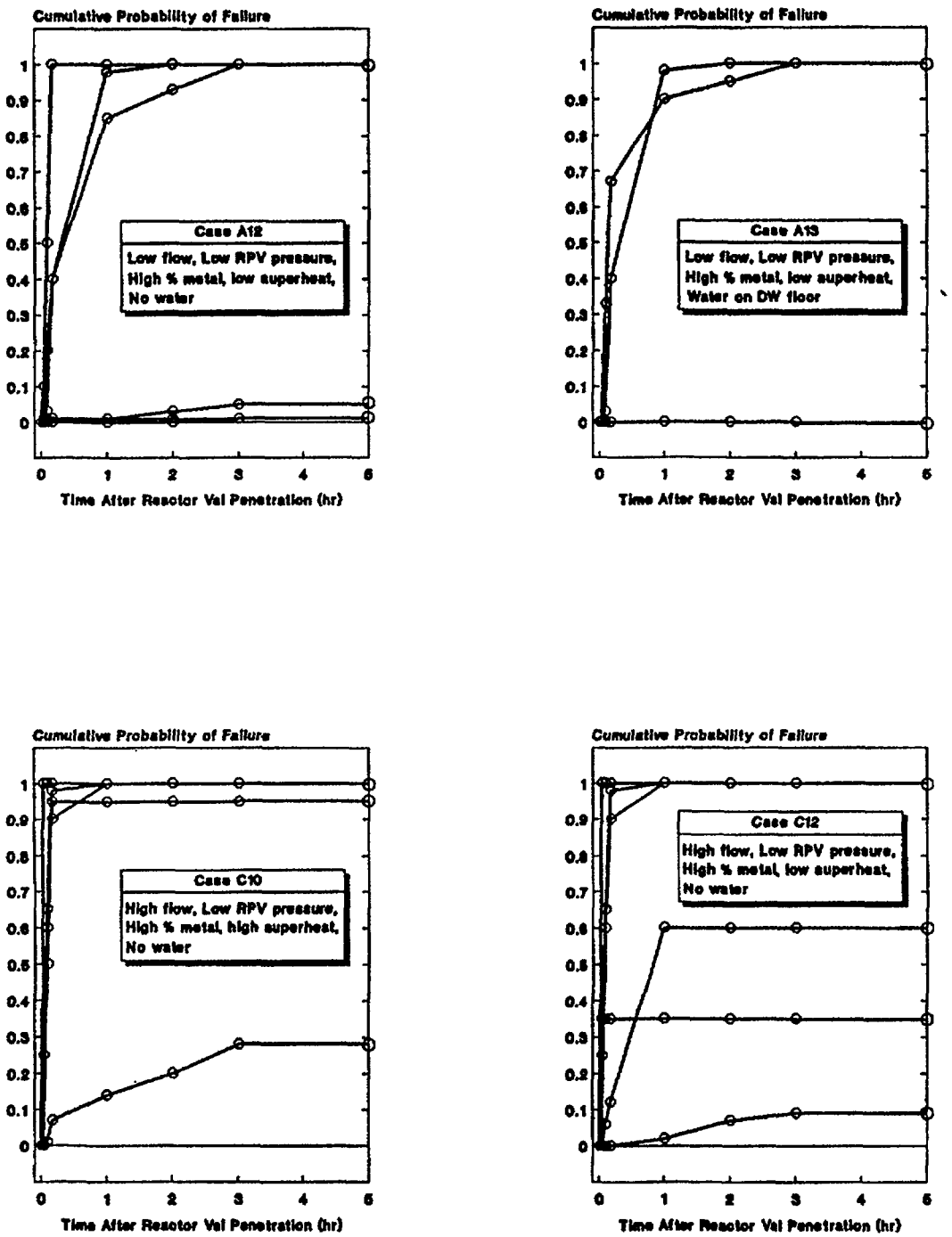

Figure C.7.4 Cumulative probability distributions composite of individuals on expert panel for this issue. (Six panelists (6 curves) are shown for each of four cases.)

the case shown in the upper right represents a scenario in which sufficient water accumulates on the floor to overfill the drywell sump. The lower two plots depict the results for two of the high flow cases (both without water on the drywell floor). One (lower left) assumes a high fraction of unoxidized metals in the melt, high debris temperatures, and low reactor pressure vessel pressure (i.e., class 2/3H in Fig. C.7.3). The plot in the lower right corner differs only by the assumption of low debris superheat.

Two important observations should be noted. First, the individual panelists' judgments appear binary (i.e., taking on values very near zero or unity). The results for the majority of cases appear this way, with at least one panelist providing a judgment at each end of the spectrum. Intermediate values were provided for relatively few cases, such as case C12 shown in the lower right corner of Figure C.7.4. This divergence of quantitative judgment explains why the values for the average probability appear constrained between 0.3 and 0.8. The average value for case A12 (upper left) is approximately 0.5 because three panelists provided values of 1 and three values of 0. In quantifying case A13 (upper right), one of the three panelists who was certain failure would occur in case A12 felt that the addition of water would prevent molten debris from reaching the drywell wall and, thus, changed his judgment from 1 to 0 for case A13. The other two panelists believe that the debris would be largely unaffected by the presence of water on the floor and did not alter their quantitative judgment. The average failure probability, therefore, changed from 0.5 to 0.33. A similar, but less dramatic, effect is observed in cases C10 and C12 (lower two plots) for which the average values changed from 0.87 to 0.68, respectively.

The second observation is that, despite an apparent consensus among panel members that the largest source of uncertainty for this issue is the initial conditions (i.e., state of core debris and drywell floor prior to reactor vessel penetration), dramatically different quantitative judgments were provided for the same initial conditions. Moreover, most panelists were very confident that their judgments were correct for many cases (i.e., a conditional probability of 1.0 or zero was provided for several types of conditions). In reviewing the elicitation of the expert panelists, one difference in rationale appears to have had a strong influence on their judgments. Some panelists believe that the flow of corium across the drywell floor is hydrodynamically limited (i.e., governed by the rheology and transport properties of the flowing core debris/concrete mixture). Others believe that the flow is thermodynamically limited (i.e., governed by the heat transfer characteristics of the mixture).

C.7.3 Treatment in PRA and Results

The probability distributions for this issue were implemented in the Peach Bottom accident progression event tree. This tree provides a structured approach for evaluating the various ways in which a severe accident can progress, including important aspects of RCS thermal-hydraulic response, core melt behavior, and containment loads and performance. The accident progression event tree is a key element in the assessment of uncertainties in risk by accommodating the possibility that a particular accident sequence may proceed along any one of several alternative pathways (i.e., alternative combinations of events in the severe accident progression). The probability distributions (or split fractions) for individual and combinations of events within the tree provide the rules that determine the relative likelihood of various modes of containment failure.

Drywell shell meltthrough is represented as an explicit event in the Peach Bottom accident progression event tree, and the probability assigned to it is dependent upon the path taken through the tree. For example, each path through the tree involves events that imply a particular combination of initial conditions for a potential challenge to drywell integrity. Values for each of the parameters defining the case structure outlined in the previous section are, therefore, established by the outcome of events occurring earlier in the tree. For example, one path may imply conditions of low reactor vessel pressure (perhaps caused by early actuation of the automatic depressurization system), high unoxidized metal content in the debris leaving the reactor vessel (from low in-vessel cladding oxidation), low debris temperature and low flow rates of debris leaving the reactor vessel (from a small hole size in the reactor vessel lower head), and, finally, no water on the drywell floor (failure of drywell sprays). For these conditions, the conditional probability of drywell shell meltthrough is represented by the distributions for case A12 (shown in Fig. C.7.4).

The distributions generated by each of the panelists are given equal weight in the accident progression event tree analysis. This is accomplished by generating an aggregate distribution for each case in the case structure that represents the composite judgment of the expert panel. The aggregate distribution is

generated by averaging the distributions prepared by the panelists. This is equivalent to randomly sampling values from each panelist's distribution but constraining the sampling process to ensure that each distribution is sampled an equal number of times. Additionally, drywell shell meltthrough is treated as a nonstochastic event (i.e., it either occurs or it does not occur). Therefore, the conditional probabilities generated by the expert panel are appropriately converted to event tree branch probabilities of 1 or zero. For example, if a conditional probability of failure equal to 0.3 is selected for a particular path in the event tree, a branch point probability of 1 would be assigned to that branch in 30 percent of the sample members. Likewise, a value of zero would be assigned for the other 70 percent of the sample members. Recall that the method used to perform the statistical uncertainty analysis is one involving multiple passes through the accident progression event tree. The values of the branch point probabilities are allowed to change from one pass to the next, generating a distribution of possible accident outcomes.

An indication of the importance of drywell shell meltthrough on the results of the Peach Bottom accident progression analysis is the mean probability that accident sequences contributing to the total core damage frequency are estimated to result in this mode of containment failure. Table C.7.1 shows the mean conditional probability of drywell shell meltthrough for several important core damage accident groups.

Another indication of the importance of drywell shell meltthrough on the Peach Bottom results is the decrease in the mean conditional probability of containment failure (i.e., given a core damage accident) when shell meltthrough is assumed to be impossible. The mean probability of early containment failure (frequency-weighted for all accident sequences*) for the base case analysis (i.e., with the drywell shell meltthrough probabilities outlined above) is 0.56. This value decreases to 0.20 if drywell shell meltthrough is assigned a probability of zero. The remaining (20%) probability of early containment failure results from other containment failure mechanisms such as overpressure failure and ex-vessel steam explosions. The latter are described further in Section C.9.

Drywell shell meltthrough is also an important contributor to each of the measures of risk for Peach Bottom. For example, Peach Bottom severe accident progressions (from all types of accident sequences) that result in drywell shell meltthrough contribute approximately 70 percent of the mean estimate for latent cancer fatality risk and 60 percent of the mean estimate for early fatality risk.

Table C.7.1 Probability of drywell shell meltthrough (conditional on a core damage accident of various types).

Type of Core Damage Accident	Mean Frequency* of Accident Type	Mean Probability of Drywell Shell Meltthrough
LOCAs	1.50E-7	0.32
Transients	1.81E-7	0.32
Station blackout	2.08E-6	0.44
ATWS	1.93E-6	0.42

*These frequencies consider internally initiated events only.

REFERENCES FOR SECTION C.7

C.7.1 M.G. Plys, J.R. Gabor, and R.E. Henry, "Ex-Vessel Source Term Contribution for a BWR Mark-I," International ANS/ENS Topical Meeting on Thermal Reactor Safety (San Diego, CA), February 1986.

C.7.2 L.S. Kao and M.S. Kazimi, "Thermal Hydraulics of Core/Concrete Interaction in Severe LWR Accidents," MIT Nuclear Engineering Dept., MITNE-276, June 1987.

C.7.3 S.A. Hodge, "BWRSAT Approach to Bottom Head Failure," Presentation to NUREG-1150 Review Group, November 1987.

*These frequencies consider internally initiated events only.

C.7.4 D.A. Powers, "Erosion of Steel Structures by High Temperature Melts," *Nuclear Science and Engineering*, 88, 1984.

C.7.5 G.A. Greene, K.R. Perkins, and S.A. Hodge, "Mark I Containment Drywell, Impact of Core/Concrete Interactions on Containment Integrity and Failure of the Drywell Liner," *Source Term Evaluation for Accident Conditions*, paper IAEA-SM-281/36, IAEA, Vienna, Austria, October 26–November 1, 1985.

C.7.6 J.J. Weingardt and K.D. Bergeron, "TAC2D Studies of Mark I Containment Drywell Shell Meltthrough," Sandia National Laboratories, NUREG/CR-5126, SAND88-1407, August 1988.

C.7.7 F.T. Harper et al., "Evaluation of Severe Accident Risks: Quantification of Major Input Parameters," Sandia National Laboratories, NUREG/CR-4551, Vol. 2, Revision 1, SAND86-1309, December 1990.

C.7.8 A.C. Payne Jr., et al., "Evaluation of Severe Accident Risks: Peach Bottom Unit 2," Sandia National Laboratories, NUREG/CR-4551, Vol. 4, Draft Revision 1, SAND86-1309, to be published.*

*Available in the NRC Public Document Room, 2120 L Street NW., Washington, DC.

C.8 Containment Strength Under Static Pressure Loads

Since the containment building of a nuclear power plant constitutes the ultimate barrier between the in-plant environment and the outside atmosphere, its anticipated performance during a severe accident has a substantial impact on the risk characteristics of the plant. Uncertainty regarding the capability of a containment to withstand the challenges associated with severe accidents can, therefore, be an important contributor to the uncertainty in risk.

In the risk models of this study, determining containment performance involves assessing the probability that the containment would be breached under a range of hypothesized severe accident conditions. In addition to the likelihood of failure, other critical factors in the characterization of containment performance are:

- *Failure size:* The larger the hole in the containment, the more rapid the escape of radioactive material in the containment atmosphere to the outside environment. This reduces the time available for radioactive material to deposit within the containment building and also reduces the opportunity for effective offsite emergency response.

- *Location of failure:* The retention of radioactive material by a breached containment building may be highly dependent upon the location of failure relative to containment systems designed to mitigate accident conditions. For example, in an ice condenser containment, failure of the containment in the lower compartment permits radioactive material to bypass the ice compartments while escaping to the outside environment. In contrast, containment failure in the upper compartment, provided the ice condenser is not degraded, requires that radioactive material pass through the ice compartments before escaping to the outside. In the latter case, retention of material by the ice would substantially reduce the radioactive release.

Consideration of these elements of containment performance, in conjunction with assessment of the degree and the timing of potential challenges to the containment, provides the basis for determining the likelihood and the consequences of scenarios involving containment failure.

C.8.1 Issue Definition

This issue addresses the response of each of the five containments to the potential pressure loads associated with severe accident conditions. Other containment failure mechanisms, such as penetration by missile, structural failure due to impulse loads (e.g., from hydrogen detonation), and meltthrough by molten material, are excluded from the scope of this issue. These are discussed elsewhere in Appendix C.

The set of plants evaluated in this study was selected to encompass a broad spectrum of containment designs. Consequently, details of important severe accident conditions and modes of containment response differ substantially among the plants analyzed. For this reason, the issue of containment performance is discussed largely on a plant-specific basis. However, it is possible to characterize broadly the range of qualitatively distinct pressure loads that may result from severe accident conditions. These are:

- *Gradual pressure rises:* Gradual pressurization of the containment building would result from the protracted generation of steam and noncondensible gases through the interaction of molten core material with the concrete floor beneath the reactor vessel. This pressurization process could last from several hours to several days, depending upon accident-specific factors such as the availability of water in the containment and the operability of engineered safety features. An additional mechanism for gradual pressurization in BWR pressure-suppression containments is the generation of steam from the suppression pool in the circumstance that pool heat removal capability is degraded.

- *Rapid pressure rises:* The high-pressure expulsion of molten material from the vessel, the deflagration of combustible gases, and the rapid generation of steam through the interaction of molten fuel with water in the containment are phenomena that could lead to pressure rises in the containment over a period of a few seconds. Such pressure rises may be viewed as rapid in a thermophysical context; however, from a structural perspective, they are effectively static. It is

essential, nevertheless, to distinguish between gradual and rapid pressure rises in the characterization of containment performance since the rate of pressure increase may have a significant influence upon determining the ultimate mode of containment failure.

This influence stems from the possibility of multiple containment failures or the development of one failure mode into another more severe mode. For example, where gradual containment pressurization results in containment breach by leakage, the pressure relief associated with the leak prevents further pressurization, and, thus, precludes more severe modes of containment failure. For rapid pressure rises, however, an induced leak would not preclude continued pressurization of the containment and, therefore, a more severe failure of the containment building could ultimately result. Hence, while the distinction between gradual and rapid pressure rises will not influence the pressure at which failure first occurs, it may influence the ultimate severity of that failure.

While the question of containment failure location is largely specific to the individual containment geometries, the approach to characterizing potential failure sizes is more generic. Three possible failure sizes were distinguished in this study: leak, rupture, and catastrophic rupture. Working quantitative definitions of each failure size were based on thermal-hydraulic evaluations of containment depressurization times.

- A leak was defined as a containment breach that would arrest a gradual pressure buildup but would not result in containment depressurization in less than 2 hours. The typical leak size was evaluated for all plants to be on the order of 0.1 ft^2.
- A rupture was defined as a containment breach that would arrest a gradual pressure buildup and would depressurize the containment within 2 hours. For all plants, a rupture was evaluated to correspond to a hole size in excess of approximately 1.0 ft^2.
- A catastrophic rupture was defined as the loss of a substantial portion of the containment boundary with possible disruption of the piping systems that penetrate or are attached to the containment wall.

A panel was assembled to address issues of containment structural performance with severe accident loads. Its members were:

D. Clauss, Sandia National Laboratories,
C. Miller, City College of New York,
K. Mokhtarian, Chicago Bridge and Iron, Inc.,
J. Rashid, ANATECH,
W. Von Riesemann, Sandia National Laboratories,
S. Sen, Bechtel,
R. Toland, United Engineers and Constructors,
A. Walser, Sargent and Lundy,
J. Weatherby, Sandia National Laboratories, and
D. Wesley, IMPELL.

The experts provided distributions that defined the probability of failure as a function of pressure and of the mode and location of failure. The distinction between rapid and gradual static pressurization cases in determining ultimate failure size was treated within the methodological framework of this study (see Section C.8.3). The experts only addressed initial failure sizes (i.e., they did not distinguish between the rapid and gradual pressurization cases).

C.8.2 Technical Bases for Issue Quantification

Detailed structural evaluations of various scopes exist for each of the containments assessed by the expert panel. These evaluations, supplemented by calculations performed by the experts in support of the elicitation process, provided the basis for quantification of this issue for each plant.

Zion

The Zion large, dry containment building, shown in Section C.5, is a concrete cylinder with a shallow-domed roof and a flat foundation slab. The thickness of the concrete is 3.5 feet in the walls, 2.7

feet in the dome, and 9 feet in the basemat. The containment wall and dome are prestressed by a system of tendons, with each tendon composed of 90 1/4-inch-diameter steel wires, while the foundation slab is reinforced with bonded, reinforcing steel. The entire structure is lined with a 1/4-inch welded steel plate attached to the concrete by means of an angle grid, stitch-welded to the liner plate, and embedded in the concrete. The free volume of the containment is approximately 2.6 million cubic feet and its design internal pressure is 47 psig.

The three experts who addressed the Zion containment performance issue had access to existing detailed structural calculations of containment response at Zion reported in References C.8.1 to C.8.3.

Two potential failure locations were identified by the expert panel: in the midsection of the cylindrical wall and at the junction between the basemat and the wall. Based upon source term considerations, the distinction between these failure locations was preserved in the risk analyses since failure in the cylindrical wall permits a direct release of radioactive material to the outside environment while failure at the cylinder-basemat intersection occurs approximately 16 feet below ground level. Some degree of ex-containment fission product decontamination prior to atmospheric release would, therefore, be anticipated in the latter case.

The mechanism for failure in the midsection of the cylindrical wall was assessed to be yielding of the hoop tendons. To develop probability distributions over potential failure pressures, a range of failure criteria of 1 to 2 percent strain in the hoop tendons was assumed. The resulting probability of failure was in the pressure range of 130–140 psig. Leak was anticipated to be the predominant failure size for failure pressures up to 138 psig. For higher failure pressures, breach by rupture was assessed to be more likely. The possibility that failure would first occur at pressures up to 150 psig was also identified, in which case catastrophic rupture was assessed to be the most likely failure size. However, it was believed that for gradual pressurization cases, the prior occurrence of a leak due to a tear in the liner would likely preclude catastrophic failure of the containment. Reference C.8.1 constituted the main analytical basis for evaluation of this failure location.

The alternative containment breach location identified involved the cracking of concrete at the shear discontinuity between the cylinder wall and the basemat. Only one of the three experts assessed this failure mode to be credible based primarily on Reference C.8.2. Uncertainty in the failure pressure associated with this location was broad. The bulk of probability was assigned to the failure pressure range of 110–180 psig. Failure by leak was assessed to be the most likely size of breach at the wall-basemat junction, although containment rupture was identified as a possibility toward the upper end of the failure pressure range.

Figure C.8.1 displays the range of failure pressures for the Zion containment at the 5th–95th percentile levels. This range is 108–180 psig, which includes all failure sizes and locations. It is based on the distribution that resulted from aggregation of the three expert-specific probability distributions.

Surry

The Surry containment building, depicted in Section C.5, is comprised of a vertical right cylinder with a hemispherical roof and a flat foundation slab. It is constructed from reinforced concrete and lined with a 1/4-inch steel plate. The containment atmosphere is maintained during operation at below ambient pressure (at approximately 10 psia), the design internal pressure is 45 psig, and the containment free volume is 1.8 million cubic feet.

Four experts addressed the issue of containment performance at Surry. The limited availability of structural calculations for the Surry containment led the experts to rely partially upon detailed calculations performed for similar containments, such as Indian Point (Ref. C.8.3).

All failure locations identified for Surry provided direct pathways to the outside environment and the distinction between these locations was, therefore, unnecessary from a risk perspective. Yielding of one of the steel hoop bars that reinforce the vertical concrete wall was identified as a likely mode of failure by all the experts. The likely location of failure was assessed to be near the intersection of the wall with the dome. Evaluation of this failure location was based partially upon the analysis of Reference C.8.4. Leakage due to the formation of a tear in the steel liner was also identified as the most likely failure mode

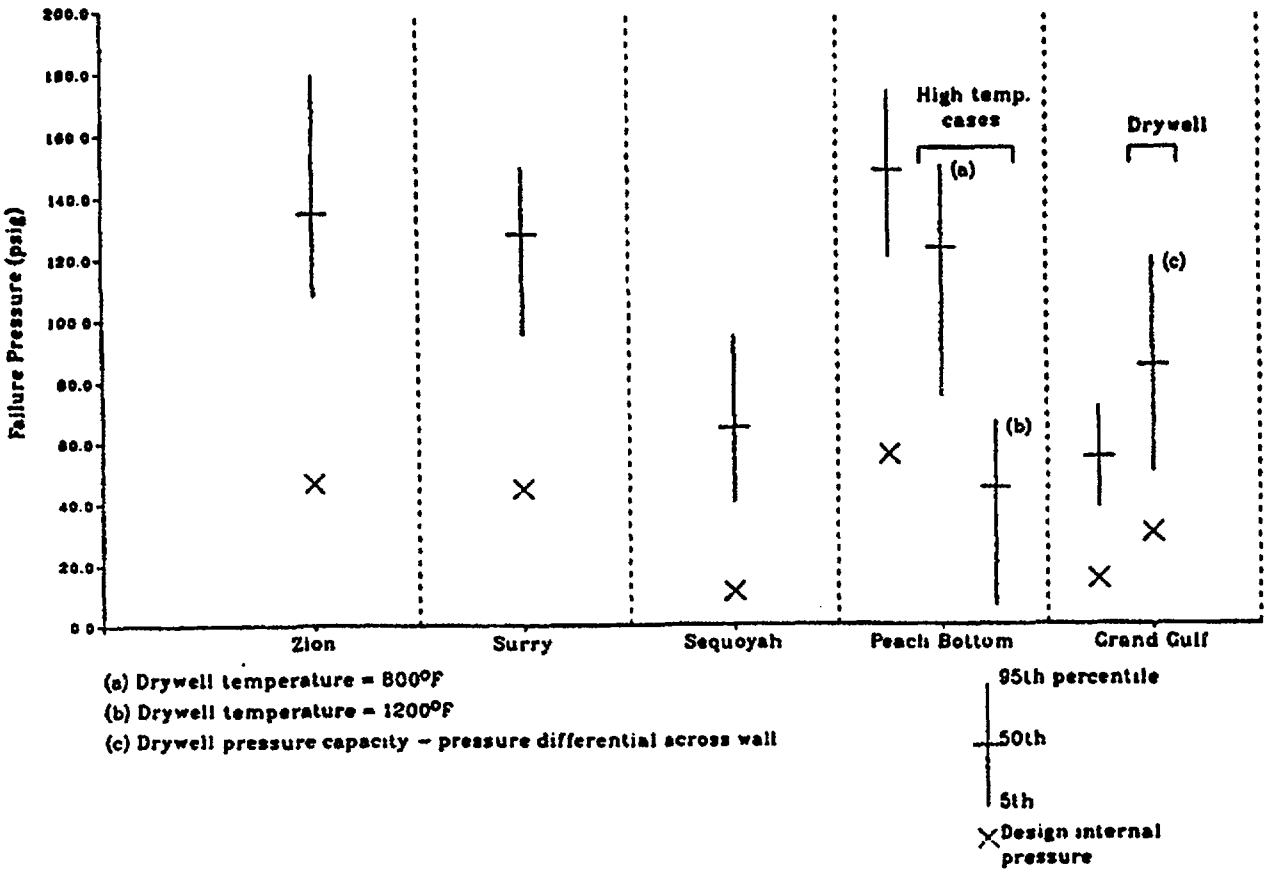

Figure C.8.1 Containment failure pressure.

in light of the results of the 1:6 scale model reinforced concrete containment test performed at Sandia National Laboratories (Ref. C.8.5). Other potential modes of containment breach identified were failure around pipe and electrical penetrations and failure due to distortion of the hatch opening. However, no consensus existed regarding the credibility of these other modes.

The probability distribution over potential failure pressures resulting from aggregating the distributions of each expert is summarized in Figure C.8.1. The 5th–95th percentile range of potential failure pressures extends from approximately 95 psig to 150 psig. Leakage was assessed as the most likely mode of failure for breaches occurring up to 140 psig, while ruptures were the most likely modes of breach for failure pressures in the 140–150 psig range. While higher failure pressures were judged unlikely, the dominant mode of failure beyond 155 psig was assessed to be catastrophic rupture.

Sequoyah

The Sequoyah ice condenser containment, shown in Section C.4, is a freestanding steel structure consisting of a cylindrical wall, a hemispherical dome, and a bottom liner plate encased in concrete. The cylinder varies from 1-3/8-inch thickness (at the bottom) to 1/2 inch (at the dome junction); the dome varies from 7/16-inch thickness (at the cylinder junction) to 15/16 inch (at the apex); and the bottom liner plate is 1/4-inch thick. Vertical and horizontal stiffeners are provided on the outside of the shell. Three volumes comprise the inside of the containment shell: the lower compartment, the ice condenser,

and the upper compartment. The reactor vessel and reactor coolant system are located in the lower compartment. The ice condenser consists of an annular volume that partially lines the containment wall (subtending an angle of 300 degrees at the center of the containment) and is comprised of a series of ice compartments located between an upper and a lower plenum. The ice condenser is lined with corrugated steel insulating panels designed to withstand an outside pressure of 19 psig. The role of the ice condenser is that of a passive heat sink intended to reduce steam pressures generated in design basis accident conditions.

The only significant structure within the upper compartment is the polar crane. Since the containment is equipped with the ice condenser pressure-suppression system, it is designed to an internal pressure of only 10.8 psig, with a free volume of 1.2 million cubic feet. A concrete shield building surrounds the steel shell. However, it is not a significant barrier to fission product release since its pressure capacity is substantially less than that of the shell.

Structural assessment of the Sequoyah containment required certain severe accident considerations specific to the ice condenser design. The location of containment failure relative to the position of the ice condenser and the structural integrity of the ice condenser are crucial factors in determining the concomitant radioactive release. If the route taken by radioactive aerosols to the outside environment involves passage through the ice, significant retention of radioactive material within the containment would be expected. Failure of the containment in the lower compartment or significant disruption of the ice would involve bypass of the ice compartments. Since the ice condenser constitutes the only passageway from the reactor vessel to the upper compartment, failure in the latter will avoid ice condenser bypass. Ultimately, however, the effect of failure location upon the source term is determined by the availability of ice, which in turn is dependent upon the accident sequence under consideration.

A further concomitant of the compartmentalized nature of the ice condenser containment is the possibility of localized accumulations of hydrogen and the possibility of containment failure through hydrogen deflagration or detonation. While the issue of containment response to hydrogen deflagration was subsumed in the case of rapid pressurization, the effects of hydrogen detonation and the associated dynamic loads were considered separately by the experts. Response of the Sequoyah containment to impulse loads is discussed in Section C.4.

Three experts addressed the issue of containment response to pressure loads at Sequoyah based on the detailed analyses of References C.8.1 and C.8.6 and on supplemental hand calculations. Membrane failure in the cylindrical wall of the upper compartment via either rupture or catastrophic rupture was identified as the most likely mode of containment failure. Failure criteria adopted involved a range of strain levels (2–10%) in the shell membrane. Since the ice condenser is attached to the cylindrical wall and subtends an angle of 300 degrees at the central containment axis, 5/6 of the ruptures in the wall of the upper compartment are expected to occur in the ice condenser. Catastrophic rupture of the wall, in contrast, would always fail the ice condenser.

One expert identified the possibility of failure in the lower compartment due to a crack in the weld at the point of embedment. Such a failure would result in ice condenser bypass. Based upon results of the 1:8 scale steel containment pressurization tests (Ref. C.8.7), two experts identified the possibility of containment leakage due to ovalization of the equipment hatch flange. The equipment hatch, a door 20 feet in diameter, is located in the upper compartment, and its failure would not result in ice condenser bypass.

Rupture or catastrophic rupture were assessed to be the most likely modes of failure in the Sequoyah containment. The only failure location associated with leakage involved ovalization of the hatch. While one expert predicted the occurrence of such a leak in the 65–70 psig range, a second expert believed that such a failure would not be likely to occur below 120 psig and that shell rupture would probably occur first. The third expert excluded this failure possibility completely. At the 5th–95th percentile levels, the range of failure pressures resulting from aggregating the individual expert distributions was 40–95 psig.

For all potential failure pressures, the probability of ice condenser bypass exceeded the probability of no bypass by factors of between 5 and 10. This stems from the dominance of the catastrophic rupture failure modes at Sequoyah. Catastrophic rupture is assumed always to fail the ice condenser since the ice compartments subtend most of the containment wall area. As discussed earlier, all failures in the lower

compartment bypass the ice. The probability distribution over potential failure pressures at Sequoyah is summarized in Figure C.8.1.

Peach Bottom

The Peach Bottom containment, shown in Section C.7, is of the Mark I pressure-suppression type. The steel "light-bulb-shaped" drywell that contains the reactor vessel is a steel spherical shell intersected by a circular cylinder. The top of the cylinder is closed by a head bolted to the drywell. The pressure-suppression chamber, or the wetwell, is a toroidal steel vessel located below and encircling the drywell. The wetwell and drywell are interconnected by eight circular vent pipes. The containment is enclosed by the reactor building, which also contains the refueling area, fuel storage facilities, and other auxiliary systems. In the event of primary system piping failure within the drywell, a mixture of drywell atmosphere and steam would be forced through the vents into the suppression pool resulting in steam condensation and pressure reduction. The design internal pressure of the containment is 56 psig and the free volumes of the drywell and wetwell are 159,000 cubic feet and 119,000 cubic feet, respectively.

From a source term perspective, the location of containment failure relative to the suppression pool and to structures external to the containment is important. Three experts evaluated containment performance at Peach Bottom. Based on prior detailed analyses of Mark I designs (Refs. C.8.1 and C.8.8) and on calculations supporting the opinion elicitation process, several failure locations were considered credible:

- *Wetwell above the water line.* In this case, the suppression pool would not be bypassed.
- *Wetwell below the water line.* Consequent drainage of the wetwell would effectively result in pool bypass.
- *Drywell near the vent pipes.* This would result in suppression pool bypass although some credit would be taken for fission product decontamination by the reactor building.
- *Drywell head.* In this case, the suppression pool would be bypassed although some credit would be taken for fission product decontamination in the refueling area.

The relative likelihood of leak versus rupture was considered dependent on the failure location and the associated failure mechanisms. For example, one expert assessed the relative likelihood of a leak occurring in the wetwell below the water line to be low since any leak at that location would develop rapidly into a rupture. The predicted failure mechanism was a crack in the hoop direction, which would rapidly unzip, given the absence of a mechanism to arrest the rupture.

Because of the small volume of the Peach Bottom containment, the possible effect upon containment pressure capacity of the high drywell temperatures expected to occur in scenarios involving the attack of concrete beneath the vessel by molten core debris was considered. Such temperatures could be as high as 800°F to 1200°F and might substantially reduce material strengths. One expert assumed, for example, that material strength in the drywell at the vent pipes would be reduced by between 25 percent and 90 percent and that gasket resiliency at the drywell head would be lost. Since wetwell temperatures were assessed to be at saturation, high drywell temperatures were determined to have little impact upon the pressure capacity of the wetwell.

In low-temperature conditions, the range of possible failure pressures for the Peach Bottom containment was determined to be 120–174 psig. This reflects the 5th–95th percentile interval of the probability distribution resulting from aggregating the expert-specific distributions. Conditional upon containment failure in the lower part of this range, 50 percent of probability was associated with leakage at the drywell head while the remaining failure probability was dominated by wetwell leakage above the suppression pool. At the top edge of the failure pressure range, wetwell rupture above and below the suppression pool were each assessed to account for 25 percent of the total failure probability, with catastrophic wetwell rupture accounting for a further 10 percent. Leakage in the drywell (principally at the head) accounted for approximately 25 percent of the conditional failure probability, with wetwell leakage accounting for the remaining 15 percent.

Two high drywell temperature cases were considered by the experts: 800°F and 1200°F. The 5th–95th percentile failure pressure ranges were assessed to be 75–150 psig and 6–67 psig, respectively. With the

drywell at 800°F, failure at the lower edge of the pressure range was assessed to be dominated by leakage in the drywell, principally (90% of the probability) through degradation of the head gasket. Toward the higher end of the failure pressure range, wetwell leaks above the suppression pool accounted for 30 percent of the failure probability, drywell leakage for a further 40 percent, and rupture at the drywell head for 12 percent. In the highest drywell temperature regime, i.e., 1200°F, the reduction in material strengths was assessed to ensure failure in the drywell. At the lower boundary of the failure pressure range, leakage in the drywell (principally at the head) was assessed to account for 95 percent of the failure probability while, at the upper boundary of the failure pressure range, drywell ruptures (principally in the main body of the drywell) were assessed to be as likely as leaks. Figure C.8.1 summarizes the aggregated probability distributions over possible containment failure pressures at Peach Bottom.

Grand Gulf

The Grand Gulf containment, shown in Section C.4, is of the Mark III pressure-suppression type. It is constructed from reinforced concrete lined with a 1/4-inch welded steel plate. The circular foundation mat, the cylindrical wall, and the hemispherical dome are 9.5, 3.5, and 2.5 feet thick, respectively. The containment volume is divided into two main compartments: the drywell, which is the central cylindrical volume of the containment and houses the reactor vessel; and the wetwell, which constitutes the outer annular volume and the dome. These compartments are connected at the base of the containment via an annular pool that provides a passive heat sink for steam in design basis accident conditions. The drywell wall, composed of reinforced concrete, is 5 feet thick and lined with 1/4-inch steel plate. Since the Grand Gulf containment is equipped with pressure-suppression features, its nominal design internal pressure is only 15 psig. The drywell has a design internal pressure of 30 psid (i.e., the differential pressure across the drywell-wetwell boundary). The free volumes of the wetwell and the drywell are 1.4 million and 270,100 cubic feet, respectively.

From a severe accident perspective, an important feature of the Mark III design is the relative configuration of the drywell, the suppression pool, and the wetwell. This configuration ensures that, provided the integrity of the drywell wall is not compromised, radioactive material released from the fuel would need to pass through the suppression pool to escape from the containment, if breached. This would result in significant radioactive material retention by the pool. In assessing performance of the Mark III, it is important, therefore, to determine the response to severe accident conditions not only of the outer containment but also of the drywell.

Given the low-pressure capacity of the Grand Gulf containment relative to anticipated pressure loads, the study project team assessed minimal uncertainty to be associated with response of the Grand Gulf containment to severe accident pressurization levels. To use expert resources most efficiently, therefore, the issue of static overpressurization at Grand Gulf was not taken to the expert panel on containment structural performance issues. The required probability distributions were developed by a structural expert at Sandia National Laboratories, who had been a member of the original panel. Detailed structural evaluations of containment performance at Grand Gulf reported in Reference C.8.1 provided a basis for the expert's evaluation. The dominant failure location of the containment due to static overpressurization was assessed to be at the intersection of the cylinder wall and the dome.

The lower bound of the Grand Gulf distribution over failure pressures was assessed to be approximately twice the design internal pressure. The upper distribution bound was identified with the calculated ultimate material strength of the steel-reinforced concrete containment. A distribution between these bounding points was then developed.

Pressure capacity distributions for the drywell were developed in a similar way. Based on the various potential failure locations in the drywell, the wall was assessed to be the weakest structure and therefore the most likely failure point. The expert determined that the failure criterion was, in terms of the pressure differential across the drywell, independent of the direction of the pressure gradient. At the 5th–95th percentile level, the range of potential failure pressures for the Grand Gulf containment and drywell were 38–72 psig and 50–120 psid, respectively. Figure C.8.1 summarizes the underlying probability distributions.

C.8.3 Treatment in PRA and Results

Within the accident progression event trees (APETs) developed in this study, the probability of containment failure associated with each identified accident progression path was determined by

comparing the value of the containment load selected from its distribution to the selected value of the load capability. As part of the overall uncertainty analyses, Monte Carlo methods were used to randomly select values for containment loads and load capacity from their distributions (Ref. C.8.9). Among the elements of each sample member were a containment failure pressure, with the corresponding failure size and failure location. For some plants, more than one load and capacity pair may be selected to simultaneously represent alternative challenges to containment integrity. In the Peach Bottom analysis, for example, one combination would dictate the containment pressure capacity, the failure size, and the failure location corresponding to rapid pressure rises at vessel breach. Another combination would characterize containment response to gradual pressure rises.

Each sample member also contained a series of pressure loads corresponding to load-generating events that occur over the time represented by the accident progression. For each accident progression, the loads and the load capacities in the sample member are compared in a time-ordered way. If the first load exceeds the corresponding pressure capacity, the containment is assumed to fail at that time (unless preceded by containment breach due to some other failure mechanism, such as impulse loading or thermal attack). The location and the size of the failure are specified in the sample member. A relative frequency of 1 (i.e., the split fraction) is then attached to the selected failure size and location conditional upon the prior path taken through the containment event tree. If none of the loads exceeded the pressure capacity, then the containment is assumed to retain its integrity unless breached by some other mechanism.

Based upon the findings of the expert panel on containment structural performance issues, the pressure at which a containment first failed was modeled to be independent of the pressurization rate. However, the ultimate size and location of failure was coupled to the pressurization rate in this study. Since the experts focused largely on the issue of the initial mode of containment failure, their distributions over failure size and location could not be used directly in the treatment of rapid pressure rises. For example, if leak were the initial failure size resulting from rapid pressurization, then, since a leak could not halt further pressurization, whether a more severe breach of the containment would occur subsequently was considered.

To generate probability distributions over ultimate failure modes in the case of rapid pressure rises, both the containment failure pressure and the peak pressure load in any one sample member were considered for each case. If the failure pressure exceeded the peak pressure, failure was assumed not to occur. If, however, the peak pressure exceeded the failure pressure, then a probability distribution over potential failure modes was constructed, which accounted for the possibility that containment rupture or catastrophic rupture could occur after a leak developed and before the peak pressurization level was reached. Sampling from this distribution provided the ultimate failure size and location.

In the Grand Gulf analysis, drywell and containment performance were evaluated in similar ways. Structural performance of the drywell became an issue for conditions in which a pressure differential is established across the drywell-wetwell boundary. This occurs in cases of rapid pressurization (e.g., hydrogen deflagration in the wetwell or loads from vessel breach) where the inertia of water in the suppression pool prevents immediate pressure equalization across the boundary. Within each sample member, the pressure differential for each accident progression was compared to the sampled drywell pressure capacity. High correlations were imposed in sampling from probability distributions over the drywell and the containment pressure capacities since the same basic uncertainties were involved in each.

Table C.8.1 summarizes the failure pressure ranges and the likely modes of containment overpressure failure identified by the expert panel for each plant.

The influence of the containment failure pressure on risk and uncertainty in risk for each plant is dependent ultimately on the predicted severe accident pressure loads and the relative likelihood of containment breach by other mechanisms, such as thermal attack. Since scenarios involving failure or bypass of the containment at or before vessel breach were found to be the dominant contributors to offsite risk, the importance of overpressure failure modes to risk may be characterized in terms of their contribution to bypass and early containment failures. Similarly, the importance of uncertainty in the failure pressure can be evaluated in terms of the impact upon the conditional probability of early containment failure of varying the failure pressure within its range of uncertainty. These importance

Table C.8.1 Containment strength under static pressure loads: summary information.

Plant	Containment Free Volume (Millions of Cubic Feet)	Design Internal Pressure (psig)	Failure Pressure Range(a) (psig)	Sizes/Locations Dominant Failure
Zion	2.6	47	108–180	Leak/rupture in cylinder wall or basemat/wall intersection
Surry	1.8	45	95–150	Leak/rupture near dome/wall intersection
Sequoyah	1.2	11	40–95	Gross rupture of the containment or rupture in the lower compartment
Peach Bottom	0.16 (drywell) 0.12 (wetwell)	56	120–174	Leak at drywell head or leak/rupture of wetwell
			high temp case: (b) 75–150	Leak at drywell head or in wetwell above suppression pool
			high temp case: (c) 6–67	Leak at drywell head or rupture of drywell wall
Grand Gulf	0.27 (drywell) 1.4 (wetwell)	15	38–72	Leak/rupture near dome/wall intersection
		Drywell: 30(d)	50–120 (d)	

(a) 5th–95th percentile range
(b) Drywell temperature at 800°F
(c) Drywell temperature at 1200°F
(d) Drywell/wetwell pressure differential in psi

measures are discussed briefly for each plant. For direct comparison among plants, attention is confined to internal initiating events.

Early containment failure scenarios dominate all offsite risk measures at Zion. The robustness of the Zion containment ensures, however, that the mean frequency of early containment breach conditional on core damage is small (approximately 1%). Ten percent of early containment failures are due to overpressure, the remainder being associated with in-vessel steam explosions (see Section C.9) and pre-existing containment isolation failures. Variations in the failure pressure within its range of uncertainty result in a minimal change to the risk profile at Zion, given the high strength of the containment relative to anticipated loads.

Similarly, the Surry containment appears to be extremely robust. Its mean frequency of early failure conditional on core damage is less than 1 percent. Accident scenarios involving bypass of the containment dominate all offsite risk measures while early containment failures contribute approximately one-quarter or less. Less than 60 percent of early failures are associated with containment overpressure. The remainder result from in-vessel steam explosions. As for Zion, variation of the containment failure pressure within its reasonable range of uncertainty would be expected to result in minimal change in the risk profile at Surry because of the high strength of the containment.

At Sequoyah, approximately 73 percent of mean early fatality risk results from scenarios involving bypass of the containment; the remaining mean early fatality risk is due to early containment failures in loss-of-offsite-power sequences. Early containment failures account for the remaining early fatality risk and for approximately one-half of the latent cancer fatality risk. Containment overpressure accounts for approximately 90 percent of early failures, while direct contact of molten debris with the steel containment, impulse loads from hydrogen detonation, in-vessel steam explosions, pre-existing isolation failures, and ex-vessel steam explosions constitute the remaining 10 percent. The mean frequency of containment failure conditional on core damage is approximately 7 percent. Comparison of this value with

the early failure frequency of the large, dry containments reflects the lower pressure capacity of the ice condenser design. The overlap between anticipated pressure loads and the range of containment failure pressures at Sequoyah leads to the conclusion that uncertainty in the overpressure criterion may have an impact on uncertainty in risk.

Scenarios involving early failure of the drywell dominate all offsite risk measures at Peach Bottom both because of the high mean conditional frequency of this mode of failure (approximately 50%) and because of the associated bypass of the suppression pool by radioactive material. The dominant mechanism for early drywell failure is attack of the drywell wall by molten debris on the cavity floor. The mean conditional frequency of early wetwell failure at Peach Bottom is approximately 3 percent. This is dominated by overpressure failures. The contribution to risk of early wetwell failure is minor, however (approximately 1% for the mean estimate of early and latent cancer fatality risk). Consequently, uncertainty in the failure pressure level at Peach Bottom has minimal influence upon uncertainty in risk.

At Grand Gulf, overpressurization is the dominant mechanism for failure of the containment and for failure of the drywell. Scenarios involving early failure of both the containment and the drywell are the principal contributors to all offsite risk measures. The mean frequency of these scenarios conditional upon core damage is approximately 20 percent. Variation of the containment failure pressure within its estimated range of uncertainty has a minimal impact on the performance of the Grand Gulf containment, given its low structural strength relative to the anticipated pressure loads, principally from hydrogen deflagration.

Considerable overlap exists between the range of drywell failure pressures and the range of anticipated pressure loads on the Grand Gulf drywell. The assumption that the drywell failure pressure lies toward the lower end of its uncertainty range could, therefore, result in a significant increase in mean offsite risk. The assumption of a high drywell failure pressure would not be expected to decrease risk significantly, however, since additional mechanisms exist for early failure of the drywell wall. These mechanisms involve pedestal collapse at the time of vessel breach, due either to overpressure or an ex-vessel steam explosion (see Section C.9), and subsequent failure of the drywell wall, due to damage incurred by penetrating pipes.

In summary, containment failures due to overpressure are significant contributors to risk at all plants except Peach Bottom. Uncertainty in structural failure pressure has the potential to significantly influence uncertainty in risk only for the Sequoyah containment and the Grand Gulf drywell. For other containment structures, there is limited overlap between the range of anticipated pressure loads and the uncertainty range of failure pressures.

More details of the treatment of containment structural performance issues in this study can be found in Reference C.8.10.

REFERENCES FOR SECTION C.8

C.8.1 IDCOR Technical Report 10.1, "Containment Capability of Light Water Nuclear Power Plants," July 1983.

C.8.2 S. Sharma et al., "Ultimate Pressure Capacity of Reinforced and Prestressed Concrete Containment," Brookhaven National Laboratory, NUREG/CR-4149, BNL-NUREG-51857, May 1985.

C.8.3 T.A. Butler and L.E. Fugelso, "Response of the Zion and Indian Point Containment Buildings to Severe Accident Pressures," Los Alamos Scientific Laboratory, NUREG/CR-2569, LA-9301-MS, May 1982.

C.8.4 W.J. Pananos and C.F. Reeves, "Containment Integrity at Surry Nuclear Power Station," Stone & Webster Engineering Corp., TP84-13, 1984.

C.8.5 R.A. Dameron et al., "Analytical Correlation and Post-Test Analysis of the Sandia 1:6-Scale Reinforced Concrete Containment Test," Fourth Workshop on Containment Integrity (Arlington, VA), June 14-17, 1988.

C.9 Containment Failure as a Result of Steam Explosions

A steam explosion is the result of rapid transfer of thermal energy from a hot liquid to water over a time scale of the order of milliseconds. Industrial experience has revealed that such explosions have the potential to do significant damage.

The possibility that certain severely degraded reactor core conditions, involving the flow of molten core material into a pool of water in the lower plenum of the reactor vessel, could be conducive to the occurrence of a steam explosion was first assessed in the Reactor Safety Study, WASH-1400. The in-vessel steam explosion scenario may be of particular significance in determining the risk profile of a nuclear power plant since, not only does this phenomenon allow the possibility of catastrophic pressure vessel breach, but the concomitant generation of a missile consisting of the upper head of the vessel could lead to failure of the containment building. An in-vessel steam explosion is a phenomenon, therefore, that could breach the last two barriers between fission products in the core and the ex-containment environment virtually simultaneously. Containment failure resulting from an in-vessel steam explosion was termed "alpha-mode failure" in the Reactor Safety Study.

The sequence of events constituting the hypothesized alpha-mode failure scenario is as follows: Because of either failure of the reactor coolant system boundary or loss of the core heat removal function, the core uncovers. The generation of fission product decay heat and the exothermic oxidation of fuel cladding results in core degradation until liquefaction of the fuel occurs. The relocation of liquefied material to cooler locations near the lower core support plate results in freezing of the fuel and the consequent formation of a crust. This crust supports the molten material that is formed. When the mass of molten material reaches a critical limit, the crust can no longer support it, and the material flows coherently into any water remaining in the lower plenum of the vessel. A steam explosion occurs, generating an upward moving slug of water and molten fuel, which lifts the upper head of the vessel. The reactor head then acts as a missile that perforates any structures above the vessel and, ultimately, penetrates the containment building.

The risk impact of a steam explosion is not confined to the in-vessel phase of a severe accident. When water is present in the reactor cavity or pedestal region at the time of vessel failure, the contact of molten core debris with the water may result in a steam explosion. If the containment geometry is such that an ex-vessel water pool could contact the containment wall or could contact structures that, if disrupted, would result in impairment of the containment function, then ex-vessel steam explosions can have potentially significant risk impact.

It should be noted that an ex-vessel steam explosion may result not only in an impulse load, but also in a quasistatic pressure load on containment structures. Indeed, in assessing pressure loads at vessel breach, the expert panel on containment loading issues accounted for the possibility of load contributions from ex-vessel steam explosions in the development of their probability distributions (see Section C.5). The current section, however, focuses upon challenges to containment structures associated uniquely with the dynamic loads resulting from ex-vessel steam explosions.

The consequences associated with in-vessel and ex-vessel steam explosions, as with other scenarios resulting in early breach of the containment building, are potentially significant. Determining the risk posed by steam explosion scenarios, however, demands not only an evaluation of the resultant consequences but also an assessment of their probability of occurrence. Evaluation of this probability is the focus of the steam explosion issue.

C.9.1 Issue Definition

The range of accident scenarios addressed in the containment analyses of this study includes alpha-mode failure and containment breach due to an ex-vessel steam explosion. The current discussion focuses on the specific accident scenarios and plants for which the steam explosion phenomenon is of the greatest potential risk significance.

C.9.1.1 In-Vessel Steam Explosions

For in-vessel steam explosions, attention is confined to large, dry containment PWR reactor systems. While there currently exists no clear basis for the assumption that other reactor/containment types are less

vulnerable to alpha-mode failure, different modes of containment breach were identified in this study as dominating at other plants. The alpha-mode probability distributions developed in the resolution of this issue were applied, however, to all the plants studied. The accident scenarios of particular concern relative to alpha-mode failure are those in which core degradation occurs at low reactor coolant system pressures since experiments indicate that high ambient pressures tend to reduce the likelihood of, although not preclude, the triggering of a steam explosion (Ref. C.9.1).

To quantify the accident progression models in these analyses, the in-vessel steam explosion issue was defined in terms of the probability, conditional upon core degradation at low ambient pressures, of the occurrence of alpha-mode failure.

While numerous small and intermediate scale simulant tests have provided substantial data, and related analytical models of steam explosion phenomena exist (Refs. C.9.2 and C.9.3), there is limited agreement within the technical community regarding the probable phenomena that govern the onset and the effects of an in-vessel steam explosion. Much of the uncertainty about steam explosion phenomenology is associated with the applicability of small and intermediate scale test results (typically involving a melt mass of less than 40 lb) to actual reactor scales and geometries (involving molten fuel masses of up to 280,000 lb in a PWR). Additionally, there is no consensus regarding the appropriateness of the various analytical models that have been used to evaluate the phenomena governing the alpha-mode scenario.

The fundamental energetic condition for alpha-mode failure is that, of the thermal energy contained in the reactor fuel, the amount converted ultimately into the kinetic energy of an upward moving missile is sufficient to permit penetration of the containment building. The maximum total heat content of the fuel elements of a typical PWR is of the order of 105 megajoules (MJ). The energy required to fail the reactor vessel is of the order of 103 MJ, while energies sufficient to fail a large, dry containment building are also of the order of 103 MJ. Simple energy balance considerations, therefore, cannot provide a basis for excluding the alpha-mode failure scenario. Hence, the crucial questions surrounding the alpha-mode issue relate to the ultimate partition of energy, both with respect to its form (thermal, kinetic, strain, and gravitational) and with respect to the mechanical elements of the system in which it resides (molten debris, in-vessel water, reactor internals, containment building shield, and upward and downward moving missiles).

The energy partition question can be addressed through decomposition of the alpha-mode failure scenario into several phases. The first phase involves the transfer of thermal energy from the molten fuel to water in the lower plenum of the reactor vessel. Subissues relating to this phase are the availability of molten core debris and water for interaction over explosive time scales, the geometry of the debris (since this determines the efficiency of the thermal interactions), and the existence of a steam explosion trigger. The second phase involves the generation of an upward moving slug (water, melt, and structural materials) within the vessel. Subissues relating to this phase are the fraction of thermal energy involved in the steam explosion that is converted to kinetic energy, possible failure of the lower head of the vessel thereby relieving the in-vessel explosive pressures, and the distribution of kinetic energy between the upward moving slug and a downward moving slug.

The third phase involves failure of the vessel upper head. Related subissues are the fraction of the initial energy of the slug that is dissipated as strain energy in the upper internal structural components of the vessel (e.g., upper core support plate, control rod drives) and, if the upper head of the vessel fails, the energy of the missile thereby generated. The fourth phase involves the impact of the missile upon the vessel shield where the relevant issue is the associated degree of energy dissipation. The final phase involves failure of the containment building. The crucial issue here is, given the loss of kinetic energy by the missile associated with its ascension to the containment boundary, the capability of the missile to penetrate the containment.

In 1984, a panel of experts was convened to summarize current understanding of steam explosion phenomena and to assess the likelihood of alpha-mode failure. The 13-member Steam Explosion Review Group (SERG) represented substantial cumulative experience in the experimental investigation and the analytic modeling of severe accident phenomena. Findings of the panel were published in June 1985 (Ref. C.9.4). The mandate of the panel also included review and assessment of analytical work undertaken by Berman et al. (Ref. C.9.5), which addressed the likelihood of alpha-mode failure. To encapsulate the spectrum of expert views on the steam explosion issue, this study drew upon both the findings of SERG

and the judgment provided by the primary author of the work reviewed by SERG. The views of each participating expert were then weighted equally in arriving at the final characterization of uncertainty in the likelihood of alpha-mode failure.

Prior to their use in this study, members of the SERG panel reviewed the probability distributions relating to alpha-mode failure that, based upon the earlier findings of SERG, had been developed at Sandia National Laboratories. Through consideration of the way in which their findings had been interpreted and of relevant information acquired since publication of the SERG report, the same panel members modified the distributions tentatively developed. These modified distributions provided the basis for this study.

C.9.1.2 Ex-Vessel Steam Explosions

Each plant evaluated in this study was screened for potential vulnerabilities to ex-vessel steam explosions. The containment design assessed to display the most significant vulnerability was Grand Gulf. The scenario of concern in the Mark III design is one in which a steam explosion impulse is delivered to the reactor pedestal through water on the drywell floor. The likelihood of a deep water pool in the drywell at Grand Gulf is high during the course of a severe accident. A dominant mechanism for this is the expulsion of water from the suppression pool as a result of pressurization of the wetwell through hydrogen deflagration. Upon receiving the explosion impulse, the pedestal collapses, resulting in failure of the drywell wall due either to impact by the unsupported vessel or damage by the penetrating steam line and feedwater pipes. Loss of the drywell wall then permits bypass of the suppression pool by fission products in the event of pre-existing or subsequent containment failure. The potentially significant risk impact of drywell failure at Grand Gulf stems from the relatively high likelihood of containment overpressure either prior to or following vessel breach.

The Zion and Surry containments were not assessed to have significant vulnerability to impulse loads from ex-vessel steam explosions since water in the cavity would not directly contact structures that are both vulnerable and essential to the containment function. Initial assessment of the Peach Bottom and Sequoyah containment designs identified potential vulnerability to ex-vessel steam explosions, associated principally with pedestal collapse (Peach Bottom) and seal table disruption or vessel dislocation (Sequoyah). However, scoping shock wave hydrodynamics calculations and application of underwater impulse correlations (based on Ref. C.9.6) revealed minimal threat to these containments from ex-vessel steam explosions.

Attention was focused therefore on the Grand Gulf containment. The ex-vessel steam explosion issue was couched in terms of three parameters:

- The likelihood (conditional frequency) of an ex-vessel steam explosion occurring conditional upon the presence of water in the cavity at vessel breach.
- The likelihood of pedestal failure conditional upon the occurrence of a steam explosion.
- The likelihood of drywell failure due to collapse of the pedestal.

Evaluation of these parameters was based upon impulse loading calculations performed at Sandia and upon the elicitation of judgments from the expert panel on containment structural performance issues (see Section C.8).

C.9.2 Technical Bases for Issue Quantification

C.9.2.1 In-Vessel Steam Explosions

The approach adopted by most of the experts in determining the probability of alpha-mode failure was decomposition of the scenario into a sequence of events and the assignment of a probability, or a range of probabilities, to each constituent event (Ref. C.9.4). These events constituted elements of the four phases of alpha-mode failure defined in the previous section. The product of event-level probabilities was then equated with the probability of alpha-mode failure. Other experts adopted variant approaches in which probabilistic judgment was exercised directly at the level of the compound-event alpha-mode failure, or in which probability distributions reflecting uncertainty in relevant physical parameters were propagated

through deterministic models to determine the probability of alpha-mode failure. These latter approaches do not permit straightforward extraction of the probabilities associated with the primary-level events, and direct comparison of the event likelihoods assessed by all the experts is therefore difficult. The range of views in each phenomenological area is described here, and direct comparisons of expert-specific probabilities are made where possible.

Initial Conditions

For the energy involved in a steam explosion to be commensurate with the energies associated with vessel and containment failure, sufficient amounts of molten material and water must be available to participate. Additionally, a coherent pour of melt into the water is required to ensure maximal participation of the melt available over explosive time scales. While some experts assigned a low likelihood to the required initial conditions, based on the premise that the meltdown process would involve the incoherent dripping of molten material into the lower plenum, others assigned probabilities in the range of 0.75 to 1.0 for the occurrence of the required conditions. These higher probabilities were based generally upon identification of a scenario in which a crust of refrozen melt at the lower core support plate breaks suddenly, permitting the coherent release of molten material into the lower plenum. Substantial uncertainty was identified regarding the process of the core degradation and fuel relocation.

Molten Core/Water Mixing

The degree of interpenetration between the melt and water in the lower plenum determines the efficiency of thermal interaction between the two media. Currently no widely accepted model of molten fuel/water mixing under severe accident conditions exists. While efficient mixing has been observed in several small and intermediate scale tests (Ref. C.9.7), various experts argued that scaling effects prevent the conclusion that efficient mixing would occur in full-scale reactor geometries. One analytical model involves a process in which hydrodynamic instabilities break up the fuel jet as it pours into the lower plenum. Rapid steam production (although not as rapid as that associated with a steam explosion) then expels water from the mixing region, thereby severely limiting the potential for effective mixing.

This process of jet fragmentation and fluidization as a result of hydrodynamic instabilities was not accepted by all participating experts, however. A process in which a blanket of steam forms around the jet body, thus limiting access by water to the jet, was the basis for an alternative model. This model confines fragmentation of the melt to the leading edge of the jet, thereby reducing the potential for mixing.

The initial mixing of melt and water as a condition for large-scale steam explosions was questioned by some experts. It was observed that, even for an initial configuration involving minimal fragmentation of the melt, the occurrence of small steam explosions sufficient to disrupt the melt could create boundary conditions conducive to the onset of a larger explosion. While no model of the net effects of preliminary steam explosions upon in-vessel melt/water configurations exists, the observation of multiple steam explosions in small-scale tests prevents the exclusion of such scenarios from consideration. Where probabilities were assigned specifically to the event of large-scale mixing conditional upon a coherent melt pour, they ranged from 10^{-2} to 0.3.

Explosion Trigger

While large-scale mixing of melt with water provides boundary conditions required for significant thermal interactions between the two media, the question of whether that interaction takes the form of a steam explosion is dependent upon whether a trigger is present. The mechanism for triggering a steam explosion is poorly understood. One model involves the onset of oscillations in the steam film barrier isolating a molten fuel fragment from water. Where these oscillations permit direct contact of fuel with water, a trigger occurs. Experiments reveal that the existence of a trigger is extremely sensitive to initial conditions (Ref. C.9.1) and that triggering becomes less likely at high ambient pressures. For low reactor coolant system pressure scenarios, those experts who provided a probability relating specifically to the occurrence of a trigger assessed it to be equal to unity.

Explosion Efficiency

Fundamental thermodynamic factors limit the efficiency with which the thermal energy involved in a steam explosion may be converted into kinetic energy. While this theoretical, maximum conversion ratio

is in the range of 40–50 percent (based upon Hicks-Menzies conditions), the value appropriate for a reactor configuration depends upon the constraints provided by the internal vessel geometry. The experts agreed that conversion ratios of up to 15 percent are possible.

Slug Formation and Vessel Head Impact

The primary mechanism for transmittal of the kinetic energy generated by the steam explosion to the upper head of the vessel is the formation of an upward-moving slug composed of molten fuel, water, and structural material. The resultant impulse upon the upper head could also be supplemented by the transmittal of an impulse from the lower core support plate, through the core barrel, to the upper head flange. The possibility also exists that the pressures generated by the steam explosion could result in failure of the lower head, thereby venting explosive pressures in the vessel and reducing the energy delivered to the upper head. Much of the uncertainty associated with the likelihood of upper head failure relates to the distribution of material within the vessel. For example, uncertainty regarding the fraction of the molten fuel and water inventories above the trigger location was taken into account explicitly by some of the experts in determining the possible mass and composition of the upward-moving slug. Uncertainty was identified also in estimating the fraction of the slug's kinetic energy dissipated as strains within the upper internal components of the vessel. Expert-specific point-value probabilities assigned to the event of upper head failure and the generation of a missile capable of failing containment (conditional upon significant thermal energy conversion) ranged from 10^{-2} to 1, although one expert provided a probability range extending from 10^{-4} to 1.

Vessel Head Failure and Containment Breach

Following bolt failure at the upper head flanges, development of the alpha-mode failure scenario involves impact of the dislocated vessel head against the missile barrier positioned above the vessel. The barrier is perforated, thus attenuating the energy of the missile. The missile continues to rise, expending kinetic energy to acquire gravitational potential energy, and ultimately impinges upon the containment wall. Some of the experts based their assessments of the likelihood of containment failure upon detailed structural calculations. Those experts who assigned probabilities to individual events within the alpha-mode scenario generally absorbed the structural uncertainties into their assessment of the probability of vessel head failure by defining such a failure as one that generates a missile capable of penetrating the containment.

C.9.2.2 Ex-Vessel Steam Explosions

The scenario of concern at Grand Gulf is one in which molten debris is released from the breached vessel into a deep water pool (about 7 meters) on the drywell floor. A steam explosion is triggered, which delivers an impulse load to the reactor pedestal. The pedestal collapses leaving the reactor vessel unsupported. The drywell wall then fails as a result of damage caused by the penetrating vessel piping or by direct contact by the vessel. The accident progression models developed for this study decompose the ex-vessel steam explosion scenario into three phases: (1) occurrence of the steam explosion, (2) subsequent failure of the pedestal, and (3) subsequent failure of the drywell wall.

Occurrence of Steam Explosion

The parameter evaluated for this phase of the scenario is the fraction of occasions upon which a steam explosion would be triggered conditional upon the release of molten debris from the vessel to an underlying water pool. An estimate of 0.86 for this parameter was based upon intermediate-scale experimental results in which 86 percent of tests involving the release of molten thermite into water at low ambient pressures resulted in a significant steam explosion (Ref. C.9.7).

Failure of Pedestal

Assessment of the dynamic load capacity of the pedestal was based upon adaptation of information elicited from the expert panel on containment structural performance issues regarding the strength of the drywell wall and upon supplementary information provided by a structural expert from Sandia, who had been a member of the original panel. The expert aggregate probability distribution over potential failure impulse levels for the Grand Gulf drywell wall extends from 3.5 to 18 psi-s. Since the pedestal and the drywell wall at Grand Gulf are both composed of reinforced concrete of similar thickness, the dynamic

load capacity of the pedestal was assumed to be comparable to that of the drywell wall. While the impulse capacity range for the drywell wall was based on the assumption of loads associated with hydrogen detonations, the similarity in impulse duration between steam explosion and gas detonation loads (typically milliseconds) was assessed to warrant adoption of the range, given its broadness. Supplementary evaluations of the pedestal impulse capacity by an internal Sandia expert on containment structural performance issues confirmed the appropriateness of this range.

Estimation of the impulse delivered to the pedestal conditional upon the occurrence of a steam explosion was based on the Similitude Equations (Ref. C.9.6). These equations, reflecting the correlation between underwater explosion size, distance from the explosion center, and impulse level, were adopted to determine the relationship between the mass of debris participating in the steam explosion and the impulse to the pedestal. Calculations revealed that, with less than 1 percent of the core participating in the explosion, the impulse to the pedestal would reach the lower edge (i.e., 3.5 psi-s) of the uncertainty range over pedestal failure loads. The upper edge of the range (18 psi-s), based upon shock wave hydrodynamics calculations, would be reached if 10 percent of the core participated in the explosion. It was noted that release from the vessel of 10 percent of the core corresponds to the 90th percentile level of the aggregate distribution over core release levels at BWR vessel breach.

It was concluded that, conditional upon the trigger of a steam explosion in the Grand Gulf drywell, failure of the pedestal is credible. To reflect maximal uncertainty regarding the fraction of ex-vessel steam explosions that would result in pedestal failure, a uniform probability distribution was assigned to the interval between the fraction zero and the fraction 1.

Failure of Drywell Wall

The final parameter associated with the ex-vessel steam explosion issue at Grand Gulf is the fraction of occasions that collapse of the pedestal results in failure of the drywell wall. This question was addressed by two members of the expert panel on containment structural performance issues. Based upon their engineering judgment and supporting hand calculations, each expert provided a single point estimate of the required parameter. These two point estimates were averaged to generate a single estimate for input to the Grand Gulf risk model. This average was 0.17.

C.9.3 Treatment in PRA and Results

C.9.3.1 In-Vessel Steam Explosions

Of the 14 experts (13 in SERG and one additional expert as discussed in Section C.9.2) participating in the steam explosion evaluation process, 12 provided probabilities for alpha-mode failure conditional upon core damage in a PWR at low reactor coolant system pressure. Two of these experts collaborated in the generation of probabilities; thus, their results reflected a single approach. Eleven independent sets of probabilities were ultimately provided.

The extreme sensitivity of the onset of a steam explosion to prevailing physical boundary conditions (Ref. C.9.7) provides a strong basis for treating alpha-mode failure as a stochastic phenomenon. This means that, conditional upon a specified plant damage state, the associated range of possible physical conditions within the vessel results in the situation that alpha-mode failure would occur only on some fraction of occasions. The probabilities assigned by the participating experts were therefore interpreted as estimates of the relative frequency of alpha-mode failure, i.e., as the fraction of severe accidents resulting in failure of the containment building due to an in-vessel steam explosion. In conformance with the approach to uncertainty characterization used in this study, probability distributions were constructed over these relative frequencies on an expert-specific basis. Aggregation over the expert distributions then provided the net representation of uncertainty regarding the frequency of alpha-mode failure.

Construction of the expert-specific distributions was based upon identification of a best-estimate frequency with the median of the distribution, identification of an upper estimate with the 95th percentile, and identification of a lower estimate with the 5th percentile. Use of an entropy-maximization algorithm (Ref. C.9.8) in conjunction with these distribution constraints ensured that uncertainty was appropriately preserved in formulation of the expert-specific probability distributions. Details of this approach to the use of probabilistic information were reviewed by each participating expert.

Figure C.9.1 displays the cumulative probability levels that bound the expert-specific distributions. These bounds exclude two experts who assessed the likelihood of alpha-mode failure to be so low that they assigned zero probability to the scenario. This figure also displays the final aggregate distribution based upon the 11 expert-specific distributions (including the two experts who assigned zero probabilities). Note that the aggregate distribution is not completely encapsulated by the bounding distributions because of the effect of the two experts who assigned zero probabilities. It can be seen that the median relative frequency of alpha-mode failure for the aggregate distribution is approximately 4E-5. That is, there is equal net probability that less than, or more than, four in a 100,000 core damage scenarios occurring at low ambient pressure will result in alpha-mode failure of the containment building. It can be seen also that the greatest median frequency proposed by any one expert was of the order of one in a 100, while the smallest finite median frequency was of the order of one in 100,000. Hence, while no consensus existed regarding details of the phenomenology of steam explosions, the conclusion that, at the median level, alpha-mode failure is unlikely was shared by each participating expert. In each plant study, the aggregate distribution displayed in Figure C.9.1 provided the basis for sampling alternative values of the frequency of alpha-mode failure conditional upon core degradation at low pressure. The frequency of alpha-mode failure conditional upon core degradation at high reactor coolant system pressure was set at one order of magnitude below the frequency associated with the low-pressure case in each sample member. This reflects the experimental observation that high ambient pressures tend to reduce the likelihood of a steam explosion trigger (Ref. C.9.1).

Although the median relative frequency of the alpha-mode scenario is low, the high relative likelihood of core degradation at low reactor coolant system pressures in PWRs (see Section C.6) has the effect of highlighting the alpha-mode scenario as a mechanism for early failure of the containment, especially at Surry and Zion for which other early failure mechanisms are of low likelihood. At Surry, for example, while about half of the mean frequency of early containment failure conditional upon core damage is

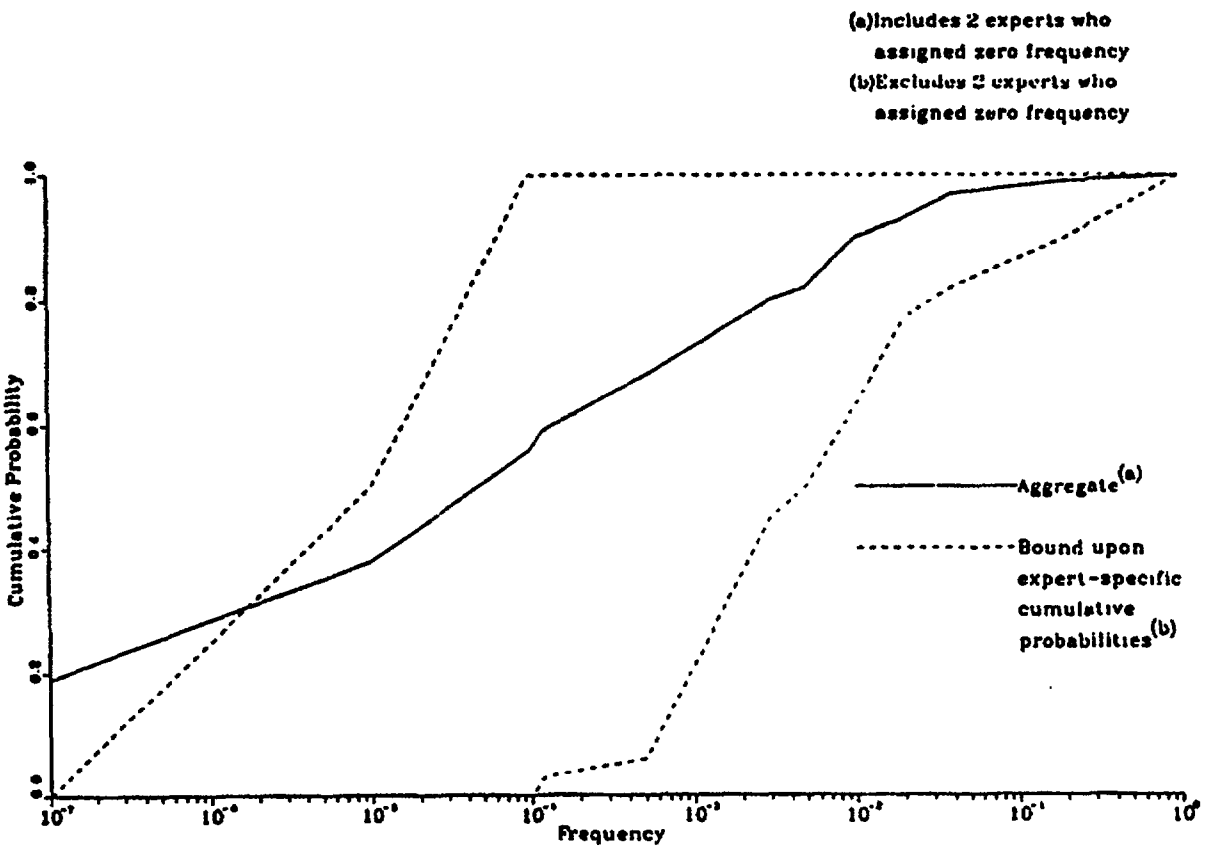

Figure C.9.1 Frequency of alpha-mode failure conditional upon core damage.

associated with the alpha-mode scenario, this total mean frequency is less than 10^{-2}. For the pressure-suppression containment types, the likelihood of alpha-mode failure is low relative to other containment failure mechanisms.

C.9.3.2 Ex-Vessel Steam Explosions

The three parameters required to characterize the likelihood of drywell failure due to ex-vessel steam explosions at Grand Gulf are defined in Section C.9.2. Each of these was an input to the Grand Gulf accident progression event tree. Conditional upon vessel breach and wet cavity conditions, the fraction of occasions upon which the drywell fails as the result of an ex-vessel steam explosion was equated with the product of these three parameters. The fraction of steam explosions leading to pedestal failure was identified as the most significant source of uncertainty because of uncertainty regarding the amount of molten material that would participate in the explosion. In the Monte Carlo uncertainty analysis, this parameter was sampled from a uniform probability distribution over the interval of fractions zero to 1. Based upon the parameter values described in the Section C.9.2, it can be deduced that the mean fraction of occasions on which failure of the vessel, in wet cavity conditions, results in breach of the drywell wall as a result of a steam explosion is approximately 0.07.

While Grand Gulf is the containment for which the threat posed by ex-vessel steam explosions is the most significant, the relative importance of this mechanism for drywell failure compared to others is small. Conditional upon core damage at Grand Gulf, less than 10 percent of early drywell failures result from an ex-vessel steam explosion. The dominant causes of drywell failure are associated with pressurization of the drywell atmosphere at the time of vessel breach.

More details of the treatment of steam explosions in this study can be found in Reference C.9.9.

REFERENCES FOR SECTION C.9

C.9.1 D.E. Mitchell, M.L. Corradini, and W.W. Tarbell, "Intermediate Scale Steam Explosion Phenomena: Experiments and Analysis," Sandia National Laboratories, NUREG/CR-2145, SAND81-0124, October 1981.

C.9.2 T.G. Theofanous et al., "An Assessment of Steam-Explosion-Induced Containment Failure," *Nuclear Science and Engineering*, 97, 259, 1987.

C.9.3 M. Berman, "A Critique of Three Methodologies for Estimating the Probability of Containment Failure Due to Steam Explosions," *Nuclear Science and Engineering*, 96, 173, 1987.

C.9.4 Steam Explosion Review Group, "A Review of the Current Understanding of the Potential for Containment Failure from In-Vessel Steam Explosions," USNRC Report NUREG-1116, June 1985.

C.9.5 M. Berman et al., "An Uncertainty Study of PWR Steam Explosions," Sandia National Laboratories, NUREG/CR-3369, SAND83-1438, July 1984.

C.9.6 R.H. Cole, *Underwater Explosions*, Princeton University Press, 1948.

C.9.7 B.W. Marshall et al., "Recent Intermediate-Scale Experiments on Fuel-Coolant Interactions in an Open Geometry," *Proceedings of the ANS/ENS International Topical Meeting on Thermal Reactor Safety* (San Diego, CA), February 1986.

C.9.8 S.D. Unwin, "IMPAGE. An Information Theory-Based Probability Assignment Generator. Brief Code Description and User's Guide," Brookhaven National Laboratory, Technical Report A-3829, August 1987.

C.9.9 F. T. Harper et al., "Evaluation of Severe Accident Risks: Quantification of Major Input Parameters," Sandia National Laboratories, NUREG/CR-4551, Vol. 2, Revision 1, SAND86-1309, December 1990.

C.10 Source Term Phenomena

The magnitude and timing of release of radioactive material from a nuclear reactor in a severe accident depend on a variety of thermal, hydraulic, and mechanical processes, as well as the chemistry and physics of fission product release and transport. Uncertainties in core melt progression, containment loads, and containment performance produce uncertainties in the release to the environment. In this study, however, each accident progression bin represents a particular state of melt progression and containment performance. Thus, uncertainties associated with how and when the containment fails are reflected as uncertainties in the likelihoods of the accident progression bins rather than in the parameters that describe the release to the environment. This section addresses the phenomena that affect the magnitude of release of the elemental groups in an accident progression bin, not its likelihood. These phenomena relate directly to the chemistry and physics of fission product release and transport. Some uncertain aspects of core melt progression (e.g., the time-temperature history of the fuel as fission products are being released) are included implicitly in the assessment of uncertainties, however.

C.10.1 Issue Definition

Following the Three Mile Island accident, the NRC established an Accident Source Term Program Office to evaluate the realism with which the analytical methods available at that time could predict severe accident source terms. In 1981, the NUREG-0772 report, "Technical Bases for Estimating Fission Product Behavior During LWR Accidents" (Ref. C.10.1), reviewed the state of the art and identified research needs in a number of areas. In response to these needs, the NRC undertook a substantial effort to direct severe accident research toward development of improved methods of analysis supported by a more comprehensive data base (Ref. C.10.2).

In 1986, the NRC published the NUREG-0956 report, "Reassessment of the Technical Bases for Estimating Source Terms" (Ref. C.10.3). One of the purposes of the present study was to develop a perspective on how changes in source term methodology, as represented in NUREG-0956, affect estimated risk to the public from severe accidents. In their review of NUREG-0956, the American Physical Society (APS) identified the principal areas of uncertainty in severe accident analysis and made recommendations for future research. The research needs that relate directly to the release and transport of radioactive materials are listed in Table C.10.1. Additional research has been performed in each of these areas subsequent to the APS review, and the results have been incorporated into the current study.

Table C.10.1 APS recommendations for source term research (Ref. C.10.3).

1.	Vaporization of low volatility fission products
2.	Release of refractory materials in core-concrete interaction
3.	Transport of radionuclides through reactor
4.	Tellurium behavior
5.	Release of volatile forms of iodine
6.	Generation mechanisms for aerosols
7.	Effectiveness of suppression pools and ice beds
8.	Growth and deposition of aerosols
9.	Change of sequence by fission product heating
10.	Intercomparison of aerosol codes
11.	Aerosol deposition on pipes
12.	Integrated severe accident code

The simplified source term codes, XSOR,* which were developed to support the uncertainty analysis for this study, represent source term processes as integral parameters such as release fractions, decontamination factors, and transmission factors. The chemistry and physics of these processes are contained in the mechanistic codes against which the XSOR parameters are benchmarked. The same parametric representation of source terms will be used in this section to discuss source term uncertainties:

*A separate code was written for each of the plants: SURSOR, SEQSOR, ZISOR, PBSOR, and GGSOR.

1. Fraction of initial inventory of species released from the fuel prior to vessel breach,
2. Fraction of release from fuel that transports from the reactor vessel into the containment,
3. Fraction of initial core inventory released during core-concrete interaction,
4. Fraction of source term to the containment atmosphere that subsequently is released to the environment,
5. Decontamination factors for engineered safety features or water pools,
6. Fraction of species deposited in reactor coolant system that is subsequently revaporized, and
7. Fraction of iodine in suppression pools or water pools that is subsequently evolved.

C.10.2 Technical Bases for Issue Quantification

The status of each of the major areas of severe accident uncertainty identified by the APS has been reviewed in Appendix J of draft NUREG–1150 (Ref. C.10.4). A "Review of Research on Uncertainties in Estimates of Source Terms from Severe Accidents in Nuclear Power Plants," (Ref. C.10.5), was also undertaken by a panel of eminent scientists under the leadership of Dr. H. Kouts. These reports discuss areas of source term uncertainties qualitatively and identify needs for further research.

In the current study, it was necessary to develop a quantitative characterization of the uncertainties in source term phenomena. A panel of experts in source term phenomena was assembled to develop the uncertainty distributions for the most important phenomena. Table C.10.2 identifies the experts and lists the issues elicited. The bases on which the experts made their judgments differed. In each case, computer analyses and experimental data were available to the experts. In many instances, the experts performed their own calculations. Each expert provided documentation on the rationale supporting his elicitation. The variety of considerations by the experts is too broad to reproduce in this appendix for the source term issues. The reader is referred to Reference C.10.6 for a detailed discussion of the bases for the elicitations.

C.10.3 Treatment in PRA and Results

In-Vessel Release

Within the range of uncertainties, the experts were not able to distinguish between the magnitude of release for different accident sequences other than for different degrees of zirconium oxidation. Thus, distributions for only four cases were developed: PWR-high oxidation, PWR-low oxidation, BWR-high oxidation, and BWR-low oxidation. The results for the four cases are similar. Figure C.10.1 illustrates the distribution obtained for the PWR case with low zirconium oxidation. The uncertainty range* for the release of iodine and cesium is from approximately 10 percent to 100 percent of the initial core inventory, for tellurium from 1 percent to 90 percent, for barium and strontium from very small to 50 percent, and for the involatiles from very small to a few percent.

In-Vessel Retention

Four cases were considered for the PWRs: setpoint pressure (2500 psia), high pressure (1200-2000 psia), intermediate pressure (150–600 psia), and low pressure (50–200 psia). Three cases were considered for the BWRs: fast (e.g., short-term station blackout), high pressure; fast, low pressure; and slow (e.g., long-term station blackout), high pressure.

In all cases 100 percent of the noble gases were assumed to escape from the reactor coolant system. For the PWR, the estimated fractional releases at setpoint pressure are typically small, as illustrated in Figure C.10.2. For all species the range is from 0.001 percent to 80 percent, with median fractional release of 9

*5th percentile and 95th percentile values are used to characterize the range.

Table C.10.2 Source term issues.

Technical Experts

P. P. Bieniarz, Risk Management Associates

A. Drozd, Stone & Webster Engineering Corp.

J. A. Gieseke, Battelle Columbus Division

R. E. Henry, Fauske and Associates

T. Kress, Oak Ridge National Laboratory

Y. H. Liu, University of Minnesota

D. Powers, Sandia National Laboratories

R. C. Vogel, Electric Power Research Institute

D. C. Williams, Sandia National Laboratories

Source Term Issues Elicited

1. In-vessel fission product release
2. Ice condenser DF—Sequoyah
3. Revolatilization (from RCS/RPV) after vessel breach
4. Core-concrete interaction (CCI) release
5. Release from containment
6. Late sources of iodine—Grand Gulf and Peach Bottom
7. Reactor building DF—Peach Bottom
8. Releases during direct containment heating

percent for iodine and 3 percent for the bulk of the other aerosols. As illustrated in Figure C.10.3, at low pressure the range for fractional release is 12 percent to 99 percent for the iodine, with a median of 50 percent, and from 4 percent to 99 percent for the bulk of the other aerosols. The high and intermediate pressure cases fall between the system setpoint case and low-pressure case.

The distributions for the BWR cases are similar to those described for the PWR cases. The distributions for the two high-pressure cases are similar to the distribution for the PWR setpoint pressure case in that the majority of the distribution indicates a small release, but at the upper end of the range the release is substantial (~80 percent). The distribution for the low-pressure case is similar to that of the PWR low-pressure case.

Core-Concrete Release

Distributions were obtained for 16 different cases. Zion, Sequoyah, and Surry were each treated separately. A common distribution was obtained for Peach Bottom and Grand Gulf because the same type of concrete was used in the construction of the two plants. For each plant, four scenarios were considered for a wet or dry cavity and high or low zirconium oxidation.

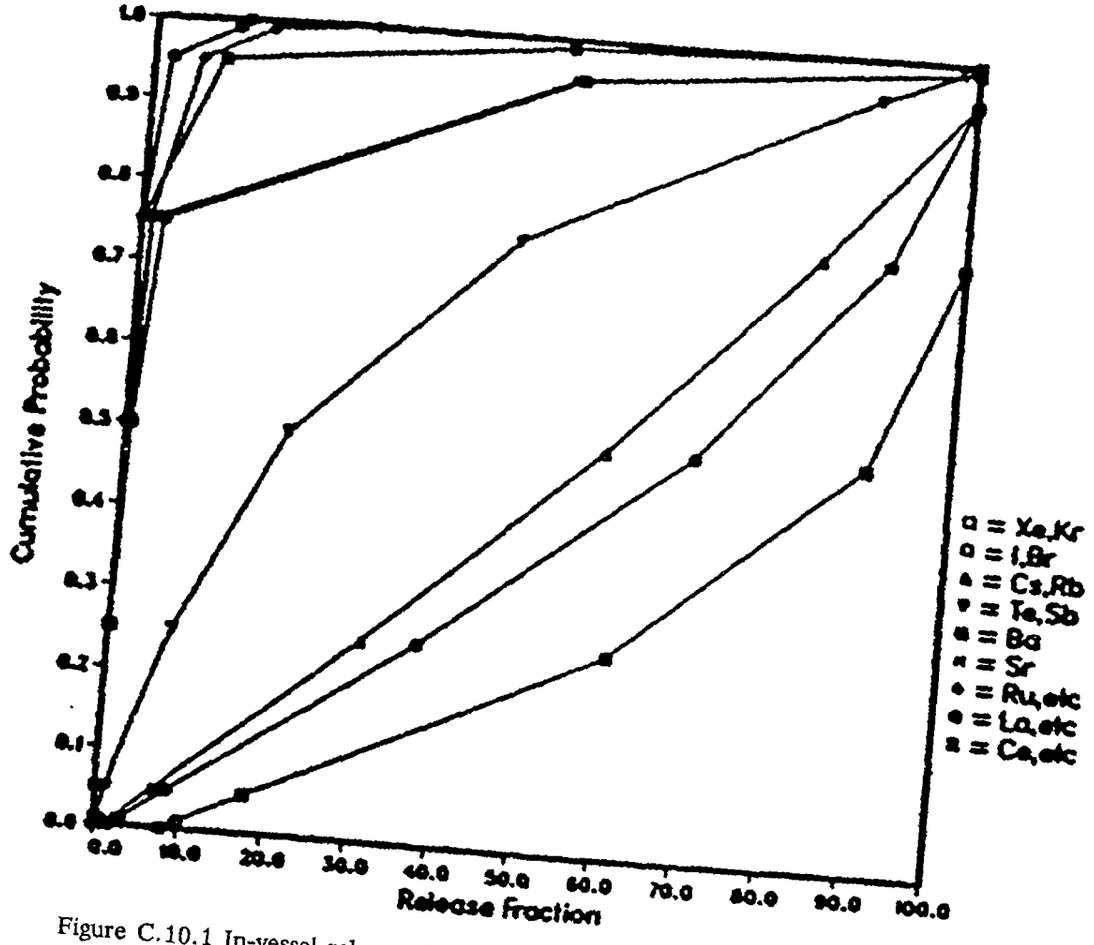

Figure C.10.1 In-vessel release distribution, PWR case with low cladding oxidation.

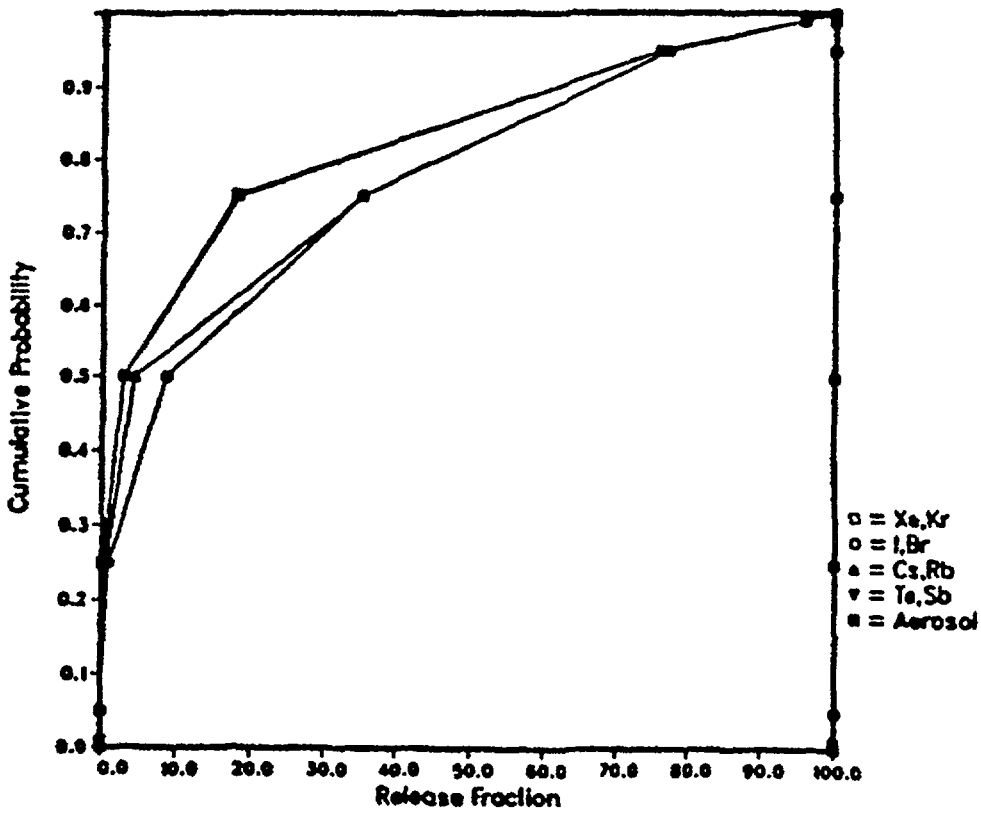

Figure C.10.2 RCS transmission fraction, PWR case at system setpoint pressure.

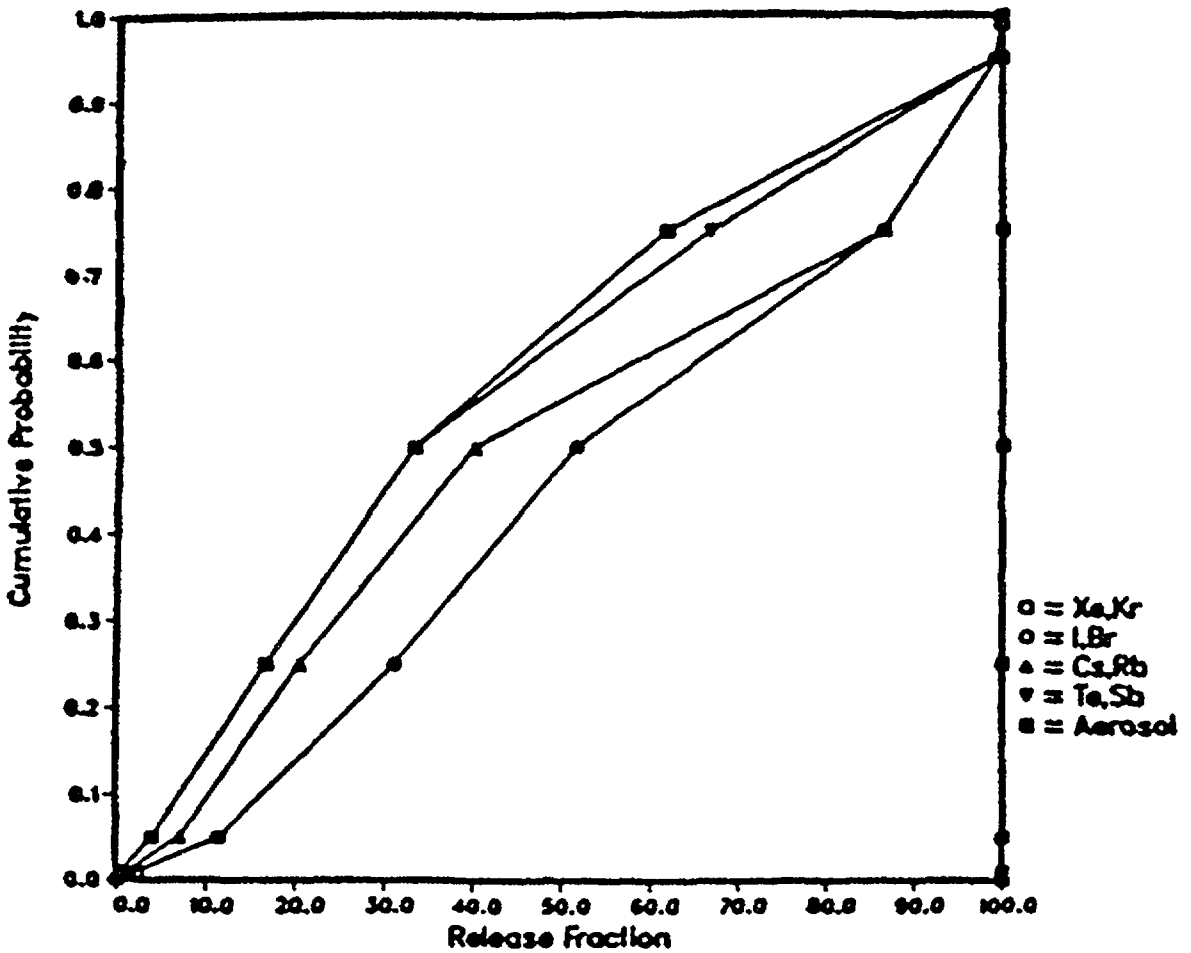

Figure C.10.3 RCS transmission fraction, PWR case with low system pressure.

Release fractions for five elemental groups were evaluated: tellurium, strontium, barium, lanthanum, and cerium. The uncertainty distributions obtained from the experts indicate broad ranges of uncertainty. The fractional release of tellurium is likely to be quite large. Median values of the release fraction for the different cases typically are approximately 50 percent, and the upper bound release is approximately 90 percent. The lower bound release fractions vary from 2 percent to 10 percent. Barium and strontium are indicated to be substantially less volatile than tellurium but at the upper end of the uncertainty range could also lead to substantial release. Median values for the release of these species vary from 2 percent to 5 percent for the different cases. The release fractions for the lanthanum and cerium groups are substantially smaller. Median values are typically less than 0.1 percent. Upper bound values are typically less than 10 percent of the inventory, except for the cerium group release in the BWR cases, which extends to 20 percent.

Containment Release Fraction

This factor is defined as the fraction of radioactive material released to the containment atmosphere that eventually leaks to the environment. Eighteen different distributions were developed associated with different plant types, whether the release was from fuel in-vessel or ex-vessel, the timing of containment failure, the mode of containment failure, and in some cases whether the suppression pool was saturated.

It is difficult to generalize the results because of the variety of containment conditions analyzed. In some early failure cases, however, the transmission fraction is quite high for the entire range of uncertainty. In an early containment failure case for the Sequoyah plant, in which the failure leads to bypass of the ice bed, the fractional release of radioactive material ranges from 25 percent to 90 percent of the material released from the reactor coolant system.

Decontamination Factors for Engineered Safety Features

Distributions for decontamination factors (DFs) were developed for suppression pools, ice condensers, overlaying water pools (for the core-concrete interaction release), containment sprays, and for the Peach Bottom reactor building. Only the ice condenser and Peach Bottom reactor building DFs were submitted to the panel of experts for quantification. The NUREG–1150 analysis staff developed the distributions for the other factors.

Although the range of uncertainty in the water pool DFs is large, water pools are sufficiently effective in decontamination that the resulting source terms are not dominant contributors to the plant risk. In comparison to the suppression pool DF, the ice condenser is not as effective in the removal of radioactive material. Four cases were considered by the experts:

Case 1: Air-return fans on, delayed containment failure, multiple passes through ice bed, no direct containment heating, low steam fraction.

Case 2: Air-return fans on, early containment failure, single pass through ice bed, no direct containment heating, low steam fraction.

Case 3: Air-return fans off, single pass through ice bed, no direct containment heating, high steam fraction.

Case 4: Direct containment heating, single pass through ice bed, high gas velocity, high steam fraction.

For a typical case, with multiple passes through the bed, low steam content, and without high-pressure melt ejection, the range of DF was from 1.2 to 20 with a median value of 3.

Distributions were developed for six cases for the DF of the Peach Bottom reactor building. The variations in conditions were associated with combinations of the mode of drywell failure (rupture, shell meltthrough, or head seal leakage) and whether the suppression pool was saturated. For the head seal leakage cases, the leak is into the refueling bay rather than into the reactor building and smaller DFs were assessed. For a typical case involving drywell rupture with the suppression pool subcooled, the range of DF is 1.1 to 10 with a median value of 3.

Revolatilization from Reactor Coolant System

Radioactive material deposited on surfaces within the BWR reactor vessel and PWR reactor coolant system can be reevolved after vessel failure because of the self-heating of the radioactive material. For the PWRs, two cases were considered: one hole in the reactor coolant system or two holes in the reactor coolant system. The latter case offers the opportunity of a chimney effect and a greatly different environment. For the BWRs, two cases were also considered: high drywell temperatures or low drywell temperatures. Variations to these cases were considered by some of the experts.

Distributions were developed for three elemental groups: iodine, cesium, and tellurium. In all cases, the fractional release is greatest for the iodine and least for the tellurium. Figure C.10.4 illustrates the distribution for the release of iodine for the PWR case with two holes in the reactor coolant system. The range for this case, which produced the greatest release, is from 0 percent to 70 percent, with a median release of 20 percent. Median releases of iodine for the other cases varied from 3 percent to 10 percent. Cesium release fractions were comparable to the iodine values but slightly reduced. The median release of tellurium was 0 percent in all cases, but the upper bound varied from 20 percent to 60 percent. This skewed distribution is indicative of a general belief by the experts that there will be little or no revaporization of tellurium but with a recognition that substantial revaporization cannot be ruled out.

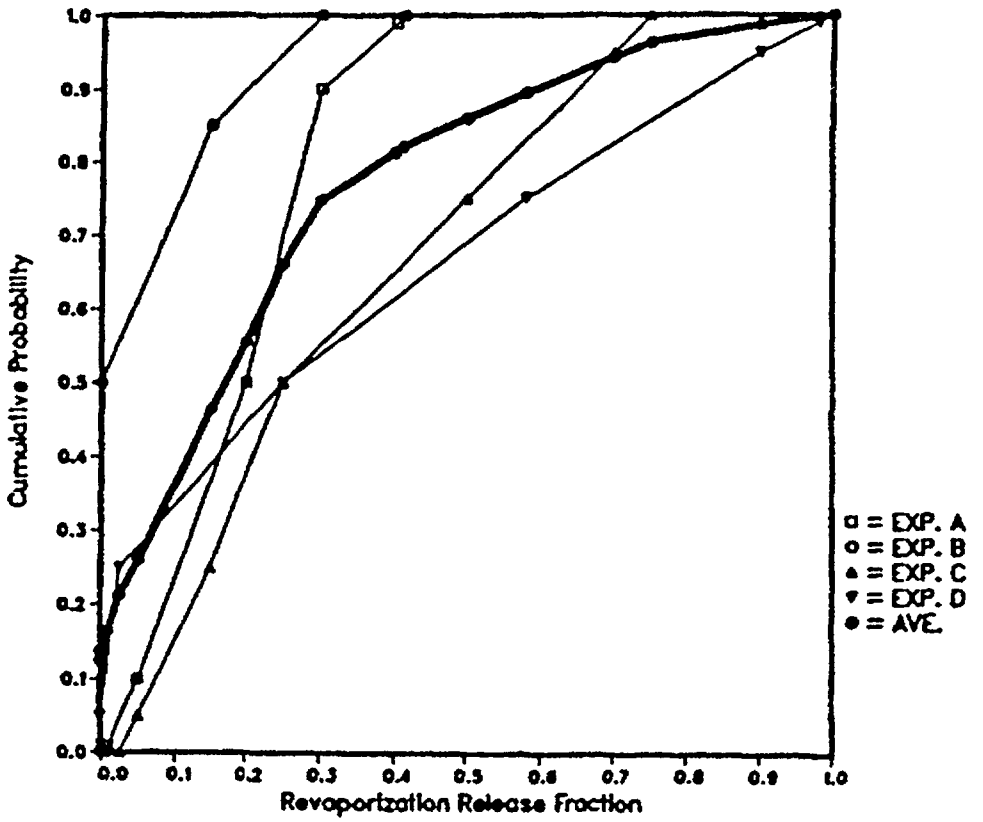

Figure C.10.4 Revaporization release fraction for iodine, PWR case with two holes.

Late Release of Iodine

This issue addresses the potential for the long-term release of iodine from suppression pools and reactor cavity water. Four cases were considered: a subcooled suppression pool, a saturated suppression pool, a flooded drywell, and a limited supply of water in the pedestal that mostly boils away.

The release from the subcooled suppression pool is limited. The upper bound of the distribution is 10 percent and the median is 0.1 percent. Release from the saturated pool is somewhat greater. The median release is 0.5 percent and the upper bound release is 80 percent.

The releases from the flooded cavity cases are substantially larger. For the case with a large volume of water, the range of release is from 10 percent to 90 percent, with a median of 50 percent. The limited water supply case has a range of 20 percent to 100 percent, with a median of 80 percent.

Summary of Results

By examining the ranges used to represent the source term factors (e.g., release from fuel in-vessel and fractional release from reactor coolant system), it is evident why the ranges of the environmental release fractions are large. To begin with, the source distributions for the release of radionuclides from fuel in-vessel and ex-vessel are very broad. Even radionuclides that are typically not considered to be volatile, such as barium and strontium, have ranges of uncertainty that extend as high as 50 percent for in-vessel release. Similarly, the decontamination factors that are applied to these release terms can vary over a range of three orders of magnitude. In some instances, the separation between the mean and the median of the source term distribution for the environmental release of a radionuclide can be as large as three orders of magnitude. These very broad distributions are the result of sampling from multiplicative factors, each of which has a wide distribution. No specific source term issues stand out as dominating the uncertainty because there are a number of contributors.

It is important to recognize that the origin of the uncertainties in the source term issues does not completely arise from uncertainties in the chemistry of fission product interactions or the physics of aerosol transport. Uncertainties in core melt progression, in thermal-hydraulic behavior within the reactor coolant system, and in thermal-hydraulic behavior within containment (and secondary buildings) also have a major effect on the uncertainties in calculated source terms.

REFERENCES FOR SECTION C.10

C.10.1 USNRC, "Technical Bases for Estimating Fission Product Behavior During LWR Accidents," NUREG-0772, June 1981.

C.10.2 J. T. Larkins and M. Cunningham, "Nuclear Power Plant Severe Accident Research Plan," NUREG-0900, January 1983.

C.10.3 M. Silberberg et al., "Reassessment of the Technical Bases for Estimating Source Terms," NRC Report NUREG-0956, July 1986.

C.10.4 USNRC, "Reactor Risk Reference Document," NUREG-1150, Appendix J of Vol. 3, Draft for Comment, February 1987.

C.10.5 H. Kouts, "Review of Research on Uncertainties in Estimates of Source Terms from Severe Accidents in Nuclear Power Plants," Brookhaven National Laboratory, NUREG/CR-4883, BNL-NUREG-52061, April 1987.

C.10.6 F.T. Harper et al., "Evaluation of Severe Accident Risks: Quantification of Major Input Parameters," NUREG/CR-4551, Vol. 2, Revision 1, SAND86-1309, December 1990.

C.11 Analysis of Seismic Issues

Since the first attempt in the Reactor Safety Study in the mid-1970's to quantify seismic risk, some 25 plant-specific seismic PRAs have been completed. These later PRAs have shown that seismic events can be significant contributors both in terms of core damage frequency and the potential for releases of radioactive material. There are many reasons for these findings. The foremost reason is that like many other external events, a seismic event not only acts as an initiator but can also compromise mitigating systems because of its common-cause effects. Secondly, the large uncertainties associated with the rare (particularly for Central and Eastern United States sites) but large seismic events that are significant to risk analyses result in large uncertainties in the outcome of the risk study. Uncertainties in these risk measures also make seismic events significant contributors when risk indices, such as mean frequencies, are used as measures. Table C.11.1 (reproduced from Ref. C.11.1) shows results of some seismic PRAs. Prior to discussing the issue of the uncertainty in the seismic hazard and its impact on PRA results and interpretation, a brief overview of both the seismic risk analysis procedure and seismic hazard methods is described in the following section.

C.11.1 Issue Definition

The elements of the seismic risk analysis procedure can be identified (Ref. C.11.2) as analyses of (1) the seismic hazard at the site, (2) the response of plant systems and structures, (3) component fragilities, (4) plant system and accident sequences, and (5) consequences. The results of these analyses are used as inputs in defining initiating events, in developing system event trees and fault trees, in quantifying accident sequences, and in modifying the accident progression event trees and consequence models to reflect the unique features of seismic events. There are uncertainties associated with each step of the risk analysis procedure. However, a number of studies (Ref. C.11.3), including the seismic risk studies performed in connection with NUREG-1150 (Parts 3 of Refs. C.11.4 and C.11.5), have shown that the uncertainties in the first element, the seismic hazard analysis, dominate the uncertainties in the overall results.

As shown in Figure C.11.1, the major steps involved in performing the site-specific hazard analysis are as follows:

- Identification of the sources of earthquakes, such as faults (F1, F2) and other seismotectonic sources (A1, A2, A3);
- Evaluation of the earthquake history of the region to assess the frequencies of occurrence of earthquakes of different magnitudes or epicentral intensities (recurrence) and determination of maximum magnitude;
- Development of attenuation relationships (including random uncertainty) to estimate the intensity of earthquake-induced ground motion (e.g., peak ground acceleration) at the site (attenuation); and
- Integration of all the above information to generate the frequencies with which different values of the selected ground-motion parameter would be exceeded (seismic hazard).

Because of the brevity of the historical record and lack of full understanding of earthquake processes and their effects in much of the United States, considerable uncertainties are associated with each of the above steps, resulting in the large uncertainties in the seismic hazard estimates. An accepted procedure for including the uncertainties of the parameters in the hazard analysis is to postulate a set of hypotheses (e.g., specific source configuration, specific value of slope parameters in recurrence relation). A probability value is assigned to each of these hypotheses, based on the analyst's expert judgment. A seismic hazard curve representing the annual frequency of exceeding a specified peak ground acceleration is generated from each hypothesis resulting in a family of different hazard curves, each representing probability of exceedance (see Fig. C.11.1(d)). Such a family of hazard curves has generally been used in past PRA applications.

Two major programs have been undertaken in the past few years to develop methods and data banks to estimate the seismic hazard at all locations of the United States east of the Rocky Mountains. The first program conducted by the Lawrence Livermore National Laboratory (LLNL) under the auspices of the NRC is entitled the Seismic Hazard Characterization Project (Ref. C.11.6). The method used in the LLNL project embodies the four steps described above. In order to capture the uncertainties, both the random (physical) uncertainty and the modeling (knowledge) uncertainty, expert judgment was used to

Table C.11.1 Seismic core damage and release frequencies from published probabilistic risk assessments.

Plant	Type	SSE (g)	Seismic Core Damage Frequency (mean) per Year	Seismic Release Frequency (mean) per Year	% of Total Core Damage	Rank of Release Sequence	Dominant Earthquake Level (g)
Zion 1 & 2	PWR	0.17	5.6E-6	———	3	1	>0.35
Indian Point 2	PWR	0.15	1.4E-4 (rev. 4.8E-5)	1.4E-4	30	1	>0.30
Indian Point 3	PWR	0.15	3.1E-6 (rev. 2.5E-5)	2.4E-6	1	8	>0.30
Limerick	BWR	0.15	4.0E-6	2.0E-7	—	1	>0.35
Millstone 3	PWR	0.17	9.4E-5	———	68	3	>0.3
Seabrook	PWR	0.25	2.9E-5	———	13	30	>0.3
Oconee 3	PWR	0.15	6.3E-5	6.0E-5	25	1	>0.15

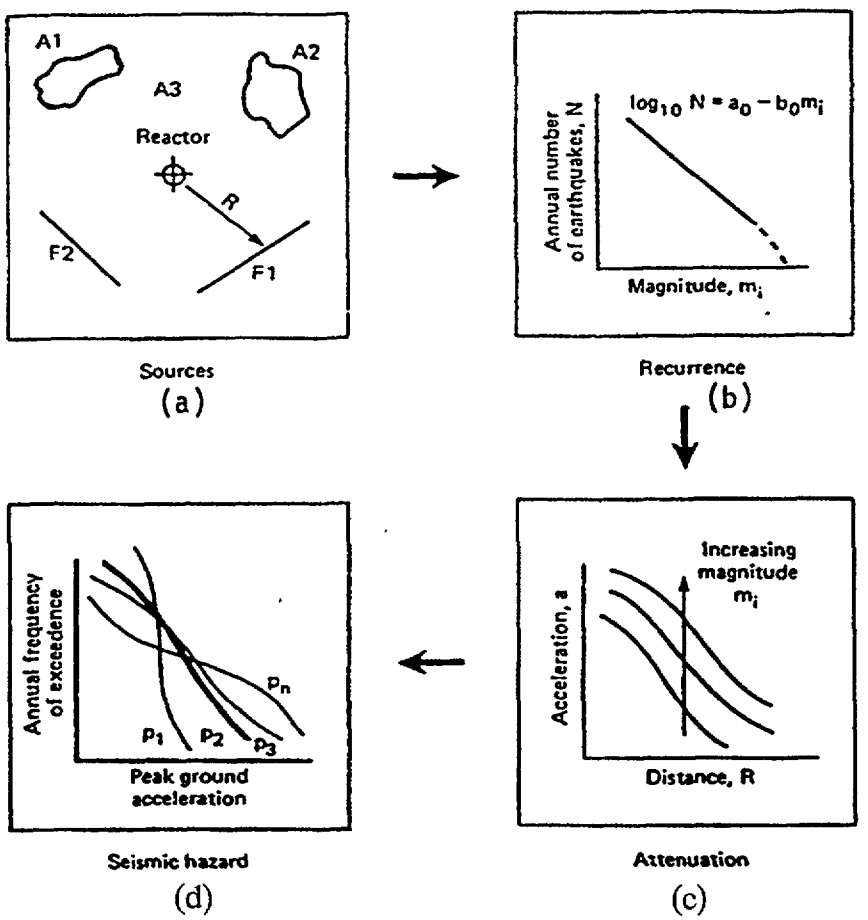

Figure C.11.1 Model of seismic hazard analysis.

assess parameter values and models in the fields of seismicity modeling and ground-motion prediction modeling. To this end two panels were formed. The S-Panel was made up of experts on seismicity and zonation; experts on ground-motion prediction formed the G-Panel. The independence of the experts was promoted by encouraging them, if they so preferred, to use their own information and data bases. The method developed was not intended to lead to some kind of artificial consensus, but rather the display of the full range of judgments was to be retained. The judgments of the experts were elicited through a series of written questionnaires, feedback meetings, and feedback questionnaires.

To propagate uncertainties in parameter values and models and develop a probability distribution of the hazard, an approach based on simulation was used. Using a Monte Carlo approach, each of the parameters was sampled a large number of times from its respective probability distribution, which described its uncertainty. With each hazard curve resulting from a given simulation was associated a weight, or probability of being the true hazard curve, which was calculated as the product of the probabilities or weights of each of the random parameter values used in that simulation. For each pair of seismicity and ground-motion experts (respectively S-Expert and G-Expert) described earlier, a typical simulation was carried out as follows:

- Draw a map from the distribution of maps for this S-Expert,
- For each one of the seismic sources in a sample map, draw a set of seismicity parameters from their respective distribution, i.e.:
  - A value for the a parameter of the recurrence law (see Fig. C.11.1(b)),
  - A value for the b parameter of the recurrence law (b is allowed to have three levels of correlation with a, as specified by the S-Expert, Fig. C.11.1(b)), and
  - The value of the upper magnitude (or intensity) cutoff;
- Draw a ground-motion model from the distribution of models; and
- Draw a value for the random uncertainty parameter, which is associated with the selected ground motion, for the appropriate Eastern United States region (Northeast, Southeast, North Central, or South Central).

The hazard was calculated for each of the seismic sources and combined for all sources. Each simulation gives a possible hazard curve. For each site, typically 2,750 curves (50 simulations for each of the possible combinations of 5 G-Experts and 11 S-Experts) were developed. Percentiles, usually the 15th, 50th, and 85th, were then used to describe the uncertainty in the hazard. Typical hazard curves are presented in Figure C.11.2 for the Peach Bottom site.

In addition to the hazard curves for 69 nuclear plant sites east of the Rocky Mountains, the LLNL project also generated uniform hazard spectra for various return periods for each site. Uniform hazard spectra for the Peach Bottom site are presented in Figure C.11.3.

The second program was undertaken by the Electrical Power Research Institute (EPRI) (Ref. C.11.7) with similar objectives to the LLNL program. While the LLNL and EPRI approaches have many similarities, that is, they rely upon expert judgment, there are significant differences in the manner in which the expert judgment was solicited and in the treatment of ground motions (Ref. C.11.8). EPRI's major effort was aimed at developing a structured approach to the delineation and characterization of seismic sources. On the other hand, LLNL's approach was that of the solicitation of expert judgment from individuals, among whom there was a moderate amount of interaction, while EPRI relied upon the use of expert teams, among whom there was a great deal of interaction through workshops and meetings devoted to specialized seismological and tectonic topics. For example, instead of the 11 individuals, (primarily seismologists) upon whom LLNL relied for the seismic zoning input, EPRI used six teams, each of which spanned the disciplines of geology, seismology, and geophysics. After discussion and interaction, each team agreed upon a common input. In order to ensure uniformity in data assumptions, EPRI compiled a common geological, geophysical, and seismological data base. With respect to seismicity recurrence parameters, a good deal of effort was expended in defining uniform statistical techniques for estimating these parameters. The teams had the option, based on these studies, of allowing variations within the

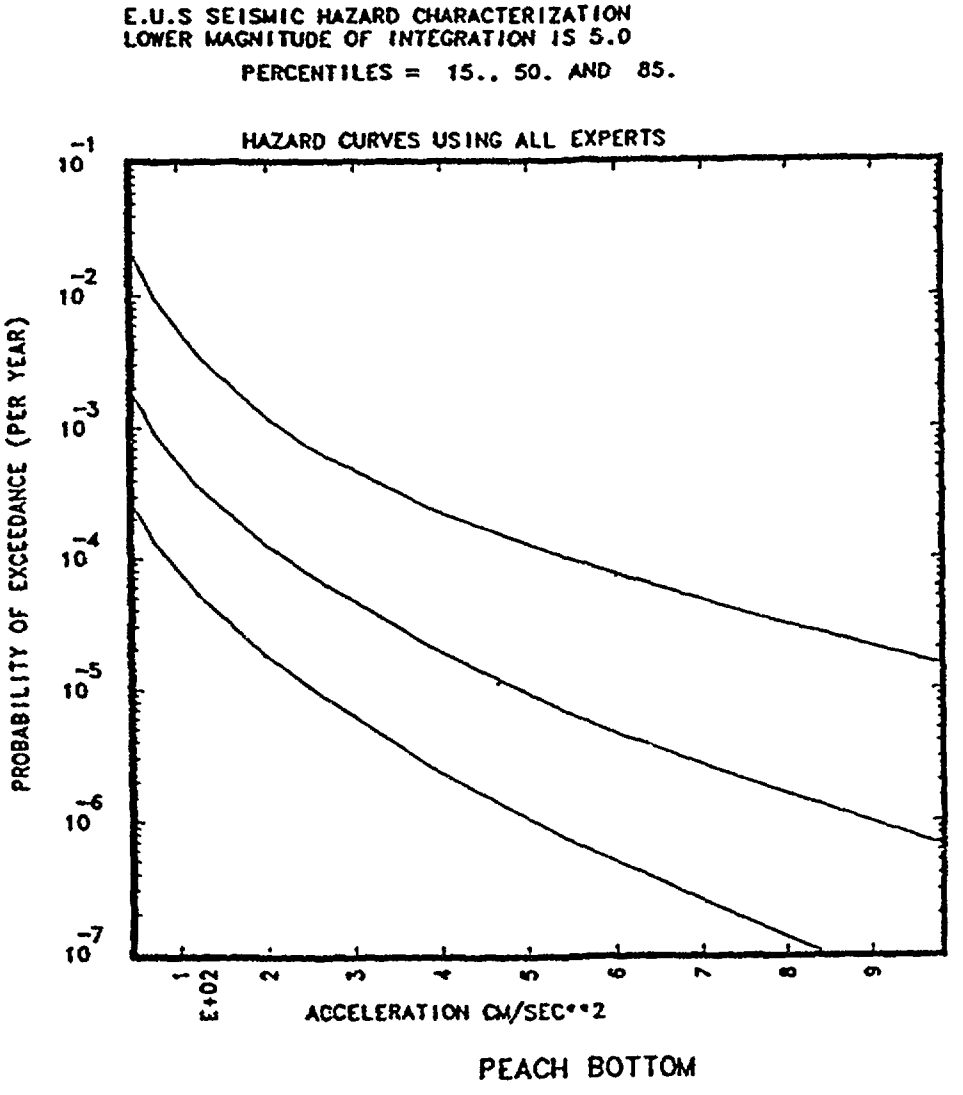

Figure C.11.2 LLNL hazard curves for Peach Bottom site.

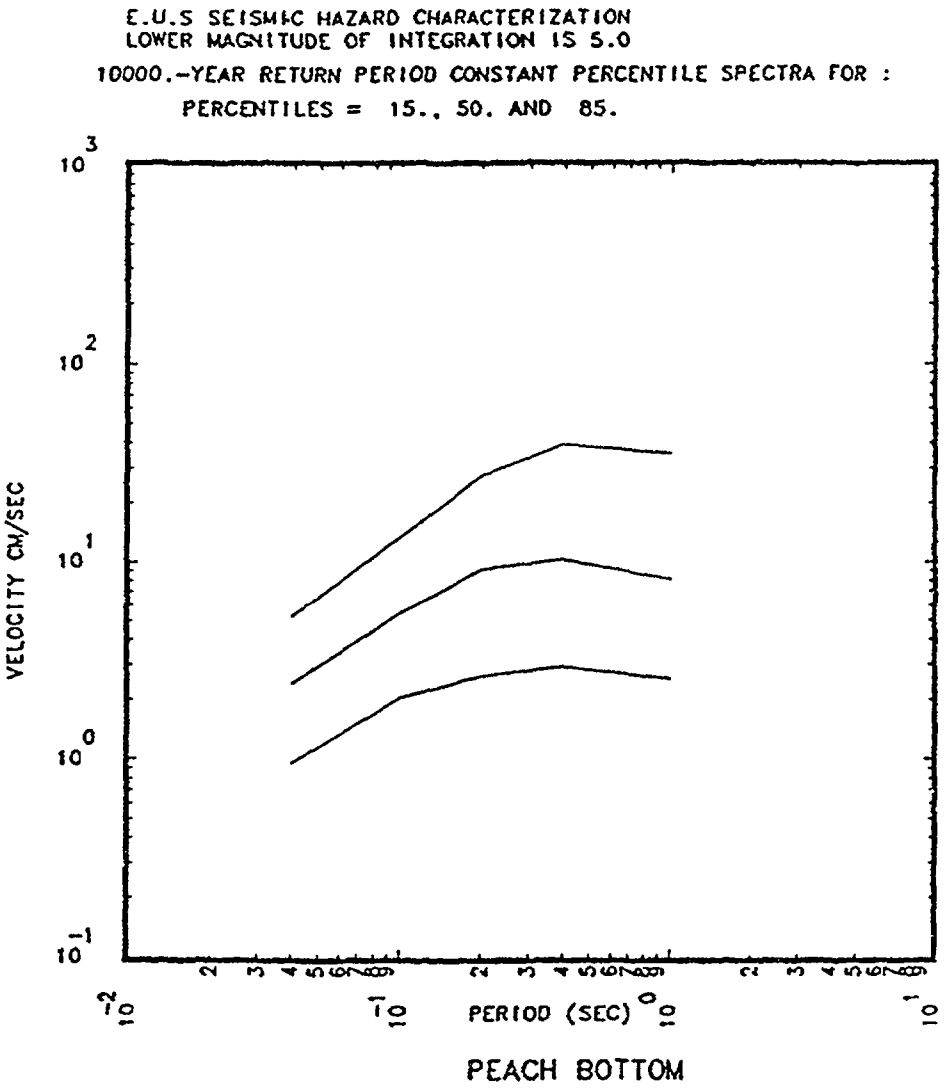

Figure C.11.3 10000–year return period uniform hazard spectra for Peach Bottom site.

seismic sources themselves. Instead of employing an expert panel for the ground motion, EPRI used three models to reflect uncertainties in the ground-motion estimates. EPRI felt that ground-motion model development is less subjective and fairly well defined and any needed evaluation could be done by its consultants (Ref. C.11.9). In the EPRI approach, in contrast to the Monte Carlo approach used by the LLNL, uncertainties in seismic sources, seismicity parameters, maximum magnitude, and ground-motion models are propagated through and represented in a logic-tree format (Fig. C.11.4). Each level of the tree represents one source of uncertainty; each terminal node represents one "state of nature." Corresponding to each terminal node, there is a hazard curve. The probability associated with a terminal node (and with the corresponding hazard curve) is the product of the probabilities associated with all intermediate branches in the path from the root to the terminal node. Results for the Peach Bottom site from the EPRI program are shown in Figure C.11.5. The uniform hazard spectra obtained from the EPRI program, in general, exhibit similar characteristics to the LLNL results. According to Reference C.11.10, which compared preliminary results of both studies of nine test sites, the most significant differences in the results of the LLNL and EPRI studies that primarily affect the uncertainty distributions are (see also Ref. C.11.11):

- A larger number of ground-motion models, encompassing a large range of opinions, are used in the LLNL project than in the EPRI study; and

- The EPRI study has less uncertainty in the seismicity parameters, leading to lower uncertainty in the estimate of the hazard.

Thus, there are now two sets of hazard curves available for use at sites east of the Rocky Mountains. Issues associated with the use of these two sets of hazard curves, associated uncertainties, and consideration of uniform hazard spectra in the PRA applications are discussed below.

The primary issue in the seismic risk analysis is the large uncertainty associated with the computed results and use of these results in decisionmaking. The uncertainties, as discussed earlier, largely stem from uncertainties in hazard estimates. In addition to the issue of the uncertainty in hazard, publication of uniform hazard spectra will also have an impact on the PRA application.

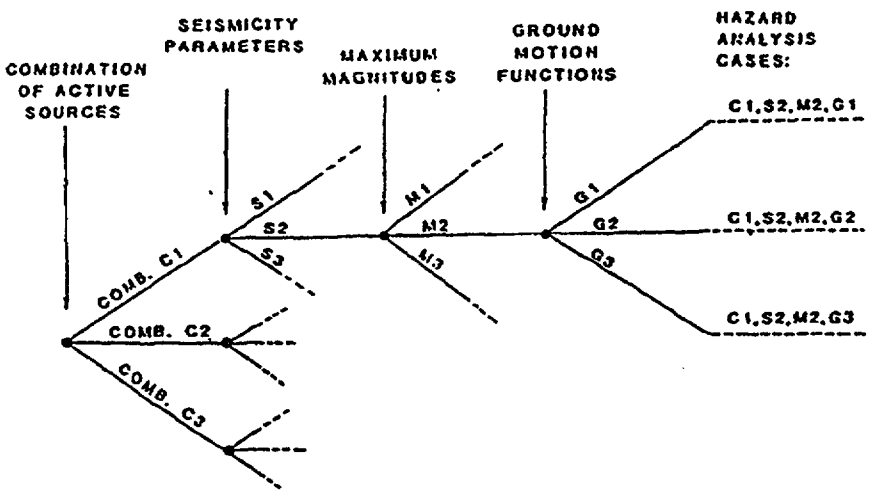

Figure C.11.4 Example of logic-tree format used to represent uncertainty in hazard analysis input (EPRI program).

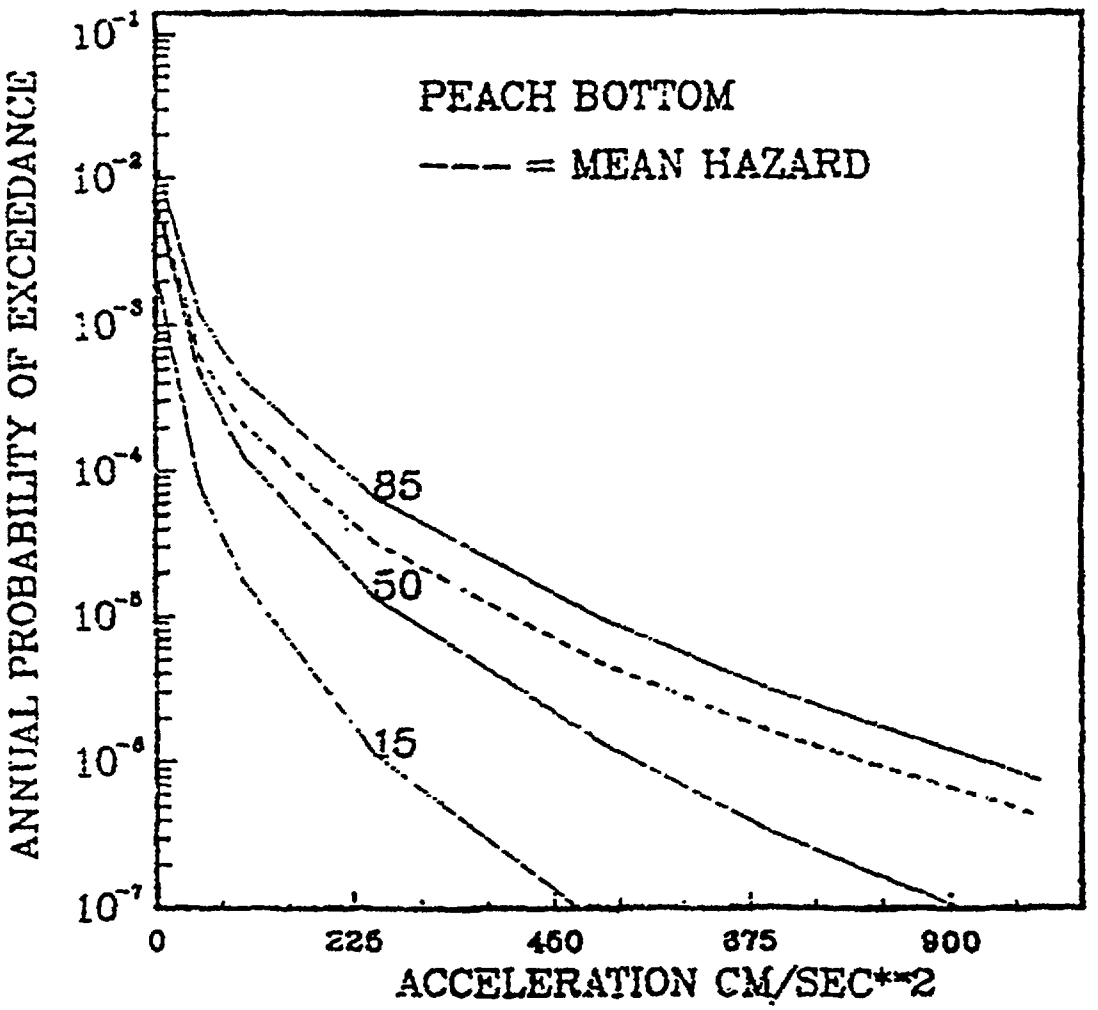

Figure C.11.5 EPRI hazard curves for Peach Bottom site.

- *Uncertainty in Hazard Estimates:* As seen in Figure C.11.2, from the large spread between the 15th percentile and 85th percentile of the hazard calculations, it is evident that seismic hazard estimates are associated with substantial uncertainties. In terms of ground-motion parameters, the LLNL results (Ref. C.11.12) indicate that, for a fixed annual probability of exceedance, the difference between the 15th and 85th percentile curves corresponds to approximately a factor of 4 or larger in both peak ground acceleration (PGA) and spectrum-related ground-motion estimates. When the probability of exceedance at the 15th and 85th percentile levels are compared at a fixed PGA, large differences, ranging from a factor of 40 to 100, can be observed, depending upon the PGA level. Sensitivity studies have shown that the largest contribution to modeling uncertainty is caused by the uncertainties associated with the models relating ground motion to distance and magnitude. It should also be noted that the mean hazard, because it is sensitive to a highly skewed distribution, can lie above the 85th percentile of the hazard. Median hazards are not strongly affected by the extreme values of the probability distributions.

  Sensitivity studies on the LLNL results indicate that individual expert judgment can, under certain conditions, dominate the hazard calculation. Specifically, if a site in question is a rock-based site where distant large earthquakes are the major contributors to the overall seismic hazard, the inclusion or exclusion of the input from one ground-motion expert (G-Expert 5) leads to significant differences in the hazard. This effect is particularly evident at the 85th percentile and mean hazard estimates.

  The widely recognized difficulties in the estimation of the likelihood of rare events are compounded in the case of seismic hazard estimation by the lack of knowledge with respect to basic causes and future locations of earthquakes in the Eastern United States. This is clearly illustrated by the results of two independent studies, the LLNL and the EPRI studies. These studies represent the most comprehensive efforts of their kind undertaken to date. Although attempts have been made (Ref. C.11.10) and studies are under way to understand and reduce the differences between the results of these studies, the methods of each of these studies should be viewed as valid. Because of the inherent uncertainties, results from both sets of hazard curves should be included in a risk study (Ref. C.11.12). Reducing the combined range of uncertainties to a single point estimate ignores the fundamental message. Enveloping the uncertainty is also inappropriate in that the least well-defined aspects are the upper and lower bounds. Therefore, in NUREG–1150 studies, both sets of curves are used independently and results are presented side by side (Figs. C.11.6 and C.11.7). The use of these two sets of hazard curves and associated risk analysis results are discussed in Section C.11.2.

- *Uniform Hazard Spectra:* As discussed earlier, the LLNL and EPRI studies have also provided estimates of uniform hazard spectra for each Eastern and Central United States site. As described in Section C.11.2, the NUREG–1150 studies used LLNL and EPRI hazard curves but did not use uniform hazard spectra. One of the major findings of both the LLNL and EPRI studies is that the estimated uniform hazard spectra for eastern earthquakes are higher at high frequencies and lower at low frequencies compared to standard broadband spectra (e.g., spectra given in Ref. C.11.13) based on recorded western earthquakes. The spectra used in the NUREG–1150 analyses were developed using primarily western records. Implications of the differences between these spectra on the risk analysis will be studied in detail in a later study but the inference for Surry is quite clear. For all structural frequencies of interest, the uniform hazard spectra are below the median spectra used in the analysis. This should result in smaller plant response for a given PGA. The overall effect, with all else remaining the same, will be a reduction in the core damage frequency. For the Peach Bottom site, the impact on the mean core damage and distribution is also not expected to be significant since, at the frequencies of important structures, both response spectra are similar. These issues will be addressed in additional staff studies. Additional issues associated with the use of uniform hazard spectra are related to partitioning of uncertainties among hazard curves, spectra, and fragility analyses. Both the PGA hazard curves and uniform spectra reflect uncertainty in the underlying seismological parameters as well as randomness in the ground-motion estimates. In addition, peak-to-valley variability and random variability between horizontal components may also be included in these two estimates. Many times these uncertainties are included in the fragility analysis. Thus, clear understanding of uncertainties is needed to avoid double counting or underestimation.

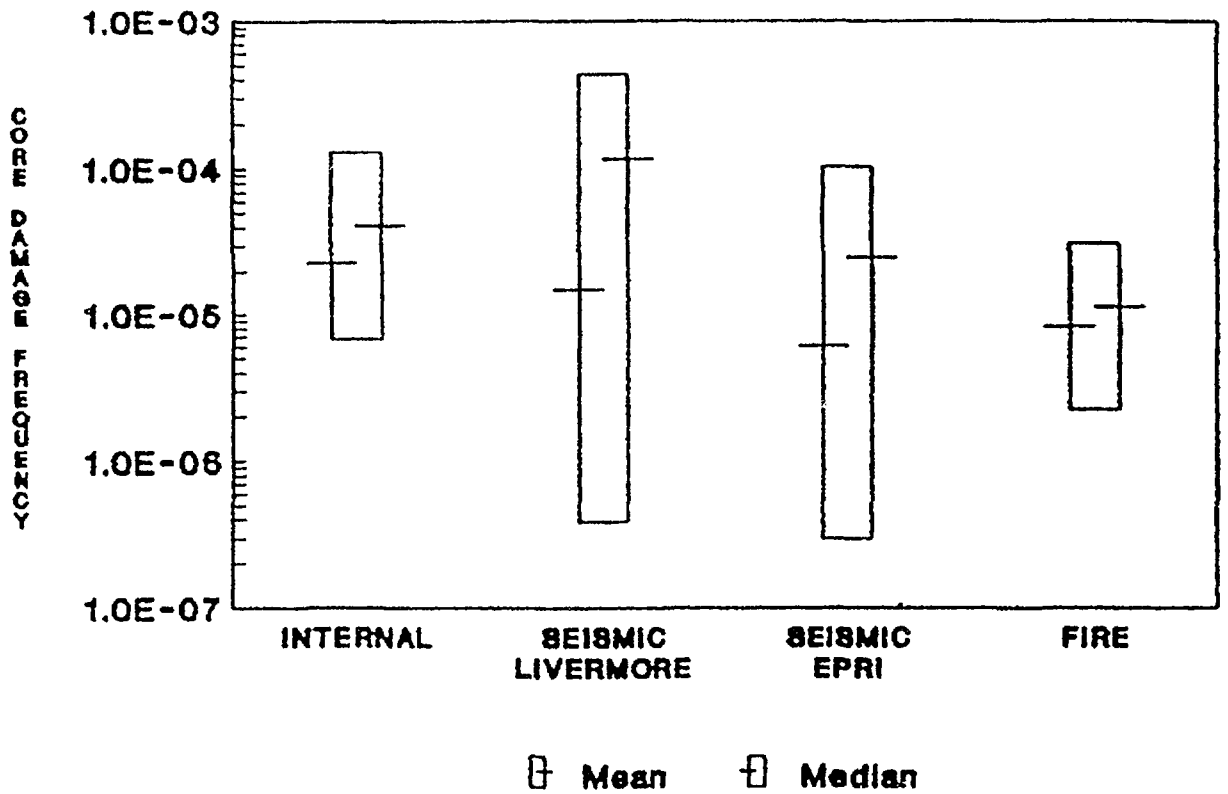

Figure C.11.6 Surry external events, core damage frequency ranges (5th and 95th percentiles).

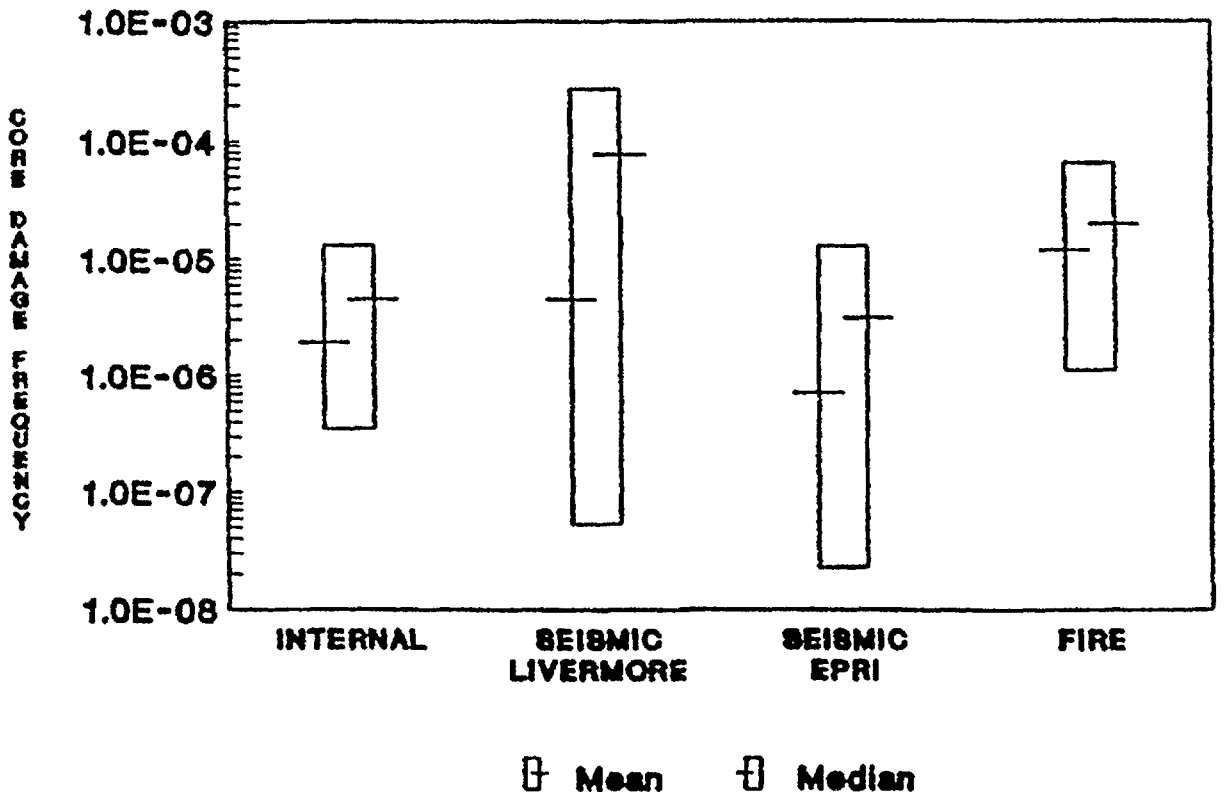

Figure C.11.7 Peach Bottom external events, core damage frequency ranges (5th and 95th percentiles).

C.11.2 Treatment in PRA and Results

In the NUREG–1150 seismic analyses, both the LLNL and EPRI hazard estimates have been used. These estimates, as shown in Figures C.11.2 and C.11.5, are given at selected confidence levels of 15 percent, 50 percent, and 85 percent and mean curves (it is also possible to get results for 5 percent and 95 percent confidence level). In principle, one can use the entire set of 2,750 hazard curves that were generated for each site in the LLNL study. However, since the results are presented in the form of Figure C.11.2, one has to resort to fitting a distribution to the hazard uncertainty at any given PGA and then discretize the distribution into a chosen set of hazard values in order to obtain a discrete set of hazard curves. This approach was used in Reference C.11.14, which also used the LLNL input. In NUREG–1150, it was assumed that the seismic hazard could be approximated by a lognormal distribution that fit the calculated 50th percentile and mean. While the lognormal assumption is a good approximation, the actual distributions vary. The differences can be seen by comparing the actual calculated hazard curves at a different percentile from the LLNL study with that determined from the lognormal fit. The EPRI hazard results can deviate more from a lognormal distribution. In the NUREG–1150 studies, the full lognormal distribution was used in drawing samples for the Monte Carlo analyses. Therefore, no discretization was necessary.

Sensitivity studies have been carried out for both Surry and Peach Bottom analyses to understand the impact of the lognormal assumption as well as to assess the potential effect of contributions from the tail of the assumed distribution. (See individual plant studies (Parts 3 of Refs. C.11.4 and C.11.5) for further discussions.) Since the distribution is derived by fitting it to the mean, there should be minimal impact on the mean core damage frequency from this approximation.

The necessity of the above approach of fitting a distribution to the uncertainty will also result in not simulating the real nature of hazard curves that may intersect each other. The correlation of hazard values at different accelerations arising out of the same source/ground-motion hypothesis model cannot also be consistently treated. The major contributions to the hazard cannot *a priori* be correlated with the size of the contributing earthquakes. For example, the study results (Ref. C.11.6) indicate that although some plant sites in the New England area exhibit relatively high seismic hazards, the contribution to the overall hazard from earthquakes with magnitudes of 6.5 or larger is significantly less than the contribution from these large earthquakes to plant sites near New Madrid, Missouri, or those near Charleston, South Carolina. Such a deaggregation of hazard curves and uniform hazard spectra can be extremely useful in understanding the relative contribution from large magnitude (potentially damaging) events versus low magnitude (less damaging) events. It is very important to understand that PGAs have not been shown to be good indicators of the damage potential of an earthquake for ductile structures/components since low magnitude events can produce a large PGA but little damage (e.g., Ref. C.11.15). (This concern has been alleviated to some extent in the LLNL and EPRI studies by the use of a minimum magnitude of 5.0, the magnitude below which damage to the engineered structures is considered unlikely.) To better characterize damage potential, information with respect to the frequency content of the motion and duration are vital. The fragility analysis used in the NUREG–1150 studies takes into account, to some extent, the earthquake magnitude effects by using the concept of an effective ductility (see Parts 3 of Refs. C.11.4 and C.11.5 for detailed discussions). However, detailed building/component response analysis (including nonlinear effects, if necessary) using magnitude-dependent spectral shapes can be used to remove further conservatisms, if any, included in the plant response/fragility analysis. Consequences of a building failure can also be evaluated more realistically.

While such understanding of hazard curves will not necessarily result in less uncertainty or changes in core damage frequencies, perspectives into which magnitude earthquakes and characteristics of the associated ground motion that contribute to these frequencies can be extremely useful. Recovery actions, not usually considered acceptable in seismic PRAs, may be feasible for the lesser magnitude events. In the additional staff studies, the deaggregation of the hazard curve into various magnitude ranges will be considered to the extent possible.

The seismic risk analysis method used in NUREG–1150 requires the use of earthquake time histories to determine the vibratory motion within the nuclear power plant. Peak ground accelerations from the seismic hazard curves were used to anchor a set of real earthquake records (time histories) for each site. These scaled earthquake records were then used to perform a probabilistic response analysis. The seismic hazard studies, while not providing time histories, do, along with defining peak accelerations, define

seismic hazard also in terms of uniform hazard spectra. They are based upon the limited data available from Eastern United States earthquakes and the most current models prepared by seismological experts in the field. They are different from the response spectra of the time histories that were used, which were derived from Western United States earthquakes. The seismic hazard spectra based on eastern earthquakes are higher at high frequencies and lower at low frequencies. Issues associated with the uniform hazard spectra and their use in the PRA application were discussed in Section C.11.1 along with the possible impact on the results of NUREG-1150 studies. This issue will be addressed in additional staff studies as discussed above.

After the establishment of the hazard curves and the spectra for use in the plant response calculations, the remaining steps of the seismic risk analysis (that is, plant system and accident sequence analysis and quantification) are described in Appendix A to NUREG-1150 and in plant-specific external-event analyses (Parts 3 of Refs. C.11.4 and C.11.5). Estimates of the core damage frequencies for the Surry and Peach Bottom plants are reproduced in Figures C.11.6 and C.11.7. Values of mean, 5th, 50th, and 95th percentile estimates are also given in Table C.11.2.

Sensitivity studies conducted specifically for Surry and Peach Bottom in this program and other sensitivity studies have shown that the uncertainty in seismic hazard curves dominates the uncertainty in the seismic core damage frequency. Table C.11.3 shows results of sensitivity analysis performed for Peach Bottom to ascertain the relative contribution of the hazard curve, the seismic response, and the seismic fragility modeling uncertainties to the overall core damage frequency.*

The base case mean, 95th percentile, and 50th percentile core damage frequencies are shown in the first column. The second column shows the corresponding values with the hazard curve fixed at its median value (i.e., with no modeling uncertainty). This results in an error factor of 3.5 versus the error factor of 30.1 for the base case. Clearly, the hazard curve is contributing the vast majority of the uncertainty to the base case results. Note also that the mean core damage frequency is reduced by a factor of 6.1 when no hazard curve uncertainty is included. The third column shows a case wherein all the fragility and response modeling uncertainties are simultaneously set to zero. The error factor for this case is 25.5, which shows that the reduction in response and fragility uncertainties has little effect on the overall core damage uncertainty. For this case, the mean core damage frequency is reduced only by a factor of 1.9. Thus, the fragility and response uncertainties play little role in determining the mean core damage frequency. However, conservatisms associated with the fragilities (median values and uncertainties) and assumed consequences, given a failure of a certain component, may have significant impact on core damage

Table C.11.2 Core damage frequencies.

	5th	Median	95th	Mean
Surry				
LLNL	3.92E-7	1.48E-5	4.38E-4	1.16E-4
EPRI	3.00E-7	6.12E-6	1.03E-4	2.50E-5
Fire	5.37E-7	8.32E-6	3.83E-5	1.13E-5
Internal	6.75E-6	2.30E-5	1.31E-4	4.01E-5
Peach Bottom				
LLNL	5.33E-8	4.41E-6	2.72E-4	7.66E-5
EPRI	2.30E-8	7.07E-7	1.27E-5	3.09E-6
Fire	1.09E-6	1.16E-5	6.37E-5	1.96E-5
Internal	3.50E-7	1.90E-6	1.30E-5	4.50E-6

*Note that the hazard curves used in this sensitivity analysis are not the same as ones used in the final calculation, however, the conclusions are the same. See Part 3 of Reference C.11.5 for the final results.

Table C.11.3 Comparison of contributions of modeling uncertainty in response, fragility, and hazard curves to core damage frequency.

P_{cm}	Base Case	No Modeling Uncertainty in Hazard	No Modeling Uncertainty in Response, Fragility
Mean	1.55E-5	2.25E-6	8.13E-6
95%	5.78E-5	6.53E-6	3.50E-5
50%	1.92E-6	1.87E-6	1.37E-6
P_{cm} (95%)	30.1	3.5	25.5
P_{cm} (50%)			
$\frac{E[P_{cm} \text{ base case}]}{E[P_{cm}]}$	1.0	6.1	1.9

frequencies if a single loss dominates the contribution. Dominant sequences and their contributions can also be affected by fragility/consequence assumptions.

These results show quite clearly that the uncertainty in the hazard curve is the dominant factor in both the mean value of core damage frequency and in the uncertainty of the core damage frequency. Further, as discussed in the plant-specific analyses (Part 3 of Ref. C.11.5), it is the mean hazard curve that drives the mean estimate of core damage frequency. Again, this shows the dominant influence of the hazard curve uncertainty (which determines the mean hazard curve) in determining the mean core damage frequency.

Sensitivity studies are also conducted in the plant-specific analyses to examine the importance of the basic seismic failure events to the estimates of mean core damage frequencies. These studies show that for a dominant component, if no failure is assumed, the percentage reduction in the core damage frequency would be in the range of 40 percent. Note that given large uncertainties associated with the seismic results, a change in the mean core damage frequency by a factor of two or so may not be that significant. However, the fragility of the plant (conditional failure probability at a given PGA) may improve appreciably.

In Table C.11.4, dominant sequences and their contributions to the mean core damage frequency are listed for the Peach Bottom plant for both the LLNL and the EPRI hazard curves. Similar studies for the Surry plant are also discussed in the plant-specific studies. Observations discussed here are equally valid for both plants. As seen from this table, although the numerical values are quite different for each sequence when the LLNL or the EPRI hazard curves are used, the order is the same and the relative contributions are slightly varied. This is not surprising since the two mean curves do not intersect each other or indicate drastically different characteristics, such as one being truncated at some acceleration value. If this were the case, then one might expect ranking of sequences and elimination or addition of some sequences. Since the order of dominant sequences remains the same for both the hazard curves, perspectives gained as to the dominant components are also robust. Perspectives as to dominant sequences and components could also be affected if the spectral shapes associated with the different hazard curves were quite dissimilar. However, the uniform hazard spectra from both the LLNL and EPRI studies seem to exhibit similar characteristics.

For the Peach Bottom plant, Figure C.11.8 shows contributions from the different earthquake ranges to the mean core damage frequencies resulting from the use of both the LLNL and the EPRI hazard curves. For both the hazard curves, the majority of contributions is coming from an earthquake range between 0.45g to 0.75g consistent with the Peach Bottom mean plant fragility curve (Fig. C.11.9) for which roughly the 50 percent conditional core damage frequency occurs around 0.6g. Thus, there is a relative robustness as to which earthquake range contributes to the mean core damage frequencies.

Table C.11.4 Dominant sequences at Peach Bottom.

Total Mean P_{cm} = 7.66E-5 (LLNL), 3.09E-6 (EPRI)				
Dominant Sequences	**LLNL**		**EPRI**	
T_1-33	3.69E-5	(48%)	1.61E-6	(52%)
ALOCA-30	1.84E-5	(24%)	6.70E-7	(21%)
RVR-1	8.92E-6	(11%)	3.27E-7	(11%)
S_1LOCA-70	6.67E-6	(9%)	1.85E-7	(6%)
RWT-1	2.76E-6	(4%)	1.75E-7	(6%)
S_2LOCA-42	1.20E-6	(2%)	4.90E-8	(2%)
By Sequence	**LLNL**		**EPRI**	
Transients (LOSP)	3.69E-5	(48%)	1.61E-6	(52%)
LOCAs	2.59E-5	(34%)	9.04E-7	(29%)
Vessel Rupture	8.92E-6	(11%)	3.27E-7	(11%)
RWT Bldg Failure	2.76E-6	(4%)	1.75E-7	(6%)

Several long-term studies are planned to better understand some of the issues associated with the hazard definition; however, it is clear that results of seismic risk analysis will have large uncertainties associated with them. From examination of Table C.11.2, it is evident that conflicting conclusions can be obtained when point estimates are used as risk indices. For example, if the median estimates are used to determine the relative importance between the seismic initiators and the internal initiators, one will conclude that for the Surry analysis, with either the LLNL hazard or the EPRI hazard estimates, the contribution to the total core damage frequency is larger from the internal initiators than the seismic initiators. Conversely, if the means are used, one would conclude that, based on the use of the LLNL hazard curves, the contribution from the seismic initiators is much larger than that from the internal initiators. Based on the results from the EPRI hazard curve, the conclusion would be that internal initiators contribute more than seismic initiators. These findings illustrate the confusion that can result if single estimates are used to characterize the risk.

One clear conclusion is that the distribution of the seismic-induced core damage frequencies are more uncertain than the internal frequencies and their distribution overlaps with the distribution from other initiators and cannot be ignored. In light of the large uncertainties, any decisionmaking should take into account the full range of uncertainty as well as engineering insights and understanding obtained regarding the integrated plant response to a seismic event. Some of the robust findings, such as perspectives regarding dominant sequences and components, were discussed in the preceding paragraphs and can be used to evaluate the need to further refine the analysis or enhance safety by improving the plant procedures or implementing cost-effective fixes.

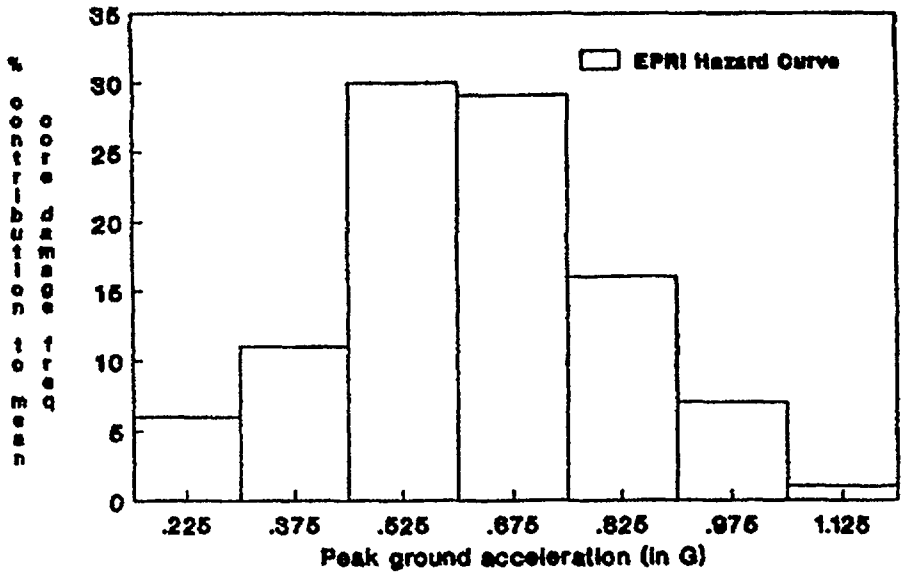

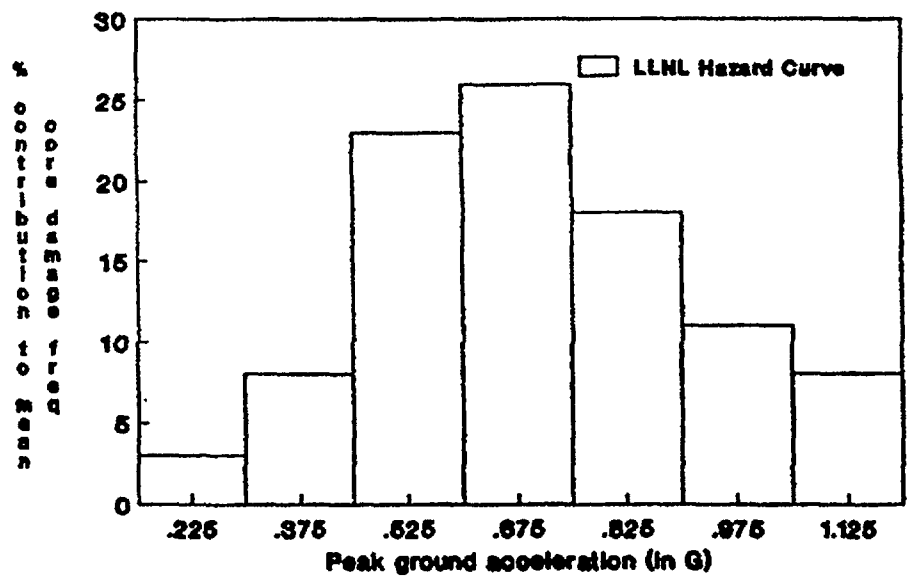

Figure C.11.8 Contribution from different earthquake ranges at Peach Bottom.

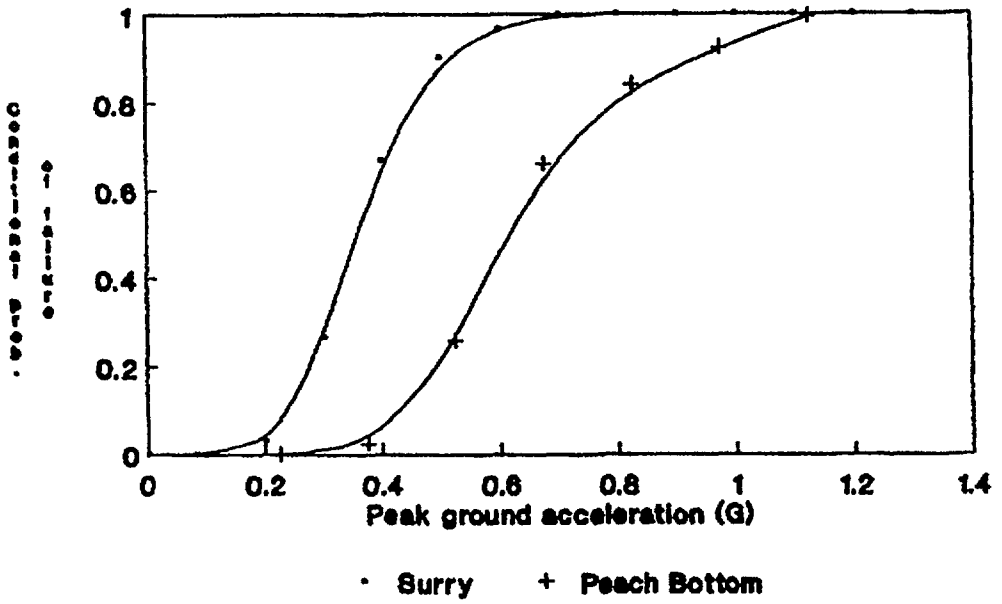

Figure C.11.9 Mean plant level fragilities.

REFERENCES FOR SECTION C.11

C.11.1 P. G. Prassinos, "Evaluation of External Hazards to Nuclear Power Plants in the United States: Seismic Hazard," Lawrence Livermore National Laboratory, NUREG/CR-5042, Supplement 1, UCID-21223, April 1988.

C.11.2 J. W. Hickman et al., "PRA Procedures Guide. A Guide to the Performance of Probabilistic Risk Assessments for Nuclear Power Plants," American Nuclear Society, NUREG/CR-2300, Vols. 1 and 2, January 1983.

C.11.3 M. K. Ravindra et al., "Sensitivity Studies of Seismic Risk Models," Electric Power Research Institute (EPRI), EPRI NP-3562, June 1984.

C.11.4 R. C. Bertucio and J. A. Julius, "Analysis of Core Damage Frequency: Surry Unit 1," Sandia National Laboratories, NUREG/CR-4550, Vol. 3, Revision 1, SAND86-2084, April 1990.

C.11.5 A. M. Kolaczkowski et al., "Analysis of Core Damage Frequency: Peach Bottom Unit 2," Sandia National Laboratories, NUREG/CR-4550, Vol. 4, Revision 1, SAND86-2084, August 1989.

C.11.6 D. L. Bernreuter et al., "Seismic Hazard Characterization of 69 Nuclear Power Plant Sites East of the Rocky Mountains," Lawrence Livermore National Laboratory, NUREG/CR-5250, Vols. 1-8, UCID-21517, January 1989.

C.11.7 Seismicity Owners Group (SOG) and EPRI, "Seismic Hazard Methodology for the Central and Eastern United States," EPRI NP-4726, July 1986.

C.11.8 L. Reiter, "Current Trends in the Estimation and Application of Probabilistic Seismic Hazard in the United States," *Proceedings of IAEA Specialists Meeting on Earthquake Ground Motion* (Moscow, USSR), March 24–28, 1986.

C.11.9 Letter from L. Reiter, NRC, to R. A. Thomas, SOG, Review Comments on EPRI Ground Motion Models for Eastern North America, dated August 3, 1988.

C.11.10 D. L. Bernreuter et al., "Seismic Hazard Characterization of the Eastern United States: Comparative Evaluation of the LLNL and EPRI Studies," Lawrence Livermore National Laboratory, NUREG/CR–4885, UCID–20696, May 1987.

C.11.11 Letter from J. E. Richardson, NRC, to R. A. Thomas, SOG, Safety Evaluation Review of the SOG/EPRI Topical Report, "Seismic Hazard Methodology for the Central and Eastern United States," EPRI NP–4726, dated September 20, 1988.

C.11.12 Memorandum from G. Bagchi, NRC, to L. Shao, NRC, Publication of NUREG/CR–5250, "Seismic Hazard Characterization of 69 Nuclear Power Plant Sites East of the Rocky Mountains," dated March 21, 1989.

C.11.13 U.S. Atomic Energy Commission, Regulatory Guide 1.60, "Design Response Spectra for Nuclear Power Plants," Revision 1, December 1973.

C.11.14 P. G. Prassinos et al., "Seismic Failure and Cask Drop Analyses of the Spent Fuel Pools at Two Representative Nuclear Power Plants," Lawrence Livermore National Laboratory, NUREG/CR–5176, UCID–21425, January 1989.

C.11.15 J. W. Reed et al., "A Criterion for Determining Exceedance of the Operating Basis Earthquake," EPRI NP–5930, July 1988.

C.12 Analysis of Fire Issue

Based on plant operating experience over the last 20 years, it has been observed that typical nuclear power plants will have three to four significant fires over their operating lifetime. Previous probabilistic risk assessments (PRAs) have shown that fires are a significant contributor to the overall core damage frequency, contributing anywhere from 7 percent to 50 percent of the total, considering contributions from internal, seismic, flood, fire, and other events (Refs. C.12.1 and C.12.2). There are many reasons for these findings. The foremost reason is that like many other external events, a fire event not only acts as an initiator but can also compromise mitigating systems because of its common-cause effects. An overview of the fire risk analysis procedure is described in the following sections. These sections will give the necessary background for the subsequent discussion of the fire issues.

C.12.1 Analysis Procedure for NUREG-1150 Fire Analysis

As described in detail in Reference C.12.3, the elements of a fire risk analysis procedure can be identified as (1) screening and (2) quantification of the remaining unscreened fire areas.

The screening analysis is comprised of:

1. Identification of relevant fire zones. Those Appendix R (Ref. C.12.4) identified fire zones that had either safety-related equipment or cabling for such equipment were determined to require further analysis.

2. Screening of fire zones based on probable fire-induced initiating events. Determination of the fire frequency for all plant locations and determination of the resulting fire-induced initiating events and "off-normal" plant states were made.

3. Screening of fire zones based on both order and frequency of cut sets.

4. Numerical evaluation and culling of remaining fire zones based on frequency.

After the screening analysis has eliminated all but the probabilistically significant fire zones, quantification of dominant cut sets is completed as follows:

1. Determine temperature response in each fire zone.

2. Compute component fire fragilities. The latest version of the fire growth code, COMPBRN III (Ref. C.12.5), with some modifications is used to calculate fire propagation and equipment damage. These fire calculations are only performed for the fire areas that survived the screening analysis.

3. Assess the probability of barrier failure for all remaining combinations of fire areas. A barrier failure analysis is conducted for those combinations of two adjacent fire areas which, with or without additional random failures, remain after the screening analysis.

4. Perform a recovery analysis. In a fashion similar to that of the internal-event analysis, recovery of non-fire-related random failures is addressed. Appropriate modifications to recovery probabilities are addressed as necessary.

5. Perform an uncertainty analysis to estimate error bounds on the computed fire-induced core damage frequencies. As in the internal-event analysis, the TEMAC code (Ref. C.12.6) is used in the uncertainty analysis.

Additional detail on the fire analysis methods used in NUREG-1150 may be found in Reference C.12.3.

C.12.2 PRA Results

Tables C.12.1 and C.12.2 provide the core damage frequency results for the Surry and Peach Bottom fire risk assessments, respectively (Refs. C.12.7 and C.12.8). All fire areas that survived the screening process are listed. When comparing fire-induced core damage frequency with the total from all other initiators (including seismic, using the LLNL seismic hazard curves), fire is 7 percent of the total for Surry and

Table C.12.1 Dominant Surry fire area core damage frequency contributors (core damage frequency/yr) (Ref. C.12.7).

Fire Area	Mean	5th Percentile	Median	95th Percentile
Emergency Switchgear Room	6.1E-6	3.9E-9	3.1E-6	2.0E-5
Control Room	1.6E-6	1.2E-10	4.7E-7	6.9E-6
Cable Vault/Tunnel	1.5E-6	6.5E-10	7.0E-7	5.8E-6
Auxiliary Building	2.2E-6	5.3E-7	1.6E-6	5.6E-6
Charging Pump, Service Water Pump Room	3.9E-8	1.4E-10	5.7E-9	1.6E-7
Total	1.1E-5	5.4E-7	8.3E-6	3.8E-5

Table C.12.2 Dominant Peach Bottom fire area core damage frequency contributors (core damage frequency/yr) (Ref. C.12.8).

Fire Area	Mean	5th Percentile	Median	95th Percentile
Emergency Switchgear Room 2A	7.4E-7	4.6E-10	1.6E-7	3.0E-6
Emergency Switchgear Room 2B	3.6E-6	3.5E-9	2.0E-6	1.3E-5
Emergency Switchgear Room 2C	4.7E-6	4.2E-9	2.2E-6	1.7E-5
Emergency Switchgear Room 2D	7.4E-7	4.6E-10	1.6E-7	3.0E-6
Emergency Switchgear Room 3A	7.4E-7	4.6E-10	1.6E-7	3.0E-6
Emergency Switchgear Room 3B	7.4E-7	4.6E-10	1.6E-7	3.0E-6
Emergency Switchgear Room 3C	7.4E-7	4.6E-10	1.6E-7	3.0E-6
Emergency Switchgear Room 3D	8.1E-7	5.3E-10	1.7E-7	3.3E-6
Control Room	6.2E-6	4.2E-10	1.4E-6	8.0E-6
Cable Spreading Room	6.7E-7	9.1E-9	1.7E-7	2.3E-6
Total	2.0E-5	1.1E-6	1.2E-5	6.4E-5

19 percent of the total for Peach Bottom. These fire areas grouped by sequence are given in Tables C.12.3 and C.12.4 for Surry and Peach Bottom, respectively.

The overall fire-induced mean core damage frequency for Surry Unit 1 was found to be 1.1E-5 per reactor year. The dominant contributing plant areas are the emergency switchgear room, auxiliary building, control room, and cable vault/tunnel. Fires in these four areas comprise 99 percent of the total fire core damage frequency. In the cases of the emergency switchgear room, cable vault/tunnel, and the auxiliary building, a reactor coolant pump seal loss-of-coolant accident (LOCA) leads to core damage. The fire itself fails cabling for both the high-pressure injection and component cooling water systems resulting in a seal LOCA. For the control room, a general transient with a subsequent stuck-open power-operated relief valve leads to a small LOCA. Failure to control the plant from the auxiliary shutdown panel results in core damage.

The overall fire-induced mean core damage frequency for Peach Bottom Unit 2 was found to be 1.9E-5 per reactor year. The dominant contributing plant areas are the control room, emergency switchgear room 2C, and emergency switchgear room 2B. Fires in these three areas comprise 75 percent of the total fire core damage frequency. In the case of the control room, a general transient occurs with smoke-induced abandonment of the area. Failure to control the plant from the remote shutdown panel results in core damage. For the two emergency switchgear rooms, a fire-induced loss of offsite power and failure of one train of the emergency service water (ESW) system occurs. Random failure of the other two ESW trains results in station blackout and core damage.

Detailed tracing of control and power cabling revealed that fires can damage the most plant safety functions in cable "pinchpoint" areas. Because of this added detail (cable location identification) as compared with past fire PRAs, many more fire scenarios arose in the initial phases of screening. However, most of these scenarios could be screened from further study by allowing for operator recovery of random failures. The final number of fire areas that survived screening and the total fire-induced core damage frequency for both Peach Bottom and Surry is similar to that found in previous fire PRAs but for dissimilar reasons involving plant-specific cabling configurations. These cable pinchpoint areas were also found in most cases to fail all containment cooling and spray systems. A review of past fire PRAs revealed a similar conclusion with respect to containment systems failure.

C.12.3 Issue Definition and Discussion

The critical fire risk issues and their effect on core damage frequency estimates will be discussed in this section. Uncertainty analysis results (documented in Refs. C.12.7 and C.12.8) highlighted the importance of most of the following issues.

A fire analysis must rely on a partitioning scheme (for fire frequency) to determine fire occurrence frequencies for any given plant area. Additional partitioning within most plant areas will occur because cable "pinchpoint" areas have typically been found to occur in 10 percent or less of these critical plant fire zones. This additional partitioning, based on fire propagation code calculations, is used to determine not only the area of influence of a fire but also the size of the fire required to damage the critical components or their cabling. In older fire PRAs (from the early 1980's), the COMPBRN I code (Ref. C.12.9) was used to determine fire zone specific area ratios and fire size estimates. Larger area ratios and longer time-to-damage estimates were calculated in the NUREG-1150 fire PRAs. As was discussed previously, the modified COMPBRN III code (Ref. C.12.5) was used for the Surry and Peach Bottom fire propagation predictions. For NUREG-1150, small fires were not found to cause damage in most cases. Therefore, fire frequencies were decreased to take credit for the fact that most fires in the data base would not have yielded damage. For plant areas where hot gas layer formation was not predicted, area ratios of 10 percent or less also led to reduced fire frequencies to reflect the situation that a postulated fire could only cause damage in a very specific area within a fire zone. These factors (area ratio and fire size estimate) reduced core damage frequency estimates from what would have been previously predicted (using COMPBRN). However, a competing effect also occurred. Shorter time to damage estimates had the effect of allowing less credit for manual suppression of these fire scenarios (with this impact being overshadowed by the other impacts noted above). Fire testing and code experts walked down each of the Peach Bottom and Surry fire areas to determine the reasonableness of the COMPBRN III predictions. It was their opinion, for the situations that occurred in NUREG-1150, that COMPBRN III yielded reasonable predictions. An analysis of the potential effect of COMPBRN results on fire-induced core

Table C.12.3 Dominant Surry accident sequence core damage frequency contributors (Ref. C.12.7).

Sequence	Fire Area	Mean Core Damage Frequency/yr
$T_3D_3WD_1$	Emergency Switchgear Room	6.1E-6
	Auxiliary Building	2.2E-6
	Cable Vault/Tunnel	1.5E-6
T_3QD_1	Control Room	1.6E-6
	Charging Pump, Service Water Pump Room	3.9E-8

KEY

Symbol	Definition
D_1	Failure of the charging pump system in the high-pressure injection mode.
D_3	Failure of the charging pump system in the seal injection flow mode.
Q	Failure of the SRVs/PORVs to close after a transient.
T_3	Transient consisting of a turbine trip with main feedwater available.
W	Failure of component cooling water to thermal barriers of all reactor coolant pumps.

Table C.12.4 Dominant Peach Bottom accident sequence core damage frequency contributors (Ref. C.12.8).

Sequence	Fire Area	Mean Core Damage Frequency/yr
$T_1BU_1U_2$	Emergency Switchgear Room 2A	7.4E-7
	Emergency Switchgear Room 2B	3.6E-6
	Emergency Switchgear Room 2C	3.6E-6
	Emergency Switchgear Room 2D	7.4E-7
	Emergency Switchgear Room 3A	7.4E-7
	Emergency Switchgear Room 3B	7.4E-7
	Emergency Switchgear Room 3C	7.4E-7
	Emergency Switchgear Room 3D	8.1E-7
$T_3U_1U_2X_1U_3$	Control Room	6.2E-6
	Cable Spreading Room	6.7E-7
$T_1BU_1W_1X_2W_2$ $W_3U_4V_2V_3Y$	Emergency Switchgear Room 2C	8.1E-7
$T_1BU_1W_1X_2W_2$ $W_3U_4V_2V_3Y$	Emergency Switchgear Room 2C	2.7E-7

Table C.12.4 (continued)

KEY	
Symbol	**Definition**
B	Failure of all ac power (station blackout).
T_1	Loss of offsite power transient.
T_3	Transient consisting of a turbine trip with main feedwater available.
U_1	Failure of the high-pressure coolant injection (HPCI) system.
U_2	Failure of the reactor core isolation cooling (RCIC) system.
U_3	Failure of the control rod drive (CRD) system (2 pump mode).
U_4	Failure of the CRD system (1 pump mode).
V_2	Failure of the low-pressure core spray (LPCS) system.
V_3	Failure of the low-pressure coolant injection (LPCI) system.
W_1	Failure of the suppression pool cooling mode of the residual heat removal (RHR) system.
W_2	Failure of the shutdown cooling mode of the RHR system.
W_3	Failure of the containment spray mode of the RHR system.
X_1	Failure to depressurize the reactor coolant system via SRVs or the automatic depressurization system.
X_2	Failure to depressurize the reactor coolant system to allow the shutdown cooling mode of the RHR system to operate.
Y	Failure of primary containment venting (including makeup to the pool as required).

damage frequency predictions was conducted as part of the Fire Risk Scoping Study (Refs. C.12.10 and C.12.11). This analysis concluded that up to a factor of 20 difference was possible for some scenarios.

A second critical issue was the probability of operator recovery from the remote shutdown panel. In the NUREG-1150 fire analysis, this recovery action was quantified on a consistent basis with recovery probabilities calculated for the internal-event analyses. However, since no detailed development of control and actuation circuits was performed, complex control system interactions were not analyzed. If these types of interactions exist for either Surry or Peach Bottom, the effect would be to decrease the credit for recovery from the remote shutdown panel and to increase the fire-induced core damage frequency.

In two studies where detailed models were developed, interactions between the remote shutdown panel and the control room were found. These interactions existed even though the remote shutdown panel was found to be electrically independent of the control room.

The control systems interaction and fire code prediction issues are two of six issues addressed in the Fire Risk Scoping Study. Four other issues that will not be covered in detail here but also have the potential to have a significant effect on fire-induced core damage frequency are:

1. Manual fire brigade effectiveness,
2. Total environment survival,
3. Fire barrier effectiveness, and
4. Fixed fire suppression system damage effects.

Since the Fire Risk Scoping Study was being conducted concurrently with the NUREG-1150 fire analyses, these issues were not addressed in the Surry and Peach Bottom studies. However, any of these issues has the potential to increase the fire core damage frequency when included in an assessment.

A final issue is the Bayesian updating of generic fire initiating event frequencies to determine plant-specific fire frequencies. Several studies have found fire frequency on a plant-wide basis of 0.15 per reactor year. Therefore, any average plant will have only three to four significant fires over its operational lifetime. As was discussed previously, the NUREG-1150 fire analyses used a Bayesian updating procedure to determine plant-specific fire frequencies (for both Surry and Peach Bottom). The plant areas updated were:

1. Control room,
2. Cable spreading room,
3. Auxiliary building, and
4. Electrical switchgear room.

When comparing the Bayesian updated frequencies with the generic fire frequencies for these areas, no more than a factor of 3 difference typically occurred. These plant-specific frequencies were found to be both higher and lower than the average depending on a given plant's operating experience. Since this affects every fire cut set, no more than a factor of 3 difference (as compared with generic estimates) in core damage frequency estimates also occurred.

REFERENCES FOR SECTION C.12

C.12.1 Public Service Company of New Hampshire and Yankee Atomic Electric Company, "Seabrook Station Probabilistic Safety Assessment," Section 9.4, December 1983.

C.12.2 Philadelphia Gas and Electric Company, "Severe Accident Risk Assessment Limerick Generating Station," Chapter 4, Main Report, Report #4161, April 1983.

C.12.3 M. P. Bohn and J. A. Lambright, "Procedures for the External Event Core Damage Frequency Analyses for NUREG-1150," Sandia National Laboratories, NUREG/CR-4840, SAND88-3102, November 1990.

C.12.4 U.S. Code of Federal Regulations, Appendix R, "Fire Protection Program for Nuclear Power Facilities Operating Prior to January 1, 1979," to Part 50, "Domestic Licensing of Production and Utilization Facilities," of Chapter I, Title 10, "Energy."

C.12.5 V. Ho et al., "COMPBRN III—A Computer Code for Modeling Compartment Fires," Oak Ridge National Laboratory, NUREG/CR-4566, ORNL/TM-10005, April 1986.

C.12.6 R. L. Iman and M. J. Shortencarier, "A User's Guide for the Top Event Matrix Analysis Code (TEMAC)," Sandia National Laboratories, NUREG/CR-4598, SAND86-0960, August 1986.

C.12.7 J. A. Lambright et al., "Analysis of Core Damage Frequency: Peach Bottom Unit 2 External Events," Sandia National Laboratories, NUREG/CR-4550, Vol. 4, Part 3, SAND86-2084, December 1990.

C.12.8 J. A. Lambright et al., "Analysis of Core Damage Frequency: Surry Unit 2 External Events," Sandia National Laboratories, NUREG/CR-4550, Vol. 3, Part 3, SAND86-2084, December 1990.

C.12.9 N. O. Siu, "COMPBRN—A Computer Code for Modeling Compartment Fires," University of California at Los Angeles, NUREG/CR-3239, UCLA-ENG-8257, May 1983.

C.12.10 V. F. Nicolette et al., "Observations Concerning the COMPBRN III Fire Growth Code," Sandia National Laboratories, SAND88-2160C, April 1989.

C.12.11 J. A. Lambright et al., "Fire Risk Scoping Study: Investigation of Nuclear Power Plant Fire Risk, Including Previously Unaddressed Issues," Sandia National Laboratories, NUREG/CR-5088, SAND88-0177, January 1989.

C.13 Containment Bypass Sequences

Accident sequences that involve bypass of the containment, thereby having a direct release path to the environment, were assessed to be important at all three PWRs and were risk dominant at the Surry and Sequoyah plants. The two categories of bypass sequences that were found to be important to the NUREG-1150 PWRs are interfacing-system loss-of-coolant accidents (ISLOCAs) and steam generator tube ruptures (SGTRs). The ISLOCA sequences can lead to a direct release path to the environment if failures occur that connect the high-pressure reactor coolant system (RCS) to a low-pressure interfacing system and subsequent failure of the low-pressure boundary occurs outside containment. SGTR sequences can lead to a direct release path to the environment if an SGTR event causes subsequent failure of the secondary side pressure boundary, usually through a stuck-open relief valve. Many different factors influence the initiation and progression of these accident sequences. Some of those factors were evaluated by expert panels, while others were evaluated by the analysis teams. Additional details on these analyses may be found in References C.13.1 and C.13.2.

C.13.1 ISLOCAs—Accident Sequence Issues

This section discusses those issues that arose in the accident sequence analysis of the interfacing-system loss-of-coolant accidents.

C.13.1.1 Issue Definitions

ISLOCAs are sequences in which the pressure isolation valves that separate low-pressure systems from the RCS fail, thus subjecting the low-pressure system piping and components to full RCS pressure. In many cases, the low-pressure system will subsequently fail, and there is a high probability that the failure will occur outside containment, usually in the auxiliary building or the safeguards area. As the RCS loses coolant inventory, makeup will be provided from the refueling water storage tank (RWST). When the water in the RWST is depleted, recirculation cooling is not possible because the water has been lost outside containment. Core damage will then occur if an alternative water supply is not provided. At issue in the accident sequence analysis is the frequency of check valve failures that represent the initiating event for this sequence. This issue was addressed by members of the accident frequency analysis expert panel, including:

Dennis Bley—Pickard, Lowe, and Garrick, Inc.,
Gary Boyd—SAROS, Inc.,
Robert Budnitz—Future Resource Associates, Inc.,
Karl Fleming—Pickard, Lowe, and Garrick, Inc., and
Garreth Parry—NUS Corporation.

C.13.1.2 Technical Basis for Issue Quantification

Three check valve failure scenarios were identified for the Surry and Sequoyah plants. (ISLOCAs were not found to be important at Zion because of the plant-specific configuration of the high-to-low pressure system interfaces.) The three scenarios considered by the expert panel were:

1. Random independent rupture (catastrophic leakage) of the two check valves in series.

2. Failure of one check valve to reclose upon RCS repressurization, followed by random rupture of the other valve.

3. The undetected failure of one valve during operation (between test periods), followed by rupture of the other valve. The undetected failure can be caused by opening of the disc or severe deterioration of the seat. This failure is not detected because the other valve is holding pressure. When the other valve fails, the ISLOCA is initiated.

The panel provided an ISLOCA initiating event frequency distribution considering the three failure modes listed above along with possible common-cause failures affecting valves in the same line. The model for Sequoyah was slightly different from the one for Surry because the accumulators inject between the two

check valves at Sequoyah, thus making failures of the outboard check valve detectable. The expert panelists considered information from valve specialists and available data bases in developing their positions. A high degree of uncertainty is evident in the distributions because of the lack of directly applicable data.

C.13.1.3 Treatment in PRA and Results

The results of the interfacing-system LOCA expert elicitation were used as the primary basis for determining the frequency of the ISLOCA initiating event. The plant analysts provided information on the check valve testing frequency and procedures that influenced the models. Additionally, for Sequoyah some ISLOCAs can be isolated, depending upon the break location. The plant analysts provided the probability that the operators would isolate the break, if possible. Except for the probability of isolating the break at Sequoyah, the ISLOCA events are assessed to proceed to core damage with unity probability, given the initiating event. The probability distributions for the initiating event that resulted from the expert elicitation are shown below. These distributions are for a single high-to-low pressure interface. At Surry, there are three such interfaces, while Sequoyah has four.

	Frequency per Reactor Year	
Percentile	**Surry**	**Sequoyah**
5th	1.3E-11	1.2E-11
50th	1.6E-8	9.5E-9
95th	1.7E-6	1.2E-6
Mean	3.8E-7	2.7E-7

C.13.2 ISLOCAs—Source Term Issues

This section discusses those issues that arose in the source term analysis of ISLOCAs. In the source term analysis, this accident was usually referred to as Event V.

C.13.2.1 Issue Definition

A number of factors influence the source terms that result from ISLOCA sequences. Because the check valve failures result in large leakage paths, the RCS will be at low pressure. The in-vessel behavior is expected to be similar to that of other, non-bypass, low-pressure sequences. Releases from the auxiliary building are strongly influenced by the location of the break in the auxiliary building and whether or not the break is ultimately covered by water, thereby leading to pool scrubbing. Fire suppression sprinklers in the auxiliary building may also act to reduce the releases. Some of these issues were addressed by the source term expert panel, some by an expert panel for the first draft of NUREG-1150, and some by the analysis teams.

C.13.2.2 Technical Basis for Issue Quantification

The releases for ISLOCA are calculated with the regular early and late release equations in the XSOR codes (see the description of the XSOR codes in Appendix A and in Ref. C.13.3). There are specific distributions for ISLOCA for the factor that accounts for the release from the vessel and for the factor that accounts for the release from the building. For ISLOCA, the vessel release factor, which represents the fraction released from the vessel to the containment in non-bypass accidents, is redefined to represent the release fraction from the vessel to the auxiliary building through the high-pressure and low-pressure piping. Because ISLOCA is a low-pressure sequence, the distributions for the ISLOCA vessel release factor are similar to those for non-bypass low-pressure accidents. For ISLOCA, the building release factors, which represent the fraction released from the containment building in non-bypass accidents, are redefined so that they account for the release fraction from the auxiliary building to the environment. These factors do not include the effects of pool scrubbing or auxiliary building sprays; reductions of the release due to mitigating effects such as these are accounted for by a separate decontamination factor. The distributions for the ISLOCA building release factor are similar to those for an early rupture of containment.

At Surry, the releases from an ISLOCA will be reduced by passage through a water pool if the pipe break location is under water. Pool scrubbing at Surry is treated by a specific pool scrubbing distribution that is used for the decontamination factor. At Sequoyah, the ISLOCA releases will be reduced if the thermally activated auxiliary building fire spray system operates. Spray scrubbing at Sequoyah is treated by a specific spray scrubbing distribution that is used for the decontamination factor. The decontamination factor is applied in addition to the building release factor. Some of the distributions used in determining the ISLOCA release were determined by the source term expert panel, some by an expert panel for the first draft of NUREG-1150, and some by the project staff.

C.13.2.3 Treatment in PRA and Results

The ISLOCAs were treated similarly to the non-bypass accidents in the PWR XSOR codes insofar as possible. The vessel release factor and the building release factor were redefined for application to ISLOCAs.

The vessel release factor is denoted FVES in SURSOR and SEQSOR. Distributions for this factor for the non-bypass accidents were determined by the source term expert panel. Distributions for FVES for ISLOCA were determined by the project staff; they were based on the low-pressure non-bypass FVES distributions of the source term expert panel. It was determined that the Ba, Sr, Ru, La, and Ce radionuclide classes would all behave as aerosols, so the distributions for these classes are identical. Three points on the distributions for the nine radionuclide classes are given below for Surry and Sequoyah. NG denotes the noble gases. In SURSOR and SEQSOR this accident is called Event V.

FVES distributions for Event V for Surry and Sequoyah

Percentile	NG	I	Cs	Te	Ba	Sr	Ru	La	Ce
5	1.0E+0	1.6E-1	1.5E-6	6.4E-2	1.0E-1	1.0E-1	1.0E-1	1.0E-1	1.0E-1
50	1.0E+6	6.1E-1	6.0E-1	2.5E-1	3.5E-1	3.5E-1	3.5E-1	3.5E-1	3.5E-1
95	1.0E+0	9.0E-1	9.7E-1	9.3E-1	9.6E-1	9.6E-1	9.6E-1	9.6E-1	9.6E-1

There are two building release factors in SURSOR and SEQSOR. FCONV is the fraction of the fission products in the auxiliary building from the RCS release that is released to the environment in the absence of mitigating factors. FCONC is the fraction of the fission products in the auxiliary building from the core-concrete interaction (CCI) release that is released to the environment in the absence of mitigating factors. The RCS release is sometimes called the early release, and the CCI release is sometimes referred to as the late release. Distributions for FCONV and FCONC for ISLOCA were determined by the project staff.

It was determined that, for the escape from the containment for the early release, one distribution could be applied to all radionuclide classes except the noble gases. FCONV is unity for the noble gases since they are not held up or absorbed in the reactor vessel. The values for the 5th, 50th, and 95th percentiles for the Surry and Sequoyah are:

FCONV distributions for Event V for both Surry and Sequoyah

Percentile	FCONV
5	1.6E-1
50	5.0E-1
95	8.6E-1

For the escape of fission products released during CCI, it was concluded that iodine and cesium would behave similarly, and all the other radionuclides except noble gases would behave as aerosols. The values for the 5th, 50th, and 95th percentiles for Surry and Sequoyah are given below.

FCONC distributions for Event V for Surry and Sequoyah

Percentile	NG	I	Cs	Te	Ba	Sr	Ru	La	Ce
5	1.0E+0	1.1E-1	1.1E-1	9.3E-2	9.3E-2	9.3E-2	9.3E-2	9.3E-2	9.3E-2
50	1.0E+0	5.0E-1	5.0E-1	4.7E-1	4.7E-1	4.7E-1	4.7E-1	4.7E-1	4.7E-1
95	1.0E+0	7.7E-1	7.7E-1	7.7E-1	7.7E-1	7.7E-1	7.7E-1	7.7E-1	7.7E-1

At Surry, much of the low-pressure piping that will be exposed to full RCS pressure in Event V is located near the floor in an area of the auxiliary building that will retain water. Since the contents of the RCS and the RWST will escape out the break before the onset of core damage, there is a good chance the pipe break will be under several feet of water when the release commences. Whether the pipe break is under water is determined in the accident progression analysis, based on the results of a panel convened for the first draft of NUREG-1150 to consider this specific question. The conclusion of this panel was that the mean probability that the Event V low-pressure pipe break at Surry will be under water is 0.85.

At Sequoyah, the pipe break is likely to be in an area of the auxiliary building that has heat-activated fire sprays (unlike Surry, which has no such sprays). There is no possibility at Sequoyah that the water escaping from the low-pressure pipe break in Event V will collect so that the pipe break will be under several feet of water when the release commences. It was decided by the project staff that there would be a high probability that the releases would be subject to scrubbing by fire sprays (the mean probability was assessed to be about 0.80).

The source term expert panel decided that the uncertainty in the distribution used for the decontamination factor for sprays or passage through a water pool was less important than the uncertainty in whether the sprays were on or whether the pipe break was under water. The decontamination factors for both sprays and pool scrubbing were therefore determined by the project staff. There is a single decontamination factor distribution that applies to all radionuclide classes except the noble gases, which are not affected by sprays or a passage through water.

Decontamination factor (DF) distribution for Event V at Surry (pool scrubbing) and at Sequoyah (sprays)

Percentile	DF
5	4.1E+3
50	6.2
95	1.8

C.13.3 SGTRs—Accident Sequence Issues

This section discusses those issues that arose in the accident sequence analysis of the steam generator tube ruptures.

C.13.3.1 Issue Definition

A steam generator tube rupture is a unique initiator because it represents a failure of the RCS boundary into the secondary side. As a result of the tube rupture, the secondary side may be exposed to full RCS pressures. These pressures are likely to cause relief valves to lift on the secondary side. If these valves fail to reclose, an open pathway from the vessel to the environment can result. Thus, this accident has some of the same characteristics as an ISLOCA. In determining the frequency of SGTR sequences, there are a number of important issues, including the SGTR initiating event frequency, the likelihood that the operators will depressurize the RCS to a pressure lower than in the secondary side so as to terminate the loss of coolant, and the response of the secondary side safety valves. The plant analysts addressed all the issues except those dealing with the safety valves; the latter were addressed in an elicitation process

involving the project staff. The nature and response of safety valves to various types of demands were the focus of the elicitation process.

C.13.3.2 Technical Bases for Issue Quantification

The consideration of secondary side safety valve behavior considered the following four questions:

1. What is the probability of a secondary safety valve demand?

2. What is the probability that, given a safety valve demand, liquid or two-phase flow through the safety valves occurs?

3. What is the probability of failure to reclose, given that the safety valves pass liquid or a two-phase mixture?

4. How many demands of the secondary safety valves will occur?

The evaluation of these questions was based on consideration of plant emergency operating procedures, thermal-hydraulic calculations, and data from actual SGTR events, such as at North Anna. The likelihood of a secondary side safety valve demand depends largely on the status of the atmospheric dump valves (ADVs) and their block valves. If the ADVs are operating in an unblocked mode, their operation may preclude demands of the safety valves. On the other hand, if the ADVs are blocked, demand of the safety valves is likely. The passage of liquid through the valves depends on the ability of the operators to prevent filling up of the faulted steam generator. The operators need to control the RCS pressure and reduce the flow from the high-pressure injection system in order to preclude liquid flow through the safety valves. Given that liquid flow occurs and that multiple demands are considered likely, it was assessed that there was a high likelihood that the safety valves would stick open.

C.13.3.3 Treatment in PRA and Results

For the PRAs, the plant analysts identified the possible situations where safety valve demand might be of concern. The mean probabilities of having a stuck-open safety valve were assessed for the eight cases identified below. Cases 2 and 6 were assessed to be inapplicable because it is impossible to control RCS pressure if safety injection is not also controlled.

Table C.13.1 Secondary side safety valve failure probabilities.

	Case							
	1	2	3	4	5	6	7	8
Primary Pressure Controlled	Y	Y	N	N	Y	Y	N	N
Safety Injection Controlled	Y	N	Y	N	Y	N	Y	N
ADVs Blocked	Y	Y	Y	Y	N	N	N	N
Mean Probability of Stuck-Open Safety Valve	.28	NA	1.0	1.0	0.0	NA	.15	.15

Cases conditional upon the failure of the operators to depressurize were assessed to be the most likely to lead to safety valve demand and subsequent failure. The plant analysts then combined this information with the analysis of operator actions to depressurize and take other mitigative steps in order to determine an overall frequency of SGTR core damage events. These frequencies were estimated to be quite low at the three PWRs in NUREG-1150; however, they remain important relative to other sequences because of the possibly large source term that can result from a bypassed containment.

C.13.4 SGTRs—Source Term Issues

This section discusses those issues that arose in the source term analysis of the steam generator tube ruptures.

C.13.4.1 Issue Definition

The magnitude of the source term from an SGTR accident depends on the integrity of the secondary system and the containment. If the integrity of both is maintained, the releases may be quite small. On the other hand, if the safety valves on the secondary system stick open, then a direct path from the vessel to the environment is created and the releases may be very high. If the safety valves on the secondary system do not stick open, the releases depend on the time at which the containment fails (if at all) as in non-bypass accidents. Thus, there are two pathways from the reactor vessel to the environment. The one pathway is through the broken steam generator tube and out through the safety valves on the secondary system. The second pathway is the same as the pathway for non-bypass transient accidents: into the containment through a safety or relief valve (if open) until the vessel fails and directly after the vessel fails; and from the containment to the environment through the failure in the containment (if it fails). If the safety valves on the secondary system stick open, the first pathway dominates. This accident is of considerable concern because of the potentially large releases that might result. If the safety valves on the secondary system do not stick open, the releases by the second (non-bypass) pathway are more important.

C.13.4.2 Technical Basis for Issue Quantification

The equation used to determine the early release for SGTR accidents differs from the usual early release equation in that it contains an additional term for the release through the secondary system and the secondary system safety valves. If the secondary safety valves are stuck open, this bypass term accounts for the bulk of the release. For the non-bypass or normal pathway to the environment via the containment, the SGTR accidents are treated no differently than similar non-bypass accidents. Only the vessel release factor has a specific distribution for the SGTR accidents. This distribution was determined by the project staff.

The additional (bypass) term for the RCS release for SGTR accidents consists of two factors. One represents the fraction released from the core that enters the secondary side of the steam generator; the second is the fraction entering the secondary side of the steam generator that is released to the environment through the safety valves. No removal factors, such as building or spray decontamination factors, are applied to this release path. For the SGTRs where the secondary system safety valves reclose, the distributions for these two factors were determined by the project staff. For the SGTRs where the secondary system safety valves stick open, the distributions for these two factors were determined by an expert panel convened specifically to consider the release from this type of SGTR.

C.13.4.3 Treatment in PRA and Results

For the non-bypass pathway to the environment via the containment, the radioactive material released from the PWRs are computed using the same equation used for non-bypass accidents. The only factor for which specific distributions are defined is the vessel release factor, FVES, which represents the fraction passing from the vessel to the containment. It cannot be the same as in a non-bypass accident since some of the fission products escape from the vessel into the steam generator. Distributions for FVES for SGTRs were determined by the project staff. In this situation, the Ba, Ru, La, and Ce radionuclide classes would all behave as aerosols so the distributions for these classes are identical. Strontium is somewhat less likely to be released.

FVES distributions for SGTRs for Surry and Sequoyah

Percentile	NG	I	Cs	Te	Ba	Sr	Ru	La	Ce
5	1.0E+2	2.4E-2	2.4E-2	8.8E-2	1.3E-2	9.4E-3	1.3E-2	1.3E-2	1.3E-2
50	1.0E+0	1.7E-1	1.7E-2	3.2E-1	5.8E-2	4.4E-2	5.8E-2	5.8E-2	5.8E-2
95	1.0E+0	8.7E-1	8.2E-1	9.5E-1	7.3E-1	6.7E-1	7.3E-1	7.3E-1	7.3E-1

In SURSOR and SEQSOR, FISG represents the fraction released from the core that enters the steam generator; and FOSG represents the fraction entering the steam generator that is released from the steam generator to the environment. For SGTRs in which the secondary system safety valves reclose, the distributions for FISG and FOSG were determined by the project staff and separate distributions were defined for each of these factors. It was determined that the Ba, Sr, Ru, La, and Ce radionuclide classes would all behave as aerosols so the distributions for these classes are very similar.

FISG distributions for SGTRs with the secondary safety valves reclosing for Surry and Sequoyah

Percentile	NG	I	Cs	Te	Ba	Sr	Ru	La	Ce
5	2.5E-1	1.1E-1	1.0E-1	2.9E-1	1.6E-1	1.7E-1	1.7E-1	1.7E-1	1.6E-1
50	5.8E-1	2.9E-1	2.8E-1	5.6E-1	3.3E-1	3.4E-1	3.4E-1	3.4E-1	3.3E-1
95	9.5E-1	8.5E-1	7.7E-1	1.0E+0	9.0E-1	9.0E-1	9.0E-1	9.0E-1	9.0E-1

FOSG distributions for SGTRs with the secondary safety valves reclosing for Surry and Sequoyah

Percentile	NG	I	Cs	Te	Ba	Sr	Ru	La	Ce
5	2.9E-1	2.0E-1	2.0E-1	2.6E-1	2.6E-1	2.5E-1	2.5E-1	2.6E-1	2.6E-1
50	6.7E-1	5.3E-1	5.4E-1	5.0E-1	5.2E-1	5.3E-1	5.3E-1	5.3E-1	5.3E-1
95	1.0E+0	1.0E+0	1.0E+0	9.2E-1	1.0E+0	1.0E+0	1.0E+0	1.0E+0	1.0E+0

For SGTRs in which the secondary system safety valves stick open, the distributions for FISG and FOSG were determined by a special source term expert panel that considered only the releases from this type of SGTR accident. The panel declined to provide separate distributions for FISG and FOSG and provided distributions for the product FISG * FOSG. Because the bypass term for the SGTR release consists of just the product of FISG and FOSG, and these factors appear nowhere else in the release equation, this was acceptable. The experts provided separate distributions for iodine, cesium, tellurium, and aerosols and specified that they applied to all the PWRs. There is no retention in the steam generators for the noble gases. The aerosol distribution applies to the Ba, Sr, Ru, La, and Ce radionuclide classes. The panel concluded that there was a very good chance that there would be little retention of radionuclides in the steam generator and the piping.

FISG * FOSG distribution for SGTRs with the secondary safety valves stuck open for Surry and Sequoyah

Percentile	NG	I	Cs	Te	Ba	Sr	Ru	La	Ce
5	1.0E+0	2.0E-5	2.8E-7	3.8E-5	3.8E-5	3.8E-5	3.8E-5	3.8E-5	3.8E-5
50	1.0E+0	2.7E-1	2.6E-1	1.7E-1	2.4E-1	2.4E-1	2.4E-1	2.4E-1	2.4E-1
95	1.0E+0	8.0E-1	7.8E-1	7.7E-1	7.6E-1	7.6E-1	7.6E-1	7.6E-1	7.6E-1

As implemented in SURSOR and SEQSOR, rather than change the equation for the SGTRs in which the secondary system safety valves stick open, the distributions for the product FISG * FOSG were placed in the data array for FISG and the data array for FOSG was set to 1.0.

REFERENCES FOR SECTION C.13

C.13.1 T. A. Wheeler et al., "Analysis of Core Damage Frequency from Internal Events: Expert Judgment Elicitation," Sandia National Laboratories, NUREG/CR-4550, Vol. 2, SAND86-2084, April 1989.

C.13.2 F. T. Harper et al., "Evaluation of Severe Accident Risks: Quantification of Major Input Parameters," Sandia National Laboratories, NUREG/CR-4551, Vol. 2, Revision 1, SAND86-1309, December 1990.

C.13.3 H. N. Jow et al., "XSOR Codes User's Manual," Sandia National Laboratories, NUREG/CR-5360, SAND89-0943, to be published.*

*Available in the NRC Public Document Room, 2120 L Street NW., Washington, DC.

C.14 Reactor Coolant Pump Seal Failures in Westinghouse Plants After Loss of All Seal Cooling

C.14.1 Issue Definition

The ability of reactor coolant pump seals to remain intact during loss of all seal cooling is a concern for PWRs. As the three PWRs studied for NUREG-1150 are all Westinghouse plants, results of the analysis of this study are only applicable to Westinghouse plants.

One of the potential concerns during a station blackout is the possibility of a loss-of-coolant accident (LOCA) created by failure of the reactor coolant pump (RCP) seals to maintain a restricted flow between the reactor coolant system and the containment.

The Westinghouse RCP shaft seal is a three-stage seal assembly, as shown in Figure C.14.1. The number one seal is a film-riding controlled leakage seal, whereas the number two and three stages are rubbing-face type seals. The leakage across the number one seal cools the seal assembly. The high-pressure subcooled leakage is supplied by an injection system upstream of the number one seal. Part of the injection water flows through the seal assembly. The remainder flows into the water coolant system as makeup water. Backup cooling is provided by a water-to-water heat exchanger parallel to the labyrinth seal. During a station blackout, both injection and cooling water would be lost.

High-temperature reactor coolant water would then flow up the shaft into the seal system. The shaft and the seal assembly would experience abnormal temperature distributions. This condition will affect the angle between the faceplates of the RCP seals and the gap between the faceplates of the number one film-riding seal.

The gap between the number one seal faceplates is determined by a force balance, which can be affected by flow rate, the angle between the faceplates of the seal ring and runner, enthalpy, and inlet pressure. The fluid pressure profile between the seal faceplates determines the opening forces on the seal. The closing force on the seal is proportional to the differential pressure across the seal and acts on the upper surface of the seal ring. If these forces are unbalanced, the gap will increase or decrease as necessary until the forces are balanced.

The number two seal stage is designed to withstand full system pressure without loss of integrity in the event that number one seal stage fails. In the event that both number one and number two seals fail, the number three seal stage is not expected to limit leakage. The size of a resultant leak rate is dependent on the combinations of seal ring failures and o-ring failures in the various seal stages.

At issue is the leak rate in gallons per minute as a function of time, due to seal failure caused by loss of cooling to the pump shaft, which is expected during station blackout. The hypothesized failure modes involve loss of the seal ring geometry and degradation of the elastomer material. (Additional detail on this analysis may be found in Ref. C.14.1.)

C.14.2 Technical Bases for Issue Quantification

For this issue, three experts participated in these evaluations:

M. Hitchler—Westinghouse Electric Corporation,
J. Jackson—Nuclear Regulatory Commission, and
D. Rhodes—Atomic Energy of Canada Limited

These experts developed a consensus structure with which to analyze the issue. The result was a logic tree that describes the possible failure combinations of seal rings and o-rings and the resultant leak rates for a single pump. This logic tree is shown in Figure C.14.2. The 21-gpm leak per pump is considered to be a successful restriction of flow.

The experts then provided assessments for the failure probabilities for the four events of the logic tree. Assessments were made for two different o-ring elastomer materials. The old o-ring material, which is currently in use at Surry, Sequoyah, and Zion, has exhibited significant degradation in some experiments.

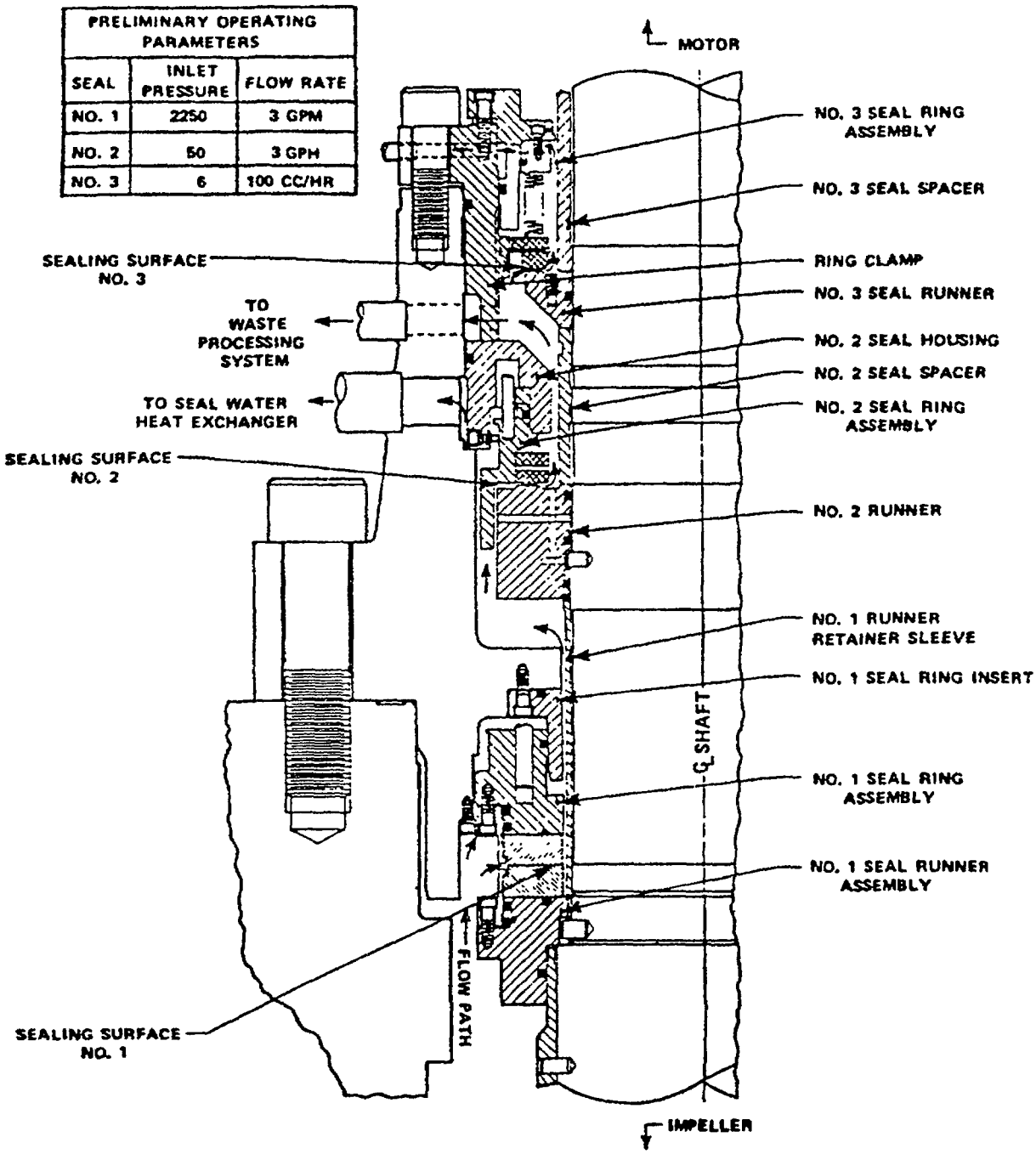

RCP Typical Shaft Seal Arrangement

Figure C.14.1 Westinghouse RCP seal assembly (Ref. C.14.1).

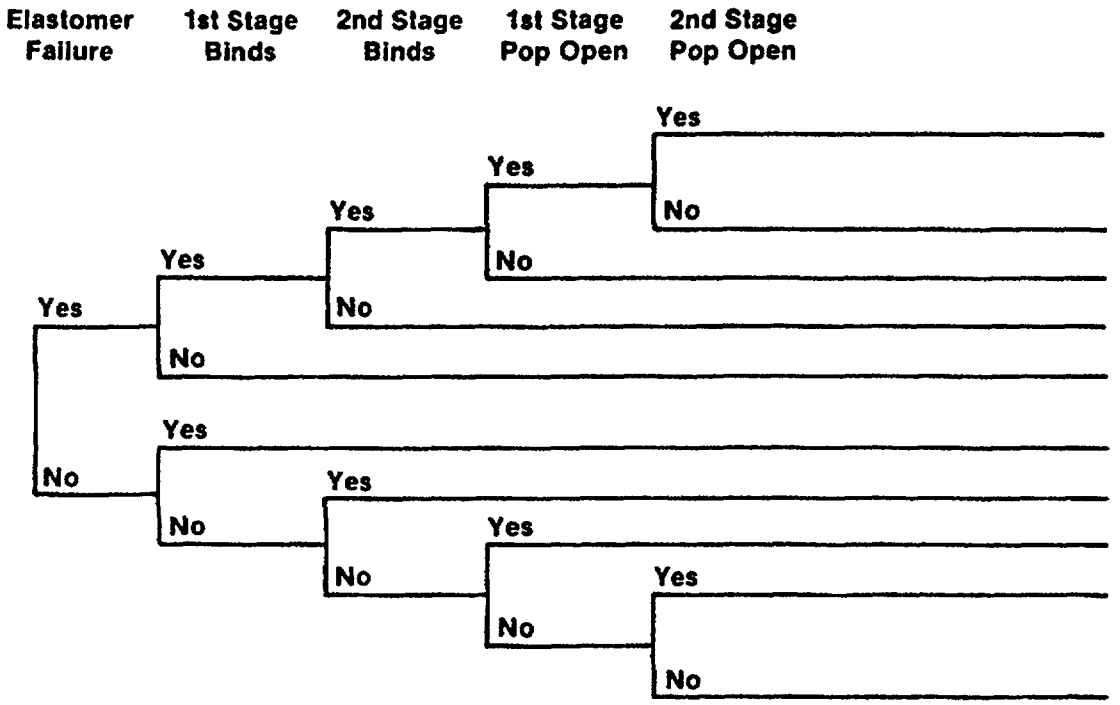

Figure C.14.2 Decision tree (Ref. C.14.1).

The new o-ring elastomer has been shown to be much less susceptible to degradation when subjected to similar experimental conditions. In addition to the type of o-ring material in the RCP seals, elicitations were taken for pressurized and depressurized reactor coolant system (RCS) status. Successful cooldown and depressurization will subject the pump seals to cooler, less harsh conditions.

Total RCS leak rate is based on leak rates from all RCP pumps (3 for Surry, 4 for Sequoyah and Zion). Therefore, in addition to developing an assessment for a single RCP, it was necessary to postulate the degree of correlation between similar failures in different pumps. That is, the assessment included consideration of whether the seals fail independently or have the same leakage.

C.14.3 Treatment in PRA and Results

In order to evaluate the station blackout event tree, it is necessary to have a relationship between leak rate and probability of leak rate versus time. The results for each expert were averaged to calculate aggregate leak rates and their probabilities. The calculations were done for the following three cases:

1. Old o-ring material—with RCS cooldown
2. Old o-ring material—without RCS cooldown
3. New o-ring material—without RCS cooldown

The experts developed very different assessments for correlating component failures between pumps. They reached a consensus on this point: if two similar components in two pumps failed (e.g., first stage seal rings in two different pumps), then the same component could be assumed to fail in all other pumps. This assumption simplified the problem of calculating total RCP seal leak rate probabilities for determining the possible failure combinations for a two-pump model for each expert.

The results are shown in Table C.14.1 for a three-loop Westinghouse plant and Table C.14.2 for a four-loop plant. These tables show the probability of various leak rates at different points in time after loss of cooling to the seals. In order to incorporate this information into the sequence models, it was necessary to calculate a time of initial seal failure and a core uncovery time for each possible failure scenario. A

Table C.14.1 Aggregated RCP seal LOCA probabilities for Westinghouse three-loop plant.*

Leak Rate (gpm)	Old O-Rings Time (h)					New O-Rings Time (h)				
	1.5	2.5	3.5	4.5	5.5	1.5	3.6	3.5	4.5	5.5
63	.306	.290	.274	.274(.258)**	.274(.241)	.817	.816	.814	.812	.811
103	–	–	–	–	–	7.7E-3	7.7E-3	7.7E-3	7.7E-3	7.7E-3
183/224***	.148	.037	.050	.048(.064)	.047(.079)	.014	.014	.016	.017	.019
294	–	–	–	–	–	1.9E-3	1.9E-3	1.9E-3	1.9E-3	1.9E-3
372	8.5E-3	5.0E-3	4.5E-3	3.7E-3	3.3E-3	4.5E-4	5.0E-3	5.3E-3	5.7E-3	6.0E-3
516/526/546	3.5E-4	3.4E-4	3.2E-4	3.2E-4	3.2E-4	.145	.145	.145	.145	.145
602/614	.001	0	0	0	0	4.7E-4	4.7E-4	4.7E-4	4.7E-4	4.7E-4
750	.530	.660	.660	.660	.660	7.7E-3	7.7E-3	7.7E-3	7.7E-3	7.7E-3
1440	4.3E-3	4.3E-3	4.3E-3	4.3E-3	4.3E-3	5.0E-3	5.0E-3	5.0E-3	5.0E-3	5.0E-3

*This table is Table 5.4-1 of Reference C.14.1.
**Parentheses denote calculations that change if no depressurization is assumed. All other probabilities are for depressurized conditions.
***Similar leak rates have been lumped together. These values are the probabilities of being at a particular leak rate at a particular time.

Table C.14.2 Aggregated RCP seal LOCA probabilities for Westinghouse four-loop plant.*

Leak Rate (gpm)	Old O-Rings Time (h)					New O-Rings Time (h)				
	1.5	2.5	3.5	4.5	5.5	1.5	3.6	3.5	4.5	5.5
	1.5	2.5	3.5	4.5	5.5	1.5	3.6	3.5	4.5	5.5
84	.302	.286	.271	.274(.255)	.271(.239)**	.810	.809	.809	.807	.805
244/245***	.148	.038	.053	.051(.067)	.049(.081)	.014	.016	.017	.0198	.020
313	–	–	–	–	–	.010	.010	.010	.010	.010
433	.011	.012	.028	9.9E-3	9.3E-3	6.0E-4	6.0E-4	6.0E-4	6.0E-4	6.0E-4
480	1.3E-3	1.3E-3	1.3E-3	1.3E-3	1.3E-3	–	–	–	–	–
543	–	–	–	–	–	2.6E-3	2.6E-3	2.6E-3	2.6E-3	2.6E-3
688/698/728	1.2E-3	1.2E-3	1.1E-3	1.1E-3	.146	.146	.146	.146	.146	.146
796	–	–	–	–	–	2.7E-3	2.7E-3	2.7E-3	2.7E-3	2.7E-3
1000/1026	.530	.659	.659	.665	.666	8.3E-3	8.3E-3	8.3E-3	8.3E-3	8.3E-3
1230	1.6E-6	1.6E-3	1.6E-3	1.6E-3	1.6E-3	–	–	–	–	–
1920	4.2E-3	4.2E-3	4.2E-3	4.2E-3	4.2E-3	4.2E-3	4.2E-3	4.2E-3	4.2E-3	4.2E-3

*This table is Table 5.4-2 of Reference C.14.1.

**Parentheses denote calculations that change if no depressurization is assumed. All other probabilities are for depressurized conditions.

***Similar leak rates have been lumped together. These values are the probabilities of being at a particular leak rate at a particular time.

series of individual scenarios were defined that identify the time of seal failure, the initial leak rate, the progression of leak rate, and the probability of the scenario.

For Sequoyah (a four-loop plant), a total of 17 scenarios were identified and are shown in Table C.14.3. They include the initial leak rate, the time of initial seal failure, any increases in leak rate, the time at which the leak rate increases, and the probability. These 17 scenarios were used to develop point estimate probabilities (i.e., no uncertainty stated) for seal failure and core uncovery. These values were not used in the uncertainty analysis. In order to calculate the probability distributions for seal LOCA sequences, the 17 scenarios were consolidated into seven states. There are six failure states and one success rate (the 84 gpm state is a success state). The seven seal states are summarized below:

Leak Path (gpm)	Time to Transfer (hours)	Probability
1000*	1-1/2	.5298
240 - 1000	2-1/2	.1253
240*	1-1/2	.049
433 - 1000	2-1/2	.0051
1920*	1-1/2	.0042
433*	1-1/2	.0042
84* (success)		.2704

*Constant leak rate

This probability distribution is interpreted as a representation of the experts' collective degrees of belief in the seven states that represent possible outcomes for seal LOCA. The occurrence of a seal LOCA is therefore treated as a modeling uncertainty with respect to time and size. These states were sampled as either a zero or unity probability in the TEMAC uncertainty analysis.

The following discussion illustrates how the seal LOCA model was integrated into the station blackout event trees. (Two constraining criteria were applied to this task: (1) the event heading for nonrecovery of ac power would be separate from the event heading for seal LOCA, and (2) a minimum number of headings would be used.)

The conclusion of the expert panel was that, at 90 minutes after loss of all cooling, the seal temperatures would have increased enough to be at risk of failure. Prior to 90 minutes, there is no risk of seal failure. After 90 minutes, with no cooling, the seal may fail or may remain intact. Leaks may slowly develop and increase with time, or they may have a constant leak rate. If a seal LOCA occurs, core uncovery can be averted if ac power is restored, thus enabling restoration of safety injection flow.

The calculation of the core damage frequency due to seal LOCA is based on a weighted average of the 17 seal failure scenarios. The conditional probability of core damage, given a station blackout, is calculated as follows:

$$P'_{CD} = P_1 * P_2 * P_3$$

where

P'_{CD} = conditional probability of core damage,
P_1 = probability of being at risk for an SLOCA,
P_2 = probability that a SLOCA occurs, and
P_3 = probability of not recovering ac power prior to core damage.

Table C.14.3 Sequoyah RCP seal LOCA model scenarios.*

Leak Path (gpm)	Time to Transfer (hours)	Probability
84**	—	.2707
240**	—	.0490
240–1000	2-1/2	.1253
240–1000	3-1/2	.0021
240–1000	4-1/2	.0021
240–1000	5-1/2	.0010
433**	—	.0042
433–1000	2-1/2	.0051
433–1000	3-1/2	.0013
433–1000	4-1/2	.0006
433–1230	2-1/2	.0013
700**	—	.0011
700–1000	2-1/2	.00007
700–1000	3-1/2	.00007
1000**	—	.5298
1230**	—	.0016
1920**	—	.0042
	TOTAL	.9995

*This is Table D.5-2 in Reference C.14.2.
**Constant leak rate

The probability of being at risk for a seal LOCA is the probability that ac power has not been restored within 90 minutes of a loss of a seal cooling. The probability of a seal LOCA is given by the results of the expert elicitation. There are 17 seal LOCA scenarios, each with a characteristic uncovery time and a specific probability. All seal failure scenarios are assumed to start at 90 minutes from loss of cooling. The probability of not recovering is just the probability of nonrecovery of ac power prior to the characteristic core uncovery time associated with each seal scenario. Note that the nonrecovery term must be conditional on nonrecovery of ac power in the first 90 minutes. The conditional probability of core damage can be written as:

$$P_{CD} = \sum_{i=1}^{17} [P(t)_{NRAC} * P(t)_{fsl(i)} * P'(t+\beta_i)_{NRAC}]$$

where

i = seal LOCA scenario index, and t, in this case, equals 90 minutes,

β_i = core uncovery time associated with the ith scenario,

$P(t)_{NRAC}$ = probability of nonrecovery of ac power by time t, given loss of power at t = 0.

$P(t)_{NRAC}$ = $1 - P'(t)_{NRAC}$ where P" is the cumulative probability of recovery of ac power,

$P(t)_{fsl(i)}$ = probability of ith seal LOCA scenario, and

$P'(t+\beta_i)_{NRAC}$ = conditional probability of nonrecovery of ac power by time $t + \beta_i$, given no recovery at time t.

$$P'(t+\beta_i)_{NRAC}] = \frac{P(t+\beta_i)_{NRAC}}{P(t)_{NRAC}} = \frac{1 - P'(t+\beta)_{NRAC}}{1 - P'(t)_{NRAC}}$$

Recognizing the form for P'_{NRAC}, the equation reduces to:

$$\sum_{i=1}^{17} P(t)_{fsl(i)} * P(t+\beta_i)_{NRAC}$$

The values for $P(t)_{fsl(i)}$ and $P(t+\beta_i)_{NRAC}$ are shown in Table C.14.4. Core uncovery times were calculated for the case with and without secondary depressurization.

Table C.14.4 Sequoyah RCP seal LOCA model.*

Leak Path (gpm)	Time to Transfer (hours)	Prob.	Time to CU (hr) (with secondary depressurization)	Time to RAC (hr) (with secondary depressurization)	Prob. NRAC (with secondary depressurization)	Prob. CD (with secondary depressurization)	Time to CU (hr) (without secondary depressurization)	Time to RAC (hr) (without secondary depressurization)	Prob. NRAC (without secondary depressurization)	Prob. CD (without secondary depressurization)
84**	—	.2707	19	20.5	.046	—	8.9	10.4	.046	—
240**	—	.0490	8.1	9.6	.046	.00225	4.6	6.1	.056	.00274
240–1000	2-1/2	.1253	2.2	3.7	.10	.01253	2.15	3.65	.103	.01291
240–1000	3-1/2	.0021	3.06	4.56	.08	.00017	2.91	4.4	.084	.00018
240–1000	4-1/2	.0021	3.9	5.4	.067	.00014	3.7	5.2	.068	.00014
240–1000	5-1/2	.0010	4.7	6.2	.054	.00005	4.4	5.9	.058	.00006
433**	—	.0042	4.2	5.9	.058	.00024	3.1	4.6	.079	.00033
433–1000	2-1/2	.0051	2.06	3.56	.108	.00055	1.96	3.46	.110	.00056
433–1000	3-1/2	.0013	2.73	4.23	.088	.00011	2.52	4.0	.093	.00012
433–1000	4-1/2	.0006	3.41	4.91	.073	.00004	3.1	4.6	.079	.00005
433–1230	2-1/2	.0013	1.86	3.36	.112	.00015	1.78	3.28	.115	.00015
700**	—	.0011	2.6	4.1	.090	.00010	2.0	3.5	.108	.00012
700–1000	2-1/2	.00007	1.8	3.3	.115	—	1.7	3.2	.118	—
700–1000	3-1/2	.00007	2.17	3.67	.103	—	2.0	3.5	.108	—
1000**	—	.5298	2.07	3.6	.105	.05563	1.85	3.35	.115	.06093
1230**	—	.0016	1.1	2.6	.135	.00022	1.1	2.6	.135	.00022
1920	—	.0042	.75	2.25	.162	.00065	.75	2.25	.162	.00068
	Total	.9995				.07283				.07919

*This is Table D.5-3 of Reference C.14.2.
**Constant leak rate.

REFERENCES FOR SECTION C.14

C.14.1 T. A. Wheeler et al., "Analysis of Core Damage Frequency from Internal Events: Expert Judgment Elicitation," Sandia National Laboratories, NUREG/CR-4550, Vol. 2, SAND86-2084, April 1989.

C.14.2 R. C. Bertucio and S. R. Brown, "Analysis of Core Damage Frequency: Sequoyah Unit 1," Sandia National Laboratories, NUREG/CR-4550, Vol. 5, Revision 1, SAND86-2084, April 1990.

C.15 Zion Service Water and Component Cooling Water Upgrade

In April 1989, the licensee for Zion Unit 1, Commonwealth Edison Co., made commitments to the NRC to make plant and procedure changes to address the major contributor to the core damage frequency, the development of an unmitigated reactor coolant pump (RCP) seal loss-of-coolant accident (LOCA) caused by a loss of the component cooling water (CCW) or service water (SW) system (Ref. C.15.1). The status of these commitments was provided in another letter to the NRC (Ref. C.15.2) in which the status was reported as:

1. Zion Station provided an auxiliary water supply to each charging pump's oil cooler via the fire protection system (FPS). Hoses, fittings, and tools are locally available at each unit's charging pump area, allowing for immediate hookup to existing taps on the oil coolers, if required. This action was completed in April 1989.

2. A formal procedure change was made to AOP 4.1, entitled "Loss of Component Cooling Water," on April 12, 1989, providing instruction to the operators to align emergency cooling to the centrifugal charging pumps. Specific instructions are included for each charging pump with a diagram of the lube oil cooling valves and piping.

3. As of May 1990, the new heat-resistant RCP seal o-rings were unavailable from Westinghouse. Therefore, during the latest unit outages, the RCP seal o-rings were not replaced. When the new o-rings are available, the existing o-rings will be changed when each pump is disassembled for routinely scheduled seal maintenance.

C.15.1 Issue Definition

The scope of this issue is the evaluation of the plant and procedure changes that provide an auxiliary source of cooling water to the charging pump oil coolers. The base case Zion analysis, as documented in Reference C.15.3, models the failure of the component cooling water (CCW) or service water (SW) systems as a challenge to the integrity of the RCP seals. The failure of CCW causes overheating of the charging pumps that supply seal injection water. CCW also provides the RCP seal cooling water. The CCW system uses the SW system as its heat sink.

The failure of both seal cooling and seal injection (via failure of the charging pumps due to overheating) places the RCP seals in jeopardy of failure. The failure model for the RCP seals states the mean probability of having a seal LOCA, given a loss of seal injection and seal cooling as 0.73. Failure of seal injection or seal cooling separately does not challenge seal integrity.

C.15.2 Issue Analysis

The changes made by Commonwealth Edison Co. are designed to break the common-cause failure mechanism represented by the CCW and SW systems. Since exact design, procedure, and training changes were not available, the following assumptions were made in the analysis:

1. The auxiliary water supply provided by the FPS is connected such that charging pump oil cooler heat is rejected without depending on the rest of the CCW system or any of the SW system.

2. The FPS does not depend on any support from the SW system.

3. The failure to provide an auxiliary water supply to the charging pump oil coolers is dominated by the operator actions to properly determine that such action is necessary and the proper execution of the task and not by hardware failures of the FPS.

4. The operator action to provide an alternative source of cooling water is comparable to the operator action to diagnose the need for feed and bleed cooling and manually starting the high-pressure injection system; therefore, a comparable failure probability may be used. To account for the large uncertainty in this value, an error factor of 10 is deemed appropriate. The failure probability assigned for the failure to provide an alternative source of water to the charging pump oil coolers is a lognormal distribution with a mean of 0.01 and an error factor of 10.

The base case analysis gave credit for the operators recovering certain CCW and SW failures by shedding unnecessary loads, starting standby pumps, and isolating piping sections where possible. These actions were modeled in the event trees as top event RE and specifically conditional split fractions (CSFs) RE1 and RE2. These CSFs were assigned a failure probability of 0.13.

The provision of an alternative water supply to the charging pump oil coolers was modeled as a change to the recoverability of the CCW and SW systems. Thus, RE1 and RE2 were changed from 0.13 to 0.01.

C.15.3 Issue Quantification and Results

The 203 highest frequency accidents and 58 plant damage states were requantified and a new Latin hypercube uncertainty analysis was performed using the failure probability data described above. Table C.15.1 shows the comparison of the plant damage state results between the base case and this sensitivity analysis. The change in the core damage frequency from a mean value of 3.4E-4 to 6.2E-5 per reactor year represents a decrease of about 81 percent.

Table C.15.1 Plant damage state comparison.

	Base Case		Sensitivity Case	
Plant Damage State	Frequency per reactor year	%	Frequency per reactor year	%
LOCAs	3.1E-4	93.2	3.9E-5	62.7
ATWS and transients	7.5E-6	4.0	1.4E-5	21.9
Station blackouts	9.3E-6	2.8	9.3E-6	15.0
Bypass	2.6E-7	—	2.6E-7	0.4
Total	3.4E-4	100.0	6.2E-5	100.0

C.15.4 Impact of Issues on Risk

The impact of the sensitivity analysis described above was a significant reduction in the mean core damage frequency, which was obtained by reducing the plant damage states involving CCW and SW induced seal LOCAs. Other plant damage states remained unchanged. Thus, in the sensitivity study, CCW and SW induced seal LOCAs contribute only 24 percent to the mean core damage frequency compared with 86 percent in the base case. This reduction in LOCAs means that other plant damage states such as bypass and station blackout (SBO) become larger contributors to the lower mean core damage frequency. The contribution of SBO accidents increased from about 2 percent to over 10 percent in the sensitivity study. Bypass accidents contributed 2.7 percent to the mean core damage frequency in the sensitivity study compared with 0.5 percent in the base case. As station blackout and bypass accidents tend to be more challenging (in terms of containment performance) than LOCAs, the risk estimates should not be reduced by as large a fraction as the mean core damage frequency. Table C.15.2 presents new mean risk estimates based on the sensitivity study and compares them with original base case risk. The results in Table C.15.2 indicate that the risk measures did in fact decrease by smaller fractions than the mean core damage frequency. The early fatality risk decreases by 75 percent and the latent cancer fatality risk by 67 percent.

The new mean risk estimates were not obtained by performing a completely new uncertainty analysis as was done for the accident frequency analysis (as described in Section C.15.3). The mean risk estimates in Table C.15.2 were obtained by using mean risk values conditional on the occurrence of the various plant damage states. The mean risk estimates that were used are given in Reference C.15.4. The conditional mean risk measures were simply multiplied by the new mean frequencies in Table C.15.1 and summed to obtain the new risk estimates. This approach is not as rigorous as a complete requantification of the uncertainty analysis in which new distributions for the risk measures would have been obtained. However, the approach is straightforward and gives a reasonable estimate of how the mean risk estimates would be

reduced by the changes made by Commonwealth Edison Company to eliminate the common-cause failure mechanism represented by the CCW and SW systems.

Table C.15.2 Comparison of mean risk values.

Risk Measure (per reactor year)	Base Case	Sensitivity Case
Early Fatalities	1.1E-4	2.0E-5
Total Fatalities—Entire Region	2.4E-2	8.1E-3
Total Fatalities—50 Miles	1.1E-2	3.3E-3
Individual Early Fatalities	1.0E-8	2.0E-9
Individual Latent Cancer Fatalities	1.1E-8	2.5E-9
Frequency of One Fatality	6.4E-7	1.2E-7
Population Dose (person-rem)—50 Miles	5.5E+1	1.7E+1
Population Dose (person-rem)—Entire Region	1.4E+2	4.6E+1

REFERENCES FOR SECTION C.15

C.15.1 Letter from Cordell Reed, Commonwealth Edison Co. (CECo) to T. E. Murley, NRC, dated March 13, 1989.

C.15.2 Letter from R. A. Chrzanowski, CECo, to NRC Document Control Desk, August 24, 1990.

C.15.3 M. B. Sattison and K. W. Hall, "Analysis of Core Damage Frequency: Zion Unit 1," Idaho National Engineering Laboratory, NUREG/CR-4550, Vol. 7, Rev. 1, EGG-2554, May 1990.

C.15.4 C. K. Park et al., "Evaluation of Severe Accident Risks: Zion Unit 1," Brookhaven National Laboratory, NUREG/CR-4551, Vol. 7, Draft Revision 1, BNL-NUREG-52029, to be published.*

*Available in the NRC Public Document Room, 2120 L Street NW., Washington, DC.

NRC FORM 335 (2-89) NRCM 1102, 3201, 3202

U.S. NUCLEAR REGULATORY COMMISSION

BIBLIOGRAPHIC DATA SHEET

(See instructions on the reverse)

1. REPORT NUMBER (Assigned by NRC, Add Vol., Supp., Rev., and Addendum Numbers, if any.)
NUREG-1150
Vol. 2

2. TITLE AND SUBTITLE

Severe Accident Risks: An Assessment for Five U.S. Nuclear Power Plants

Appendices A, B, and C
Final Report

3. DATE REPORT PUBLISHED

MONTH	YEAR
December	1990

4. FIN OR GRANT NUMBER

5. AUTHOR(S)

6. TYPE OF REPORT
Final Technical

7. PERIOD COVERED (Inclusive Dates)

8. PERFORMING ORGANIZATION - NAME AND ADDRESS (If NRC, provide Division, Office or Region, U.S. Nuclear Regulatory Commission, and mailing address; if contractor, provide name and mailing address.)

Division of Systems Research
Office of Nuclear Regulatory Research
U.S. Nuclear Regulatory Commission
Washington, DC 20555

9. SPONSORING ORGANIZATION - NAME AND ADDRESS (If NRC, type "Same as above"; if contractor, provide NRC Division, Office or Region, U.S. Nuclear Regulatory Commission, and mailing address.)

Same as 8. above.

10. SUPPLEMENTARY NOTES

11. ABSTRACT (200 words or less)

This report summarizes an assessment of the risks from severe accidents in five commercial nuclear power plants in the United States. These risks are measured in a number of ways, including: the estimated frequencies of core damage accidents from internally initiated accidents, and externally initiated accidents for two of the plants; the performance of containment structures under severe accident loadings; the potential magnitude of radionuclide releases and offsite consequences of such accidents; and the overall risk (the product of accident frequencies and consequences). Supporting this summary report are a large number of reports written under contract to NRC which provide the detailed discussion of the methods used and results obtained in these risk studies.

Volume 2 of this report contains three appendices, providing greater detail on the methods used, an example risk calculation, and more detailed discussion of particular technical issues found important in the risk studies.

12. KEY WORDS/DESCRIPTORS (List words or phrases that will assist researchers in locating the report.)

severe accidents
risk analysis
probabilistic risk analysis

13. AVAILABILITY STATEMENT
Unlimited

14. SECURITY CLASSIFICATION
(This Page)
Unclassified
(This Report)
Unclassified

15. NUMBER OF PAGES

16. PRICE

THIS DOCUMENT WAS PRINTED USING RECYCLED PAPER.